AD NUMBER

AD443589

LIMITATION CHANGES

TO:

Approved for public release; distribution is unlimited.

FROM:

**Distribution authorized to U.S. Gov't. agencies and their contractors;
Administrative/Operational Use; 27 JAN 1999.
Other requests shall be referred to Defense Special Weapons Agency, 6801 Telegraph Road, Alexandria, VA 22310-3398.**

AUTHORITY

DTRA CPWC/TRC ltr dtd 6 May 1999

DASA-1285 (V)

NUCLEAR GEOPLOSICS

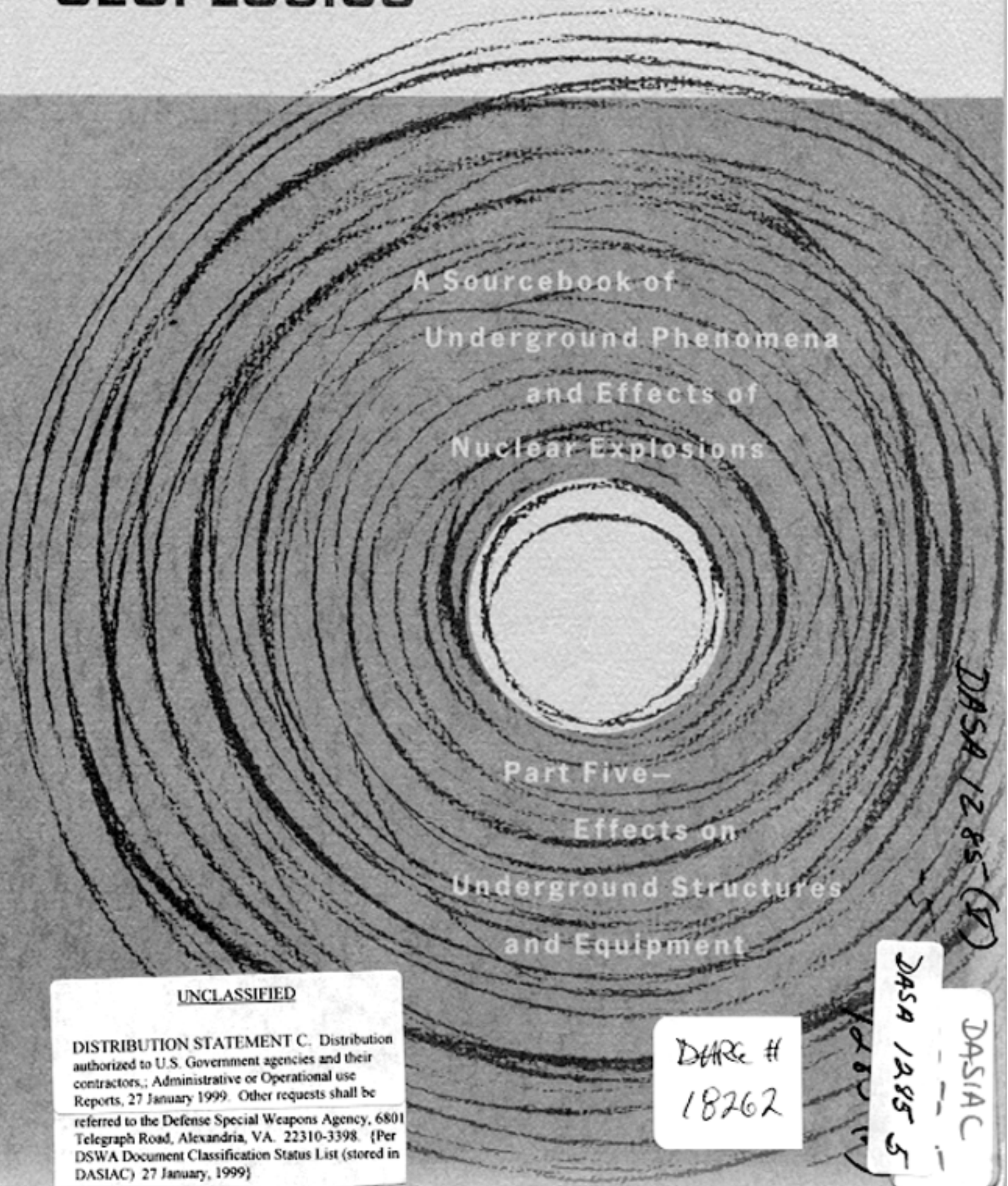

A Sourcebook of Underground Phenomena and Effects of Nuclear Explosions

Part Five– Effects on Underground Structures and Equipment

This report was prepared for the Defense Atomic Support Agency under Subtask 13.036.

DASA-1285 (V)

NUCLEAR GEOPLOSICS

A Sourcebook of Underground Phenomena and Effects of Nuclear Explosions

Part Five— Effects on Underground Structures and Equipment

By: J. L. Merritt and N. M. Newmark
N. M. Newmark Associates
Urbana, Illinois

Prepared for The Defense Atomic Support Agency
Washington 25, D.C., under Contract Nos. DA-49-146-XZ-027
and DA-49-146-XZ-030

Compiled for Publication by Stanford Research Institute
Fred M. Sauer, Editor-in-Chief

May 1964

FOREWORD

This is Part V of a sourcebook, comprised of five parts, on underground phenomena and effects of nuclear explosions. The compilation of this sourcebook is sponsored by the Defense Atomic Support Agency. The sourcebook is divided into the following parts:

Part		Authorship
I	Theory of Directly-Induced Ground Motion	Jacques Naar, Stanford Research Institute
II-1	Mechanical Properties of Earth Materials--Soils	R. V. Whitman, Massachusetts Institute of Technology
II-2	Mechanical Properties of Earth Materials--Rocks	G. B. Clark, University of Missouri School of Mines & Metallurgy
III	Test Sites and Instrumentation	Phyllis Flanders, Stanford Research Institute
IV	Empirical Analysis of Ground Motion and Cratering	Fred M. Sauer, Stanford Research Institute, with contributions by Illinois Institute of Technology Research Institute and University of Missouri School of Mines & Metallurgy
V	Effects on Underground Structures and Equipment	J. L. Merritt and N. M. Newmark, (Newmark Associates)

PREFACE

Earth motion is by no means a new study -- as early as 132 A. D. the Chinese scholar-astronomer Chang Hen devised an instrument to record earth motion during earthquakes. What is new, or comparatively so, is the study of explosively induced earth motion. With the discovery of high explosives man had at his disposal a force capable of causing earth motion of significant magnitude, and as a result there developed an interest in explosion effects in earth (geoplosics), an interest which until World War II was centered chiefly in preventing damage caused by blasting in construction, quarrying, and mining operations. When World War II brought the use of large high-explosive bombs burst at the surface and within the earth, interest quickened in the effects of earth motion as a factor in the design of fortifications. But it was not until the development of nuclear explosives that man succeeded in harnessing a force that matched natural seisms in the creation of earth motion of tectonic proportions. Interest in geoplosics now came to maturity because the physical devastation demonstrated by airblast from nuclear weapons made it imperative that one line of our defense be underground structures housing missiles, men, and materiel.

Earth motion has been measured on all nuclear weapons effects tests since the first test device, Trinity, was fired near Alamogordo, New Mexico, in the summer of 1945. In addition, earth motion from high-explosive detonations and its effect on structures has been studied under programs sponsored by various government agencies. An ever-increasing amount of effort has gone into the study of earth motion, both theoretical and experimental, but unlike the relatively uncomplicated physics of the shock wave in the medium of air, understanding the stress wave in earth is confounded by the very properties of the medium in which the wave moves. Despite the quantity of useful theory and data developed by these efforts, many old questions remain unanswered and with every advance in missile technology new questions arise, so that geoplosics can be expected to remain a dynamic science for some time to come.

With this in mind, it seemed an appropriate time to sum up our understanding of the behavior of explosions underground, especially those burst within the surface, which are the explosions of practical interest, the propagation of explosively-induced waves through the earth, how the earth is transformed under their influence, and how these waves affect buried structures. In the process it will become clear what we do not yet know and what we need to know.

This book is not meant to be a handbook of design specifications. It is meant to be an authoritative sourcebook. Between these two is the difference, for example, between the laboratory course and the lecture course. It contains more philosophy than figures, more hypotheses than certainties. These hypotheses are given whenever possible with the empirical information and the theory upon which they are based so that the reader can make his own judgment of their validity. We strive to avoid the temptation to speculate intuitively without factual or theoretical foundation for the arguments presented, and we attempt to present objectively all approaches, favored and unfavored, with the reasons for preference of one or another type of analysis or procedure clearly stated. So that the sourcebook need not be classified, a few relevant references are not discussed. In addition new material appearing during the late stages of compilation of the sourcebook is not referenced. It is hoped that these deficiencies will be corrected in future editions.

The editor-in-chief expresses his indebtedness to his associates at Stanford Research Institute, Drs. R. B. Vaile, Jr., E. G. Chilton, G. N. Bycroft, L. Seaman, and Mr. L. M. Swift, for review of material and many helpful suggestions. In particular, the editor wishes to acknowledge his debt to his associate editor, Mrs. Phyllis (Flanders) Dorset, without whom this sourcebook would not have been attempted. Thanks are also extended to Mr. John Lewis, Commanders James Andrews and Worthen Walls, Majors Bruce Carswell, Merrill Barnes, Patrick Donohoe, and Floyd Henk, Lieutenant Commander John Healy, and Captain James Choromokos, all of the Defense Atomic Support Agency, who over the years have given their wholehearted support to the project. In addition, we wish to thank the many people and organizations who have contributed to this effort by making data, photographs, and drawings available, which were not readily available in reports or other doucments. These contributions are gratefully acknowledged.

Fred M. Sauer

ACKNOWLEDGMENT

The writers acknowledge the help and advice in this study of N. Khachaturian, A. R. Robinson, R. E. Fulton, H. Kane, J. W. Melin, J. P. Murtha, S. L. Paul, W. C. Schnobrich, G. K. Sinnamon and R. N. Wright. Valuable consultation with W. J. Hall and J. D. Haltiwanger is also acknowledged.

J. L. M. and N. M. N.

NOTATION

CHAPTER V-1

a = particle acceleration

A = the cross sectional area included in the width b

b = unit width or spacing between ribs or beams

c = seismic velocity (dilatation)

c_1 = seismic velocity in medium (dilatation)

c_2 = seismic velocity in structure (dilatation)

c_R = Rayleigh wave velocity

c_s = seismic velocity (shear or distortion)

$C_f = t\left(\frac{\partial S}{\partial t}\right)_f$ = specific heat under constant tension

C_p = the specific heat at constant pressure

d = effective depth of structural member

d_1 = depth below surface to loaded element

d_2 = depth below surface to base of footing

e = base of natural logarithms (2.718 . . . .)

E = modulus of elasticity

E_s = modulus of elasticity at constant entropy

E_t = modulus of elasticity at constant temperature

f = axial stress

G = modulus of rigidity

G_s = the dynamic modulus of rigidity

G_t = the static modulus of rigidity

I = effective moment of inertia

K = bulk modulus of elasticity

K_s = bulk modulus corresponding to the adiabatic compression or the dynamic bulk modulus

K_t = bulk modulus corresponding to the isothermal compression or the static bulk modulus

L = span or length

m = mass per unit of length

m' = mass of buried element and portion of overburden

p = peak intensity of load or stress on structural element

p_m = peak intensity of force on single-degree-of-freedom system

$p(t)$ = force acting on standard linear oscillator

P = compressive force

q = plastic resistance of structural element

q_y = force causing yielding of structural element

r = mean radius of arch or great circle of dome

R' = constant associated with natural period of vibration of reinforced concrete beams

R_o = constant associated with natural period of vibration of beams

s = specific entropy

t = thickness of arch or dome (Section V-1.5.2)

t = absolute temperature (Section V-1.6.2)

t_d = effective duration of force on single-degree-of-freedom system

t_m = time of maximum response of single-degree-of-freedom system

t_r = rise time of loading on single-degree-of-freedom system

T = natural period of vibration of single-degree-of-freedom system

T' = modified period of vibration of buried structure

T_a = natural period of vibration of arch

T_d = natural period of vibration of dome

T_r = natural period of vibration of rectangular element

v = particle velocity (Section V-1.3.1)

v = specific volume (Section V-1.6.2)

v_o = particle velocity at impacted end of rod

v_u = critical impact velocity

V_a = original volume of arch

W = weapon yield

x_m = maximum deflection

x_y = effective yield deflection

y = depth below the surface

$\ddot{y}$ = acceleration of base of standard linear oscillator

z_1 = depth for a given overpressure at which a given stress occurs from a detonation of yield W_1

z_2 = depth for a given overpressure at which a given stress occurs from a detonation of yield W_2

β = the ratio of the damping present to the critical damping

Δp_m = peak overpressure in psi

ΔV_a = change in volume for arch

ΔV_r = maximum change in volume for rectangular structure

ϵ = strain

ϵ_u = strain corresponding to the ultimate strength of the material

λ = wave length (Rayleigh)

μ = ratio of maximum to effective yield resistance of structural element

μ_c = ratio of maximum circumferential strain to yield strain in arch

μ_r = ratio of the maximum deflection to the yield deflection

ν = Poisson's ratio

ρ = density

ρ_1 = density of medium

ρ_2 = density of structure

σ = stress

σ_1 = incident stress in medium

σ_2 = stress in structure

σ_h = horizontal stress

σ_r = reflected stress in medium

σ_v = vertical stress

φ = angle of internal friction (Section V-1.4.4)

φ = percentage of tensile reinforcement at midspan (Section V-1.5.2)

CHAPTER V-2

$a = \frac{2K \tan \varphi'}{b_d}$

$A = \frac{c}{R}$

$b = \frac{2K \tan \varphi'}{b_c}$

b_c = width of buried structure

b_d = width of ditch

$B = \frac{K \tan \varphi}{R}$

c = cohesive strength of soil

D = depth factor for cratering

e = base of natural logarithms (2.718 . . . .)

E = modulus of elasticity of medium

$\tilde{E}$ = modulus of elasticity of liner

h = height above roof of structure

h_e = height of equal settlement (measured from roof of structure)

$K = \frac{\tan^2 \varphi + 1 - \tan \varphi}{\tan^2 \varphi + 1 + \tan \varphi} = \frac{1 - \sin \varphi}{1 + \sin \varphi}$ (Section V-2.1.2)

K = ratio of horizontal to vertical stress in soil (Section V-2.2.3)

K_A = coefficient of "active pressure" in soil

K_o = coefficient of "earth pressure at rest"

$L = 230 \text{ ft} \left(\frac{100 \text{ psi}}{p_s} \right)^{0.5} \left(\frac{W}{1 \text{ mt}} \right)^{1/3}$

p = vertical stress at any depth

p_a = radial stress acting across the structure-soil interface

p_b = circumferential stress in liner

p_c = circumferential stress in medium adjacent to liner

p_m = peak intensity of force on single-degree-of-freedom system

p_o = vertical stress acting on roof of structure (Section V-2.2.3)

p_o = horizontal radial stress in medium at large distances from structure (Section V-2.2.1)

p_s = peak overpressure

p_y = vertical stress in medium at depth y including effects of attenuation

p_z = horizontal stress at depth z on a cylinder with radius r

p_∞ = horizontal stress at an infinite depth

q_y = force causing yielding of single-degree-of-freedom system

r = radius of liner; radius of great circle for spherical liner

R = ratio of area of roof of structure to perimeter of roof lying between assumed planes of slip

S = soil factor for cratering

t = thickness of liner or diaphragm

t_d = effective duration of force on single-degree-of-freedom system

T = natural period of vibration of single-degree-of-freedom system

u = displacement at any depth

u_o = displacement of roof

w = unit weight of soil

W = weapon yield

x = vertical coordinate measured from roof of structure

x_m = maximum deflection of single-degree-of-freedom system

x_y = effective yield deflection of single-degree-of-freedom system

y = depth below surface

z = depth below surface

α = slope of mound over structure with respect to horizontal (Section V-2.2.1)

α = limiting value of constant defining displacement at which shear failure occurs in soil (Section V-2.2.3)

$\alpha = \dfrac{1}{1 + \frac{y}{L}}$ (Eq. V-2.9)

β = constant for decay of displacement

$\gamma = \dfrac{1 - \nu^{-2}}{1 - \nu^2} \dfrac{Er}{\bar{E}t}$ = relative stiffness of medium and liner

ϵ = circumferential strain in medium or lining at structure-soil interface

λ = scaled slant range

λ_c = scaled depth of charge for cratering

ν = Poisson's ratio of medium

$\bar{\nu}$ = Poisson's ratio of liner

τ = shear stress at any depth

τ_{max} = limiting shear stress

φ = angle of internal friction of natural soil

φ' = angle of internal friction of the backfill

NOTATION

CHAPTER V-3

B = horizontal span or width of opening

c = seismic velocity (dilatation)

$\bar{c}$ = cohesive strength

C = width of opening

D = thickness of the spall

E = modulus of elasticity of lining material

E_c = modulus of elasticity of the critical stratum

E_f = energy absorption per unit of surface area

E_m = the modulus of elasticity of medium

E_ℓ = the modulus of elasticity of lining

h = height of tunnel

H = height of opening (Section V-3.1.1)

I = moment of inertia of lining

K_C = maximum compressive strain (stress) concentration factor

K_t = maximum tensile strain (stress) concentration factor

L = span of slab in stratified formations or width of pillar in homogeneous formations

L_p = length of pulse

p = amplitude of sinusoidal component of loading on structural lining

p_1 = amplitude of p giving a compatible stress and deformation between the structural lining and the packing

q = magnitude of uniform component of stress on structural lining

q_{cr} = approximate critical buckling load (a uniform stress) of structural lining

r = mean radius of lining

r_f = plastic resistance of the filler or crushable material

R = range measured from point of detonation

R_c = empirical range from center of detonation corresponding to closure from spalling

t = thickness of a solid lining

t_c = thickness of critical slab

t_f = thickness of the filler or crushable material

v = velocity of initial spall

v_{max} = average shearing stress

w = unit weight of rock

w_c = effective unit weight of critical stratum

w_e = effective unit weight of single stratum

W = width of opening or width of pillar (Table V-3.1)

W = weapon yield (Section V-3.1.2)

W' = width of pillar

y = depth

Δ = minimum deformation of surface of rock

Δ_m = maximum deformation of surface of rock opening

δ = total maximum deflection of structural lining

δ_{max} = maximum deflection of critical slab

δ_1 = value of δ corresponding to p_1

ϵ = peak radial strain in medium

$\bar{\epsilon}$ = strain corresponding to ultimate tensile strength

ϵ_p = effective strain in stratified formation

ϵ_t = strain corresponding to modulus of rupture

ϵ_u = ultimate compressive strain in rock

ζ, η, ξ = coefficients defining shape of ovaloidal openings

ν_m = Poisson's ratio of medium

ρ = density of medium

σ_h = horizontal stress

σ_{max} = maximum stress produced by flexure

σ_u = unconfined compressive strength

σ_v = vertical stress

σ_v = vertical component of static stress

τ_{max} = maximum shearing stress

φ = angle of internal friction

NOTATION

CHAPTER V-4

A = spectrum acceleration

$\bar{A}$ = ratio of maximum internal energy to internal energy at initial yielding of spring in simple oscillator

D = spectrum displacement

D_y = yield value of spectrum displacement

E = modulus of elasticity of material

f = natural frequency of vibration of simple oscillator

g = acceleration of gravity

h = length of time interval in numerical integration

i = impulse or area under force-time curve

I = moment of inertia of cross section of beam

K = elastic stiffness of simple oscillator representing beam

K' = plastic stiffness of simple oscillator representing beam

L = span of beam

M = mass of simple oscillator representing beam with elastic response

M' = mass of simple oscillator representing beam with plastic response

M_c = bending moment at center of beam for elastic response

M'_c = bending moment at center of beam for plastic response

M_x = bending moment at any point x along beam

m = mass of beam per unit of length

P = magnitude of total uniformly distributed load applied to beam

P_n = magnitude of nth component of load

P = concentrated load acting on mass of simple oscillator representing beam with elastic response

P' = concentrated load acting on mass of simple oscillator representing beam with plastic response

$\bar{P}$ = "effective" average force acting during time from zero to t_y

P_m = maximum value of force acting on structure

R = value of force developed by spring in simple oscillator

R_y = force developed by spring in simple oscillator at initial (or effective) yielding

S_a = ratio of errors in devised and assumed acceleration

$S_{\bar{M}}$ = error in bending moment represented by neglecting all but fundamental mode in response of simple beam to step pulse of loading with infinite duration

$S_{\bar{y}}$ = error in deflection represented by neglecting all but fundamental mode in response of simple beam to step pulse of loading with infinite duration

$S_{\bar{\bar{y}}}$ = error in deflection represented by neglecting all but fundamental mode in response of simple beam for impulsive loading

s = length over which curvature occurs in beam deformed beyond its yield strength

T = period of vibration of simple oscillator

T_n = natural period of vibration in nth mode

T_s = pseudo period of solution by numerical integration

t = time variable

t_d = effective duration of positive phase of loading or ground displacement

t_l = "duration" of impulse

t_m = time of maximum response of simple oscillator

t_r = rise time or time from zero to maximum of applied force

u = relative displacement between mass and ground

$\dot{u}$ = relative velocity between mass and ground

$\ddot{u}$ = relative acceleration between mass and ground

V = spectrum pseudo-velocity

x = absolute displacement of ground or coordinate measured from support of beam

$\dot{x}$ = absolute velocity of ground

$\ddot{x}$ = absolute acceleration of support or "ground"

x_m = maximum displacement of ground

$\dot{x}_m$ = maximum velocity of ground

$\ddot{x}_m$ = maximum acceleration of ground

x_{ave} = average displacement of ground

$\dot{x}_{ave}$ = average velocity of ground

$\ddot{x}_{ave}$ = average acceleration of ground

y = displacement of mass

$\bar{y}$ = approximate displacement of mass

$\dot{y}$ = absolute velocity of mass

$\ddot{y}$ = absolute acceleration of mass

y_c = correction in displacement applied in solution of "plastic" response of simple oscillator

y_b = deflection at center of beam produced by static load

$\bar{y}_b$ = deflection at center of beam produced by step pulse of force with infinite duration

$\bar{\bar{y}}_b$ = deflection at center of beam produced by impulse

y_m = maximum displacement of simple oscillator

y_s = static displacement caused by load P

y'_s = displacement of simple oscillator produced by the supported mass

y_y = deflection corresponding to initial (or effective) yielding of spring in simple oscillator

α = a parameter defined by: $\alpha^2 = \dfrac{\theta^2}{1 + \beta\,\theta^2}$

β = parameter defining variation of acceleration with time

γ = pseudo damping parameter in numerical integration

θ = product of natural circular frequency and time interval

μ = "ductility factor" which is ratio of maximum to yield deflection

ψ = pseudo natural circular frequency in solution by numerical integration

ω = natural circular frequency of vibration of simple oscillator

NOTATION

CHAPTER V-5

A = spectral value of acceleration for single-degree-of-freedom system

a_n = coefficient of series

D = spectral value of displacement for single-degree-of-freedom system

E = modulus of elasticity of material

g = acceleration of gravity

i, j = subscripts denoting modes

I = moment of inertia of section

K = stiffness of part of structure; subscripts define position in structure

L = span

L = Lagrangian function

M = mass of part of structure; subscripts define position in structure

M_x = moment at position x in beam

n = mode designation or general position designation (in structure)

p = intensity of load on beam

P = static pressure acting on structure

$\overline{P}$ = peak value of pressure acting on structure

R = resistance of structure

R_y = resistance of structure at general yielding

t = time

U = potential (or strain) energy

$u(t)$ = deflection response for a single-degree-of-freedom system subject to ground motion

V = kinetic energy

V = spectral value of velocity for single-degree-of-freedom system

w = weight of beam per unit of length

x = coordinate defining distance from support of beam

y = absolute deflection of mass; subscripts define position in structure

$\dot{y}$ = absolute velocity of mass

$\ddot{y}$ = absolute acceleration of mass

y_a = arbitrary deflection pattern

y_m = computed displacement

y_{m-1} = assumed displacement

$\bar{y}_m$ = maximum transient displacement of structure

α = modal quantity

γ = scale factor for modal quantities (deflection, velocity, force, etc.), modal excitation factor

ΔF_n = force in nth spring

Δy_n = deflection of nth spring

μ = ductility ratio, ratio of maximum transient displacement to displacement at general yielding

ξ, η, ζ = Cartesian coordinates

ω = circular natural frequency of vibration

NOTATION

CHAPTER V-6

A_c = core area of column

A_g = gross area of column

A_s = cross-sectional area of tensile reinforcement

A_{st} = total area of longitudinal reinforcement

b = width of member or of the "compression flange"

b' = width of stem of a T-section

c = distance from neutral axis to "extreme fiber"

d = effective depth of member

E = modulus of elasticity

e = eccentricity of load

f = stress at "extreme fiber"

f'_c = ultimate strength of concrete

f_r = modulus of rupture of concrete

f'_s = yield strength of spiral reinforcement

f_y = yield stress for tensile reinforcement

h = total depth of member

I_c = moment of inertia of "transformed section"

I_g = gross moment of inertia of a beam

j = dimensionless parameter defining the distance between the centroid of the internal compressive and tensile forces

L = span of member

L_a = total length of column

L_s = shorter span of slab

M = moment at mid-span

M_c = bending (or resisting) moment at initial cracking

M_u = bending (or resisting) moment at ultimate conditions

M_y = bending (or resisting) moment at general yielding

N_u = axial force on column at ultimate conditions

N_y = axial force on column at general yielding

p = tensile reinforcing ratio

p' = compressive reinforcing ratio at mid-span

p_1 = tensile reinforcing ratio at one support

p_2 = tensile reinforcing ratio at another support

p_a = average value of tensile reinforcing ratio over supports

p_c = tensile reinforcing ratio at mid-span

p_g = gross reinforcing ratio

p_{Lc} = tensile reinforcing ratio parallel to longer span of slab at (or near) mid-span

p_{Le} = tensile reinforcing ratio parallel to longer span of slab at (or near) the support

P_m = magnitude of dynamic pressure acting on beam

p_{max} = maximum value of tensile reinforcing ratio

p_{min} = minimum value of tensile reinforcing ratio

p_s = spiral reinforcing ratio

p_{sc} = tensile reinforcing ratio parallel to shorter span of slab at (or near) mid-span

p_{se} = tensile reinforcing ratio parallel to shorter span of slab at (or near) the support

p_v = volumetric reinforcing ratio of web reinforcement

R_1 = resistance at initial yielding in indeterminate beam

R_c = cracking resistance of beam

R_u = ultimate resistance of beam

R_y = resistance of a beam at general yielding for uniformly distributed loading (R_y is a pressure)

R_{ys} = resistance at general yielding and at ultimate conditions for beam subjected to combined shear and flexure

V_{max} = maximum shear in member

y_1 = deflection at initial yielding in indeterminate beam

y_2 = deflection at general yielding in indeterminate beam

y_E = deflection at mid-span

y_y = mid-span deflection at yielding in indeterminate beam

y'_y = mid-span deflection at yielding in simple beam

y_{ya} = deflection at yielding in column under axial load

α = aspect ratio for a slab

β = factor relating strength of two-way slab to strength of one-way slab

ϵ_u = maximum compressive strain at which crushing of the concrete begins

ϵ_y = strain in tensile reinforcement corresponding to initial yielding

θ = ratio of tensile reinforcing ratio at the supports to that at mid-span

μ_m = maximum ductility ratio

ϕ = ratio of compressive to tensile reinforcing ratios

CONTENTS

ILLUSTRATIONS

TABLES

CHAPTER V-1

GENERAL LOADING AND RESPONSE OF STRUCTURES

V-1.1 INTRODUCTION

Explosion-generated motion propagating through soil or rock may be characterized in several ways. In the earlier parts of this book the nature of the motion and the factors which influence its strength and propagation in the free field are discussed. Most of the manifestations of the motion have an influence on an underground structure embedded in the medium. Which of the manifestations predominate in the behavior of the structure depends upon how the properties of the structure differ from those of the medium. The problem of determining the influence on the structure of the ground motion in the vicinity of the structure introduces the concept of "structure-medium interaction."

A knowledge of the effects induced in the free field, the factors influencing these effects, the structure-medium interaction, and the factors influencing interaction is implicit in the study of behavior of underground structures. This chapter summarizes these various phenomena as they apply to underground structures in general. Behavior of specific structural types is discussed in Chapters V-2 and V-3.

As described in Part III many methods have been used to measure the intensity and variation in time and space of the free-field motion. The characteristics of free-field motion are important in the definition of the nature of the waves induced in the medium and the conditions which affect the behavior of a structure located in the medium. It is emphasized that, for each of the parameters discussed below, the magnitude, direction, and the variation with time and space of the free-field effects should generally be known.

Although the behavior of a structure may be influenced by other factors than the external loading, the outer shell of a buried structure must have a strength capable of resisting the forces applied to it. Consequently, knowledge of the contact stresses acting on the structure is required. These may often differ from the free-field stresses, but nevertheless they are related to them. Hence the stress intensities in the free field are important.

For open unlined cavities in rock or for structures in soil extending over large lengths or areas, the free-field strains may be more important than the stresses in determining the conditions of failure. Moreover, the distribution of strain must be known to define displacement. For many situations this distribution can be inferred from the mode of stress wave propagation.

In the determination of the behavior of equipment mounted within a structure, knowledge of the absolute motions of the structure is required. In many instances the effects on equipment, as well as on component parts of the structure itself, can be stated in terms of the response spectrum, which can often be described adequately enough for design purposes from only the maximum values of medium displacement, velocity, and acceleration.

In the consideration of the desirable depth of cover over a structure, both for structural strength and for response of contained equipment, the attenuation with depth and the decay with distance of the various stress wave parameters must be known.* For example, changes in displacement with horizontal or vertical distance are important because effects sometimes vary significantly with distance along a structure; this variation can cause serious problems in a large structure.

V-1.2 SOURCES OF DATA

Although theories and experimental evidence related to the propagation of stress waves in elastic homogeneous materials were relatively well known prior to World War II, only limited inferences could be drawn pertaining to the behavior of protective

*Thermal and nuclear radiation from a nuclear explosion are not important in a discussion of structural behavior under blast loading. Even for completely exposed structures, the short duration of the intense thermal wave renders it of little significance in causing other than surface damage. Because of the insulation provided by the earth cover, thermal radiation has no effect on the behavior of underground structures. Yet it cannot be neglected a priori in the design of ventilation systems; this subject however is not a part of this book. Even though nuclear radiation is intense, it generally does not have sufficient duration or sufficient energy to cause significant changes in structural materials. Although it is not germane to this book, the effects of nuclear radiation must be accounted for in the general problem of designing an underground structure to insure protection from radiation of the contents or inhabitants of a buried structure. This requires sufficient cover to attenuate the radiation reaching the structure to tolerable levels.

structures located in soil and rock. Consequently it was necessary to conduct tests of buried structures subjected to the forces of both contact and remote explosions. The results of the tests involving high explosives were summarized by Christopherson (Ref. V-1.1) in Great Britain and by Lampson (Ref. V-1.2) in this country. Results obtained in these experiments of importance to this book were: (1) Development of techniques for measuring pressure in the free field and stress on structures (See Part III); (2) documentation of the means by which stress waves propagate through soil and subsequent analyses of these phenomena (See Part IV); and (3) determination of damage criteria for buried structures. Relative to these damage criteria, it should be noted that the instruments of warfare at the time differed in many respects from nuclear weapons. For example, armor piercing projectiles and bombs were commonly used against fortifications; also delivery systems for the weapons were such that the total energy available in the projectiles and bombs were limited to a few tons of high explosive. Consequently, the buried structures tested were representative of typical reinforced concrete fortifications common to the era which were designed to prevent penetration of and spalling on interior surfaces caused by armor piercing weapons. To provide this protection required thick structural elements and reinforcement concentrated on the interior surfaces of the structure. Yet because this reinforcement was provided mainly to prevent spalling, it offered relatively limited strength to the members for resisting the explosion generated stresses from remote detonations. In fact the analysis of the elements in these structures indicates that the amount of reinforcement provided was significantly less than the percentage required to cause the ultimate strength to equal the cracking strength. Although they were adequate to protect against the weapons in use at the time, the fortifications considered by Lampson and Christopherson proved inadequate for resisting the effects of nuclear weapons. This resulted primarily because of the many-fold increase in the yield of nuclear weapons with the attendant increase of positive phase duration and in area subject to stress in comparison to the size of the fortifications.

Field tests of protective structures are important for many reasons. Paramount among these reasons are: (1) Knowledge of the phenomena is not sufficient to allow reliable scaling from microscale laboratory experiments; (2) it is difficult to simulate the natural conditions which prevail; and (3) it is difficult to simulate the loading induced by a nuclear detonation. This is not to say that laboratory and theoretical investigations are of little value; on the contrary they are indispensable and must always accompany field experiments of any kind. Yet field data have been most useful in providing checks and controls on the theoretical analyses. Full-scale tests should never be considered ends in themselves; science is advanced when a theory is generated which explains fully the empirical observations.

Although a wealth of data has been accumulated through the years of testing, theoretical development unfortunately did not keep pace with the data collection in many cases. This gap is now being closed, but many of the empirical observations require additional explanation. In the sections which follow the inferences which may be drawn from the field tests are discussed whenever they are pertinent.

For practical reasons tests on underground structures made in a laboratory must normally be geometrically scaled. Also to gain fundamental understanding of a problem individual parts of that problem must be studied rather than the entire problem. Even though simulation, or even approximate simulation, of physical conditions may be impossible, much can be learned at least qualitatively about any complex problem through scaled tests. For example the properties of materials in the environment associated with the over-all problem can be studied in detail. Following such a study, investigation of the behavior of individual structural elements of the same environment is desirable. Additional steps follow until the entire problem is understood.

For the situation considered in this chapter the major characteristic of the environment influencing the behavior of structural elements is the variation of loading with time. Many tests have been made on various materials wherein the effect of strain rate on the mechanical properties of structural materials has been studied. Although these effects are now reasonably well documented, a theory which completely explains the observations is as yet lacking. Studies in this area are continuing. These studies are summarized in Section V-1.6.

Studies also are continuing of the behavior of individual structural elements subjected to dynamic loads. For the types of construction which have been investigated it appears that static theories are appropriate in the definition of the strength provided that the governing stresses of the component materials are augmented to reflect the effect of strain rate. Yet in some areas, notably diagonal tension in reinforced concrete, reliable static theories are not available. Studies of the static and dynamic behavior of individual structural elements are continuing. The results of some of these studies are presented in Chapter V-6.

A problem which only relatively recently has been studied experimentally involves the interaction of soil and structure. This is a most complex problem; experimental studies are hampered by the lack of equipment to apply transient loads to the relatively large samples of soil required and by the difficulty in measuring the states of stress and deformation in the soil. Techniques are being developed currently and testing in this area is proceeding at U. S. Navy Civil Engineering Laboratory (NCEL), U. S. Army Waterways Experiment Station (WES), U. S. Air Force,

Eric H. Wang Shock Tube Laboratory, MIT Soils Laboratory, Armour Research Foundation, and University of Illinois, Department of Civil Engineering, among others.

Another problem which is difficult to study experimentally involves the assessment of shock vulnerability of equipment. Although shake and spin tables and impact machines have been available for testing various components, the inputs imparted by these machines frequently do not simulate the inputs associated with stress waves produced by an explosion in or over soil or rock. This area of investigation also is receiving much attention.

Development of a unified theory of the behavior of buried structures has been impeded by a lack of understanding of the precise phenomena involved. Although the general phenomena which should influence this behavior have been understood reasonably well for some time, the manner in which these phenomena are coupled and bounded has not been clear. Consequently, analyses have evolved as the data from field and laboratory experiments became available. In most cases these experiments were designed to investigate the influence of parameters which a particular theory indicated should be of importance.

Because of the extreme complexity of the general problem, the evolution of theoretical solutions has occurred rather slowly. Individual idealized problems have been solved, and in general the correlation between the results of these solutions and experience depends upon the degree to which the idealizations match the physical situation. Fewer idealizations, and consequently better correlations, should be expected as ultra-high-speed digital computers become more generally available.

V-1.3 INFLUENCE OF STRESS WAVE ON TYPE OF RESPONSE

In the earlier parts of this book are presented detailed discussions of the manner in which the stress wave forms and propagates. Therefore, only the aspects of these phenomena that are pertinent to the behavior of buried structures are reviewed in this section. For example, the relative strength of the airblast- and directly-induced stress waves influences significantly the response of the structure. Also the change in shape of the stress wave as it propagates through the medium influences structural response.

As discussed in Part I, near the point of detonation of an underground or surface burst the medium may be treated as if it were a fluid under the action of the intense stress and velocity fields. Structures can only survive in the hydrodynamic region if they can withstand the major rigid body displacement caused by the intense stresses in this region.

Changes in air shock and ground motion parameters with time and distance depend implicitly on the type, size, and point of burst of a weapon. Much of the data from field tests of import to the current discussion has been obtained from detonations of high explosives. Several conditions accompanying a high explosive detonation differ from those involved in a nuclear detonation. For this discussion, these differences are assumed to be defined uniquely by the energy equivalence factors of the type discussed in detail in Ref. V-1.3.

Structural response is a function of the ratio of the effective duration of the stress wave to the appropriate natural period of vibration for the structural element on which the stress is acting. Although the effective duration of the stress wave is influenced by many parameters, the primary influence is a function of the size of the weapon as measured by the absolute energy yield. Despite the fact that the effect of the ratio of duration to natural period, in many instances, can be expressed as a continuous function (Ref. V-1.4), the physical effects can be understood more clearly by recognizing three cases; viz., shock inputs which are (1) nearly impulsive, (2) nearly infinite in duration and (3) intermediate between impulsive and infinitely long.

The location of the point of detonation relative to the surface of the ground influences the amount of energy which directly enters the medium as contrasted to the amount of energy released into the air as discussed in the introduction and in Part IV. This division of energy can be important to the behavior of a structure because it defines the relative intensity of the airblast- and directly-induced motion which reaches the vicinity of the structure.

V-1.3.1 Airblast-Induced Ground Motion

Theoretical Developments. When airblast-induced motion predominates in causing damage to underground structures, it is important to recognize the changes which occur as the wave moves through the medium. It is especially important to distinguish between the changes resulting from the wave passing through the medium and those resulting from the interaction between the medium and the structure.

To facilitate analysis, changes in stress-wave intensity resulting from propagation through the medium can be considered a result of two separate causes. The first, and major one, is spatial dispersion; the second is the complex dissipation resulting from nonlinear behavior, damping, and inertial effects in the medium. For airblast-induced ground motion, effects of spatial dispersion can be estimated if it is recognized that the airblast produced by a large nuclear detonation loads a large annular area surrounding the burst point. The radius of the air-shock front and of any contour of constant overpressure behind the shock front is so large compared to the practical depths of interest that these fronts may

be approximated by straight lines over a relatively large distance transverse to the direction of shock propagation. By use of this assumption a numerical solution for the stress field taking into account dispersal was generated by integration of the static (Boussinesq) solution for stresses produced in an infinite, elastic, homogeneous half-space (Ref. V-1.5). The mass of the medium cannot be included directly in this treatment because the static solution inherently disregards inertial effects. Thus, the results in Ref. V-1.5 are consistent with an assumption that the stress waves propagating from all points on the ground surface reach the point in the medium below the surface instantaneously. A graphical solution of the same problem (Ref. V-1.6), but considering the contours of constant overpressure to be arcs of circles, was based on charts developed in Ref. V-1.7 and gives results almost identical to those in Ref. V-1.5. The theoretical attenuation of vertical and horizontal stress with depth is shown in Figs. V-1.1 and V-1.2 which are taken directly from Ref. V-1.5. Typical shapes of the stress-time curves at selected depths also are shown in Figs. V-1.3 and V-1.4. It is important to recognize both the decrease in stresses and the increase in rise time with depth in the latter figures. Both of these changes in the stress wave can be very significant to the response of a structure.

Figures V-1.2 and V-1.4 are based on Poisson's ratio for the medium of 0.50; vertical stresses (Figs. V-1.1 and V-1.3) are independent of Poisson's ratio. Also the stresses computed from static theory are independent of the modulus of elasticity. None of the stress components includes the effect of the weight of soil above the horizontal plane at which the stresses are computed. As noted in the captions of the figures all computations were made for an ideal waveform of the surface overpressure. The scaling referred to in Figs. V-1.1 and V-1.2 illustrates how the data presented can be used to obtain stresses for nuclear devices of different yield. This scaling is based on the following relationship:

$$\frac{z_1}{z_2} = \left(\frac{W_1}{W_2}\right)^{1/3} \qquad \text{(V-1.1)}$$

where z_1 = depth for a given overpressure at which a given stress occurs from a detonation of yield W_1

z_2 = depth for a given overpressure at which a given stress occurs from a detonation of yield W_2.

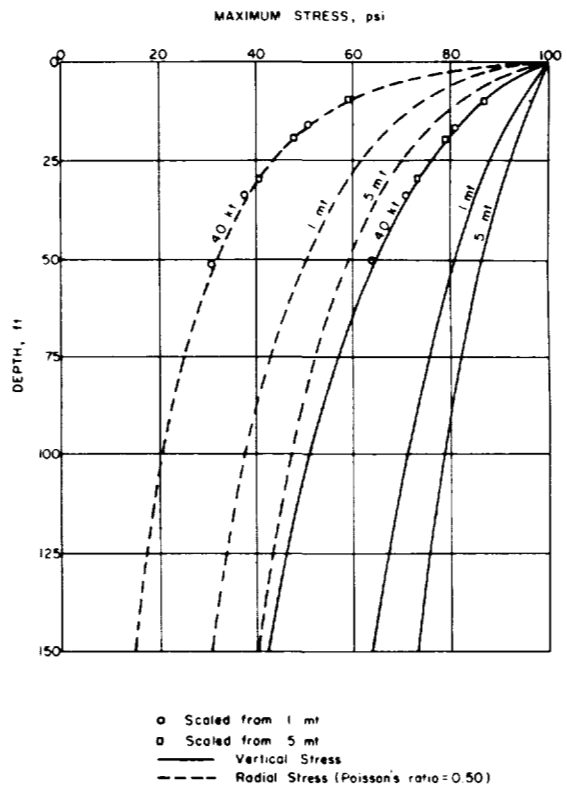

FIG. V-1.1 MAXIMUM AIRBLAST-INDUCED STRESS VS DEPTH FOR 100-PSI IDEAL OVERPRESSURE FROM SURFACE BURST

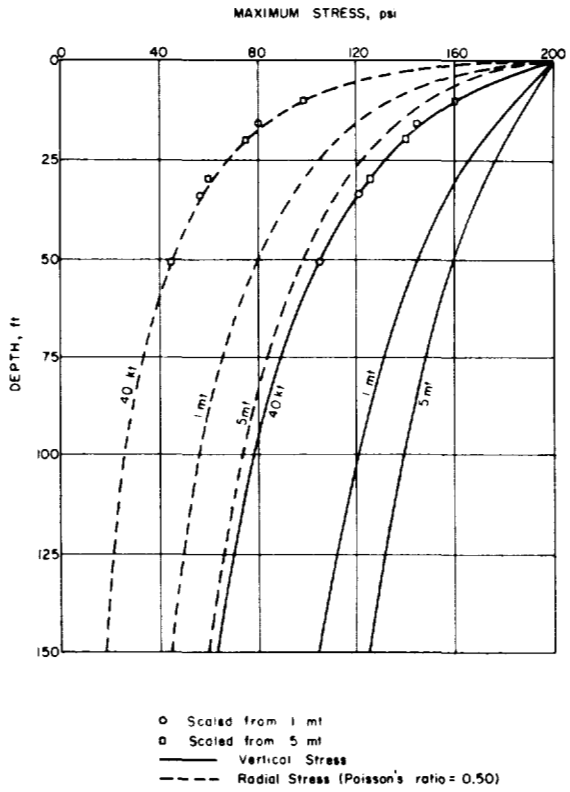

FIG. V-1.2 MAXIMUM AIRBLAST-INDUCED STRESS VS DEPTH FOR 200-PSI IDEAL OVERPRESSURE FROM SURFACE BURST

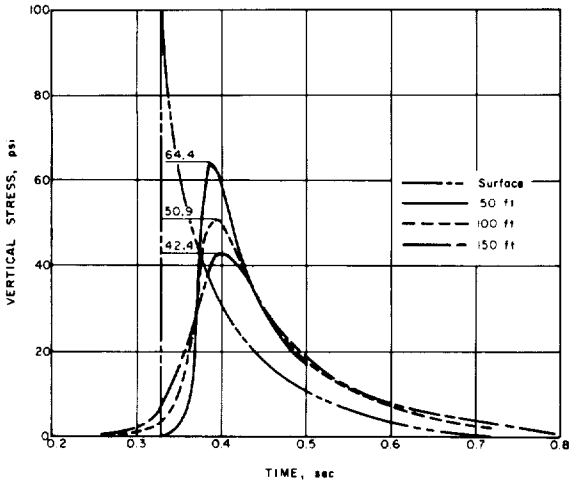

FIG. V-1.3 VERTICAL AIRBLAST-INDUCED STRESS VS TIME, EFFECT OF SPATIAL DISPERSION, 40-KT SURFACE BURST, 100-PSI IDEAL OVERPRESSURE WAVEFORM

Figures V-1.3 and V-1.4 illustrate the change in shape of the stress wave with depth. A distinct reduction in radial stress at all depths is apparent at a time approximately corresponding to the time of arrival of the surface overpressure at the vertical plane considered. This results from the fact that purely vertical stress at a point has a smaller influence on horizontal stress at the same point than does a vertical stress applied at a point removed from the point in question. A manifestation of this relative significance of the influence of vertical stress on horizontal (or radial) stress also is apparent in the earlier arrival of the horizontal stress compared to that of the vertical stress and the increase in rise time of radial stress with depth. In both figures, the earlier arrival of horizontal stress at greater depths than at smaller depths results from the implicit assumption that stress waves propagating from all points on the contour of constant overpressure reach the point instantaneously.

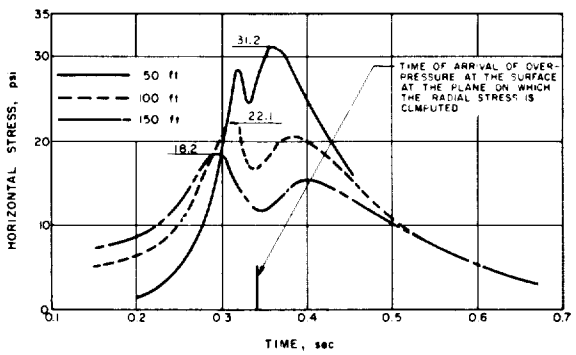

FIG. V-1.4 RADIAL AIRBLAST-INDUCED STRESS VS TIME, EFFECT OF SPATIAL DISPERSION, 40-KT SURFACE BURST, 100-PSI IDEAL OVERPRESSURE WAVEFORM

To eliminate partially the effect of this last assumption, the transit time from various points on the surface, corresponding to points on each contour of constant overpressure, to the point at which the vertical stress in the medium was computed, was included in the graphical solutions of the Boussinesq equations (Ref. V-1.6). Figure V-1.5 presents the results obtained at a range corresponding to 200-psi overpressure produced by a 5-mt surface burst (4320 ft). The seismic velocity of the medium (2000 ft/sec) considered in this figure is representative of many soils. Comparison of the peak values in Fig. V-1.5 with those in Fig. V-1.1 illustrates that the effect on the peak vertical stress of the finite seismic velocity is less than 10% for the depths considered.

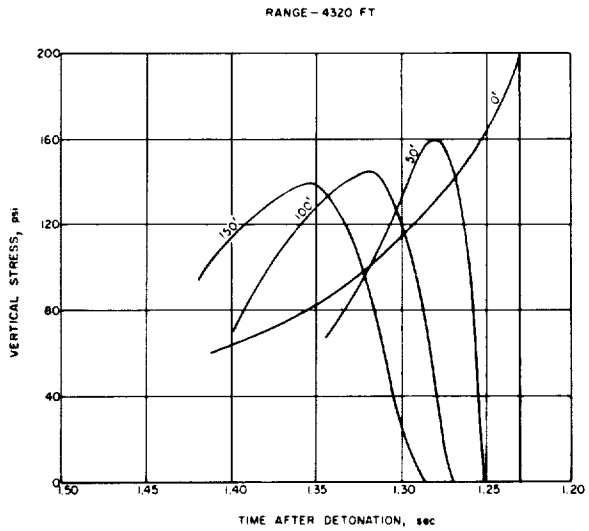

FIG. V-1.5 PRESSURE VARIATION WITH TIME AT DEPTHS INDICATED: SEISMIC VELOCITY IN SOIL TAKEN TO BE 2000 FT/SEC

Also in Ref. V-1.6 the radial stress was computed for a Poisson's ratio equal to 0.15. The results of this computation are compared with similar results for Poisson's ratio of 0.50 in Fig. V-1.6.

Recognizing that the airblast produced by a large yield nuclear device loads an annular ring with center at the point of detonation nearly uniformly circumferentially and radially over distances of several tens of feet suggests that a condition of one-dimensional strain might be nearly approached in the medium loaded by the airblast. If additionally the lateral stresses associated with a condition of one-dimensional strain are neglected, the behavior of the soil under the action of the airblast can be studied qualitatively by considering a one-dimensional rod.

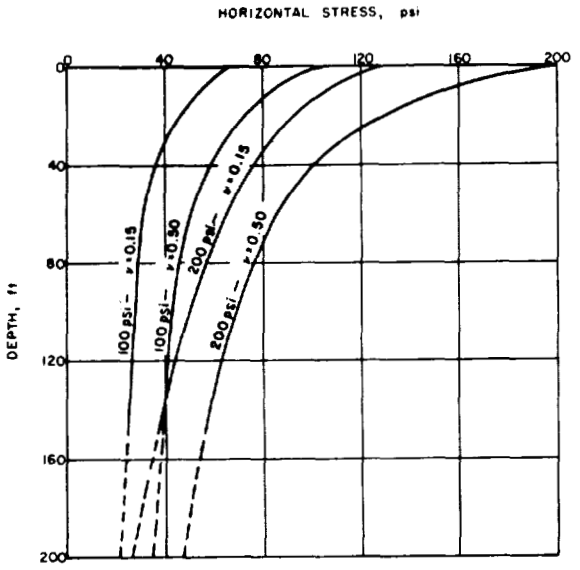

FIG. V-1.6 CHANGE IN MAXIMUM RADIAL STRESS WITH DEPTH NEGLECTING TRANSIT TIME, 5-MT SURFACE BURST

Recent theoretical work in studying specifically the propagation of waves in "rods" of soil appears in Refs. V-1.5 and V-1.8. Both of these references, in the evaluation of results, employ experimental data on the dynamic properties of soils (Ref. V-1.9 and associated reports). These experiments are described in Part II of this book.

In Ref. V-1.5 a viscoelastic model was postulated which deviates only slightly from a standard linear model in that a mass is added between the spring and the parallel combination of dashpot and spring common to the standard linear model (Fig. V-1.7). This division of mass was included primarily for ease in calculations. The springs in the model were not restricted to elastic action, and computations were made for nonlinear spring forces. A detailed study of the effects of varying each of the parameters was carried out to study the characteristics of the model and the stability of the numerical integration. Also experimentally determined parameters (Ref. V-1.9) were used, and except for the initial portion, the model solution checked the experimental stress-time curves well. The static stress-strain curve used in the solutions to compare with the experimental results is shown in Fig. V-1.8. Actual comparisons of theoretical and measured results are portrayed in Figs. V-1.9 through V-1.12. The parameters used in the computations are summarized in the insert for each figure. The value v_o is the particle velocity of the impacted end of the specimen. The lack of correlation in the initial part of the stress-time curves, especially at the impact end apparent in Figs. V-1.9 through V-1.12, was attributed to the effects of lateral inertia which were neglected in the model. The effects of lateral inertia theoretically should have been pronounced in the ex-

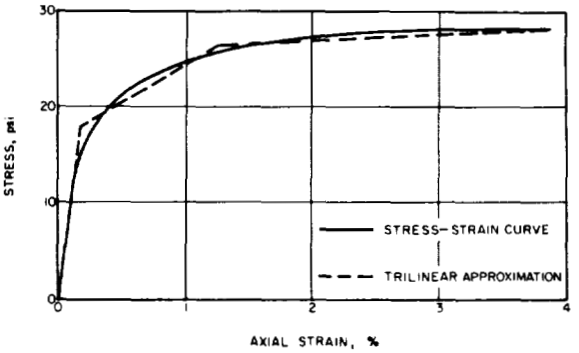

FIG. V-1.8 STATIC STRESS-STRAIN CURVE FOR OTTAWA SAND (REF. V-1.9)

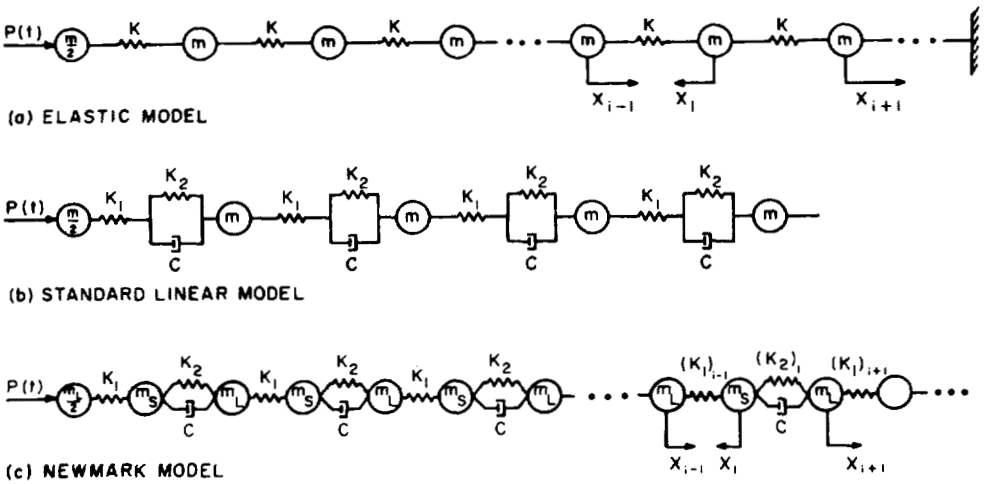

FIG. V-1.7 COMPARISON OF CERTAIN MODELS USED TO STUDY STRESS WAVE PROPAGATION IN ONE-DIMENSIONAL RODS

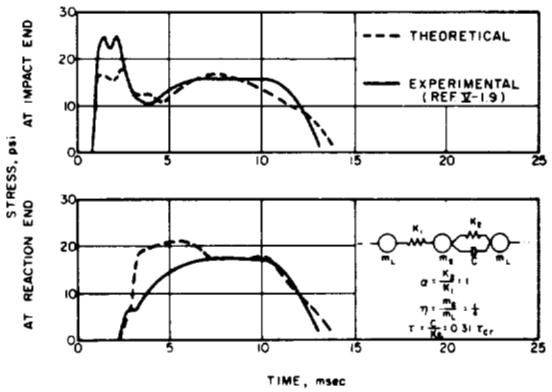

FIG. V-1.9 STRESS VS TIME FOR 20-IN. OTTAWA SAND SPECIMEN, V_o = 15 IN/SEC

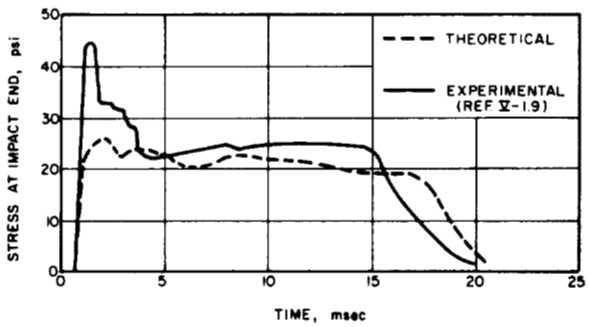

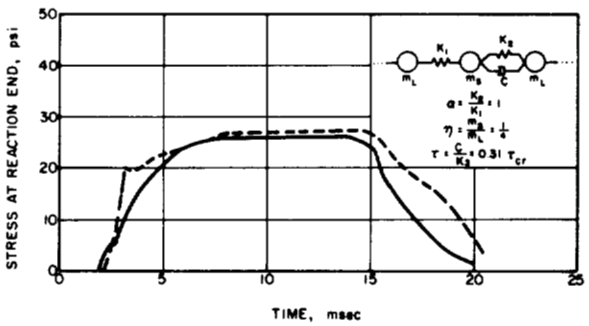

FIG. V-1.10 STRESS VS TIME FOR 20-IN. OTTAWA SAND SPECIMEN, V_o = 45 IN/SEC

perimental results because of the relatively small length-diameter ratio of the specimens. (See discussion by Whitman in Ref. V-1.8.)

Parkin (Ref. V-1.8) agrees that the effect of lateral inertia should be pronounced for the experimental data, but he presents a different analysis which neglects lateral inertia. In his theory Parkin

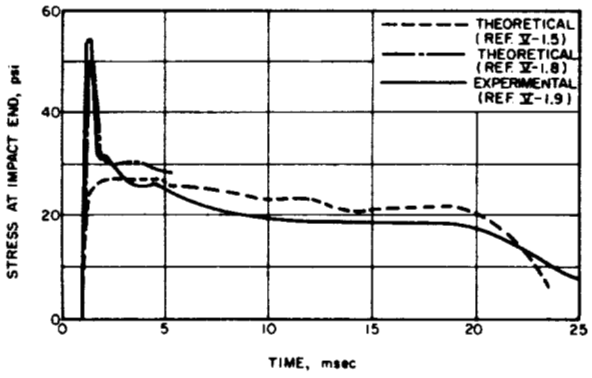

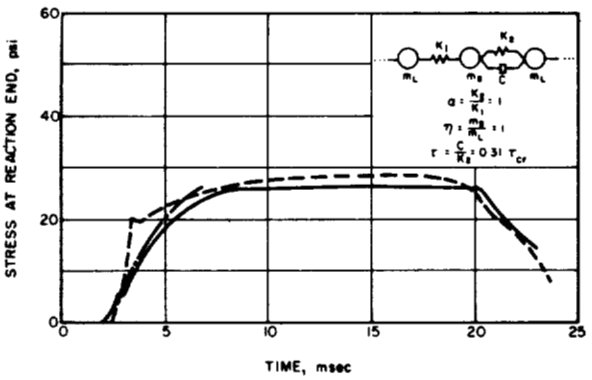

FIG. V-1.11 STRESS VS TIME FOR 20-IN. OTTAWA SAND SPECIMEN, V_o = 60 IN/SEC

approximates an experimental stress-strain curve for Ottawa sand by either a portion of an ellipse or by two straight lines. Additionally it is assumed that the stress-strain relation for the sand depends upon the strain rate induced. By the method of characteristics several solutions were obtained and with the proper choice of parameters the experimental results in Ref. V-1.9 are reproduced closely by this model. Of particular importance is the fact that Parkin's solution also predicts the large initial amplification of stress observed in the experiments, despite the neglect of lateral inertia in his model. A comparison of Parkin's results with those by Smith and Newmark and the experimental curves is shown in Fig. V-1.11. A complete curve from Ref. V-1.8 is shown in Fig. V-1.13.

Thus, Parkin's solution reproduces the entire curve obtained in the laboratory while the solution presented in Ref. V-1.5 does not predict reliably the initial portion of these curves especially at the impacted end. At the moment the validity of either of the solutions cannot be determined. Common to the theories is the fact that both rely on experimentally determined "constants" and both require that part of the input data be inferred on the basis of intuition

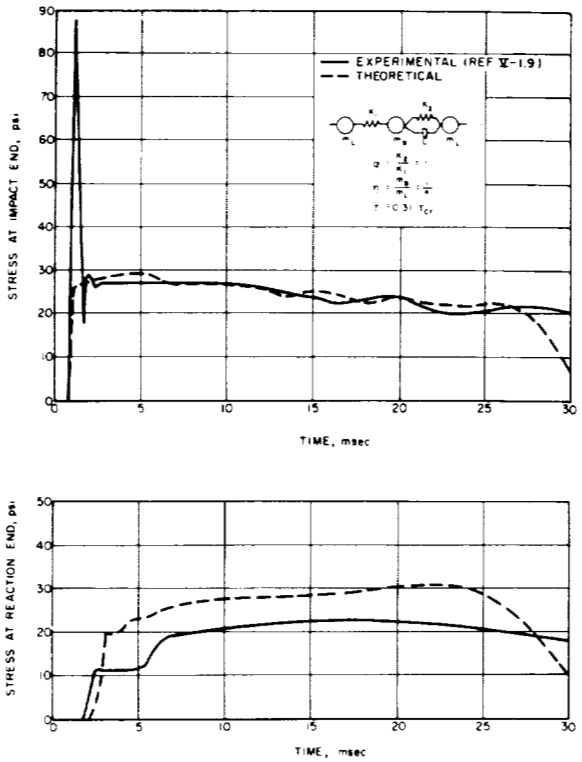

FIG. V-1.12 STRESS VS TIME FOR 20-IN. OTTAWA SAND SPECIMEN, V_o 90 IN SEC

since some of the required data do not lend themselves easily to direct measurement. For example, both theories require the knowledge of stress-strain characteristics; for the Newmark model (Ref. V-1.5) the damping characteristics must be inferred; and for Parkin's approach (Ref. V-1.8) the mass and stiffness of a gage placed over the end of the laboratory specimen had to be inferred. The inferences in both cases appear quite realistic, and they are documented by detailed analyses.

It is suggested that the two solutions really may be nearly the same in producing qualitative measures of the behavior of the Ottawa sand tested. In the Newmark model the strain-rate effect is included implicitly by the inclusion of Newtonian dashpots; Parkin's development on the other hand utilizes an algebraic function expressing the strain-rate effect in terms of the difference between the applied stress and the static stress-strain characteristics at a particular strain. The lumped mass-spring model presumably could be adjusted to approximate the function assumed to represent the strain-rate effect. Also it should be recognized that a large number of masses is required to obtain a stable solution for a step-stress pulse applied to a lumped mass-spring model. This is caused by the very high frequencies implied by a step function; the model must be capable of compatible frequencies to obtain a solution.

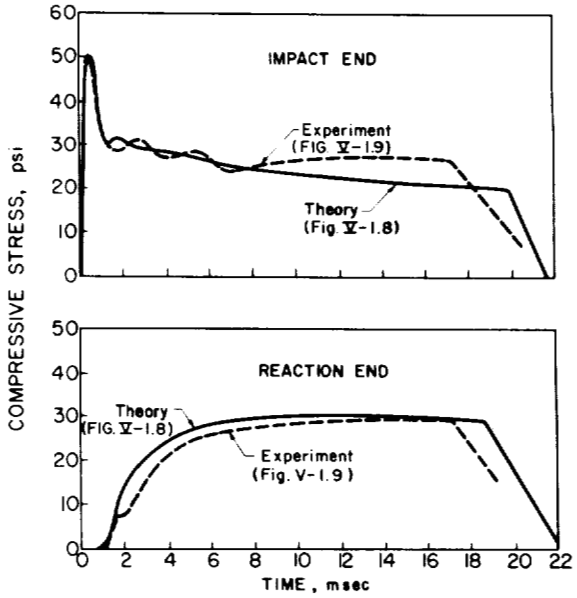

FIG. V-1.13 EXPERIMENTAL AND THEORETICAL IMPACT STRESS HISTORIES FOR A 60-IN./SEC IMPACT ON 14-IN. COLUMN OF OTTAWA SAND

Consequently in Ref. V-1.5 a relatively long finite rise time was assumed for the pressure pulse, an expediency required by the capacity of the digital computer used in the solution. A similar expediency was not required in the approach by Parkin since his solution was based on the method of characteristics wherein the properties of the pressure pulse are not critical in limiting the results.

Another one-dimensional analysis should be mentioned (Ref. V-1.10). In this development an undamped homogeneous material was assumed and bilinear stress-strain relations were considered. A solution was generated by the method of characteristics. Vertical stress and particle velocity at selected depths are derived in this procedure. In general an input of 184,000 psi surface overpressure consistent with ranges very near the point of detonation was specifically considered in the study. The results indicate a maximum vertical stress of 16,500 psi at a depth of 500 ft and 10,700 psi at 700 ft for a plastic-elastic stress-strain curve of the type shown in Fig. V-1.14. The decay of the stress with time for depths below the surface is much smaller than that of the overpressure.

Near the surface of the ground relatively large rotations of a small structure or of portions of a large structure can occur under blast loading. It would appear that these rotations are primarily a result of Rayleigh wave effects. For most soils a Rayleigh wave probably cannot develop fully because it propagates with a velocity of approximately one-

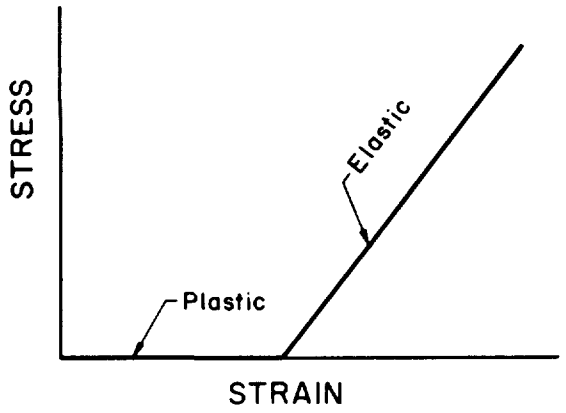

FIG. V-1.14 PLASTIC-ELASTIC STRESS-STRAIN CURVE USED IN REF. V-1.10

half that of the dilatational wave, and this velocity is normally significantly less than the velocity of propagation in air for the pressures of interest. For example, if a soil exhibits a dilatational wave velocity of 2000 ft/sec, the Rayleigh wave velocity would be approximately 1000 ft/sec. Since the air-shock velocity is greater than 1100 ft/sec for all positive pressures the air-shock wave would always outrun the Rayleigh wave generated by the air-shock. Consequently the surface overpressure interferes with the development of the Rayleigh wave. However, in some unusual cases, when the shock velocity in air is nearly coincident with the velocity of the Rayleigh wave, the amplitude of these waves can reach large values since the airblast would constantly feed energy into the Rayleigh wave. A detailed discussion of these effects is presented in Ref. V-1.11, but the analysis therein is more qualitative than quantitative.

Normally for soils the effects of Rayleigh waves are limited to regions near the surface because the displacements associated with these waves decay in proportion to e^{-fy} where e is the base of natural logarithms (2.718...); y is depth below the surface; and f is a function of the wave length λ and Poisson's ratio ν (For $\nu = 1/2$, $f = 1/\lambda$ and for $\nu = 1/4$, $f \cong 1/0.84\lambda$). Thus, for depths corresponding to 2 wave lengths (Rayleigh wave) the displacements corresponding to the Rayleigh wave would be approximately one-eighth of the surface displacements.

Empirical Results. Laboratory investigations of the propagation of stress waves through soil were mentioned in the preceding section. Also they are discussed in detail in Part II of this book.

Much significant information on the propagation of stress waves through soil has been obtained in field tests. Also because the gages used to measure the stress intensity in the soil actually are miniature structures, these data also pertain to the problem of structure-soil interaction. However, only stress propagation will be discussed here; interaction is discussed in Chapter 2.

Continuing investigations of stress propagation have been conducted by Sandia Corporation (Ref. V-1.12). Also a minor number of correlative measurements were obtained by the University of Illinois on Operation Upshot-Knothole (Ref. V-1.13). A different system of measuring devices (in the sense that a stress gage is a miniature structure, a small structure is a stress gage) were employed by the University of Illinois in Operation Plumbbob (Ref. V-1.14) to measure attenuation of airblast-induced stress with depth. On Operation Plumbbob, Sandia Corporation (Ref. V-1.15) and Stanford Research Institute (Ref. V-1.16) measured attenuation of various ground motion parameters to greater depths than had previously been investigated.

All of these investigations indicate a significant attenuation of airblast-induced motion with depth in dry-granular soils. Curves of stress and time at various depths are shown in Fig. V-1.15 which is copied from Ref. V-1.13. Although the waveform for the overpressure was not ideal, it is significant to note the decrease in maximum stress and the increase in rise time with depth in this figure. Stresses produced by overpressures with ideal waveforms exhibit similar effects as shown in Part IV of this book. These phenomena are qualitatively in agreement with the results of the Boussinesq solution discussed in the preceding section.

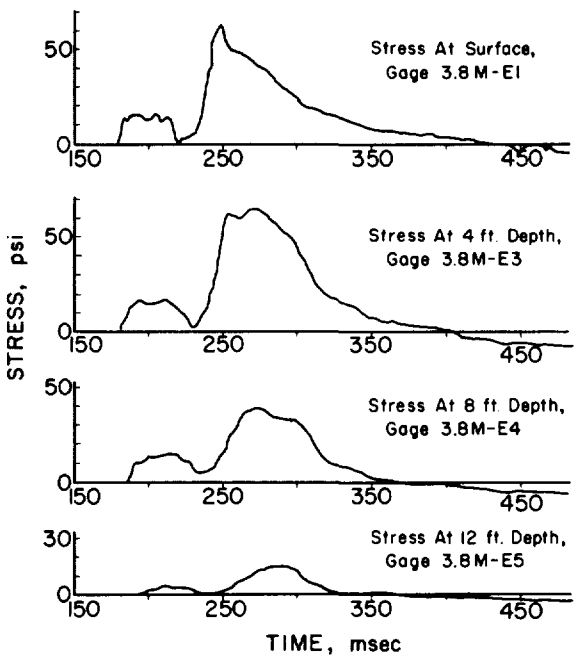

FIG. V-1.15 VERTICAL STRESSES IN FREE EARTH FROM 14.9-KT DETONATION

Where acceleration, velocity, and displacement have been measured in addition to stress, reasonable correlation among these measurements can be obtained (Ref. V-1.17) by considering an elastic rod of soil which is much simpler than the models assumed in Refs. V-1.5 and V-1.8. For an elastic rod, the particle velocity v can be expressed (Ref. V-1.18) in terms of the stress σ or strain ϵ (which need not be elastic) by the following simple relation with modulus of elasticity E and seismic velocity c:

$$\frac{\sigma}{E} = \epsilon = \frac{v}{c} \quad \text{or} \quad v = c\epsilon \qquad \text{(V-1.2)}$$

and particle acceleration a by:

$$a = c^2 \frac{\partial \epsilon}{\partial y} \qquad \text{(V-1.3)}$$

where y is a space coordinate measured vertically from the surface. Displacement can be estimated, if reflections from underlying layers are negligible, by integrating the strain in the soil from an infinite depth up to the surface. The estimates based on a simple elastic rod do not precisely represent the measured quantities, but with use of measured seismic profiles and measured stress-strain properties including strain rate effects consistent with the measured seismic velocities reasonable correlation is obtained. (See Part IV and Ref. V-1.17.) The ability to predict airblast-induced ground motions is important in providing the input used to assess the damage to equipment mounted in a structure.

Another important observation gained from the field measurements is that the soil appears to approach a condition of one-dimensional strain under airblast loading. At least the ratio of measured horizontal to vertical stress in the soil in Ref. V-1.12 can be consistent with that predicted assuming a condition of unidimensional strain for reasonable dynamic values of Poisson's ratio. This ratio can be expressed theoretically by the following, with σ_h and σ_v being horizontal and vertical stress, respectively, and ν Poisson's ratio.

$$\frac{\sigma_h}{\sigma_v} = \frac{\nu}{1 - \nu} \qquad \text{(V-1.4)}$$

This ratio of pressures is important in determining the arching forces which might develop above a structure and the forces acting on vertical elements of the structure.

V-1.3.2 Directly-Induced Ground Motion

Theoretical Developments. Probably the earliest development of the problem of stress waves propagating through a nonlinear soil medium was carried out by Lampson (Ref. V-1.19). In this study the changes in the wave caused by the curvature of the stress-strain curve were investigated. Also the spherical dispersion of the wave as it propagated outward from the center of detonation was studied. For the concave downward stress-strain curve assumed (Fig. V-1.16), Lampson proved that the rise-time of the radial stress in the medium must increase with distance measured from the center of the burst. Also he showed that the peak magnitude of radial stress must decrease in proportion to the reciprocal of the distance traversed. Finally from the principle of conservation of momentum, it was shown that the duration of the radial compressive stress must increase with distance traversed. These conclusions were in qualitative agreement with the experimental data obtained in the tests conducted as part of the study.

From considerations of dimensional similitude scaling laws also were developed in Ref. V-1.19. With minor modification, these laws continue to be used; their present form is given in Part IV of this book.

A spherical wave in a homogeneous infinite elastic medium was studied by Sharpe (Ref. V-1.20). These studies are generally qualitative, but they show that the waves disperse in direct proportion to the reciprocal of the radius measured from the point of the disturbance.

Empirical Results. Although laboratory experiments have been conducted on the problem of waves propagating in solid media these studies have been somewhat limited. Reference V-1.21 summarizes many of these studies. Field tests have provided a wealth of data, but most of these data are difficult to interpret since the airblast-induced ground motion is superimposed on the directly-induced ground motion. This, of course, is not true for the completely contained bursts. The contained bursts have occurred in rock. The writers are not aware of an instrumented detonation in soil which has produced a deep camouflet where the airblast-induced effects would mainly be eliminated.

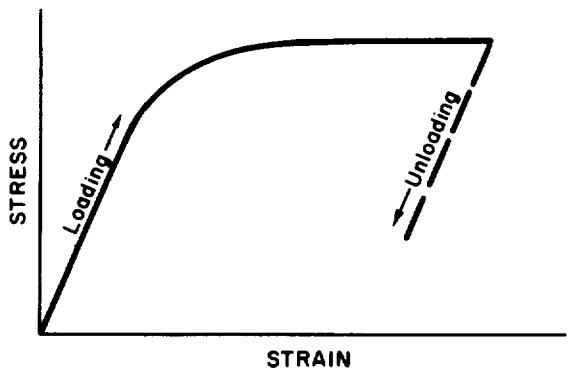

FIG. V-1.16 CONCAVE DOWNWARD STRESS-STRAIN CHARACTERISTIC OF MEDIUM

The inability to separate clearly the airblast-induced shock from the directly-induced effects has hampered analysis of the data. However, significant conclusions can be drawn from them insofar as structural behavior is concerned. These conclusions are detailed in the following chapter. Thus, only the sources of the data will be mentioned here.

The investigations by Christopherson (Ref. V-1.1) and Lampson (Ref. V-1.2) already have been mentioned. These involved small detonations compared with the yield of a nuclear detonation. Furthermore, the detonations occurred at scaled depths of burial which generally would be unattainable for large yield nuclear weapons, except perhaps for cases of sabotage. Similar scaled depths were used in the Underground Explosion Tests (Ref. V-1.22) and for many of the tests in Project Mole (Ref. V-1.23). Yet important inferences can be drawn from these data provided that: (1) An energy equivalence may be specified to allow converting from TNT to nuclear conditions; and (2) a conversion may be defined which relates the effects of a burst deeply buried to one at or near the surface. On the basis of the craters formed, energy equivalences have been defined (Ref. V-1.3). These equivalences can vary markedly depending on the position of burst relative to the ground surface. Nuclear detonations on the surface of rock are of the order of 1% effective as compared to a buried TNT charge (Ref. V-1.17). On the other hand nuclear detonations on the surface of soil are somewhat more effective compared with a buried TNT charge (Ref. V-1.17). The large difference between soil and rock possibly can be attributed to the competency of the rock in shear providing a much higher degree of coupling for the buried charge.

V-1.3.3 Importance of Type of Stress Wave in Causing Structural Damage

Consideration of the effects of airblast- and directly-induced effects can become tedious, but when the difference between the seismic velocity of the medium and the sonic velocity in air is relatively large the analysis is straightforward. When these velocities are nearly matched, the problem becomes especially nebulous. The effects produced by airblast and directly through the medium must be considered in conjunction with one another in such cases.

Because of the dependence of the character of the stress wave on the seismic velocity in the medium to the shock velocity in air, the position of a structure relative to the surface as well as to the point of burst is important. A structure near the surface of soil and near the burst may be subjected to the effects of the airblast-induced ground motion long before the directly-induced motion arrives. To illustrate this effect, suppose a structure is just below the surface at a range of 3000 ft from a large yield device (corresponding to an overpressure of approximately 130 psi from a 1-mt surface burst). If the average velocity of the airblast were 6000 ft/sec while the seismic velocity in the soil were 3000 ft/sec, the airblast-induced motion would reach the structure in one-half second while the directly-induced motion would arrive in one second. For the structure located 3000 ft directly below a surface burst, the other conditions remaining the same, the directly-induced effects would arrive significantly before the airblast-induced motion. With intermediate locations of the structure the two sources of ground motion would more nearly superimpose on arrival at the structure. From this example, however, it should not be assumed that the directly-induced effects would always predominate for a structure located near the surface in soil at a range where these effects arrive before the airblast; i.e., at a range where the seismic velocity of the medium is significantly greater than the average air-shock velocity between the point of burst and the location of the structure. Such an inference is not valid because the intensity of the airblast generally is much greater than that of the directly-induced stress at large ranges. This generality results from the experimental observation that the airblast overpressure diminishes much less rapidly with distance than does the directly-induced stress wave in soil. The airblast overpressure is approximately proportional to the inverse cube of the distance for overpressures in excess of 100 psi, but to the inverse first power of the distance for overpressures less than 1 psi; directly-induced stress is proportional approximately to the inverse cube of the distance for even relatively small stresses. Both types of stress have nearly the same magnitude at the edge of the apparent crater (Ref. V-1.24).

A different situation develops in competent rock. First of all, the experimentally observed magnitude at a given range for directly-induced ground motion in competent rock is significantly larger than that in soil (Refs. V-1.22 - V-1.24). The increase in magnitude of motion in rock compared to that in soil probably is a result of the better so-called tamping afforded by the more competent medium. There also is some indication (Ref. V-1.17) that the stress wave diminshes less rapidly in rock than in soil. This may be a result of the Coulomb damping in a granular medium (soil) being greater than the viscous damping in a more continuous medium (rock) (Ref. V-1.26). Similarly the seismic velocity of competent rock normally is comparable to the shock velocity of the airblast just beyond the fireball. Consequently in such a medium the directly-induced effects normally arrive before the airblast-induced effects.

V-1.4 EFFECT OF TYPE AND PROPERTIES OF MEDIUM

As implied immediately above, the type of medium may be divided into two general classes: rock and soil. The demarcation however is not clearcut; a highly weathered rock may behave more like soil than rock, or on the other hand a well-cemented soil may behave in a manner similar to

rock. Empirical data (Ref. V-1.23) also indicate that soil should be divided into two subcategories: saturated (including plastic clays) and non-saturated. Again a nebulous area exists in these subcategories; if the moisture content is at either extreme the situation is obvious, but there is no definition currently available specifying the degree of saturation at which a soil behaves as though it were completely saturated. The problem here involves whether the wave propagates by intergranular contact or by hydrostatic conditions developing in the fluid filling the voids. Even when a soil is not completely saturated relatively small changes in volume could effectively produce a completely saturated condition.

One of the most important properties of the medium which influences both airblast- and directly-induced effects in the free field is the seismic velocity of the medium. The effective dynamic characteristics of an inhomogeneous medium include the average nature of the medium which lies between the point of burst and the location of the structure as well as layering of the strata above and below. For example, if the medium is homogeneous or if the structure is located in the same geologic stratum as that at the point of detonation, the directly-induced effects may predominate. If stratification exists between the structure and the point of burst the airblast-induced effects may predominate. In either case the properties of the medium through which the wave propagates influence the character of the stress reaching the vicinity of the structure.

The stress-strain characteristics and the mechanism of failure of the medium, in addition to its geologic characteristics, may influence the character and strength of shock reaching a structure.

Shapes of dynamic stress-strain curves for the medium in situ can influence both the intensity of stress transmitted and the variation with time of the various stress-wave phenomena. If the medium is homogeneous and elastic, a characteristic of some rock, the stress wave decays with distance mainly as a result of geometric dispersion. For a stress-strain curve of the type shown in Fig. V-1.16 the stress propagates with increased rise time with distance traveled because the higher intensity stress propagates more slowly than the lower intensities. In addition this stress-strain characteristic may result in a diminution of stress with distance since the unloading wave can overtake the loading wave. A similar diminution of stress with distance can occur for a locking medium; a stress-strain curve characteristic of such a medium is shown in Fig. V-1.17.

V-1.4.1 Seismic Velocity and Density

The seismic velocity implicitly includes many characteristics of the medium. The dilatational wave (seismic) velocity c may be expressed in terms of the modulus of elasticity E, Poisson's ratio ν, and density ρ.

$$c = \sqrt{\frac{E(1-\nu)}{\rho(1+\nu)(1-2\nu)}} \qquad \text{(V-1.5)}$$

Velocities of other waves can be important, and they can be expressed as a fraction of the dilatational velocity. The shear wave (distortion) velocity c_s is:

$$c_s = c\,\frac{1-2\nu}{2(1-\nu)} \qquad \text{(V-1.6)}$$

Rayleigh waves propagate with a velocity c_R which is a complex function of Poisson's ratio; for $\nu = 0$, $c_R = 0.8740\, c_s$ and for $\nu = 1/4$, $c_R = 0.9194\, c_s$. For nonlinear media of the type shown in Fig. V-1.16 the modulus of elasticity may be interpreted as the instantaneous tangent modulus consistent with the intensity of stress considered; for locking media (Fig. V-1.17) as the secant modulus consistent with stress intensity. Thus, although the seismic velocity depends upon the stress-strain characteristics, these characteristics are not defined by it.

The seismic velocity has a two-fold significance in evaluating the behavior of a structure. First if the wave is plane or nearly so and it impinges on a plane surface of a structure, the stresses transmitted to the structure are related to the incident stresses in the medium by the relative acoustic impedance of the two materials so long as they remain in contact (Ref. V-1.27). Acoustic impedance is the product of the mass density ρ and seismic velocity c for each material. If the subscript 1 denotes conditions in the medium, subscript 2 denotes conditions in the structure, and continuity of stress and displacement across the plane interface is maintained.

$$\frac{\sigma_2}{\sigma_1} = \frac{2\rho_2 c_2}{\rho_1 c_1 + \rho_2 c_2} \qquad \text{(V-1.7)}$$

The stress reflected back into the medium σ_r has an intensity given by:

$$\frac{\sigma_r}{\sigma_1} = \frac{\rho_2 c_2 - \rho_1 c_1}{\rho_1 c_1 + \rho_2 c_2} \qquad \text{(V-1.8)}$$

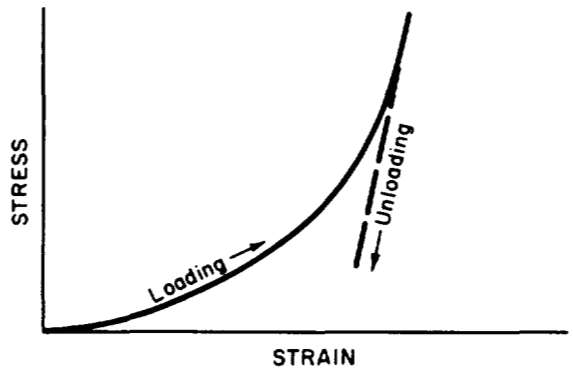

FIG. V-1.17 STRESS-STRAIN CHARACTERISTICS FOR LOCKING MEDIUM

Secondly the seismic velocity influences the behavior of a structure by defining the time required for the wave to envelop the structure and the relative motions which might develop along the sides of the structure parallel to the direction of shock propagation. The time required for a wave to envelop a structure is important in the determination of the time the structure remains relatively stationary while the soil in the vicinity of the structure moves past it. In tending to move past the structure, soil can cause increased stress to develop on the face of the structure perpendicular to the direction of shock propagation. The increased stress may remain until the wave has propagated a sufficient distance to produce motion of the medium beyond the structure. Relative motions along the sides of the structure parallel to the direction of propagation can produce the effects pictured in Fig. V-1.18 if the stress wave in the structure propagates with a higher velocity than that in the medium. If the relationship among the velocities is reversed, the direction of the shearing forces in Fig. V-1.18 would be reversed.

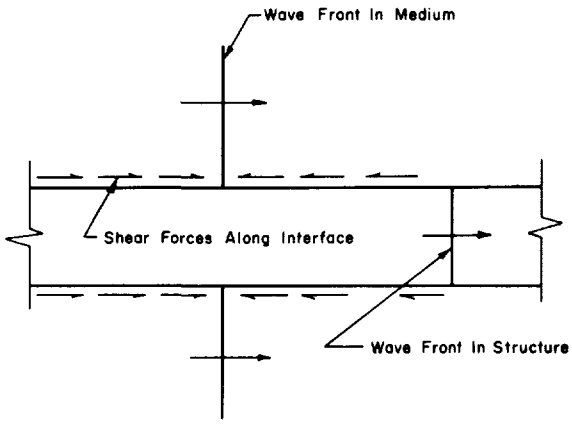

FIG. V-1.18 EFFECT OF RELATIVE MOTION BETWEEN SOIL AND STRUCTURE WITH LONGITUDINAL AXIS OF STRUCTURE PARALLEL TO DIRECTION OF SHOCK PROPAGATION

V-1.4.2 Stress-Strain Characteristics

Some of the effects of the stress-strain characteristics already have been mentioned; namely: (1) The shape of the stress-strain curve and the "elastic properties" of the medium influence the manner in which the ground motion propagates and (2) the conditions of stress and strain in the medium and their influence on the character of stress at a point. Therefore, the discussion in this section will be restricted to the influence of stress-strain characteristics on the forces acting on a structure.

For a static condition of hydrostatic stress in an elastic medium, the stress transmitted across a spherical interface between two elastically dissimilar materials is related to the relative compressibility of the two materials (Ref. V-1.28). If the inner sphere (inclusion) is more compressible than the surrounding medium the stress at the interface is reduced below that in the surrounding medium and is increased if the inclusion is less compressible.

However, it already has been mentioned that a condition of unidimensional strain may be approached in the medium at relatively large ranges from surface or air bursts with yields of tens of kt or more. Thus, it is unlikely that the inferences drawn from consideration of a hydrostatic state of stress are appropriate. Alternatively it would appear that for walls of structures parallel to the direction of shock propagation at least, complete rigidity of the walls would produce stresses acting normal to the wall which are identical to the tangential stresses in the medium away from the wall. This results from the fact that the rigid wall identically satisfies a condition of one-dimensional strain at the structure-medium interface. Furthermore, this argument would imply a reduction in stress for structural walls which were not rigid. It will be shown later that this implication is not clearly supported by empirical measurements. Although there frequently is major scatter in the empirical data, it appears that gages and structures in soil "feel" the same pressure as that which exists in the field.

This observation can be explained on the basis of the normal large difference between the elastic properties of soil and a structure. These elastic properties, of course, define the relative stiffness or compressibility. The modulus of elasticity of structural materials generally is several orders of magnitude greater than that of soil. Consequently many structural elements can be expected to be as much as an order of magnitude stiffer than the surrounding soil. Such structural stiffness frequently is required to resist the static loads alone. Thus, buried structures usually will approach more nearly a rigid than a flexible condition compared with the deformational characteristics of the surrounding soil. If the soil surrounding the structure is not "elastic" and a condition is approached wherein essentially a constant stress for relatively long periods of real time is propagated irrespective of the magnitude of the strain (Fig. V-1.16), this effect of rigidity should be magnified. On the other hand should the soil be locking (Fig. V-1.17), the rigidity of the medium might become greater than that of the structure, and a significant reduction in stress acting on the structure might be expected. However, the magnitude of strain developed in the medium, except in the "plastic zone" of the crater (Ref. V-2.24), does not appear to be large enough to cause locking in most soils.

The relative rigidity of rock compared to a structure located in it can be very large. Therefore, an entirely different condition than that just described might be expected for structures located in rock. However, from a practical standpoint it is impossible to construct a lined tunnel which will be

truly in contact with the face of the rock. Such construction is possible with reinforced concrete, but the irregular boundary which almost always exists between the rock and the concrete suggests that the behavior of a reinforced concrete lining would not be consistent with the assumption of a continuous boundary between the rock and structure. This effect could be magnified by the difference in properties of the concrete filling the irregularities and the surrounding rock.

The empirical data applicable to the hypotheses regarding relative stiffness of soil and structure are numerous. First of all it should be noted how the "true" intensity of stress in the medium is assessed before discussing the specific types of measurement. In static laboratory tests sufficient measurements can be made to infer the average intensity of stress developed within a specimen of soil. In field tests the manner in which the stress propagates can be inferred on the basis of the theoretical conditions already discussed. If the measurements are consistent with the theoretical inferences, the gage or structure, on which the measurements are taken, is considered to have "felt" the same effects as those which exist in the free field. Furthermore for stress measurements taken on structures, the validity of the measurement can be established independently by analyzing the structure using the measured force to determine if the computed deformations are consistent with those observed.

Many static laboratory experiments have been conducted to determine the characteristics of soil pressure cells. These experiments have been hampered generally by difficulty in duplicating the properties of the soil surrounding the gage in a series of tests. Yet it is concluded in Ref. V-1.29 that an inclusion in soil would have to be very "hard" before a significant degree of over-registration would occur; on the other hand an inclusion only slightly "softer" than the surrounding soil would register a significant reduction in pressure. A similar evaluation of the behavior of gages is presented in Ref. V-1.30.

The empirical data from field tests presented in Refs. V-1.12 to V-1.16 were obtained by soil pressure and stress gages, soil strain gages, structures, simulated structures, accelerometers, and displacement gages. In general, the side-on overpressure measurements and peak particle velocities prior to arrival of the directly-induced wave computed from the accelerograms agree with the theoretical predictions from Eq. V-1.2 (Fig. V-1.19). At the maximum depth of 5 ft considered in the figure, little attenuation would be expected and the free-field stress should equal the overpressure. Accelerations also were measured at depths up to 150 ft, but the particle velocities computed from these data exhibit so much scatter that no clearcut correlation with vertical stress can be detected.

The simulated structures (Ref. V-1.14) consisted of steel drums with aluminum diaphragms clamped over either or both ends. The diaphragms were calibrated against strain and deflection by applying gas pressure to them before being buried in the soil. Conventional Carlson cells were buried near the drums. These drums indicated a lesser stress than that measured by the Carlson cells or predicted on the basis of the static (Boussinesq) attenuation. Similar behavior was noted in the more flexible steel beams in the roof of the structure tested (Ref. V-1.13). However, as will be discussed later much of this difference in stress on the structures can be attributed to arching of the soil around the simulated structures or structure.

V-1.4.3 Tensile Strength

The tensile strength of the medium has an important effect both on the propagational characteristics and on the behavior of a structure. Unless a soil is cemented or highly cohesive, its tensile strength is effectively zero. For cemented or cohesive soils and most rocks the ultimate tensile strength is approximately an order of magnitude less than the ultimate compressive strength.

From Eq. V-1.8 it is obvious that a tension wave is reflected from a boundary where the acoustic impedance of the structure is less than that of the medium. This reflected wave superimposes itself on the incident wave, and in many cases a net tension develops. If this net tension equals the ultimate tensile strength of the medium, fractures develop (Ref. V-1.27). Multiple fractures can develop when the wave length of the incident pulse is long compared with the thickness of the spall (the material thrown off as a result of the tensile failure). Spalls are thrown off with a velocity consistent with the momentum trapped within them.

A decrease in acoustic impedance obviously exists for an opening in rock. However, an analogous situation can develop if for any reason a structure deforms away from the adjacent medium. For the latter case developing in soil, the soil adjacent to the structure would fail immediately because of its inherent lack of tensile strength.

Another mechanism of failure which might occur for unlined openings in rock involves tensile stresses along the sides of the opening for normal incidence of the shock with respect to the axis of the opening. For a circular opening subjected to uniaxial static compression a circumferential tensile stress equal to the compressive stress develops at the extremes of the diameter parallel to the direction of applied stress (Ref. V-1.28) as shown in Fig. V-1.20. A study (Ref. V-1.31) considers a circular hole in an infinite medium subjected to the effects of a step

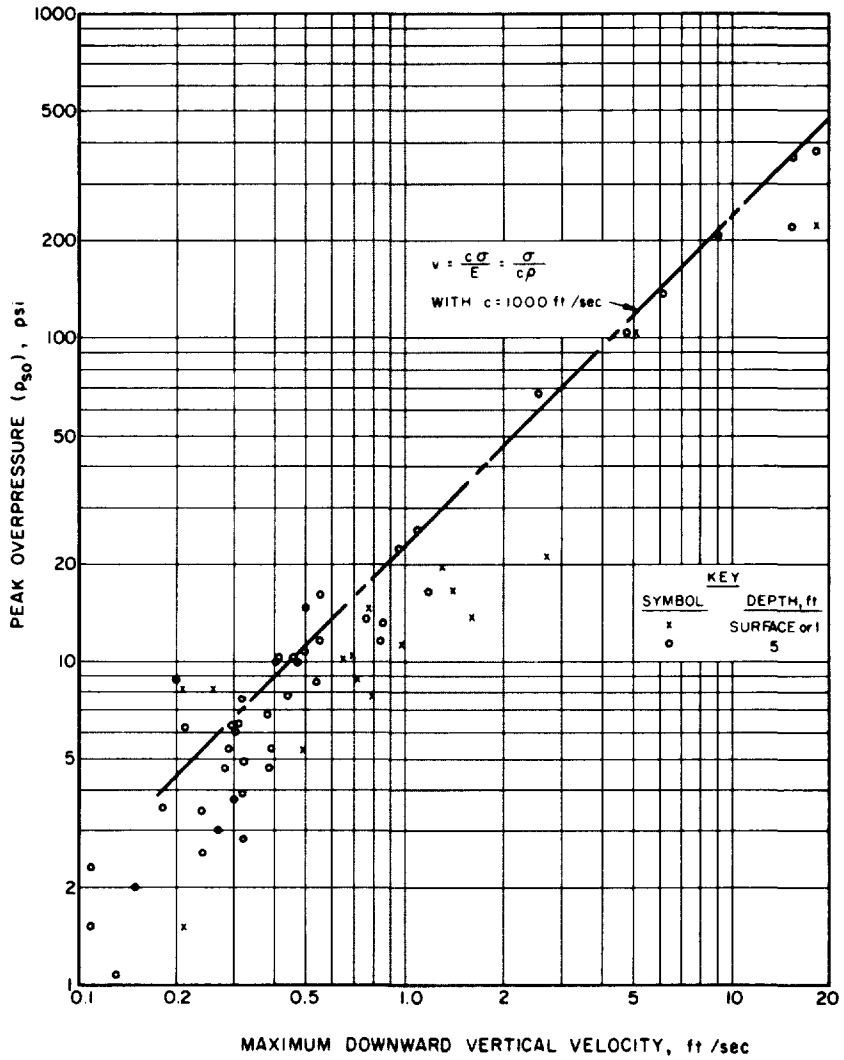

FIG. V-1.19 MAXIMUM DOWNWARD VERTICAL VELOCITY VS PEAK OVERPRESSURE (NTS – VELOCITY COMPUTED FROM ACCELEROGRAMS PRIOR TO ARRIVAL OF DIRECTLY-INDUCED WAVE)

pulse compression wave of infinite duration. For this wave the maximum tensile stress was 1.16 times the magnitude of the applied stress; the maximum compressive stress was 3.28 times the magnitude of the applied stress. A solution for a shear (distortion) wave intersecting the opening was obtained in the same reference; the maximum stress in this case was 4.37 times the magnitude of the applied stress. These three dynamic stress coefficients should be compared with the static values of 1.00, 3.00, and 4.00, respectively. Thus even for a step pulse the maximum stresses are predictable with a high degree of accuracy on the basis of the static solutions.

The large tensile stresses implied by these solutions indicate a distinct possibility that tensile fractures can occur radially along the boundary of an opening in rock. Because of natural joints or planes of weakness caused by driving the tunnel, it is possible that rock can be dislodged should these radial tensile failures develop.

V-1.4.4 Cohesion and Internal Friction

Strength of soils, like that of many other materials, can be measured by the Mohr envelope of failure (Ref. V-1.32) as shown in Fig. V-1.21. As indicated in the figure the intercept of the Mohr envelope on the shear axis for soils is defined as the cohesive strength. Cohesion normally is present for soils containing relatively high clay contents; however other constituents such as caliche can produce

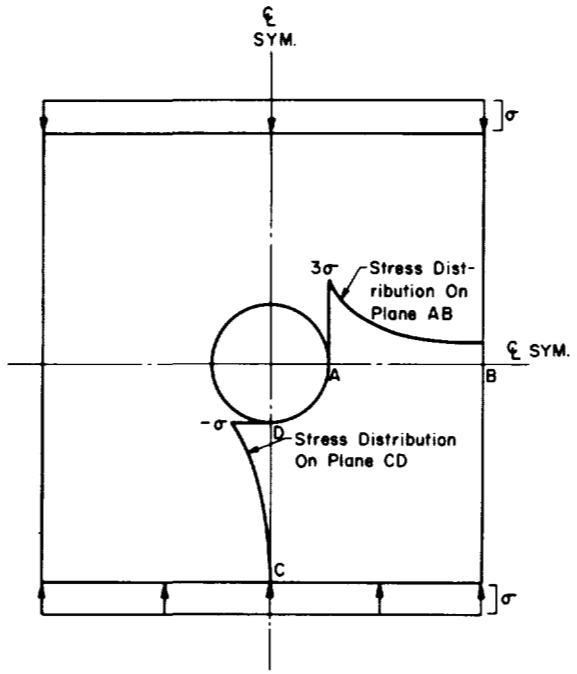

FIG. V-1.20 CIRCUMFERENTIAL STRESSES PRODUCED BY UNIAXIAL STATIC COMPRESSION ON A CIRCULAR HOLE IN AN INFINITE PLATE

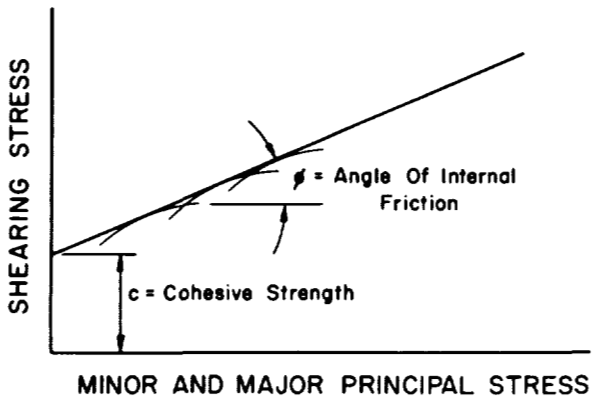

FIG. V-1.21 MOHR'S ENVELOPE OF RUPTURE AND NOTATION USED FOR SOIL FAILURE

cohesion. The slope of the Mohr envelope is defined as the internal friction, tan φ, with φ the angle of internal friction. Internal friction normally is present in soils containing relatively high sand contents. Plastic clays, generally clays with high moisture contents, frequently exhibit zero internal friction. Thus, the Mohr envelope for such a material is a horizontal line.

Since the strength of soils generally can be measured by their cohesion and internal friction, behavior of soil under load is inherently related to these parameters. Arching above a structure and the resistance mobilized as a result of structural deformation should depend on these parameters. The phenomenon of arching is developed in the following chapter. Therefore, the discussion here will be limited to the resistance mobilized in the soil by structural deformations. These resistances can develop along the exterior surfaces or beneath the foundations of a structure. Generally the forces mobilized in the soil are a result of the structure's deforming into the soil.

Structural deformations tend to be antisymmetrical with respect to the axis of the structure because the loading traverses the structure in a finite time. As a result, buried structures tend to move in the direction of shock propagation thereby mobilizing resistance in the surrounding soil opposing the motion (Fig. V-1.22). It is probable that the resistances developed in the soil under these conditions are the active and passive pressures which depend directly on the cohesion and internal friction (Ref. V-1.32). The transient loading acting on the surface however produces a tremendous surcharge (when compared with static cases) on the zones of soil defined by the classical planes of failure and the ground surface. Consequently a much larger passive force is available to resist deformations of a structure subjected to airblast-induced stress compared with the force on the same structure subjected to static load.

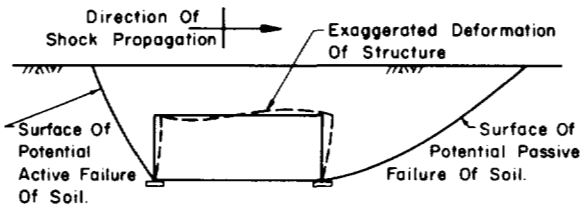

FIG. V-1.22 POTENTIAL SURFACES OF FAILURE IN SOIL SURROUNDING A STRUCTURE

V-1.5 EFFECTS OF STRUCTURAL TYPES AND PROPERTIES

The type of deformation induced in a buried structure influences the resistance mobilized in the surrounding medium. These resistances in turn define the loading on the structure and hence the deformations. The mutual dependence of structural deformations and medium resistances is extremely important in evaluating the behavior of an underground structure. Included in this section are: (1) a general discussion of the character of the deformation induced in various structural types; (2) com-

ments on the relative compressibility, natural periods of vibration, strength, and ductility of structural types and (3) concepts of virtual mass. Speculation of the character of the deformation is required to give a basis for the comments on compressibility and natural periods of vibration.

V-1.5.1 Structural Deformation and Damage

Field tests have not included all conceivable types of underground structures; as a matter of fact, the tests have included a relatively small number of buried structures. Therefore, this section includes speculations on the character of deformation expected in various types of buried structures. In the following chapter experimental and analytical studies of the response of buried structures are summarized.

Rectangular Structures. Rectangular structures are those consisting of several plane elements forming the exterior surfaces of a rectangular parallelepiped. The interior may be free of structural members or it may include columns and/or walls and girders supporting the roof and exterior walls at intervals. Each of the individual exterior elements of such a structure deform under the influence of the stress in the medium adjacent to the member. In turn the interior elements or foundations supporting these members respond to the load transmitted to them. At the same time the over-all structure begins to respond as a rigid body under the influence of the motions of the medium in the vicinity of the structure. This rigid body motion contributes additional deformation to the individual elements of the structure.

Perforce the span of separate members of such a structure is small, at most limited to a few tens of feet, since longer spans require thicknesses of elements which are prohibitive in cost when proportioned for loads of 30 psi or more. For example, it can be shown from the equations of Chapter V-6, that a reinforced-concrete, one-way slab with a depth of 12 in. would be adequate for a span of approximately 10 ft and loading of approximately 30 psi while doubling the span to 20 ft would require a slab approximately 24 in. thick. Because the added cost of formwork can be offset by savings in material, arches or domes become more economical than rectangular structures when large clear spans are required. Because the spans of members in rectangular structures generally are short the wave envelops them quickly and the transient response induced by the envelopment can be expected to be a small fraction of the response caused by the loading which develops on the complete member after envelopment. Thus, each member should respond primarily in its fundamental mode.

The over-all structure may translate in the direction of shock propagation as illustrated in Fig. V-1.22. However, this translation mobilizes resistance in the surrounding medium, and this resistance impedes the translation. For structures near the surface this resistance is augmented by the overpressure after the airblast envelops the structure. Consequently for structures near the surface and subjected to airblast-induced effects, major translation exists only so long as the wave is enveloping the structure.

In a vertical direction, gross translation results from the loads transmitted through the structure to the foundation and from the motion of the medium in the vicinity.

Arches and Domes. Although the curved surfaces of arches and domes complicate the picture showing the mobilization of resistance in the surrounding medium (Fig. V-1.22), these resistances must develop. Consequently gross horizontal translation of these structures also is impeded after the wave envelops the arch or dome. Yet because these structural configurations can have significantly larger spans, this envelopment may require longer periods of actual time than that required for rectangular structures in the same medium. Nevertheless, this time generally is small compared to the time of maximum response in flexural modes so that primary response of the shells might be expected to occur in the fundamental or "breathing mode" of vibration. For example, it can be shown from the equations of Chapter V-6, that the period of vibration in the first flexural mode for a 180° arch of reinforced concrete with span of 100 ft designed for 100 psi (hoop compression) would be approximately 3 sec. The time of maximum response would depend upon the variation of loading with time, but it would be of the order of 1 sec. For an air-shock velocity of 3000 ft/sec (corresponding to 100-psi overpressure), the time required for the wave to envelop the arch would be approximately 0.033 sec or about one-thirtieth of the time of maximum response in the flexural mode.

Tunnels in Rock. Damage to lined or unlined tunnels in rock generally occurs by mechanisms which differ from those associated with structures located in soils. In the early field tests (Ref. V-1.23) four types of damage to unlined tunnels were recognized. These types were described by zones (Fig. V-1.23). The mechanisms believed to be effective in defining the types of damage observed are:

Zone I, Closure:

Closure occurs when the rock in the vicinity of the tunnel is literally crushed so that there is gross movement of the rock into the tunnel opening. The failure apparently can be defined by the ultimate compressive strength or by the strains associated with the ultimate compressive strength; the strains considered should be the strains induced in the vicinity of the tunnel opening by the stress wave.

No augmentation of this strain (by a stress, or strain, concentration factor) should be considered; i.e., the rock appears to fail generally around the opening when the peak strain in the free field is equal to or greater than the strain corresponding to failure of the rock in partially-confined compression. Therefore, the condition which defines the limit of Zone I involves equating the peak radial strain in the free field to the strain corresponding to the ultimate compressive strength in partially-confined compression.

Zone II, Zone of General Compression Failures:

This region, extending beyond Zone I, is characterized by rock being displaced from the surface of the tunnel opening; the thickness of the rock displaced decreases with increasing distance from the point of detonation. Until recently this was believed to be a manifestation of classical spalling defined by a compressive wave intersecting a free surface, but it is now believed, on the basis of results from Hard Hat (Ref. V-1.53), that the mechanism of damage involves the general crushing locally of the rock. The limit of Zone II failure may be defined by equating the maximum local strain developed at the surface of the opening (including an appropriate strain, or stress, concentration factor) to the strain corresponding to the ultimate compressive strength of the rock in partially-confined compression.

Zone III, Zone of Local Compression Failures:

Although continuous spalling of the type observed in this zone could result from a compression wave intersecting a free surface, it is considered more likely, and the test results (Ref. V-1.53) are not inconsistent with an assumption, that the stress wave in diffracting around the opening generates local compressive stresses of sufficient magnitude to cause compressive failure of the rock. These compressive failures develop when the maximum compressive strain around the opening (including an appropriate strain or stress concentration factor) equals the strain corresponding to the ultimate strength in unconfined compression. By equating these two values of strain one finds the limiting range at which this type of failure develops.

Zone IV, Intermittent or Minor Spalling:

Degradation of the stress wave with distance results in diminishing the damage to a rock opening with increased distance from the point of detonation. This accounts for the dislodged rock becoming intermittent beyond the limit of Zone III damage. Furthermore it is apparent that tensile failures of the rock surrounding the opening can occur. These tensile failures develop essentially in a radial direction, and the openings produced would allow rock disturbed by the original driving of the tunnel to fall by gravity into the opening. The limit of Zone IV damage, the maximum extent of observed damages produced in tunnels in rock, is defined by equating the tensile strain which develops locally on the surface of the tunnel (requiring consideration of the appropriate strain, or stress, concentration factor) to the actual, or effective, tensile strength of the rock. Care must be exercised in defining the tensile strength of the rock. Most conventional tests of the properties of the rock are performed on sound samples taken from the formation; in many cases the rock contains numerous joints which may or may not be cemented. Thus, the effective tensile strength may be much less than that defined by laboratory tests and may approach zero. To estimate this strength, consideration must be given to laboratory tests, to lithostatic conditions, and to tectonic forces.

Even though the use of the numbered zones defined above has been common since 1953 (Ref. V-1.25), it now is suggested that more definitive descriptions, based upon the type of failure involved as discussed above, can be assigned to these phenomena and to their limits. Consequently hereinafter the following terms will be used:

- Zone of Closure and Limit of Closure instead of Zone I and Limit of Zone I Damage.
- Zone of General Compression Failures and Limit of General Compression Failures instead of Zone II and Limit of Zone II Damage.
- Zone of Local Compression Failures and Limit of Local Compression Failures instead of Zone III and Limit of Zone III. Damage.
- Zone of Minor Spalls and Limit of Damage instead of Zone IV and Limit of Zone IV Damage.

Similar zones of failure were observed in tests employing completely contained nuclear detonations

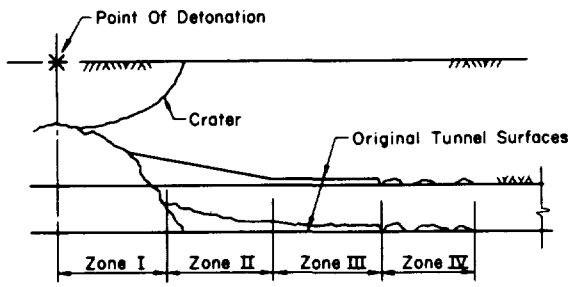

FIG. V-1.23 DAMAGE ZONES IN ROCK TUNNELS

(Ref. V-1.33). In these tests a conventional tunnel lining generally was provided, and the tunnels frequently were oriented with respect to the point of burst differently from the tunnels subjected to the effects of high explosive charges.

When a lining is introduced into a tunnel, this lining is subjected to the effects resulting from the failure of the rock described above. To survive, the lining must resist either closure, spalling, or slabbing. Upon consideration of the inherent strength of the rock it is doubtful that linings can be proportioned to survive the conditions associated with complete closure of the tunnel. However, it is probable that a lining could survive the effects of spalling or slabbing of the surrounding rock.

V-1.5.2 Relative Characteristics of Various Structural Types

An underground structure normally is less dense, frequently is stiffer and usually has greater effective strength than the soil it replaces. On the other hand tunnel linings in rock normally are more flexible and usually have less effective strength than the rock they replace. Each of these parameters may influence the stress and motion acting on the structure.

Compressibility. Compressibility can be computed as the ratio of the change in volume to the original volume. Therefore, the compressibility of a rectangular structure compared to that of an arch or dome can be assessed if the change in volume produced by the loading can be defined. The change in volume can be derived from the deflections of the elements of the structure. For a one-way slab of unit width or a series of beams continuous over several supports, the effective change in volume implied by the maximum deflection can be defined in terms of the span L, the intensity of load p over the unit width or over the spacing b between adjacent beams, the modulus of elasticity of the material E, and the effective moment of inertia of the section I for a unit width or for a single beam of a set with spacing b. The effective moment of inertia is the actual value for homogeneous construction and the transformed value for reinforced concrete or other composite construction. To derive the effective change in volume the static deflected shape for a beam supporting a uniformly distributed load and fixed at both ends was assumed on the basis of the Rayleigh-Ritz approximation. Also the deflection at yielding of the material was chosen to balance the area between the theoretical and effective resistance (Fig. V-1.24). Using the parameter μ_r to represent the ratio of the maximum deflection to the effective yield deflection x_y defines the maximum change in volume ΔV_r for each slab of constant thickness, fixed at both ends, assuming a step function loading of inifinite duration:

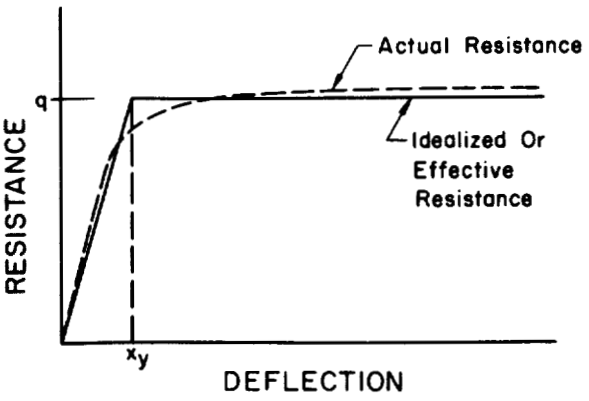

FIG. V-1.24 CONVENTIONAL ELASTO-PLASTIC RESISTANCE FOR STRUCTURAL ELEMENTS

$$\Delta V_r \cong \frac{pL^5}{200\ EI}\left(\frac{2\mu_r^2}{2\mu_r - 1}\right) \qquad (V\text{-}1.9)$$

For a comparable flat slab or plate the change in volume normally would be somewhat less than that in a one-way slab.

A circular arch or cylinder of uniform thickness with radius r and thickness t in which all deformation is restricted to shortening of the rib will experience a change in volume ΔV_a under the action of a step function loading p, if higher order terms are neglected:

$$\Delta V_a \cong 2V_a \cdot \frac{pr}{Et}\left(\frac{2\mu_c^2}{2\mu_c - 1}\right) \qquad (V\text{-}1.10)$$

where V_a is original volume and μ_c is the ratio of maximum circumferential strain to yield strain. If the arch is ribbed with b the spacing between ribs and A the cross sectional area included in the width b, the change in volume in the ribs alone for width b is:

$$\Delta V_a \cong 2V_a \cdot \frac{pbr}{EA}\left(\frac{2\mu_c^2}{2\mu_c - 1}\right) \qquad (V\text{-}1.11)$$

For a dome of constant thickness, the change in volume would be approximately three-fourths that of the arch with the same thickness and radius or approximately one and one half times that of the arch designed for the same loading.

From the above equations the compressibility of a rectangular structure can be obtained by summing the changes in volume for the individual elements neglecting the change in volume produced by axial deformation, which is small in comparison,

and dividing this total volume change by the original volume of the structure. The compressibility of a cylinder is defined directly by the equations given. It is difficult to generalize the possible structural configurations, but taking practical structures it is apparent that an arch almost always is considerably more compressible than a rectangular structure of the same length and enclosing the same volume. A dome is even more compressible than the comparable arch.

Footing Motions. Phenomenologically an increase in compressibility can be produced by motions of footings of structures. If by design, the footings of any structure, or supports of a structural element, can be forced to move, the effective compressibility can be significantly enhanced. A brief study of the motions of footings has been made (Ref. V-1.34). This study considered a model (Fig. V-1.25) of the overall structure subjected to overpressure on the roof (thus corresponding to conditions near the surface) with the footings subjected to accelerations identical to those in the surrounding soil. The accelerations in the soil were computed from Eq. V-1.3 and the data from the Boussinesq solution (Section V-1.3.1) by assuming that the observed attenuation with depth resulted from an increase in rise time of vertical stress with depth and that the stress in the free medium was effective in the vicinity of the footings.

These analyses result in two equations (V-1.12 and V-1.13) for the net stress on the loaded element p expressed as a ratio to the peak overpressure at the point above the structure Δp_m.

$$\frac{p}{\Delta p_m} = 1 - \frac{18 \times 10^{-5} \, \Delta p_m^{2/3}}{W^{1/3}} \left(d_2 - \frac{d_1}{2}\right) \qquad \text{(V-1.12)}$$

or

$$\frac{p}{\Delta p_m} = 1 - \frac{d_1}{2d_2} - \frac{9 \times 10^{-5} \, \Delta p_m^{2/3} \, d_1}{W^{1/3}} \qquad \text{(V-1.13)}$$

where Δp_m = peak overpressure in psi (must be greater than approximately 30 psi)

W = weapon yield in mt

d_1 = depth below surface to loaded element in ft

d_2 = depth below surface to base of footing in ft (must be less than approximately 50 ft)

The limitations on overpressure and depth result from the fitting of algebraic equations to the positive phase duration of the triangular representation of the impulse in ideal wave shapes for the overpressure and Boussinesq solutions, and these equations do not match the solutions they approximate outside of the given limits. Also Eqs. V-1.12 and V-1.13 are derived for a soil with seismic velocity of 2000 ft/sec. The net stress acting on the loaded element is the larger value of p determined from the two equations.

Study of these equations indicates for most practical structures, the effect of footing motion is relatively insignificant for weapon yields greater than approximately 100 kt since d_2 would normally be only a few feet more than d_1.

Natural Period of Vibration. Another structural parameter of fundamental importance in assessing the behavior of members subjected to dynamic loads is the natural period of vibration. Because most structural elements have distributed mass, they possess an infinite number of periods. However, on the basis of the discussion of types of deformation in Section V-1.5.1 only certain periods predominate in the response of elements of underground structures.

For the type of deformation which normally occurs in completely buried rectangular structures, it appears that the fundamental period of vibration for each member is of major importance. For homogeneous materials this period can be defined as (Ref. V-1.35):

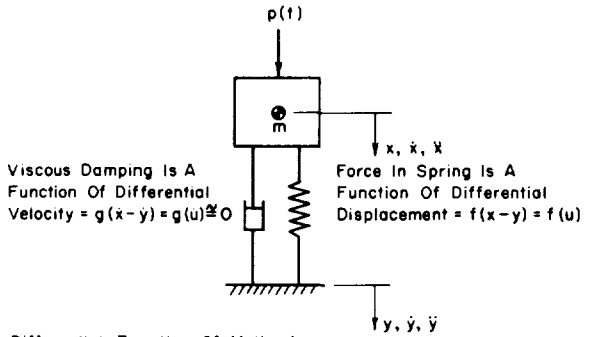

Differential Equation Of Motion:

$$m\ddot{u} + f(u) = p(t) - m\ddot{y}$$

$p(t)$ = force acting on mass

m = magnitude of mass

$x, \dot{x}, \ddot{x}$ = absolute displacement, velocity and acceleration of centroid of mass

$y, \dot{y}, \ddot{y}$ = absolute displacement, velocity and acceleration of support

$u, \dot{u}, \ddot{u}$ = displacement, velocity and acceleration of centroid of mass relative to support

FIG. V-1.25 MODEL AND NOTATION FOR GENERAL SINGLE-DEGREE OF FREEDOM SYSTEM

$$T_r = R_o L^2 \sqrt{\frac{m}{EI}} \qquad \text{(V-1.14)}$$

where m = mass per unit of length

R_o is a constant for any given condition of support. Values for the normal conditions are: 0.636 for simple supports; 0.318 for complete fixity at each end; and 0.423 for complete fixity at one end and simple support at the other.

All other symbols have been previously defined.

For reinforced concrete the fundamental period of one-way slabs or beams can be expressed by (Ref. V-1.36):

$$T_r = \frac{R_o L^2}{R'd} \qquad \text{(V-1.15)}$$

where d = effective depth of member

$R' = 2250$ ft/sec $\sqrt{\varphi}$

φ = percentage of tensile reinforcement at midspan

To account for burial, the period for the roof elements of rectangular structures must be modified in accordance with the virtual mass discussed in Section V-1.5.3.

Since, antisymmetrical deformations in arches and domes are largely eliminated by the resistance mobilized in the soil, the primary response occurs in the so-called "breathing mode." The period for arches T_a and domes T_d is defined by Eqs. V-1.16 and V-1.17, respectively, (Ref. V-1.36):

$$T_a = \frac{2\pi r}{c} \qquad \text{(V-1.16)}$$

$$T_d = \frac{2\pi r}{c\sqrt{2}} \qquad \text{(V-1.17)}$$

where $c = \sqrt{E/o}$ = dilatational velocity for the material (approximately 12,000 ft/sec for concrete and 16,700 ft/sec for steel). All other terms have been previously defined. In this case also the period must be modified to account for the virtual mass as discussed in Section V-1.5.3.

If the effect of virtual mass is neglected and if it is recognized that for structures of comparable span the quantity L^2/d is large relative to r, it can be illustrated that the natural period of arches and domes is much smaller than the period of the rectangular element. Also it is apparent that for practical structures the periods are of the order of tens of milliseconds or less. These periods may be comparable with the rise time of the loading but generally they are extremely small compared to the effective duration of the loading from nuclear weapons. The effect of rise time is known (for example Ref. V-1.37) but for a precise analysis, it is a very difficult quantity to generalize; response is critically dependent on the ratio of rise time to period. Fortunately in design, however, its effect can be taken into account relatively easily because normally the design must consider such a range of values that the controlling condition is obvious. The fact that the duration of loading produced by nuclear weapons with yields currently considered important is very large compared to the fundamental natural period of vibration results in relatively simple analyses of the response of buried elements. With little error the loading frequently can be considered a step pulse of infinite duration. For this case and representing the peak magnitude of load or stress, on the element by p, the plastic resistance of the element by q, (Fig. V-1.24) and the ratio of the maximum displacement to the effective yield displacement x_y by μ, it may be shown (Ref. V-1.4) that:

$$\frac{p}{q} = 1 - \frac{1}{2\mu} \qquad \text{(V-1.18)}$$

To define the appropriate elasto-plastic resistance function requires computation of the resistance at yielding and the deflections at yielding and at failure. These computations require consideration of the particular mode of failure induced in the structural element by the loading. These modes of failure and the associated deflections are discussed in the following two chapters.

It should be noted here, however, that in general an arch will have a yield resistance which is at least an order of magnitude larger than the resistance of a slab of the same thickness or span. The yield resistance of a dome normally is twice that of an arch of the same thickness and span. Thus an arch or dome will resist forces of much larger intensity than a comparable slab.

Ductility. The effect of ductility of a structural element on the force it can resist is obvious from a consideration of Eq. V-1.18. For a given resistance, the larger the ductility ratio μ the larger the force resisted. Ductility ratios depend directly on the mode of failure induced in a member and upon the material used to fabricate a structure. If buckling of outstanding legs is prevented, steel can be more ductile under many conditions than reinforced concrete. However as may be seen from Eq. V-1.18, the effect of ductility decreases very rapidly once the ductility ratio becomes large. Thus if a mode of failure develops which implies a relatively large ductility factor, the difference in load resisted by a steel or reinforced concrete structure becomes relatively insignificant.

Frequently an arch or dome, especially if fabricated in reinforced concrete, is less ductile than a comparable slab because shells are subjected primarily to direct compression while slabs are subjected primarily to flexure. However, the decrease in ductility is subordinate in effect to the increase in strength for the shell compared to the slab.

V-1.5.3 Virtual Mass

Rectangular Structures. The unity of action between the structure and the surrounding soil has been mentioned frequently in the preceding discussion. One action of the soil, that of stiffening the structure, was alluded to in Section V-1.5.1; it will be discussed in more detail in the following chapter. Additionally the soil adds mass to the structure, and it is this added mass which will be discussed in this section. The mass of soil which must be accelerated along with an element of a buried structure classically is referred to as the virtual mass. This mass can have a significant effect upon the response of an element.

Although no theoretical solution exists which defines the virtual mass of a structure buried in soil, there are several means for estimating its effect based on empirical data from the response of buried structures. Two basic methods have been used to determine this parameter. The first, and probably the more reliable, involves consideration of the free vibration of an element after the load is no longer acting (Ref. V-1.17). For this method an analysis was made of strain and deflection measurements on simply supported steel beams of varying stiffness forming the roofs of buried reinforced-concrete boxes tested on Operation Upshot-Knothole (Project 3.8). The roofs in three separate structures were arranged such that the depth of burial was 0.125, 0.500, and 1.000 times the span of 8 ft. Analysis of the free vibration evidenced by these roofs indicated a period consistent with the stiffness of the element alone vibrating in its fundamental mode and the total of the mass of the beam and the entire overburden. Consequently the fundamental period T should be modified by the square root of the ratio of the total mass of the beam and overburden per unit of length m' to the mass per unit of length of the beam alone to define the effective period T':

$$T' = T\sqrt{\frac{m'}{m}} \qquad \text{(V-1.19)}$$

It is important to note that consideration of the apparent period manifest in the free vibration of these elements is independent of the magnitude of force acting on the member. Therefore, the means of determining the virtual mass just described does not require inferring the character of the loading reaching the structure. In addition it is worthy of note that for rectangular structures buried in soil the maximum depth of burial has equaled the span of the element. Furthermore, the structures tested in soil were constructed by cut-and-cover methods. Yet for the specific structures cited here, a later test [Operation Teapot (Ref. V-1.38)] revealed that the caliche in the soil at Frenchman Flat had largely recemented the cover above the two deeper structures. (The cover over the shallowest structure was removed prior to this test to repair the waterproofing of the roof.) In these tests as well it appears also that the virtual mass consisted of the mass of the beam plus the mass of the entire overburden. Nevertheless, it is doubtful that the relation obtained from these results would remain unchanged for depths of burial significantly greater than the span and probably for structures in soil placed by tunneling methods. The latter condition is suspect because of the difference in the stress state induced by tunneling compared to cut-and-cover procedures. Consequently it would appear unsafe to assume a virtual mass which is greater than that implied by a depth equal to the span for beams buried to depths greater than the span until further theoretical or empirical results justify such an assumption.

Arches and Conduits. A second method of estimating the virtual mass from empirical data involves a specification of the forces acting on the structure and the time variation of these forces. A model of the structure also is assumed, and the response is computed using the specified forces. By trial and error the characteristics of the force and of the model are varied until a computed response agrees with that observed. This procedure has been used in the analysis of the behavior of many structures tested in the field including those discussed above. For the latter structures, detailed instrumentation was provided, and this method of computation also indicated that the virtual mass consisted of the total mass of the beam plus the entire overburden. The fact that this procedure gives results identical to those obtained by considering the free vibration lends support to the validity of the trial and error procedure. Without this support the trial and error process is questionable since theoretically there are an infinite number of assumptions which would produce a similar computed response of a structural element.

This trial and error procedure was used in an attempt to determine the virtual mass for the buried arches and conduits which have been included in several field tests (Ref. V-1.34). In most cases the instrumentation either was not sufficiently complete or the records were not of sufficient length to allow a determination of the period of vibration which occurred during the free vibration. The analyses assumed that the structures were subjected to the surface overpressure (the airblast-induced stress without attenuation) and that the response occurred only in the breathing mode. In computing the period consistent with the breathing mode a virtual mass was assumed which was equal to the average depth of burial of the arches and to the average depth of burial over the upper half of the conduits but, on the basis of the results of the beams, not greater than the diameter of the structure in either case. Because of the sensitivity of the computed response to the magnitude or time variation of the assumed loading, these computations were performed by assuming values for the maximum response

and computing the peak overpressure consistent with these values. In Ref.V-1.34 these computations were made both including and neglecting the effect of footing motion as described in Section V-1.5.2. These computations (summarized in Table V-1.1) indicated that the assumed value of virtual mass was reasonable since the computed overpressures corresponding to failure were greater than the observed values and none of the structures failed. The correction of the yield strength referred to in the footnote to the table was required because it was learned after the analyses were completed that the yield point of the materials used in the corrugated metal structures was approximately 30,000 psi while 40,000 psi was used in analysis. The correction was accomplished by taking a simple ratio of yield points and multiplying by the overpressure. A small error is caused in this process since the effective duration of the overpressure varies with the overpressure.

Additional experimental evidence supporting the conclusions drawn from these computations was gained in non-destructive tests conducted on the arches and conduits in Operation Plumbbob (Ref. V-1.39). These tests were conducted after the nuclear operation, and they employed both small high explosive charges and mechanical methods for deforming the structures. The measurements of free vibration determined from strain gages and accelerometers indicated a period consistent with the breathing mode with a mass as described in the discussion of the preceding computations.

Therefore it appears that the effective period of vibration for buried arches and conduits also may be determined by application of Eq. V-1.19 if T is the period for the breathing mode and m' is the mass of the shell plus the mass of the average overburden per unit length but not greater than the shell diameter. For the arches and conduits there is limited experimental evidence to indicate that the average overburden should not be assumed larger than the diameter of the shell.

Domes. The only completely buried domes which have been tested had such small response that it is difficult to interpret their behavior. However, by inference from experience with buried arches, the virtual mass for a dome should be governed by a relation similar to that for an arch.

TABLE V-1.1 COMPARISON OF COMPUTED OVERPRESSURE LEVELS WITH OBSERVED EXPERIENCE IN OPERATION PLUMBBOB

Structure No. and Description	Weapon Yield	Overpressure for Failure by General Yielding (Breathing Mode)		Max. Observed Overpressure, No Failures Observed	Overpressure for Failure by Shearing of Bolts
		Footings Immovable	Footings Movable		Footings Movable
	(kt)	(psi)	(psi)	(psi)	(psi)
3.1a, b, c and n---Buried R/C Semi-Circular Arch---8'-0" radius	40	480	600	190	---
3.2e, j, and ℓ Buried R/C Pipe 8'-0" diameter	40	750	1100[b]	136	---
3.2d and h---Buried 10 ga. Corrugated Metal Pipe---8'-0" diameter	40	190[a]	200	136	165[a]
3.2a, b, c, f, g, k, and m---Buried 10 ga. Corrugated Metal "Cattle Passes"---2'-6" radius	40	330[a]	400	153	450
3.3b---Buried 10 ga. Corrugated Metal Semi-Circular Arch without Stiffeners---12'-6" radius	40	70[a]	75	56	60[a]

[a]Corrected for yield strength but not for effective duration. Correcting the effective duration would result in a somewhat lower value for 40 kt.

[b]A result possibly outside the range of applicability of the theoretical expression.

Lined Tunnels in Rock. For lined tunnels for protective construction the concept of virtual mass currently is believed to be basically irrelevant since it seems impractical to place a metal lining in continuous contact with the rock. Also rock generally is much stronger than reinforced concrete so that use of such construction would appear to provide no added safety against explosion generated loads over merely the bare rock tunnel. Current concepts for the design of protective linings in competent rock therefore include the provision of a highly deformable material between the face of the rock and the lining. This deformable material normally would respond with the lining; however, its mass generally would be so small that it would cause a negligible change in the period of the lining.

V-1.6 DYNAMIC PROPERTIES OF STRUCTURAL MATERIALS

It already has been shown that the behavior of structural elements depends directly on their strength, ductility, and natural period of vibration. These parameters depend upon the mechanical properties of the materials used in the construction. In this section the dynamic properties of the materials normally used in construction, steel and concrete, are summarized.

Engineering materials generally behave differently under dynamic loads than they do under static loads. Static loads are essentially independent of time. Distinctions may be made among the types of loads which vary with time (Ref. V-1.21). Gradually applied loads are those which change with a time scale which is measurable in seconds or longer; even these loads, however, may exhibit a dynamic effect. Rapidly applied loads are those defined by a time scale measurable in milliseconds. Finally, impulsive or impact loads are those with a time scale which is less than a millisecond and may be of the order of microseconds.

V-1.6.1 Fundamental Concepts

Mechanical properties of materials, i.e., those which relate the various deformations in a material to loads or stresses are generally determined from the engineering stress-strain diagram, in which the stress is determined by dividing the total load by the original cross-sectional area, and strain is determined by dividing the change in length by the original length of the specimen.

The shape of stress-strain diagram may be continuous and unbroken as it is for materials which have no distinct yield plateau. Aluminum, copper, and concrete are in this group. Some heat-treated or work hardened steels are also in this category.

The shape of a stress-strain diagram may be discontinuous with a distinct yield point and plastic region. Standard structural alloy steels are in this category. In this type of material, as the load is increased beyond the so-called elastic limit, a stress level is reached at which the material yields and this stress increases with the rate of loading. Knowledge of the amount of increase in yield point for a given type of dynamic loading is essential in the design of structures for shock loads.

Materials which have continuous stress-strain diagrams and have no distinct yield point (although they may at very high strain rates), generally do not show an appreciably different yield stress when loaded rapidly. In these materials the yield stress or strength is frequently defined as the stress corresponding to 0.2% permanent set (or other convenient strain), and this stress does not necessarily increase with the rate of loading. In fact, for cast magnesium alloy (Dowmetal H) the yield point drops appreciably when the rate of loading is increased (Ref. V-1.40).

When the load is increased beyond that corresponding to yielding eventually the ultimate strength of material is reached which is the maximum stress developed by the material before fracture occurs. The rate of strain also influences the ultimate strength of a material. To define an ultimate factor of safety a knowledge of the ultimate strength of a material for a given dynamic loading is desirable. In some materials, such as concrete, it is essential.

Materials which exhibit a definite yield point in their static stress-strain diagrams may have a measurable time delay associated with the initiation of plastic deformations. In materials which have a continuous stress-strain diagram without a distinct yield point a measurable time delay has generally not been observed.

The delay time for the initiation of plastic flow, while not significant for conventional loads, is an important property when the loads are rapidly applied because if the duration of loading, or more precisely the time of maximum response, is less than the time delay, the material will not yield.

Critical impact velocity is also an important property of the material when the loads are impulsive. Critical impact velocity may be defined as the velocity at which the specimen fractures at the point of impact. Theoretically it can be shown (Ref. V-1.40) that

$$v_u = \int_0^{\epsilon_u} \sqrt{\frac{d\sigma/d\epsilon}{\rho}}\, d\epsilon$$

where v_u = critical impact velocity

$d\sigma/d\epsilon$ = is the slope of the stress-strain diagram and a function of ϵ

ρ = density

ϵ_u = strain corresponding to the ultimate strength of the material

If the impact velocity is less than the critical impact velocity, the specimen will suffer deformation but no fracture will take place immediately. At velocities above the critical impact velocity fracturing can be expected at the impacted end. This phenomenon has been studied experimentally (Refs. V-1.27 and V-1.42).

V-1.6.2 Mechanical Properties of Materials in the Linear Elastic Range

At low levels of stress or strain materials normally act elastically. A material is elastic when its deformations are linearly related to the stresses and are also reversible; that is, upon removal of the load the material returns linearly to its original state. At high levels of stress or strain all materials suffer a certain amount of permanent deformation.

Some important mechanical properties when the material acts elastically are the modulus of elasticity E, modulus of rigidity G, and the bulk modulus of elasticity K. These quantities are related by the following expressions:

$$K = \frac{E}{3(1-2\nu)}$$

$$G = \frac{E}{2(1+\nu)} \qquad \text{(V-1.21)}$$

$$K = \frac{2G(1+\nu)}{3(1-2\nu)}$$

$$\text{and } \frac{1}{E} = \frac{1}{3G} + \frac{1}{9K} \qquad \text{(V-1.22)}$$

where ν = Poisson's ratio.

When a material is deformed, there tends to be an increase or decrease in temperature. Under static loading the heat manifested by the change in temperature is dissipated to the air nearly as rapidly as it is generated. This condition approaches an isothermal transformation in which the temperature of all parts of the material is kept constant while the loads do work on the body.

On the other hand when a dynamic load is applied there would be little time for dissipation of heat. This condition approaches an adiabatic transformation in which no heat is allowed to enter or leave any part of the body. In reality this condition may not be reached, since time of loading is finite; however, it is possible to approximate it.

The bar shown in Fig. V-1.26a is subjected to a compressive force P. Figure V-1.26b shows the variation of the stress f with length L. Point A corresponds to a condition in which the stress is f and the length is L. Let the curve designated t represent the relationship between f and L under an

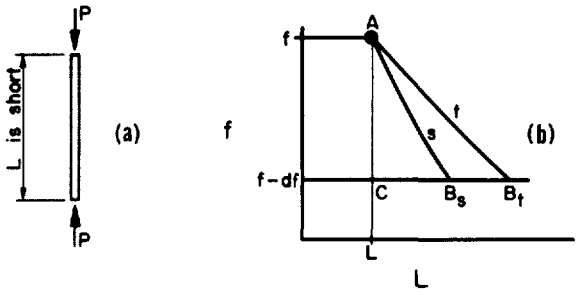

FIG. V-1.26 CONDITIONS AND NOTATION FOR THEORETICAL DERIVATION FOR STRAIN RATE EFFECT

isothermal condition (static load) and that marked s represent an adiabatic condition (dynamic load). The increase in length, when stress is reduced to f - df, will be smaller under adiabatic than it will under isothermal conditions.

Using the conditions shown in Fig. V-1.26, Jeffreys (Ref. V-1.43) derives certain relations among the elastic constants, Eqs. V-1.23 and V-1.24.

$$\frac{E_t}{E_s} = 1 - \frac{tvE_t}{C_f A}\left(\frac{1}{L}\frac{\partial L}{\partial t}\right)_f^2 \qquad \text{(V-1.23)}$$

where E_t = modulus of elasticity at constant temperature (isothermal)

E_s = modulus of elasticity at constant entropy (adiabatic)

t = absolute temperature

v = specific volume

$C_f = t\left(\frac{\partial s}{\partial t}\right)_f$ = specific heat under constant tension

s = specific entropy

$\frac{1}{L}\left(\frac{\partial L}{\partial t}\right)_f$ = coefficient of linear expansion under constant tension.

$$\frac{K_t}{K_s} = 1 - \frac{tvK_t}{C_p}\left(\frac{1}{v}\frac{\partial v}{\partial t}\right)_p^2 \qquad \text{(V-1.24)}$$

where K_t = bulk modulus corresponding to the isothermal compression or the static bulk modulus

K_s = bulk modulus corresponding to the adiabatic compression or the dynamic bulk modulus

$C_p = t\left(\frac{\partial s}{\partial t}\right)_p$ is the specific heat at constant pressure and $\left(\frac{1}{v}\frac{\partial v}{\partial t}\right)_p^2$ is the coefficient of cubical expansion under the constant pressure p, with v the specific volume of the material.

From Eq. V-1.23 it is apparent that E_s is always greater than E_t unless the coefficient of linear expansion is zero. It can be shown also that for ordinary materials the term $tvE_t/C_fA\ (1/L\ \partial L/\partial t)_f^2$ is normally less than 0.01, and therefore experimental difficulties make it impossible to measure differences between E_t and E_s within one percent.

For ordinary solid materials the term, $\frac{tvK_t}{C_p}\left(\frac{1}{v}\frac{\partial v}{\partial t}\right)_p^2$ in Eq. V-1.24, is less than 0.04.

It can be shown (Ref. V-1.43) that the dynamic modulus of rigidity G_s is equal to the static modulus G_t.

It should be emphasized that the above analyses are only applicable to perfectly elastic and reversible deformations. Furthermore, the values of elastic constants are difficult to verify experimentally. In fact some investigations (Ref. V-1.44) have shown that the static modulus of elasticity is greater than the dynamic modulus of elasticity. This discrepancy is believed to be the result of distinctly different procedures used to measure load and strain in static and dynamic tests and the inherent inaccuracies in each because as indicated by Eq. V-1.23, the dynamic modulus of elasticity must be greater than the static value.

In several investigations the tangent or a secant modulus of elasticity has been measured in materials with no distinct yield point or elastic limit. Several investigations also have been carried out to determine the properties of concrete under dynamic loads in which the variation of modulus of elasticity has also been studied (Ref. V-1.45). It can be stated generally that the secant modulus of elasticity increases with the rate of loading; however, quantitatively, the effect of rate of loading on the modulus of elasticity seems to vary through a wide range and there appears to be no common base for comparing the various results.

The theory discussed in this section is an important guide in understanding the deformations of a material when the stress is low. However, it should be applied judiciously.

V-1.6.3 Dynamic Strength and Behavior

In studying the influence of rapid loading on the behavior of materials generally two types of investigations have been employed. The first type is called strain-rate testing in which a constant rate of strain is applied to each specimen and its rate is varied between specimens. The other type is generally called load testing in which a loading pulse with a sharp rise is applied to a specimen which has a very small mass.

Results for Metals from Strain-Rate Tests. Tests on metals have covered a wide range of strain rates (Refs. V-1.40 and V-1.46-V-1.48). Data are available for the variation of yield stress of low carbon steel when rate of strain varies from 10^{-6} in./in./sec to more than 10^2 in./in./sec. As a rule it is impossible to find a common base for comparing the results of all tests. The size and type of specimen chosen and the type of testing machine and measuring device all influence the results. Figure V-1.27 shows the influence of the rate of strain on the yield point of various types of steel. The curve corresponding to Manjoine's tests (Ref. V-1.46) is for low carbon steel and the rate of strain varies from 10^{-6} in./in./sec to 10^2 in./in./sec. If we assume 10^{-3} in./in./sec as a base value of strain-rate for static loads, the increase in yield strength for a rate of strain of 1 in./in./sec will be about 30%. Figure V-1.27 also shows results of tests by Jones and Moore (Ref. V-1.40) on SAE 1020 and SAE 1045 steel. The range of variation of strain rate was considerably smaller in the latter tests.

Results for Steel from Load Tests. Several investigators have accumulated data for load tests (Refs. V-1.44 and V-1.49-V-1.51). In this type of test a load causing stresses in excess of those normally corresponding to yielding, is applied rapidly to a specimen which has little mass. First the strains increase linearly with stress during which time the test is essentially equivalent to a strain-rate test. The strain corresponding to the applied stress may be approximated by dividing the stress by the dynamic modulus of elasticity of the material (Ref. V-1.44). If the peak value of the stress is equal to or greater than the yield stress corresponding to the strain-rate the specimen will yield without delay. For example reference to Manjoine's curve (Fig. V-1.27) illustrated that the yield strength of mild steel is 42 ksi for a strain rate of 1 in./in./sec. Thus, if a peak stress of 45 ksi were applied to the specimen in about 1.5 msec which corresponds to a strain rate of 1 in./in./sec, the specimen would yield immediately. On the other hand, if the peak stress is less than the yield stress for the corresponding strain rate (less than 42 ksi applied in 1.5 msec for the preceding example), the straining will stop for some finite time after the load has reached its peak and before yielding begins. During this delay time the specimen will support a stress in excess of that commonly associated with static yielding.

Figure V-1.28 shows results on ASTM A-7 rolled bars obtained by Massard (Ref. V-1.51). In this figure the dynamic yield stress is plotted against time from application of load to initiation of yielding (time to yield). The time to yield for conventional static tests may be taken as that corresponding to the maximum strain-rate permissible under the ASTM Specifications. Since in the strain-rate tests a base value for the strain-rate representing static conditions was taken as 10^{-3} in./in./sec, the base value for time to yield in the load tests may be taken roughly as one second. This, of course assumes that yielding occurs at a strain of 0.001 in./in. For the

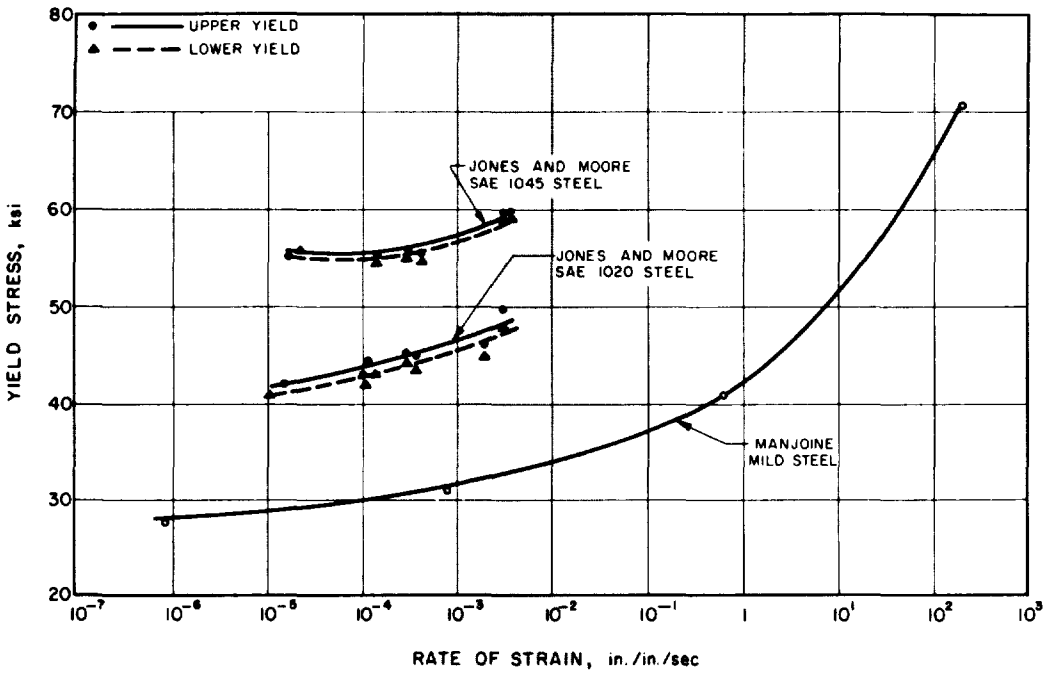

FIG. V-1.27 EFFECT OF STRAIN RATE ON YIELD STRENGTH OF MILD STEEL

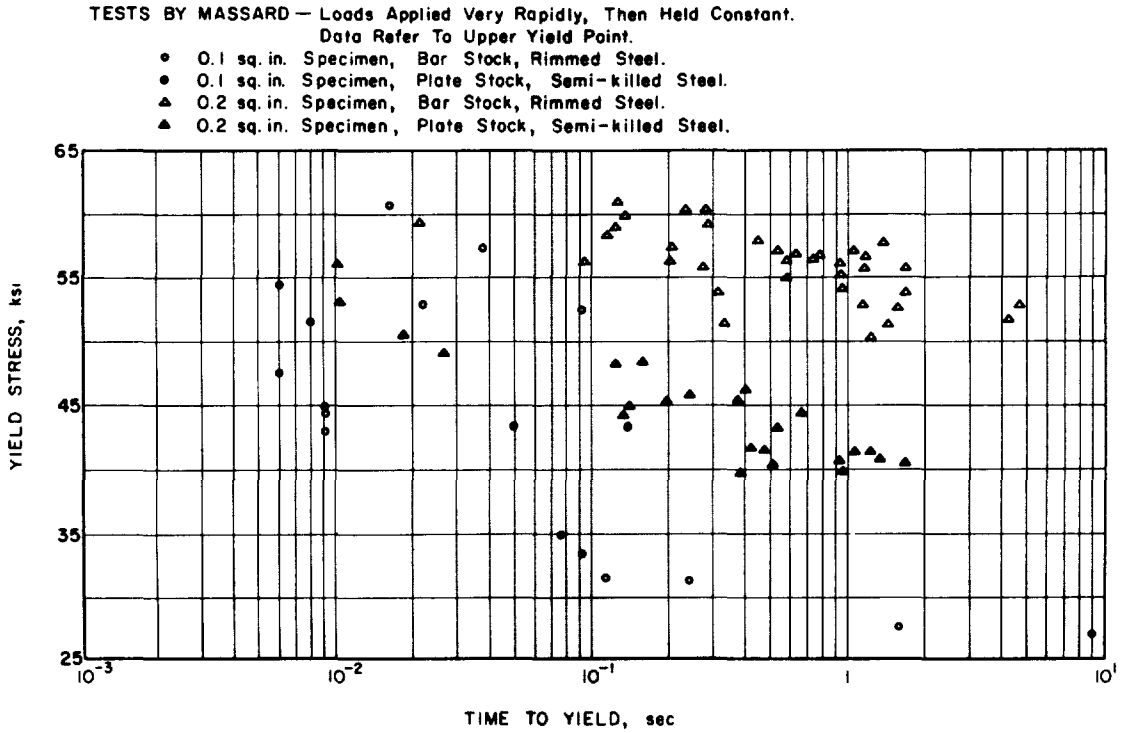

FIG. V-1.28 EFFECT OF MANUFACTURING PROCESS AND SIZE OF SPECIMEN ON DYNAMIC YIELD STRESS FOR STRUCTURAL (A7) STEEL

larger specimens, Massard's tests indicate a dependence of the dynamic yield strength on the manufacturing process used in making the steel. For a particular size of specimen or a particular steel manufacturing process the increase in strength produced by dynamic load is definitely supported.

Figure V-1.29 shows results of load tests on intermediate grade (ASTM A-15) reinforcing bars carried out by Keenan and Feldman (Ref. V-1.44). In this figure the dynamic yield stress is also plotted against time to yield. Three bar sizes were tested in this investigation: Nos. 6, 7 and 9. This figure also contains the results obtained by Clark and Wood (Ref. V-1.50) which were carried out on A-7 bars.

Several interesting observations can be made from Fig. V-1.29. The data from Clark and Wood's experiments indicate a static upper yield point for ASTM A-7 steel which is significantly higher than the minimum lower yield point of 33 ksi specified for this steel. Although there can be a marked difference between the upper and lower yield points for mild steel, this difference becomes small for low strain rates. Thus, for Clark and Wood's data with times to yield of 1 sec or more the upper and lower yield point should be nearly the same. The difference between the measured and specified values of yield point has been observed frequently in the past, and a study of the static yield point of structural steel is presented in Ref. V-1.52. These tests represent 3,974 individual tests sampling 33,000 tons of steel. A median yield point of approximately 38 ksi for ASTM A-7 steel was found. This median value is quite consistent with the data presented in Fig. V-1.29 for A-7 steel. Thus, the data by Clark and Wood might be considered indicative of the median behavior of A-7 steel under conditions of rapidly applied constant stress.

Since the minimum specified yield point for intermediate grade reinforcing steel (ASTM A-15) is 40 ksi while that for structural steel (ASTM A-7) is 33 ksi it should not be surprising that the tests on reinforcing steel show strengths usually larger than the strengths of structural steel. However, the tests by Keenan and Feldman on No. 6 bars are generally in agreement with the tests on structural steel. This could be a result of the normal variation in strength which might occur for a particular grade of steel. Yet the quality of this group of No. 6 bars is somewhat suspect since the specified cross sectional area is 0.44 in.^{2} while the measured value was 0.51 in.^{2}.

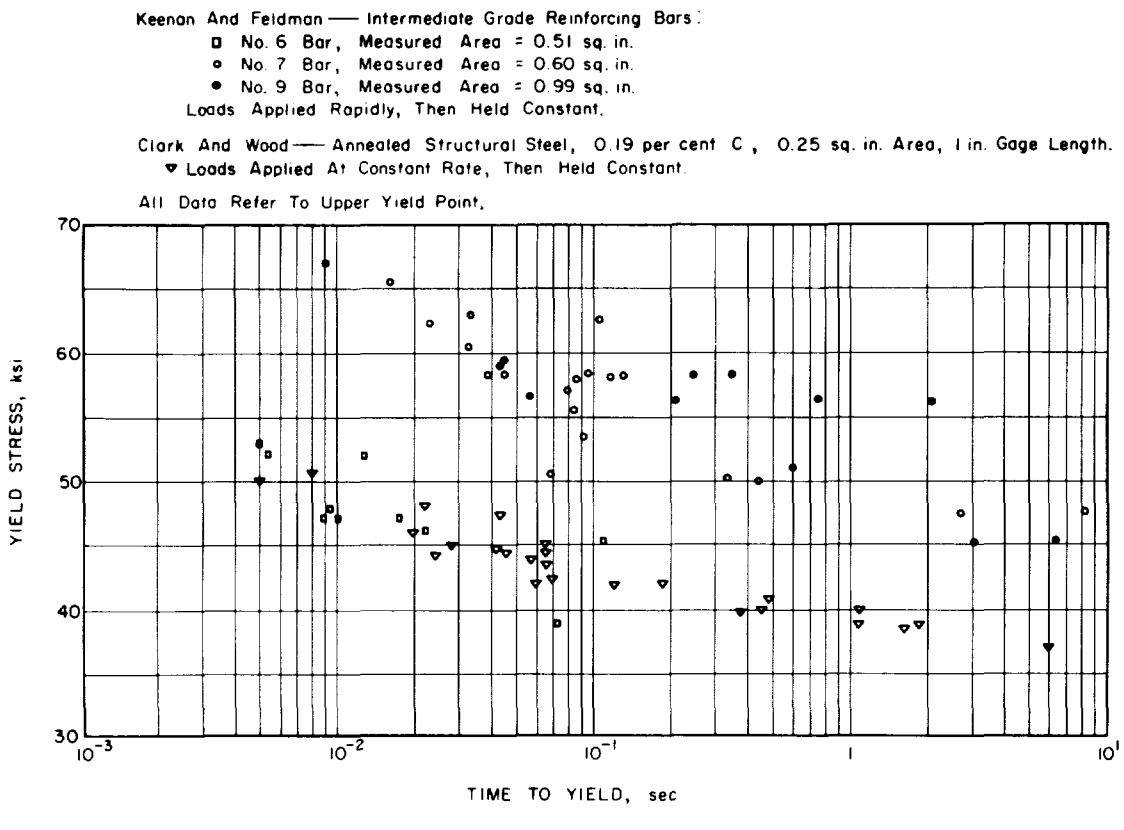

FIG. V-1.29 DYNAMIC YIELD STRESS FOR STRUCTURAL (A7) AND CONCRETE REINFORCING (A15-INTERMEDIATE GRADE) STEEL

Although the sizes of reinforcing bars now are specified by weight, it is doubtful that this particular No. 6 bar would meet the specified tolerances on weight. The remaining results in this study for the larger bars appear entirely reasonable. Thus, it is believed that the results for the larger intermediate grade bars indicate that the magnitude of the yield point which might be expected under conditions of rapidly applied loads.

It should be emphasized that for steels with a definite yield point the increased strength produced by dynamic loads is a clearly documented phenomenon. Furthermore, the increased strength exists throughout the normally plastic region until work hardening begins. Thus, the effective strength of the material to be used in analysis should be augmented always to account for the dynamic effect. At the same time however analyses are complicated by the fact that a finite time is required to initiate yielding in the material. This finite time also must be considered in analysis for it is possible that the structural element will not yield if the time of maximum response is less than the time delay to yielding. On the other hand in design this complication normally need not be considered because the loading generally is not known with sufficient accuracy to specify with safety a particular value of the time of maximum response; the material is assumed to yield without a time delay in this case.

Results for Concrete from Strain Rate Tests. Figure V-1.30 shows the data from three separate investigations on compressive strength of concrete (Ref. V-1.45). In this figure the ratio of dynamic strength to static strength is plotted against the rate of strain. In the plot it is assumed that the base for static loads is 6.95×10^{-5} in./in./sec. This base is consistent with the ASTM Standard. Although in the original report by Watstein a base of 10^{-6} in./in./sec was used to define a static load, the data have been re-evaluated in terms of the ASTM Standard.

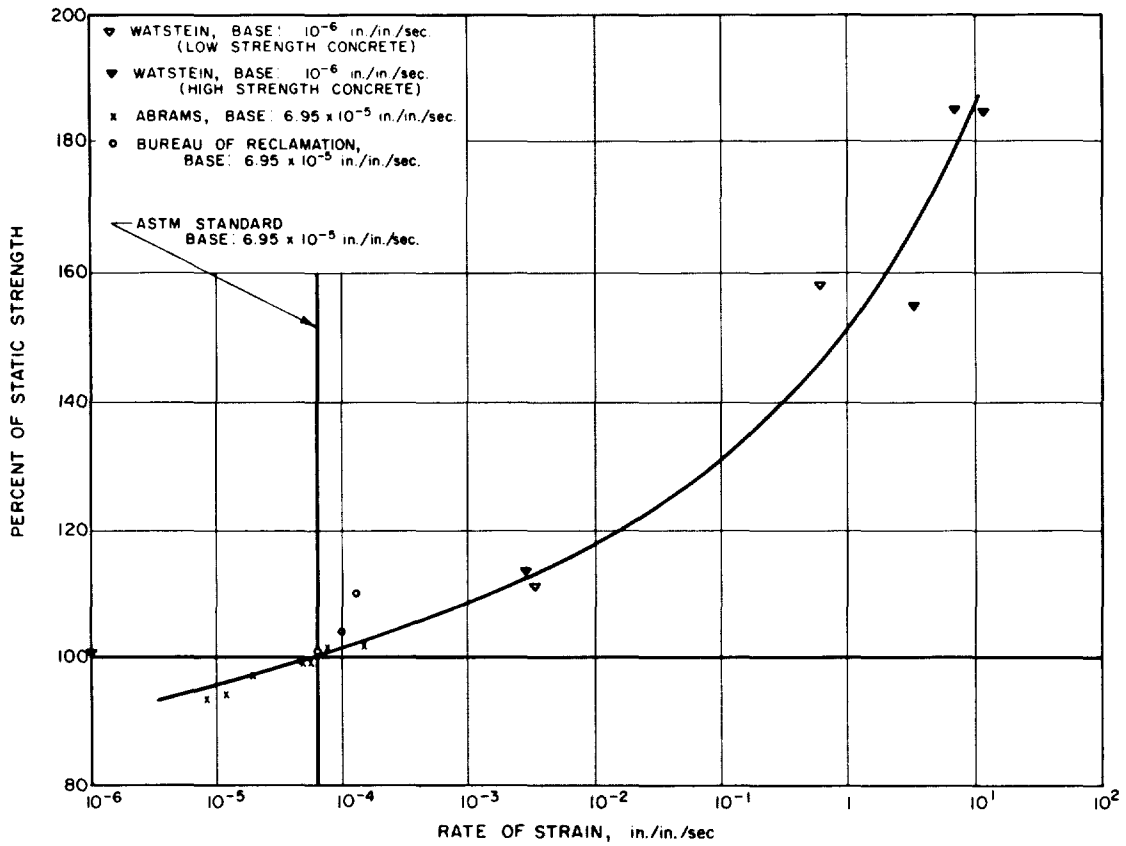

FIG. V-1.30 EFFECT OF RATE OF STRAIN ON COMPRESSIVE STRENGTH OF CONCRETE

It should be noted that references for studies on the dynamic behavior of concrete in shear have not been located. Thus, it would appear that no specific studies of this phenomena have been made. In the dynamic tests of reinforced concrete beams, the members were designed to obtain primarily flexural behavior; consequently these tests do not allow inferences regarding the behavior of reinforced concrete under the action of combined flexure and shear. To understand fully the behavior of reinforced concrete members it is necessary to know the dynamic behavior of plain concrete in shear and reinforced concrete in combined shear and flexure.

V-1.7 METHODS OF STRUCTURAL ANALYSIS

Although much of Chapter 4 is devoted to this subject, the concepts are briefly summarized here.

V-1.7.1 Single-Degree-of-Freedom System

Most prominent among the problems associated with analysis of structures subjected to transient loads is the definition of the mathematical model which represents the actual structural system. Once the model is defined, specification of the parameters needed to assess behavior becomes relatively simple. Behavior of exterior elements and other parts of buried structures can be interpreted by considering a single degree of freedom model of the element.

A general single-degree-of-freedom system and the notation are shown in Fig. V-1.25. In most cases the important loading consists of the force p(t) applied to the mass; this force is related inherently to the force acting on the exposed surface of the element. Sometimes the motion of the support, normally defined by the acceleration $\ddot{y}$, can be important. Because of the linearity of the differential equation, the effect of this base motion can be combined with the force acting on the mass, producing an effective force of $p(t) - m\ddot{y}$. In measuring the more significant response of a member related to its failure, the viscous damping inherent in most structural materials is so small that it can be neglected; consequently this term has been omitted in the differential equation of motion shown in Fig. V-1.25. However, damping is an important consideration in the assessment of potential damage to equipment and personnel and for rebound.

It is convenient to measure response in a dimensionless form. Normally this dimensionless parameter is taken as the ductility ratio μ which is defined as the quotient of the maximum displacement x_m to the displacement x_y corresponding to initial yielding of the structural element. Usually however computation of the degree of damage measured by μ or x_m is not as reliable as calculation of force consistent with a particular value of ductility ratio. This results from the fact that small changes in the magnitude or variation with time of the applied force can cause disproportionate changes in the deflection of a structural member. Therefore, the most significant parameters in measuring behavior are those associated with the force p(t) in Fig. V-1.25 (Refs. V-1.4 and V-1.37). Here also it is convenient to specify the relevant characteristics of the force in a dimensionless form:

(1) Peak magnitude of force p_m is expressed as a ratio to the effective force q_y causing yielding of the element.

(2) Rise time t_r (the effective time required for the force to build-up from zero to its maximum) is expressed as a ratio to the effective natural period of vibration of the element T.

(3) Effective duration t_d (the time that the force is effective in causing initial deflection) is expressed as a ratio to the effective natural period of vibration of the element T.

A solution to the single-degree-of-freedom system for $t_r = 0$ is shown in Fig. V-1.31 which uses these parameters.

V-1.7.2 Multi-Degree-of-Freedom System

When the structure or the loading is very complex, it frequently is necessary to consider a multi-degree-of-freedom model in place of the single-degree system. In underground structures consideration of multi-degree systems most often is required in analyzing the potential damage to contents and equipment. Analysis of such systems is more complex than for single-degree systems, and generalizations of the behavior normally cannot be made. Thus, each problem must be considered separately. However, a method which often is useful, consists of a modal analysis wherein the eigenvalues and eigenvectors for the system are computed. From these the participation factors for each mode excited by the force are found, and combinations of the modal responses can provide upper bounds or probable values of the solution (Ref. V-1.37).

V-1.8 REBOUND PHENOMENA

As in the preceding section, much of Chapter 4 is devoted to a discussion of rebound phenomena; consequently, this subject is only briefly summarized here.

When a structural element is subjected to a dynamic load, it first deflects in the direction of the applied load. At some later time it may tend to deflect in an opposite direction; i.e., rebound as a result of strain energy stored in the element. For short duration loads on an elastic element not in contact with soil, the rebound can equal the maximum primary deflection. However, for loads of long duration the rebound normally will be less than the primary

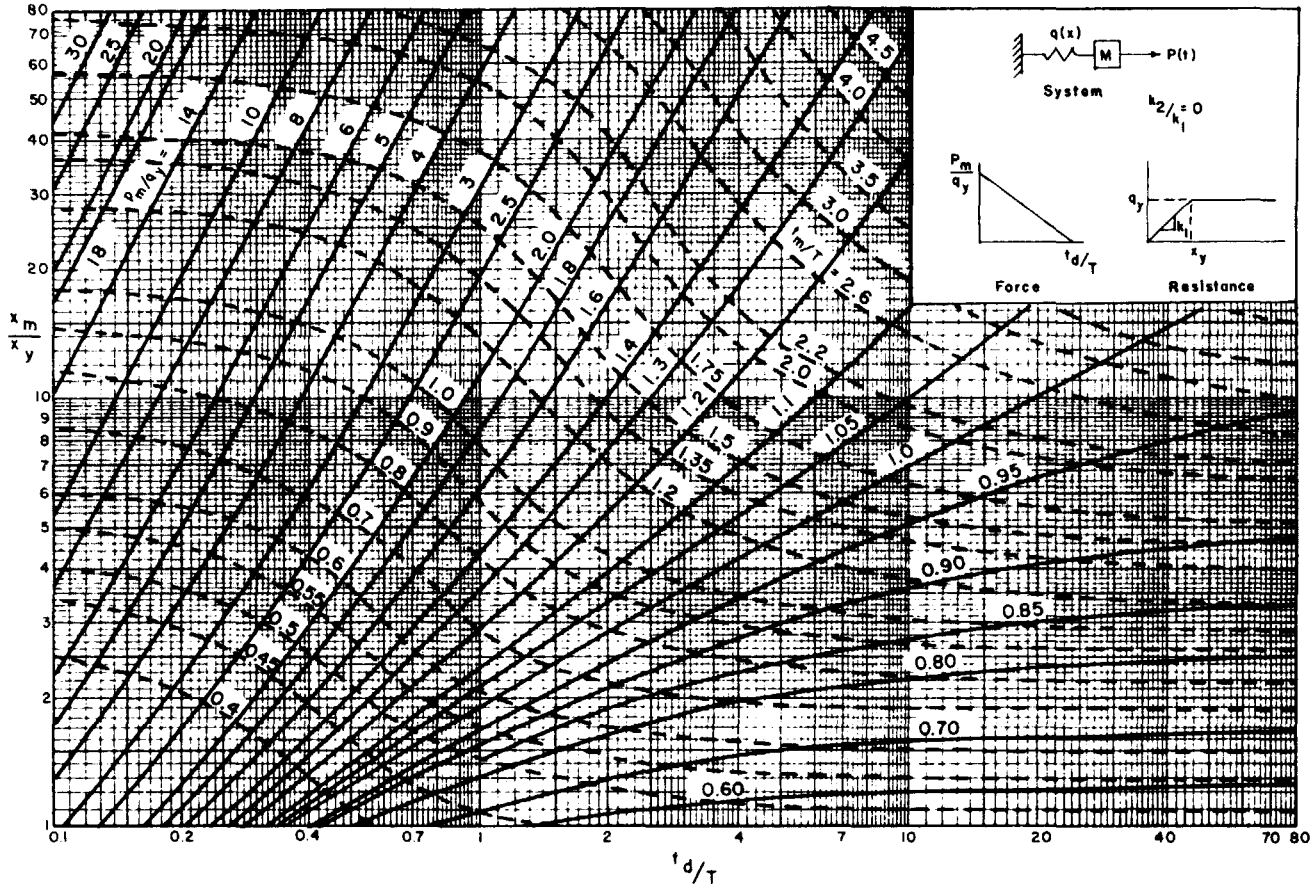

FIG. V-1.31 MAXIMUM RESPONSE OF SIMPLE SPRING-MASS SYSTEM TO INITIALLY PEAKED TRIANGULAR FORCE PULSE

displacement. For buried structures rebound may not occur since to deflect in a direction opposite to the load, the structure must overcome the resistance offered by the soil; definite data or analyses are not as yet available for this case.

From a detailed study of the response of a single-degree-of-freedom system with an elasto-plastic resistance function subjected to the effects of an initially peaked triangular load (Ref. V-1.17) approximate solutions to the problem of rebound were generated (Fig. V-1.32). The maximum error associated with the approximation pictured produces a rebound resistance which is approximately 20% greater than the theoretical value; thus, the error is conservative, and it should be emphasized that this error is the extreme. In most cases of interest the error is much smaller.

Viscous damping can significantly reduce rebound. Reduction factors to be applied to the values in Fig. V-1.32 are given in Table V-1.2. The notation in Fig. V-1.32 and Table V-1.2 is identical to that in the preceding section. The parameter β, which is the ratio of the damping present to the critical damping, has been added.

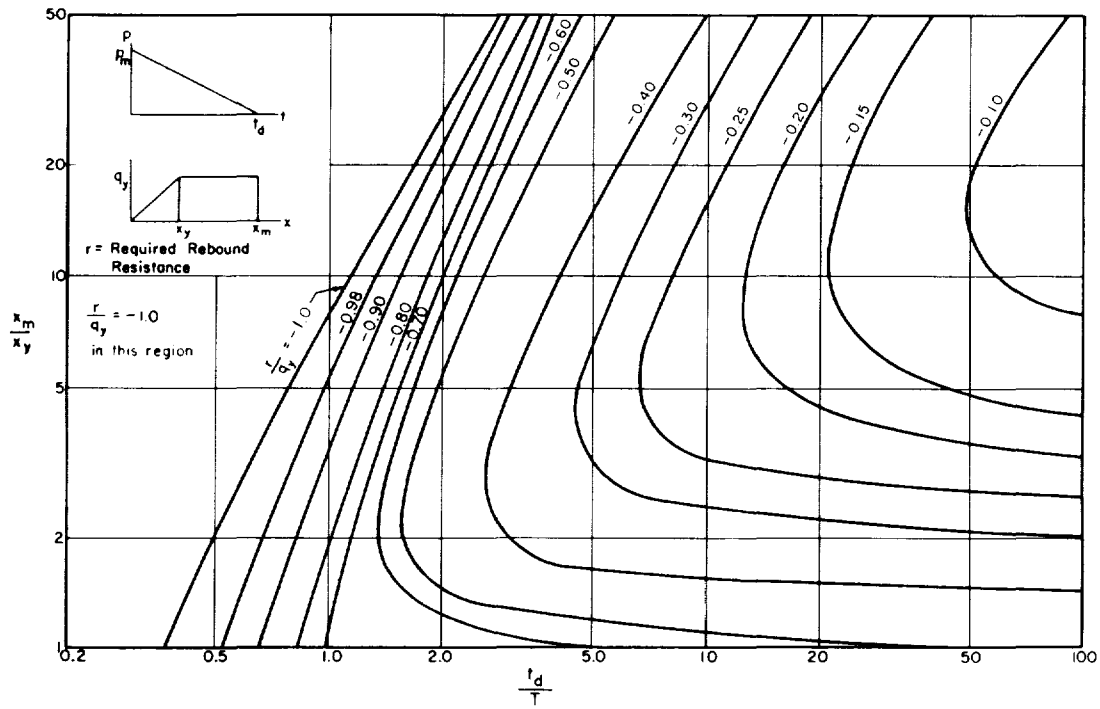

FIG. V-1.32 DESIGN CHART FOR ELASTIC REBOUND

TABLE V-1.2 REDUCTION FACTORS FOR DAMPED REBOUND

$\frac{t_d-t_m}{T}$	β \ $\frac{p_m}{q_y}$	0.125	0.25	0.5	0.75
0	0	1.0	1.0	1.0	1.0
	0.025	0.925	0.925	0.925	0.925
	0.05	0.853	0.853	0.853	0.853
	0.1	0.728	0.728	0.728	0.728
0.5	0	0.875	0.760	0.588	0.530
	0.025	0.841	0.736	0.565	0.515
	0.05	0.808	0.702	0.540	0.495
	0.1	0.742	0.644	0.492	0.455
1.0	0	0.875	0.750	0.500	0.250
	0.025	0.775	0.665	0.442	0.221
	0.05	0.745	0.592	0.394	0.195
	0.1	0.685	0.512	0.314	0.160
1.5	0	0.875	0.750	0.500	0.250
	0.025	0.775	0.665	0.455	0.261
	0.05	0.725	0.594	0.402	0.236
	0.1	0.662	0.475	0.316	0.192
2.0	0	0.875	0.750	0.500	0.250
	0.025	0.748	0.614	0.410	0.205
	0.05	0.714	0.530	0.336	0.170
	0.1	0.652	0.450	0.230	0.116
2.5	0	0.875	0.750	0.500	0.250
	0.025	0.740	0.614	0.412	0.220
	0.05	0.706	0.505	0.340	0.182
	0.1	0.645	0.438	0.225	0.125
3.0	0	0.875	0.750	0.500	0.250
	0.025	0.735	0.572	0.380	0.190
	0.05	0.702	0.482	0.285	0.145
	0.1	0.641	0.430	0.168	0.085
3.5	0	0.875	0.750	0.500	0.250
	0.025	0.732	0.570	0.380	0.195
	0.05	0.701	0.475	0.290	0.154
	0.1	0.640	0.420	0.165	0.092
4.0	0	0.875	0.750	0.500	0.250
	0.025	0.731	0.535	0.354	0.175
	0.05	0.700	0.470	0.245	0.124
	0.1	0.639	0.420	0.124	0.064
∞	0	0.875	0.750	0.500	0.250
	0.025	0.684	0.446	*	*
	0.05	0.623	0.391	*	*
	0.1	0.510	0.294	*	*

*For $p_m/q_y > \dfrac{1}{1 + \exp \dfrac{\beta\pi}{\sqrt{1 - \beta^2}}}$

as $(t_d-t_m)/T \to \infty$ the system will not rebound past the equilibrium position; under such conditions the rebound is effectively zero.

REFERENCES

V.1 Newmark, Hansen, and Associates, Protective Construction Review Guide, prepared for OASD under Contract SD52, Revised June 1961.

V.2 Newmark, Haltiwanger, et al, Air Force Design Manual: Design of Protective Structures to Resist the Effects of Nuclear Weapons, Draft, Vol. 1 and 2, prepared for AFSWC under Contract 29(601)-2390, May 1961 (Confidential).

V.3 Office, Chief of Engineers, Design of Structures to Resist the Effects of Atomic Weapons, Engineering Manual, Military Construction, EM 1110-345-413.

V-1.1 Christopherson, Structural Defence, 1945, Ministry of Home Security (Gt. Br.), RC 450 (Confidential).

V-1.2 Lampson, Final Report on Effects of Underground Explosions, NDRC A-479, OSRD 6645, Washington, 1946 (Unclassified).

V-1.3 Christensen, Cratering from Atomic Weapons, AFSWP (DASA) 514, 29 June 1956 (Secret Restricted Data).

V-1.4 Newmark, An Engineering Approach to Blast Resistant Design, Trans. ASCE, 121, 45-64, 1956.

V-1.5 Smith and Newmark, Numerical Integration for One-Dimensional Stress Waves, Department of Civil Engineering, University of Illinois, SRS 162, Urbana, 1958 (Unclassified).

V-1.6 Newmark, Considerations in the Design of Underground Protective Structures, Vol. III Final Report to USBMD by AMF under Contract AF-04(647)-156, 1958 (Secret).

V-1.7 Newmark, Influence Charts for Computation of Stresses in Elastic Foundations, University of Illinois, Engineering Experiment Station, Bulletin 338, 1942 (Unclassified).

V-1.8 Parkin, Impact Wave Propagation in Columns of Sand, RM 2486, Rand Corporation, Santa Monica, 1959, Unclassified and Impact Waves in Sand: Theory Compared with Experiments on Sand Columns, Proceedings ASCE, 87, No. SM 3, June 1961. See Also discussions by Fulton and Hendron and by Selig and Vey, 87, No. SM 6, Dec. 1961 and by Whitman, 88, No. SM 1, Feb. 1962.

V-1.9 Taylor and Whitman, The Behavior of Soils Under Dynamic Loadings, 3: Final Report on Laboratory Studies, Soil Mechanics Lab, MIT, AFSWP 118, 1954 (Unclassified).

V-1.10 Weidlinger, et al, On the Application of the Theory of Locking Media to Ground Shock Phenomena, Mitre Corporation, SR-18, Bedford, Mass., 1960 (Unclassified).

V-1.11 Sutcliffe, The Analysis of an Elastic Half-Space Subjected to a Simulated Blast Load, PhD Thesis, Dept. of Civ. Eng., Univ. of Ill., Urbana, Ill., 1960 (Unclassified).

V-1.12 (a) Perret, Attenuation of Earth Pressures Induced by Air Blast, SC, Operation Buster-Jangle, WT-302, 1952 (Secret Restricted Data).

(b) Perret, Earth Stresses and Earth Strains, SC, Operation Tumbler-Snapper, WT-503, 1952 (Confidential Restricted Data).

(c) Perret, Vertical Earth Stress and Earth Stress and Strain Systems, SC, Operation Upshot-Knothole, WT-716, 1954 (Secret Restricted Data).

V-1.13 Newmark and Sinnamon, Air Blast Effects on Underground Structures, Univ. of Ill., Operation Upshot-Knothole, WT-727, 1954 (Confidential Restricted Data).

V-1.14 Bultmann, McDonough, and Sinnamon, Loading on Simulated Buried Structures at High Incident Overpressures, Univ. of Ill/SWC Operation Plumbbob, WT-1406, 1959 (Confidential Formerly Restricted Data).

V-1.15 Perret, Ground Motion Studies at High Incident Overpressures, SC, Operation Plumbbob, WT-1405, 1960 (Unclassified).

V-1.16 Swift and Sauer, Ground Acceleration, Stress, and Strain at High Incident Overpressures, SRI, Operation Plumbbob, WT-1404, 1960 (Unclassified).

V-1.17 Newmark and Hall, Preliminary Design Methods for Underground Protective Structures, AFSWC-TR-60-5, 1959 (Secret).

V-1.18 Strutt (Lord Rayleigh), The Theory of Sound, Vols. I and II, reprinted in U.S. New York: Dover Press, 1945.

V-1.19 Committee on Fortification Design, National Research Council, Interim Report No. 26, Vol. I, Subsurface and Target Phenomena, Vol. II, Subsurface and Surface Phenomena, Vol. III, Resulting Damage to Structures, Washington, 1944 (Unclassified).

V-1.20 Sharpe, The Production of Elastic Waves by Explosion Pressures, Geophys., 7, 144-152, 1942.

V-1.21 Rinehart and Pearson, Behavior of Metals Under Impulsive Loads, ASM, Cleveland, 1954.

V-1.22 Engineering Research Associates, et al, Underground Explosion Test Program, Vol. I Soil, St. Paul, 1952 (Unclassified).

V-1.23 Sachs and Swift, Small Explosion Tests, Project Mole, Vols. I and II, AFSWP (DASA)-291, SRI, Menlo Park, 1955 (Unclassified).

V-1.24 Capabilities of Atomic Weapons, AFSWP (DASA), TM 23-200, 1957 (Confidential).

V-1.25 Engineering Research Associates, et al, Underground Explosion Test Program, Final Report, Vol. II, Rock, St. Paul, 1953 (Confidential).

V-1.26 Born, The Attenuation Constant of Earth Materials, Geophys., 6, 1941.

V-1.27 Kolsky, Stress Waves in Solids, London: Oxford Univ. Press, 1953.

V-1.28 Timoshenko and Goodier, Theory of Elasticity, New York: McGraw-Hill 2nd ed., 1951.

V-1.29 Taylor, Review of Pressure Distribution Theories, Earth Pressure Cell Investigations and Pressure Distribution Data, WES, Vicksburg, 1947.

V-1.30 Kallstenius and Bergau, Investigations of Soil Pressure Measuring by Means of Cells, Royal Swedish Geotechnical Institute, Stockholm, 1956.

V-1.31 Baron, Bleich, and Weidlinger, Theoretical Studies on Ground Shock Phenomena, Mitre Corporation, SR-19, Bedford, Mass., 1960 (Unclassified).

V-1.32 Terzaghi and Peck, Soil Mechanics in Engineering Practice, New York: John Wiley & Sons, Inc., 1948.

V-1.33 Lee and Wong, Evaluation of Effects on Tunnel Support Structures, Operation Hardtack II, ITR-1714, 1959 (Confidential).

V-1.34 Newmark, Briscoe, and Merritt, Analysis and Design of Flexible Underground Structures, Contract DA-22-079-eng-225 with WES, Vol. II, Urbana, 1960 (Confidential).

V-1.35 Timoshenko, Vibration Problems in Engineering, New York: D. Van Nostrand, Inc., 3rd ed., 1955.

V-1.36 Merritt and Newmark, Design of Underground Structures to Resist Nuclear Blast, Dept. of Civ. Eng., Univ. of Ill., SRS-149, Urbana, 1958 (Unclassified).

V-1.37 Melin and Sutcliffe, Development of Procedures for Rapid Computation of Dynamic Structural Response, Final Report on Contract AF33(600)-24994 with Physical Vulnerability Division, USAF, Univ. of Ill., Dept. of Civ. Eng., SRS-171, 1958 (Unclassified).

V-1.38 Woodring, Sinnamon and Newmark, Air Blast Effects on Underground Structures, Univ. of Ill., Operation Teapot, WT-1127, 1958 (Confidential Formerly Restricted Data).

V-1.39 Sievers, Structural Response and Permanent Displacement Measurements, Operation Hardtack-II, Project 26.7, WT-1708, 1960 (Unclassified).

V-1.40 Jones and Moore, An Investigation of the Effect of Rate of Strain on the Results of Tension Test of Metals, Proceedings, ASTM, 40, 1940.

V-1.41 Von Karman and Duwez, The Propagation of Plastic Deformation in Solids, Jour. App. Phys., 21, 987, 1950.

V-1.42 Duwez and Clark, An Experimental Study of the Propagation of Plastic Deformation Under Conditions of Longitudinal Impact, Proceedings, ASTM, 47, 502, 1947.

V-1.43 Jeffreys, Cartesian Tensors, Cambridge University Press, 76-81, 1957.

V-1.44 Keenan and Feldman, The Yield Strength of Intermediate Grade Reinforcing Bars Under Rapid Loading, Univ. of Ill., Structural Research Series No. 197, March 1960.

V-1.45 McHenry and Shideler, Review of Data on Effect of Speed in Mechanical Testing of Concrete, Bulletin D9, Portland Cement Association, Skokie, 1956.

V-1.46 Manjoine, Influence of Rate of Strain and Temperature on Yield Stresses of Mild Steel, Jour. App. Mech., 11, 4, 1944.

V-1.47 Fry, Speed in Tension Testing and Its Influence on Yield Point Values, Proceedings, ASTM, 40, 1940.

V-1.48 Klinger, Effect of Strain Rate on the Tensile Properties of SAE 4340 Steel, WADC Technical Report 53-507, WPAFB, 1955 (Unclassified).

V-1.49 Vreeland, Wood, and Clark, A study of the Mechanism of the Delayed Yield Phenomenon, Metal Prog., 1952.

V-1.50 Clark and Wood, Time Delay for the Initiation of Plastic Deformation at Rapidly Applied Constant Stress, Proceedings, ASTM, 1949.

V-1.51 Massard, The Stress-Deformation Characteristics of Some Mild Steel Subjected to Various Rapid Uniaxial Stressings, PhD Thesis, Univ. of Ill., Urbana, Ill., 1955.

V-1.52 Norris, et al, Structural Design for Dynamic Loads, New York: John Wiley & Sons, Inc., p. 5, 1959.

V-1.53 Kane, Cox, and Planomdon, Evaluation of Tunnel Liners in Granite, Shot Hard Hat, Operation Nougat (U), RTD-TDR63-3041, prepared for Air Force Weapons Lab. by Dept. of Civ. Eng., Univ. of Ill., Kirtland AFB, Sept. 1963 (Secret).

CHAPTER V-2

STRUCTURES BURIED AT SHALLOW DEPTHS

Normally underground protective structures buried at shallow depths are placed by cut and cover techniques, or they might actually project above the surface with an extensive earth mound placed over the projection. Such structures would generally be buried in soil because there is little advantage in terms of protection gained in placing a structure near the surface in rock. Furthermore, a shallow buried structure would not ordinarily be located below the water table if it could be reasonably avoided.

Consequently, this discussion is restricted to consideration of structures located in unsaturated soil at depths of cover less than 100 to 200 ft. Because the structures are located in unsaturated soil, for which the seismic velocity generally is less than 2000 ft/sec, they are subjected primarily to the effects of airblast-induced motion. Thus, the average air-shock velocity between the point of burst and the structure generally will be greater by a considerable margin than the wave velocity in the soil. Supporting this contention is the fact that shallow-buried structures become economically feasible generally for overpressures of the order of 30 psi at which the air-shock velocity has reduced to approximately 1900 ft/sec (Ref. V.1). Other means of protection are usually more desirable for overpressures in excess of perhaps 500 to 1000 psi.

Structural configurations normally constructed by cut-and-cover techniques include rectangles wherein all elements are plane, horizontal arches or cylinders, vertical cylinders, domes and combinations of one or more of these basic configurations. A distinction is made between horizontal and vertical cylinders because their behavior under airblast-induced loading depends upon orientation. The basic configuration to be used for a particular purpose is normally dictated by the required architectural layout.

V-2.1 STATIC LOADS

Because important insight into the behavior of structures subjected to blast loads can be gained from study of behavior under static loads, the conditions associated with static loading are summarized in some detail. Also in some cases, as discussed later, the behavior under static loading may influence the dynamic loading reaching structural elements.

The magnitude of static load is influenced primarily by the type of soil and means of excavation, type of structure, and the depth of cover. These effects are related but in the following discussion each is treated separately.

V-2.1.1 Effect of Soil Type and Means of Excavation

At shallow depths in some soils with high cohesive strengths, it is possible to obtain stable vertical cuts. In other cases vertical slopes may be employed if only intermittent bracing is used. When vertical slopes are possible, the surface of the cut can actually be used as the outer form for the structure. In such soils the static load on vertical surfaces of the structure can be very much reduced compared with the load when the walls are backfilled after completion of construction.

When the structure itself is used as a caisson to accomplish the excavation, reductions in lateral forces on the structure also can be expected when the soil has relatively high cohesive strength.

The potential planes of failure which might develop in the soil, for an unbraced trench (Fig. V-2.1), explain why initial reduction in lateral force may be expected if the final structure rests directly against the surface of the cut. If the walls of the cut will stand vertically (that is, when the force produced by the overburden is less than the shearing force developed along the potential plane of failure), the strength of the soil is already mobilized and failure does not occur. Thus, the walls of the structure initially are subjected to zero static load. Vibrations induced during construction, percolation of water through the surrounding soil and other conditions will cause the walls of the structure to gain static load with time. However, these loads should not ordinarily exceed the lateral stresses associated with the normal "active" conditions. In developing these lateral stresses arching around the structure may also develop. Possible development of arching during the redistribution of stress makes consideration of effects of cohesive strength on means of excavation important.

This is in contrast to the conditions where a relatively large cut is provided and is backfilled following completion of the walls of the structure, a procedure frequently required in non-cohesive soils. Between the surface of the cut and the backfill, zones of weakness, similar to the potential planes of failure in Fig. V-2.1, are introduced into the soil. If the soil is cohesive, considerable time must elapse before cohesion is re-established along these zones of weakness.

Consequently in such a situation the walls of the structure might immediately be subjected to static load consisting of lateral stresses associated with the backfill, corresponding to a situation normally between the "active" and the "at rest" conditions*. For cohesionless soils the empirical "coefficient of earth pressure at rest" K_o, the ratio of horizontal to vertical stress at a point, ranges from 0.4 to 0.5 for natural deposits but may be as high as 0.8 in carefully controlled backfill (Ref. V-1.32). The "coefficient of active earth pressure" K_A, the ratio of horizontal to vertical stress when the active condition exists, is defined for cohesionless soils as:

$$K_A = \tan^2\left(45^\circ - \frac{\varphi}{2}\right) \qquad \text{(V-2.1)}$$

where φ = angle of internal friction.

Although sophisticated procedures are available (cf. Ref. V-1.32, p 147ff) to define K_A for cohesive soils, it is suggested that it may be sufficient to define an effective "coefficient of active pressure" by defining a pseudo-value of angle of internal friction φ from the Mohr envelope of rupture (cf. Fig. V-1.21) for the cohesive soil; i.e., an angle of internal friction is chosen which reproduces approximately the states of stress for a given loading.

At shallow depths (of the order of 25 ft) the static stresses on vertical surfaces of a structure, irrespective of the construction procedure used, frequently are small compared with the stresses produced by blast. For large depths the lateral static stresses are significant and a method for estimating their magnitude on vertical cylinders is presented in Section V-2.1.3.

The static loads reaching horizontal surfaces depend upon the characteristics of the structure relative to the soil surrounding it and upon the characteristics of the backfill placed around the structure. If the structure is rigid or is founded on relatively rigid strata, these loads can be much larger than would be the case for a flexible structure. Alternatively if the backfill is highly compressible compared with the natural soil, these loads can be greatly reduced, and this reduction may be independent of the properties of the structure. The dependence of the structural loading on the relative motions between structure and soil is referred to generally as arching.

*The active condition corresponds to a so-called state of plastic equilibrium where the soil has moved establishing shearing forces along a plane of potential failure which maintains equilibrium. "At rest" condition refers to the case where no movement has occurred in the soil.

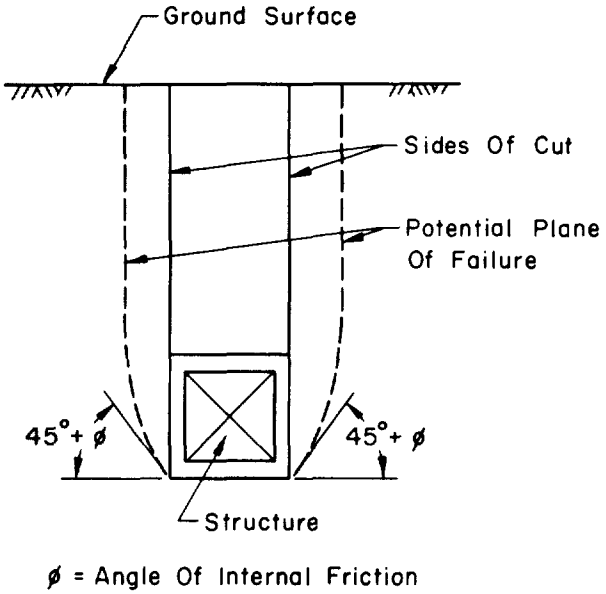

FIG. V-2.1 DEVELOPMENT OF STATIC LOADS ON BURIED STRUCTURES

V-2.1.2 Arching

Natural arching of deformable media was probably first recognized as a practical problem in the design of grain bins (Ref. V-2.1). This recognition resulted from observations that the pressures on the floor of a grain bin were much smaller than would be implied by the weight of the grain. At the same time the vertical stresses in the walls of the bins were much higher than expected. A similar problem was recognized later by foundation engineers. Despite early recognition, the mechanism of formation of an arch in granular media still is not fully understood although studies by Terzaghi (Refs. V-1.32, V-2.2-V-2.4) have given important insight into the static problem.

In general, arching refers to the situation in which the stress in a body of soil is carried through a portion of the soil by the formation of a structural arch in the soil. Arching develops most frequently when a structure or structural element buried in soil tends to move away from the soil it supports. When this occurs, the load above the structure, under certain conditions, may continue to be supported by the formation of an arch in the soil, which carries the load beyond the structure or to the less deformable parts of the structure; thus, reducing the load carried by the deformable parts of the structure. A phenomenon called negative arching also may be inferred from the evidence available. Negative arching results when a structure remains relatively stationary while the surrounding soil moves past it, the moving soil causing an increase in force on the loaded face of the structure.

In grain bins the conditions producing the arching are apparent; the walls of the bin are relatively rigid and shearing forces can develop between the grain and these walls. These forces in turn form the reactions for an arch which develops in the grain as a result of the inherent internal friction. The inherent internal friction of granular soils can produce similar conditions when an element tends to move relative to surrounding elements of soil. A formal attempt to account for such behavior in soil was done by Marston (Ref. V-2.5). Experimental proof that soil can develop an arch above a yielding surface was illustrated conclusively by Terzaghi's classic trap door experiments with dry and saturated sands (Ref. V-2.3).

In Ref. V-2.5 is presented an analytical study of arching including limited experimental validation of the theory. Four conditions are postulated (Ref. V-2.5) which are summarized in Fig. V-2.2. Although circular conduits such as water mains are specifically illustrated, the theory neglects the actual characteristics of the buried structure except to note that the structure is stiffer than the soil it replaces. The theory defines the total vertical load P which acts on a plane tangent to the crown of the cylinder buried in granular (cohesionless) soil. In the associated experimental studies circular pipes were employed.

For the complete ditch condition (Fig. V-2.2a) with a rigid structure on a rigid foundation, the backfill in the trench tends to move downward relative to the original sides of the trench. As it does shearing forces develop which support a part of the backfill relieving part of the force on the structure in the sense that the conduit does not have to support the entire overburden. The amount of relief depends on the effective angle of internal friction of the backfill φ' and of the original soil φ and the effective normal stress across the potential planes of failure (the sides of the original trench). The unit weight of the soil is w. Cohesion can be considered separately or included in the definition of the effective angle of internal friction.

For complete ditch condition with a rigid conduit on a rigid foundation (Fig. V-2.2a), $P = P_{dr}$:

$$P_{dr} = wb_d^2 \frac{1 - e^{-ah}}{2K \tan \varphi'} \qquad (V\text{-}2.2)$$

where

$$a = \frac{2K \tan \varphi'}{b_d}$$

and

$$K = \frac{\tan^2 \varphi + 1 - \tan \varphi}{\tan^2 \varphi + 1 + \tan \varphi} = \frac{1 - \sin \varphi}{1 + \sin \varphi}$$

For a complete ditch condition (Fig. V-2.2a) with a flexible structure or a rigid structure on a flexible foundation and with the natural soil along the sides of the ditch having the same stiffness as the structure and soil surrounding it, $P = P_{df}$:

$$P_{df} = w b_c b_d \frac{1 - e^{-ah}}{2K \tan \varphi'} \qquad (V\text{-}2.3)$$

Negative arching can occur statically whenever the structure and soil above it remains stationary while the soil to the sides of the structure tends to move downward. Alternatively negative arching can develop if a structure, such as a footing, is forced into the soil. Perhaps the most obvious example of negative arching occurs when a structure is placed on natural ground and a fill is placed over it (Fig. V-2.2b). Normally the structure is stiffer than the backfill. Consequently the vertical column of soil including the structure generally is more stiff than adjacent similar columns of soil alone. The adjacent columns of soil deform more than the column including the structure thereby producing shearing forces which act downward on the soil above the structure. As a result the structure carries a load which is larger than the force implied by the overburden. In this case the load $P = P_p$ is

$$P_p = wb_c^2 \frac{e^{bh} - 1}{2K \tan \varphi'} \qquad (V\text{-}2.4)$$

where

$$b = \frac{2K \tan \varphi'}{b_c}$$

To distinguish between complete ditch and complete projection conditions the concept of the plane of equal settlement is introduced. This is the plane in the soil above which the settlement in the column of soil bounded by vertical planes tangent to the sides of the structure is equal to the settlement of the columns of soil adjacent to the one including the structure (Ref. V-2.5). For the complete ditch condition the plane of equal settlement is below the structure; it is above the surface of the backfill placed over the entire area including the structure for the complete projection condition. When the incomplete ditch or projection conditions develop, the plane of equal settlement falls between the structure and the surface of the ground. Whether a ditch or projection condition develops depends upon the direction of settlement between the columns of soil of interest: if the column including the structure settles downward relative to the adjacent columns an incomplete ditch develops (Fig. V-2.2c); the reverse direction of settlement produces the incomplete projection (Fig. V-2.2d). Before the location of the plane of equal settlement and the direction of settlement below this plane can be determined, the deformation characteristics of the structure, of the

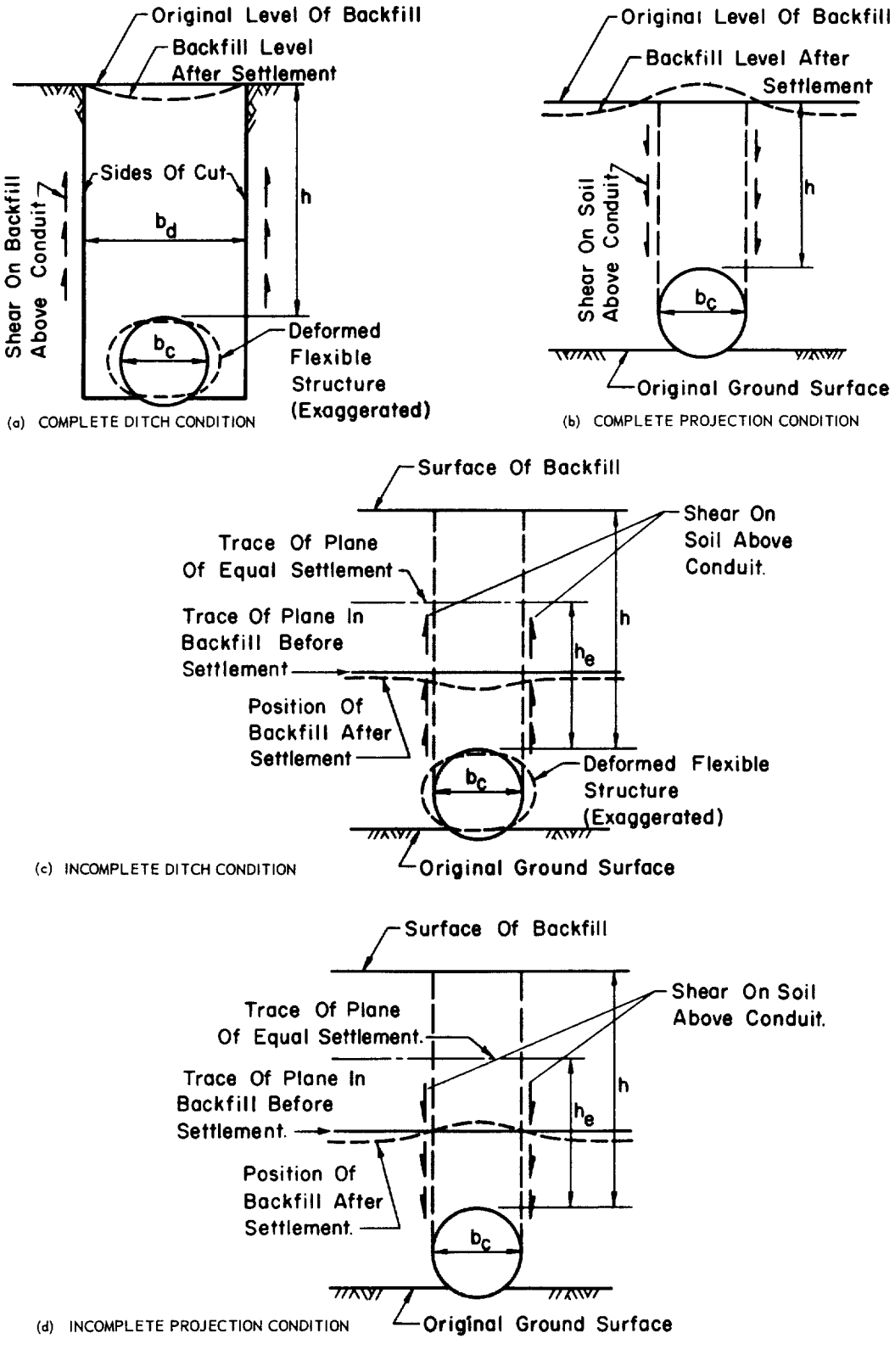

FIG. V-2.2 CONDITIONS AFFECTING STATIC LOADS ON BURIED STRUCTURES

backfill and of the soil on which the conduit is placed must be known. A semi-empirical procedure for sewers or water mains with conventional bedding (special backfill) is suggested in Ref. V-2.5 for roughly evaluating these deformational characteristics: the Boussinesq solution (cf. Section V-1.3.1) is suggested for computing displacements in the soil, and approximate procedures are mentioned for determining displacements in conventionally bedded structures. A qualitative discussion of relative displacements for structures without conventional bedding is presented in Section V-2.1.3.

If the height of equal settlement can be estimated for a particular case the static load $P = P_i$ is:

$$P_i = wb_c^2 \frac{e^{\pm bh_e} - 1}{\pm K \tan \varphi'} + \left(\frac{h}{b_c} - \frac{h_e}{b_c} \right) e^{\pm bh_e} \qquad (V\text{-}2.5)$$

where the positive signs apply to the incomplete projection condition and the negative signs apply to the incomplete ditch condition.

For the complete ditch condition, the backfill placed in the ditch forms an arch whose abutments are the sides of the ditch and positive arching occurs. On the other hand for the complete projection condition, negative arching develops since the shear forces acting on the column of soil immediately above the conduit augment the force imposed by the weight of material. Intermediate cases can produce either positive or negative arching depending upon the direction of the shear forces shown in Fig. V-2.2.

Arching is also produced by deflection of the entire structure or of parts of the structure such that an opening tends to develop between the top of the structure and the soil. In Terzaghi's initial experiments (Ref. V-2.3) an actual opening was introduced by removing a portion from the bottom of a box containing sand. It was found that only a volume of sand approximating a half cylinder with a diameter equal to the smaller span of the opening dropped through the "trap door," and all sand above this half cylinder remained essentially stationary. Thus, an arch across the opening must have formed in the sand. Complementing these trap door observations Terzaghi placed a flexible member across the opening and deflected it away from the sand. A minimum load approximately consistent with the weight implied by the half cylinder of sand which fell through the open "trap door" in the preceding case was obtained at a deflection of 1/73 times the smaller span. The load observed was found to be independent of the depth of sand above the structure (if this depth is greater than one or two times the relevant span of the structure) for depths less than approximately five times the span. For greater depths the load on the structure increased in proportion to the overburden.

Terzaghi also found that after the arch was established, it was not disturbed by subsequent percolation of water through the sand. These tests indicated additionally that vibrations (presumably of small amplitude and frequency) did not destroy the arching action.

If Terzaghi's classic trap door experiments (Ref. V-2.3) are evaluated in terms of the preceding discussion, a deflection of the top surface of the structure of the order of one percent of its span would produce a height of equal settlement equal to approximately five times the span and the overburden above the height of equal settlement would be resisted by the roof of the structure.

Another manifestation of arching is exhibited in the data presented in Ref. V-2.6. Here a series of static and dynamic tests of gages embedded in a urethane rubber compound (Hysol 8530/CH2) and in clay were conducted. The static and dynamic measurements were compared in each case to the gage response produced by air pressure applied to the sensing element (diaphragm) of the gage. Also the effects of gage orientation and of relative dimensions of the embedding cylinder to the dimensions of the gage were investigated. For this discussion the series of static tests using Hysol to study relative dimensions are most interesting. For the two smallest depth ratios (height of Hysol above the gage to diameter of gage which was 5/8 in.), the gages recorded stresses less than the stress applied to the end of the specimen, and for greater depth ratios, stresses which were greater than the applied stress. The amount by which the recorded stress exceeded the applied stress increased nearly uniformly with the increase in depth ratio up to the largest value of 6.1 used (Fig. V-2.3). This is consistent with the concept of height of equal settlement because if this height falls within the material above the structure (gage in this case) the stress on the structure increases in proportion to the overburden or to the surcharge. The observation that the smallest depth ratios produced measured stresses less than the applied stress does not agree with this concept. However, for the two smallest depth ratios, 0.20 and 1.3, the discrepancy could be attributed to a different distribution of stress in the specimen. This distribution could be caused by the shear acting along the top and bottom of the embedding cylinder causing a restraint to the lateral deformation of this cylinder, a contention supported by the marked dependence of stress on the diameter of the Hysol (Fig. V-2.3): the larger the diameter, the smaller the stress recorded by the gage. Such action has been observed many times in static axial compression tests especially where relatively large strains occur. This action could cause perturbations of the stress field in the vicinity of the gage if the gage is located near the loaded surface.

On the other hand, for the type of gage used in these static tests, significant arching of the load across the sensitive element of the gage could occur

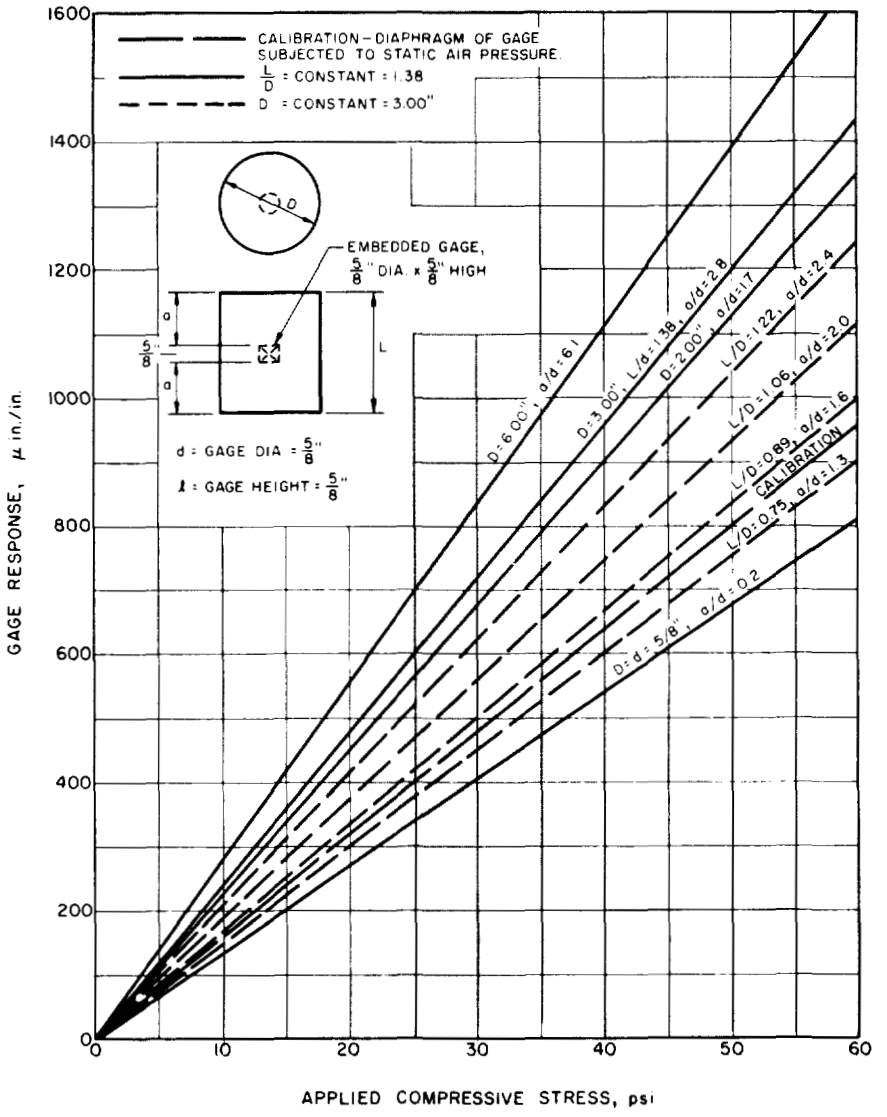

FIG. V-2.3 ARCHING AROUND STRESS GAGE EMBEDDED IN HYSOL 8530/CH2

especially for the smallest depth ratio (0.20) wherein the diameter of the cylinder of Hysol was equal to the diameter of the gage. The sensing element consisted of a thin brass diaphragm soldered across the end of a relatively rigid steel right circular cylinder. As the diaphragm deflects under the applied load, the load may be transferred to the relatively rigid wall of the cylinder. However, the dome of arching found in Terzaghi's experiments could not form in the Hysol since the thickness of material above the diaphragm was only 20% of the diameter. Here the dome probably formed partially in the Hysol and partially in the plate used to distribute the load across the surface of the specimen. Such action could be enhanced by the confining effect produced by shear on the face between the loading plate and the specimen mentioned above.

From the foregoing discussion it appears that static arching is a complex function of the deflections of the structure, the stiffening effect of the structure on the surrounding medium and the cohesion and internal friction of the soil. Precise formulation of the mechanism involved does not appear to have been accomplished although procedures adequate for static design have been advanced (Ref. V-2.4).

V-2.1.3 Structural Type

A qualitative effect of structural type on the static loads reaching the structure is implicitly included in the theory discussed in the preceding section (Ref. V-2.5). However, no direct quantitative data are given in Ref. V-2.5 for estimating the deformational characteristics of structures located directly in natural soil. These deformational characteristics can be measured by the compressibility of the structure relative to the soil replaced, yet the compressibility depends on the load reaching the structure which in turn depends on the compressibility. Mutual dependences of this type suggest a trial and error process in which a load is assumed and a compressibility computed from which a new load is computed. Yet computations of the height of equal settlement for a given structure is a particularly difficult problem since it depends both on the characteristics of the structure and on the characteristics of the surrounding soil. At the moment quantitative values related to either of these characteristics are not defined, but certain qualitative observations can be made.

Conventional rectangular structures can develop the incomplete ditch condition (Fig. V-2.2c) since parts of the roof (slabs) will be more flexible than other parts (beams and columns); thus the slabs deflect more than the beams and columns causing a reduction in load on the more flexible parts with corresponding increases on the more rigid parts.

Arches and domes are inherently more flexible, in flexure at least, than rectangular structures with the same plan area and proportioned for the same loads. Thus, arches and domes can deflect locally a sufficient amount to force the static loads to assume more uniform distribution. Furthermore the geometrical configuration of arches and domes coupled with their inherent flexibility causes an arch or dome to exist in the soil; this is especially apparent if it is recognized that the normal slopes of the cuts made to construct the structure are at an ideal angle to act as abutments of an arch formed in the backfill over the structure. From this consideration alone it would appear that in most cases the theory (Ref. V-2.5) summarized in the preceding section would constitute a lower bound for the amount of static arching to be expected over arches and domes.

For the vertically oriented cylinder the horizontal force produced by static load can significantly influence the behavior since at large depths the dead load can be even larger than the dynamic load. From formulas developed by Terzaghi (Ref. V-2.4) the stress distribution along the height of the surface of a flexible vertical cylinder can be related to the stress at an infinite depth in dry granular soil by assuming: (1) that a condition of plastic equilibrium exists in the soil in the vicinity of the cylinder; and (2) that the tangential stress in the soil is nearly equal to the vertical stress. The relation between these stresses (Fig. V-2.4) has the form:

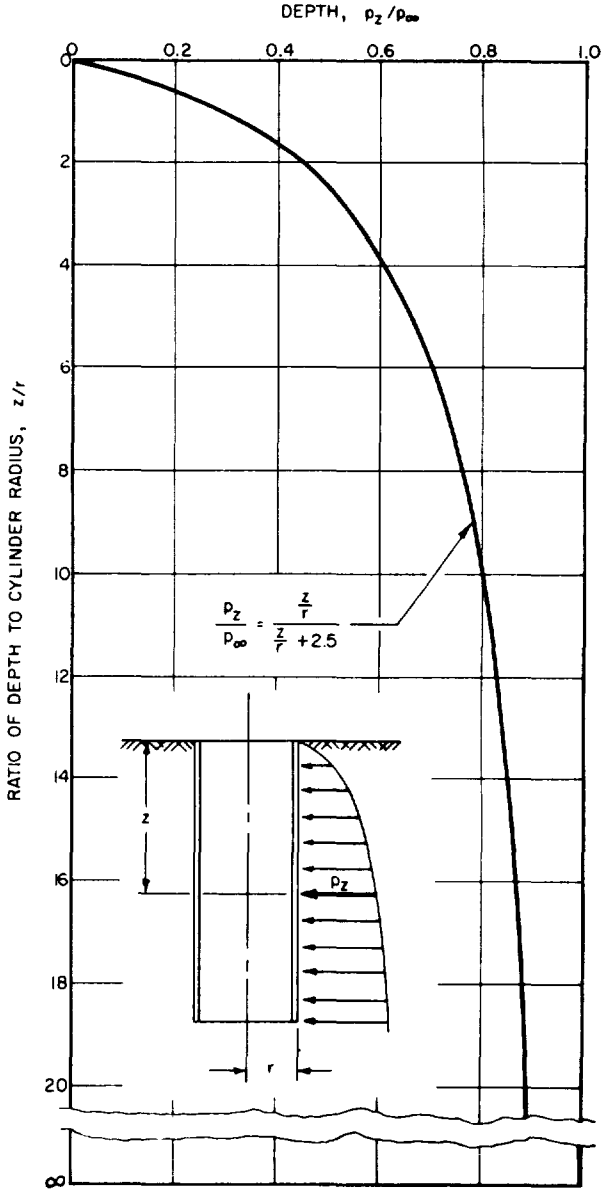

FIG. V-2.4 HORIZONTAL STATIC STRESS DISTRIBUTION AGAINST VERTICAL CYLINDER

$$\frac{p_z}{p_\infty} = \frac{z/r}{z/r + 2.5} \qquad \text{(V-2.6)}$$

where p_z = horizontal stress at depth z on a cylinder with radius r

p_∞ = horizontal stress at an infinite depth.

The horizontal stress at an infinite depth can be formulated in terms of the unit weight of soil w and the angle of internal friction φ. These relations are shown in Fig. V-2.5 which is an extension of a graph presented in Ref. V-2.4. These stresses, however, depend greatly on the construction procedures, and should not be used where the conditions of deformation during construction are not consistent with the assumption of the theory; i.e., the sand in the vicinity of the shaft is in a state of plastic equilibrium and that the shaft lining is relatively flexible.

V-2.1.4 Moisture Content

An additional problem which frequently must be considered as the depth of burial increases is the position of the water table in the soil. The depth to the water table may vary seasonally, and it is desirable to locate any buried structure above the water table. When a buried structure is constantly submerged the provision of effective waterproofing may prove to be the most difficult practical problem to be solved. Additionally the static loads in saturated soils are generally larger than those in non-saturated soils, particularly for vertical surfaces of a structure, because the stresses produced by water pressure are hydrostatic and increase linearly with depth below the water table. The stresses, in addition to the water pressure, caused by the submerged soil normally are small in comparison to the pressures induced by the water.

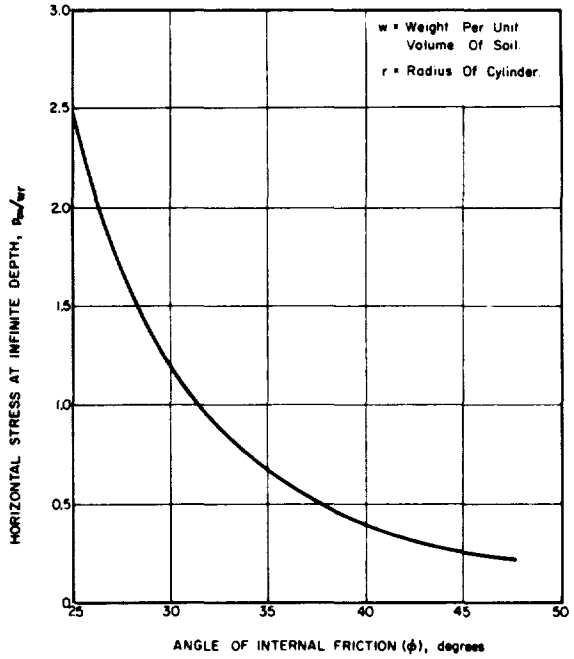

FIG. V-2.5 MAGNITUDE OF HORIZONTAL STATIC STRESS ON CYLINDER AT INFINITE DEPTH

V-2.2 LOADS PRODUCED BY BLAST

V-2.2.1 Effect of Structural Type

As discussed in Section V-2.1.2 the amount of arching appears to depend primarily on the compressibility of a structure relative to the compressibility of the soil replaced by the structure. Additionally, arches and domes geometrically force the soil above the structure to form an arch around the structure for static loads; a similar condition should also exist for blast loads. Consequently, the amount by which the blast load acting on the surfaces of a structure is reduced, can be influenced by the geometrical shape of the structure. However, there are insufficient data to indicate clearly what effect the shape of the structure has on the loads acting on it.

An attempt was made (Ref. V-2.7) to provide some insight into the effect of the structural shape on the stresses acting on a buried structure and the stresses in the medium adjacent to the structure. The conditions assumed are summarized in Fig. V-2.6. A complete derivation is given (Ref. V-2.7) based on the following assumptions:

(1) The circumferential strain in the medium in contact with the structure is equal to the circumferential strain in the structure.

(2) The medium is in a state of one-dimensional strain; i.e., only strains perpendicular to the ground surface exist.

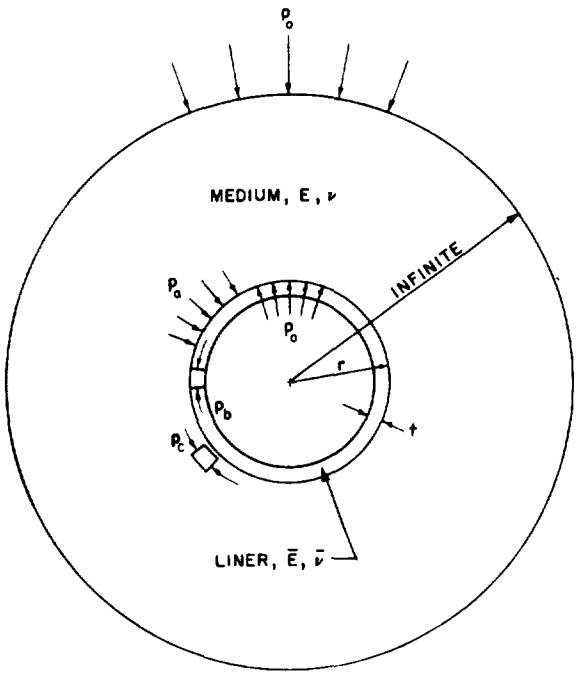

FIG. V-2.6 THIN LINER IN HOLE IN SOIL MASS

TABLE V-2.1 STRESS AND STRAINS AROUND LINED HOLES IN ELASTIC MEDIA

Stress or "Strain" Ratio	Structural Configuration		
	Vertical Cylinder	Horizontal Cylinder	Sphere
$\frac{p_o}{p_y}$	$\frac{\nu}{1-\nu}$	1	1
$\frac{p_a}{p_o}$	$\frac{\frac{1}{1-\nu}}{\frac{1}{1-\nu}+\gamma}$	$\frac{2}{\frac{1}{1-\nu}+\gamma}$	$\frac{\frac{3}{1+\nu}}{\frac{1}{1-\nu}+\frac{\gamma}{1+\overline{\nu}}}$
$\frac{p_c}{p_o}$	$2-\frac{p_a}{p_o}$	$2-\frac{p_a}{p_o}$	$\frac{\left(3-\frac{p_a}{p_o}\right)}{2}$
$\frac{\epsilon}{p_o}\cdot\frac{E}{1+\nu}$	$\frac{p_c}{p_o}-1$	$\frac{p_c}{p_o}-2\nu$	$\frac{p_c}{p_o}-\frac{3\nu}{1+\nu}$
$\frac{p_b}{p_o}$	$\frac{r}{t}$	$\frac{r}{t}$	$\frac{r}{2t}$

(3) The cylindrical liner is in a state of plane strain; i.e., the longitudinal strain vanishes parallel to the axis of the cylinder.

(4) The spherical liner is in a state of plane stress; i.e., the radial stress vanishes.

(5) The vertical component of stress in the medium at any point is p_y, including the effects of attenuation with depth.

Results of this study are summarized in Table V-2.1 where the following notation is used:

p_y = vertical stress in medium at depth y including effects of attenuation

p_o = horizontal radial stress in medium at large distances from structure; for practical purposes a large distance might be of the order of four times the radius

p_a = radial stress acting across the structure-soil interface

p_b = circumferential stress in liner

p_c = circumferential stress in medium adjacent to liner

ϵ = circumferential strain in medium or lining at structure-soil interface

E = modulus of elasticity of medium

ν = Poisson's ratio of medium

$\overline{E}$ = modulus of elasticity of liner

$\overline{\nu}$ = Poisson's ratio of liner

$\gamma = \frac{1-\overline{\nu}^2}{1-\nu^2}\frac{Er}{\overline{E}t}$ = relative stiffness of medium and liner

r = radius of liner; radius of great circle for spherical liner

t = thickness of liner.

The relations summarized in Table V-2.1 are believed to represent qualitatively the distribution of stress and displacements (as measured by the strain ϵ since, for the conditions considered, radial displacement equals $r\epsilon$) for buried cylinders and spheres under dynamic loading. It is restricted to dynamic loading primarily because the soil under these loads probably does not have the time to creep significantly or experience sizable plastic deformations.

Symmetrical and Unsymmetrical Components of Loading. It is apparent that the soil surrounding a buried structure significantly stiffens it. If a sufficient amount of soil cover over the structure is provided, the structure will not deform antisymmetrically even though the loading may be highly antisymmetrical during the envelopment. When a structure is completely exposed, pronounced antisymmetry in loading develops, and the over-all structure is subjected to a net force which acts in the direction of shock propagation. However, for buried structures this translational force acts on the soil and not directly on the structure. If the extent of the soil cover over the structure is sufficient, the forces reaching the structure can be mitigated by two primary effects: (1) The soil cover effectively streamlines the structure reducing the drag coefficient*; and (2) forces acting on the surface of the soil can be partially resisted by shear developed in the surrounding soil mass before reaching the structure.

These effects are illustrated qualitatively in Fig. V-2.7. Here, only the forces on the windward face are illustrated. However, a similar effect develops on the leeward face of the soil cover except that no reflected pressures develop and the side-on overpressure acts in a direction opposite to the drag. Although shock tube studies apparently have not defined the variation in reflection coefficient† with angle of incidence for all angles of incidence**, it is apparent that the reflection coefficient becomes small as the slope of the soil mound (tan α in Fig. V-2.7) becomes small. For α equal to 90° the drag coefficient becomes large, sometimes as high as 1.0 to 2.0; however, the drag coefficient is reduced as the shape of the earth mound approaches that of a cylinder. For a cylinder the drag coefficient may be of the order of 0.3 to 1.0 or more (with higher values applicable to high overpressures) while it becomes zero if there is no projection above the surface of the ground. (For a discussion of reflection and drag coefficients, see Ref. V-2.8). Thus, placing soil around a surface structure may reduce the forces acting on the structure directly. Also from the geometry shown in Fig. V-2.7, it is apparent that the forces associated with diffraction and drag on the surfaces of the mound can refract into the soil ahead of the structure thereby reducing the loading on the structure enclosed by the soil.

*The drag coefficient is a number which is multiplied by the dynamic (q) pressure in air produced by particle velocity to determine the drag pressure on a given configuration exposed to the "blast wind." It depends on the shape of the element and upon the Reynolds number primarily.

†The reflection coefficient is a number which is multiplied by the overpressure to determine the diffraction pressure acting upon an obstacle in the path of the airblast.

**That is, the observed variation of reflection coefficient with angle of incidence in the region of angles of incidence around 45° is subject to large scatter. The results are much more smooth and repeatable between tests for angles of incidence outside this region.

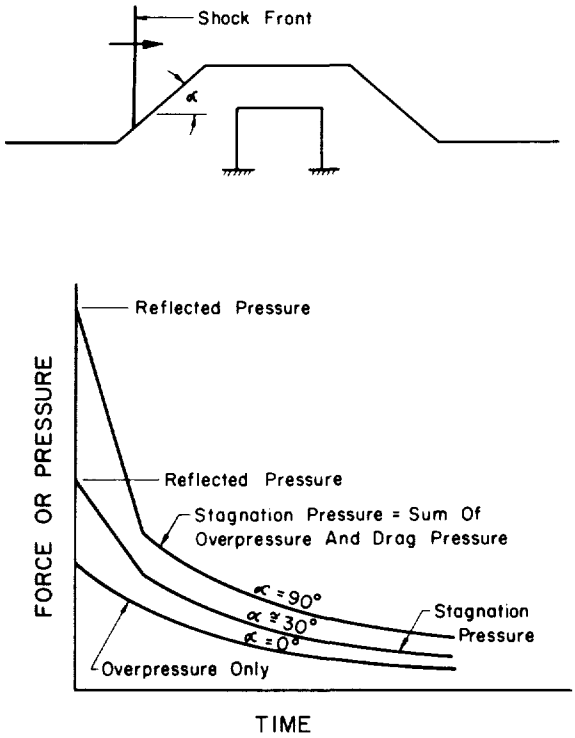

FIG. V-2.7 PRESSURES ACTING ON WINDWARD FACE OF SOIL MOUNDED OVER A STRUCTURE

Results of field tests and subsequent theoretical analyses show that, for configurations of earth cover at least meeting the criteria summarized in Fig. V-2.8, the type of action postulated in the foregoing actually develops. These studies indicate further that even though translational forces may reach the structure, significant antisymmetrical deformation of the fully buried structure (with cover requirements meeting or exceeding those shown in Fig. V-2.8) does not develop. These antisymmetrical deformations appear to be impeded by the resistances mobilized in the soil, as well as by the tremendous surcharge imposed by the side-on overpressure.

Before discussing the theoretical analyses some comments relative to the origin and evolution of Fig. V-2.8 are in order. The configuration of the mound placed over structures to streamline them as well as to provide radiation protection has been studied almost continuously in field tests since Operation Greenhouse (1951). The shape and amount of cover has varied between tests. Probably the first attempt was made in Ref. V-1.36 to specify a general design rule to be followed in constructing mounds to obtain essentially fully-buried conditions. This general rule was established by studying the observed response of the structures tested in the field and by speculating on the amount of additional cover which might be required to essentially eliminate the antisymmetrical deformations observed in the tests.

Initially a slope of 1 on 3 was specified for the minimum cover; subsequent speculation resulted in increasing the maximum slope to 1 on 4. Also for radiation protection additional cover beyond the minimum might be required which dictated the addition of "Region A" (Fig. V-2.8). Allowing a greater slope (to 1 on 2) in "Region A" was consistent with the hypothesis that the earth mound must streamline the enclosed structure since increasing the slope in "Region A" did not produce a sharp discontinuity in the earth contour. It is emphasized that the recommendations (Fig. V-2.8) were initially suggested as design rules based on extrapolations of field data and some correlative data from shock tube studies (Ref. V-2.9). Subsequent analyses have indicated that the design rules for full burial are reasonable.

For depths of cover less than those portrayed in Fig. V-2.8 the behavior of buried structures is not clearly defined. The empirical data indicate that some antisymmetrical deformations develop if the extent of fill over the structure is less than that defined herein. The procedure normally used to design such structures (Ref. V.1) requires estimating the forces acting on the partially buried structure by linear interpolation between the forces which exist when the structure is completely exposed and the forces which exist when the structure is fully buried.

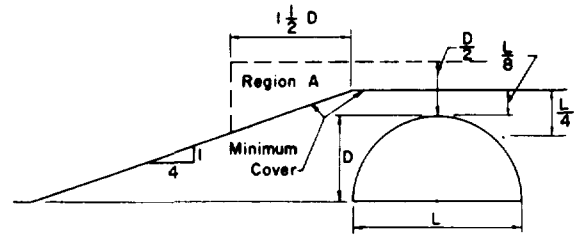

(a) Arch or Dome

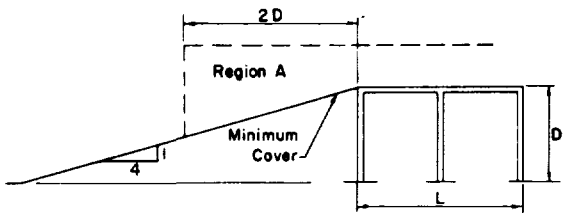

(b) Rectangular Structure

In Region A, maximum slope permitted is 1 on 2. Elsewhere no limitations apply, except cover must be greater than minimum shown.

FIG. V-2.8 DEFINITION OF FULL COVER

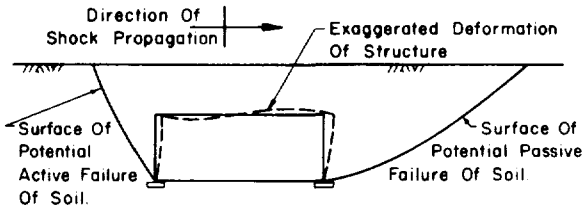

FIG. V-2.9 POTENTIAL SURFACES OF FAILURE IN SOIL SURROUNDING A STRUCTURE

Rectangular Structures. In Fig. V-2.9 are shown the translation and potential planes of failure in the surrounding soil produced by airblast-induced ground motion. The primary mode of failure observed in exposed retangular structures without earth cover occurs as a result of the translation pictured in Fig. V-2.9. For a completely buried structure, however, this mode of failure appears unimportant because the structural deformations immediately mobilize sizable passive resistances in the surrounding soil to prevent such deformation (by inference from the discussion below of the behavior of arches). Consequently the translation is not critical in defining the moments and stresses for which the overall frame must be designed; in a buried rectangular structure it seems only necessary to consider the loading on the individual parts in analysis. These loads in turn are those produced directly by the blast-induced stresses reaching the element because the passive pressures induced in the soil generally are small compared to the dynamic stresses and because the passive pressures normally are short in duration lasting approximately only as long as it takes the wave to traverse the structure.

Arches and Cylinders. The potential planes of failure induced by deformation of an arch or cylinder while the wave is enveloping the structure are much more complex than those shown in Fig. V-2.9 because of the curved surfaces which contact the soil. Nevertheless a condition of passive pressure must also develop for these configurations as the wave envelops the structure. In Ref. V-2.10 potential failure planes similar to those shown in Fig. V-2.9 were assumed, with the plane of failure intersecting the springing line of the arch. The analyses performed on the basis of this assumption are qualitatively consistent with experimental observations in the field (Refs. V-2.11 and V-2.12).

The analyses (Ref. V-2.10) assume that the arch may be replaced by a series of four straight-rigid bars (Fig. V-2.10). Mass, flexural stiffness, and applied forces (including restraint of the soil) were concentrated at the intersection of each pair of bars. The overpressure was applied to the surface

of soil above the arch, and initially it was treated as being equivalent to a surcharge* on the classical wedges of active and passive states of plastic equilibrium in the soil (cf. Fig. V-2.9). However, the overpressure was considered to propagate along the surface with a velocity corresponding to the air-shock velocity and to build up and decay following the ideal waveform (cf. Part II). Comparisons (Ref. V-2.10) of the results of the analyses with the observed behavior (Refs. V-2.11 and V-2.12) indicated that the overpressure could not have been equivalent to surcharge; that is for this model to predict the observed deformations of the arches tested, the surcharge had to be reduced below the value of overpressure throughout its time history. This result could indicate that the model does not represent the actual structure reliably or that the overpressure is, in fact, not fully effective in producing the conditions of plastic equilibrium in the soil, a condition which seems tenable in that the overpressure (varying with time) must change the resistance in the soil from classical "at rest" to plastic equilibrium conditions.

Airblast-induced stresses were assumed (Ref. V-2.10) to propagate in the soil at the seismic velocity (dilatation). Various values of the ratio of horizontal to vertical induced stress were assumed in the general studies presented.

In Ref. V-2.13 the model discussed immediately above was used to study specifically the response of the structures in the field test (Refs. V-2.11 and V-2.12). Although a consistent set of results (Table V-2.2) between the model and prototype were obtained using reasonable values of the parameters as summarized below the table, Whipple notes several conditions which do not match the properties of the model:

(1) The arches were short relative to their diameter so that the end bulkheads could significantly stiffen the arch rib.

(2) Accelerometers attached to the footings of some structures indicated significant motions while the model assumes footings immovable. (The test data in Table V-2.2 are adjusted by subtracting the footing motion directly from the deflections of the arch.)

(3) The model assumed pinned supports of the haunches while the test structures may have developed some restraint at the springing line.

Despite these discrepancies the analyses indicate that the model can be adjusted using reasonable values of the parameters to reproduce the observed behavior.

*The surcharge would be the hypothetical weight of soil acting at the surface producing the same vertical stress as the overpressure.

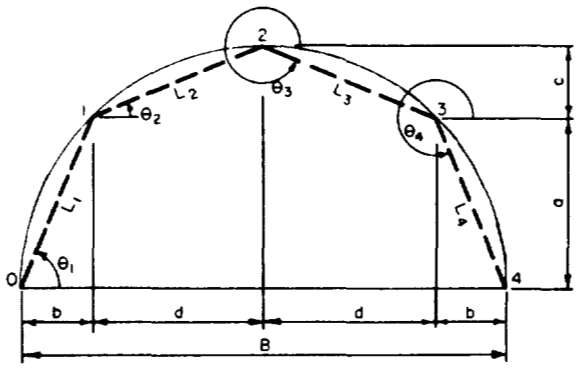

FIG. V-2.10 MODEL CONSIDERED IN ANALYSIS (REF. V-2.10)

Prevention of disastrous flexural deformations by unity of action between circular structures and soil indicates that these configurations can be much more flexible than rectangular structures for which large flexural resistance is inherent because of the action of the individual elements. The flexibility of arches also suggests a hazard which might develop in arched or cylindrical structures: the reduction in flexural stiffness in the member may induce buckling phenomena. However, a brief study conducted by Duberg (Ref. V-2.14), using a model of the same type as Whipple's (Ref. V-2.10) and similar assumptions pertaining to the behavior of soil, suggests that elastic buckling is improbable for practical structures buried sufficiently deep to inhibit flexural deformations produced by the stress wave enveloping the structure.

Domes. In general a dome will be approximately only half as thick and hence only half as stiff as an arch of the same major span and proportioned for the same loading. This increased flexibility should magnify the mobilization of resistance in the surrounding soil of the type discussed for an arch. That is, the resistance mobilized in the soil opposing antisymmetrical deformations in a dome should be greater than that developed in a corresponding arch. If sufficient cover is provided to mobilize the magnitude of the soil resistances required, then a dome should respond primarily as though it were acted upon by a uniform pressure all around at any instant of time. Greater flexibility in a dome should also magnify the tendency toward elastic buckling, but it would appear such buckling is improbable for practical structures.

Domed configurations located entirely below the ground surface have been included in some early field tests (Greenhouse and Jangle). These were precast structures consisting of relatively rigid concrete panels bolted together at intervals, and by virtue of this construction they are very difficult to analyze. However it is important to note that none of the precast domes buried below the surface experienced significant deformations.

TABLE V-2.2 COMPARISON OF MEASURED (REFS. V-2.11 AND V-2.12) WITH COMPUTED DEFLECTIONS (REF. V-2.13) OF ARCHES

	Inward Radial Deflection of Crown, ft.	
	Test*	Calculated†
Reinforced Concrete Arch	0.098	0.101
Corrugated Steel Arch	0.166	0.163

*Adjusted by subtracting the deflection of the floor from the deflection of the crown.

†Input Parameters:

Seismic velocity of soil = 3000 ft/sec

Unit weight of soil = 100 pcf

Cohesionless soil with angle of internal friction of 30°.

Friction angle between soil and arch = 20° (Concrete arch) = 10° (Steel arch)

Ratio of horizontal to vertical stress induced in the soil = 0.15

"Coefficient of pressure at rest" = 0.50

Overpressure = 130 psi (measured)

Ratio equivalent surcharge to overpressure = 0.11 (Concrete arch) = 0.12 (Steel arch)

V-2.2.2 Effect of Pulse Length and Source of Loading

Laboratory investigations (Ref. V-1.30 for example) related to the problem of determining the effect of density and stiffness of a model structure (or gage) have involved loading statically the soils in which these gages were embedded. These studies have progressed with extreme difficulty because of problems encountered in reproducing the properties of the soil from test to test. Yet an important conclusion (Ref. V-1.30) has been obtained which is that thin pressure cells which are volumetrically stiffer than the soil, such as Carlson cells, actually measure approximately the stress truly existing in the medium. The actual magnitude of the error is at the moment indeterminate.

Dynamically a similar situation might develop since small gages and structural models are enveloped by the shock so rapidly that reflections are cancelled as nearly as quickly as they develop by the gage's being "carried along with" the soil. That is, an imminent reflection would tend to drive the gage into the soil beyond it. This soil would be in motion a short time following the onset of the reflection. The gage or small structure in turn in "catching up" with the moving soil would effectively cancel the reflected stress.

In Table V-2.3 empirical data obtained from tests of structural models are summarized; these data with other similar results also are shown in Fig. V-2.11 (Ref. V-2.15). Not all of the data shown in the figure are included in the table because only the information in the table was investigated (Ref. V-2.15) to determine the consistency of the structural motions with the stresses acting on the structure. Investigation of this consistency was not possible for the other cases because sufficient data generally were not obtained in the test to permit the analysis to be made. The analyses were performed assuming two limiting conditions: zero and infinite stiffness of the soil beyond the structure. In every case the computed deflection of the front (loaded) wall of the structure relative to the supports of the wall using the measured stress to define the loading and zero soil stiffness was compatible with the measured relative deflection. Since this is the lower bound solution for relative deflections and since the stiffness of the soil should be nearer the lower bound, it would appear that the measured pressures on the structure are approximately correct.

Although it varies, the empirical ratio of the stress on the structures (most of which were located in the crater) to the approximate stress in the medium is consistently much greater than two, which is the maximum value consistent with Eq. V-1.7 from consideration of acoustic impedance. Unlike the case of the small gages imbedded in soil, however, these data indicate a reflection of stress at the interface.

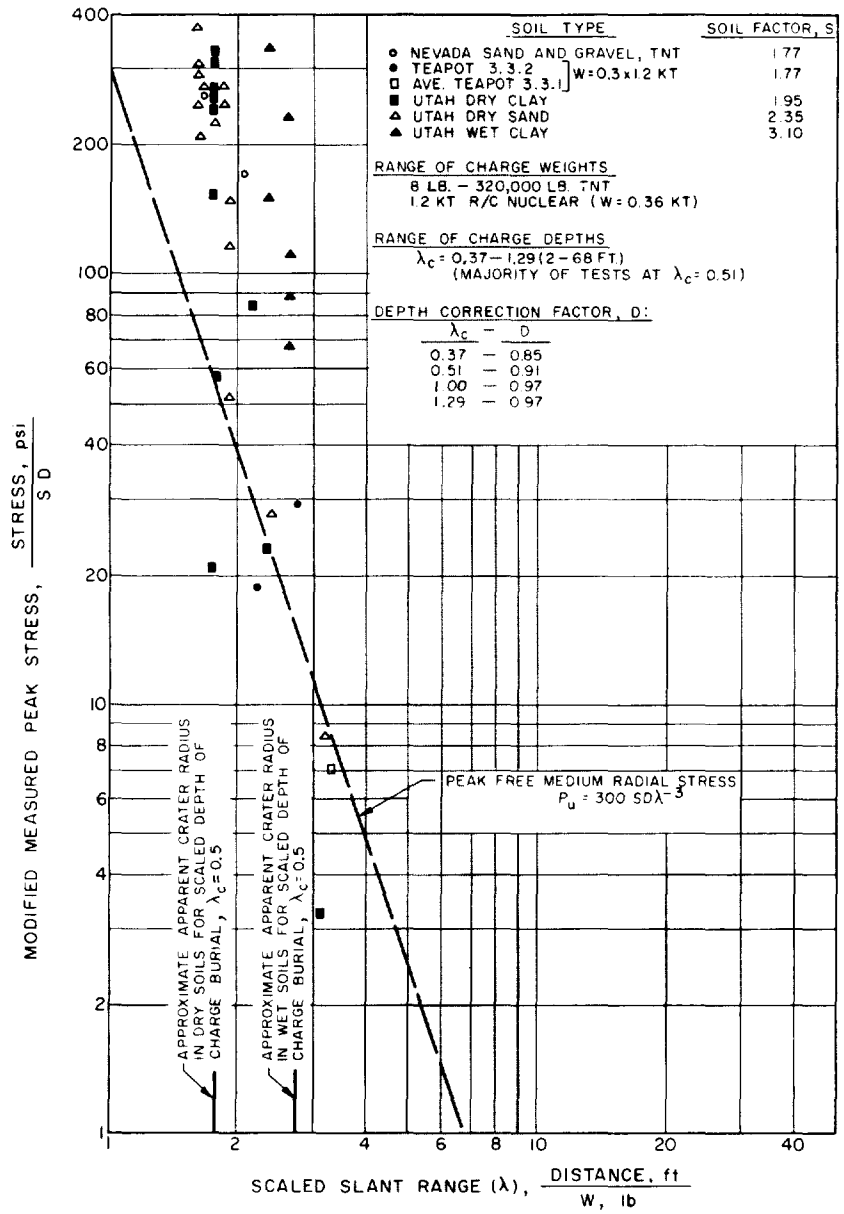

FIG. V-2.11 COMPARISON OF STRUCTURE AND RADIAL MEDIUM STRESSES

A logical explanation of this reflection is indicated in Fig. V-2.11. In this figure the vertical scale has been normalized by the apparent radius of the crater* in an attempt to eliminate the effect of the soil type and to compare all data on a single plot. A yield (total energy) equivalence between nuclear and HE of 0.3 as noted in the legend was used to reduce the nuclear data for direct comparison to HE. This equivalence was determined (Ref. V-2.15) by comparison of crater radii following the method presented in Ref. V-1.3. Use of apparent crater radius to normalize the data has been justified empirically (Ref. V-1.23). The approximate apparent crater radius has been superposed on Fig. V-2.11 for the two basic types of soil: "dry" or "wet." The true crater radius is larger than the

*The crater radius (Ref. V-2.15) was defined by the product of two factors. S = soil factor and D = depth correction factor which depends on scaled charge depth λ_c. Thus D is a normalized curve defining crater radius as a function of λ_c and S is the normalizing factor for each soil type.

TABLE V-2.3 COMPARISON OF APPROXIMATE CONDITIONS IN MEDIUM WITH CONDITIONS ON STRUCTURES TESTED IN UET PROGRAM

Structure Number	Approximate Peak Radial Stress in Medium (psi)	Approximate Peak Stress on Structure (psi)	Ratio Structure Stress to Medium Stress	Approximate Length of Pulse (ft)	Length of Structure (ft)
DRY SAND PROGRAM ($c \cong 1500$ ft/sec)					
2Aa 108	150	700	4.7	8	5.00
2Ab 109	150	820	5.5	9	8.33
2Aa 111X	90	300	3.3	13	5.00
2Aa 106	150	631	4.2	6	5.00
2Ab 107	150	454	3.0	10	8.33
2Aa 104	130	850	6.5	7	5.00
5Aa 114	150	670	4.5	13	12.5
5Aa 112	160	700	4.4	13	12.5
DRY CLAY PROGRAM ($c \cong 3000$ ft/sec)					
2Aa 405S	100	320	3.2	27	5.00
2Aa 406X	100	500	5.0	27	5.00
2Ab 308	100	725	7.3	52	8.53
10Aa 319	100	428	4.3	102	25.0
WET CLAY PROGRAM ($c \cong 5000$ ft/sec)					
2Aa 405	70	300	4.3	50	5.00

apparent one. Consequently it may be inferred that all of the structural models exhibiting large reflection coefficients for the loaded face were located within the true crater. This implies that the loading was produced by airblast and not by stress waves propagating through the soil. Since the maximum theoretical reflection coefficient for airblast striking a rigid object is eight (or more), the reflections indicated in Table V-2.3 also support the inference drawn. On the other hand, for those structures located outside the crater it would appear that the average stress on the structure was nearly equal to the radial stress in the medium.

On the other hand it may be argued, on the basis of the comparison of the length of pulse and the length of the structure in Table V-2.3, that impeded motion of the structure during the early phase of loading caused a major increase in the pressure acting on the loaded face. There are not sufficient data to reconcile these observations, but it is believed that the airblast argument is more tenable than the possible lack of rigid body motion.

In many of the field tests the fireball has intersected the ground surface. Thus, much of the empirical data include a superposition of the airblast- and directly-induced effects although in many of the tests the height of burst probably was sufficient to subordinate the directly-induced effects. Assuming that damage to a structure is inherently related to the stresses existing in the medium in the vicinity of the structure allows using a direct comparison of the airblast- and directly-induced stresses to evaluate the importance of each type of stress in causing damage. Damage to a structural element depends directly on the peak intensity and effective duration of force acting on it. Therefore, by comparing the peak intensity and duration of stress in the free field caused by: (1) A burst condition where airblast-induced stress predominates; and (2) a burst condition where the directly-induced effects are maximized, the critical condition for the structure becomes apparent. This can be accomplished by utilizing airblast data obtained by measurements from nuclear bursts on the surface and in air and stresses measured below ground from buried nuclear bursts. Use of the airblast data assumes that the stress induced in the medium is equal to the overpressure. Near the surface this should be nearly correct for soils with seismic velocity less than the average air-shock velocity for the pressures of interest. Comparisons are shown in Figs. V-2.12 and V-2.13 between the intensity and duration of side-on overpressure produced by detonations at different heights of burst in Yucca Flat. The effects for airbursts were constructed from data given in Ref. V-1.24 while the data for overpressures from particular bursts were obtained from the several reports summarizing measurements from the Jangle and Teapot Operations. (Notably Refs. V-2.16 and V-2.17).

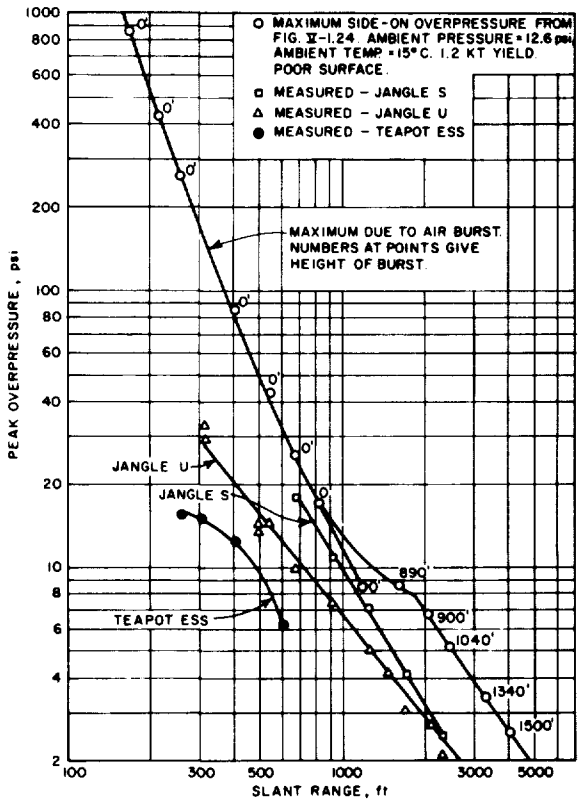

FIG. V-2.12 MAXIMUM SIDE-ON OVERPRESSURE PRODUCED BY SEVERAL DETONATIONS AT YUCCA FLAT

The data from airbursts in Figs. V-2.12 and V-2.13 were selected on the basis of the maximum overpressure produced at a given range from the surface zero (the point on the ground surface vertically below the point of detonation). Therefore, this curve is a composite of data from detonations at various heights of burst which causes the unusual cusp at approximately 1900 ft slant range; this cusp, in this case, is not a real phenomenon. To illustrate the magnitude of overpressures produced by a zero height of burst, the curve was extended to a slant range of 1200 ft. Beyond this range, the curve constructed from data in Ref. V-1.24 approaches the Jangle S data asymptotically. These figures graphically illustrate that the overpressure is a maximum for surface bursts while the positive phase duration is comparable for the bursts considered within the range of interest for buried structures (above approximately 30 psi). In addition they show, as would be expected, that the part of the mechanical energy producing airblast is diminished for buried charges. On the assumption that the intensity of airblast-induced ground motion varies directly with the intensity of overpressure, Figs. V-2.12 and V-2.13 suggest that a surface burst might be more critical than an underground burst in causing damage to a structure located in soil with a seismic velocity less than the average air-shock velocity. At least, for horizontal surfaces of structures located near ground surface the airblast-induced stresses should prove to be more critical than the directly-induced stresses since the proximity of the free surface will diminish the vertical component of compressive stresses from the directly-induced wave.

For vertical elements of structures near the surface, a comparison is needed of the horizontal stresses induced by airblast with the horizontal stress produced by airblast and directly-induced effects in combination. To make such a comparison requires a specification of the magnitude of maximum horizontal stress produced by airblast. Study of the data in Refs. V-1.12 and V-1.13 indicates that, for the dry-granular soil common to Frenchman and Yucca Flats at the Nevada Test Site, the maximum horizontal stress induced by airblast (at depths of 20 ft or less) is approximately one-quarter of the maximum overpressure. This factor was employed in constructing the curve shown in Fig. V-2.14 from the similar curve in Fig. V-2.12. In addition Fig. V-2.14 shows the pressures in the soil measured by neoprene-bags in Aquagel at depths ranging from 10 to 68 ft and the radial horizontal stresses measured by Carlson gages at a depth of 10 ft. Finally, Fig. V-2.14 contains the overpressure-slant range curves for the specific nuclear bursts in Fig. V-2.12 for direct comparison with the stresses measured in the medium.

Several interesting effects are apparent in Fig. V-2.14:

(1) The neoprene bags in Aquagel measured pressures in the Jangle S detonation which were 0.1 to 0.6 times the overpressure.

(2) The neoprene bags in Aquagel, on an average, measured a pressure essentially equal to the overpressure in the Jangle U detonation.

(3) The Carlson cells buried in soil measured stresses which at small slant ranges were larger while at large slant ranges were smaller than the overpressure.

(4) On the basis of the average measurements from the surface and underground detonations, the peak radial stress in the medium was comparable to the hypothetical stress computed from one-quarter of the maximum overpressure produced by surface or airbursts.

The observation that the neoprene bags in Aquagel measured pressures of the order of the overpressure in the actual detonations might be a result of the overpressure inducing a nearly equal stress in the fluid column including the gage; that this be the case however is not clear in the records because of difficulty in distinguishing the effect of the directly-induced stress. On the other hand, the lack of a consistent pattern showing a definite attenuation with

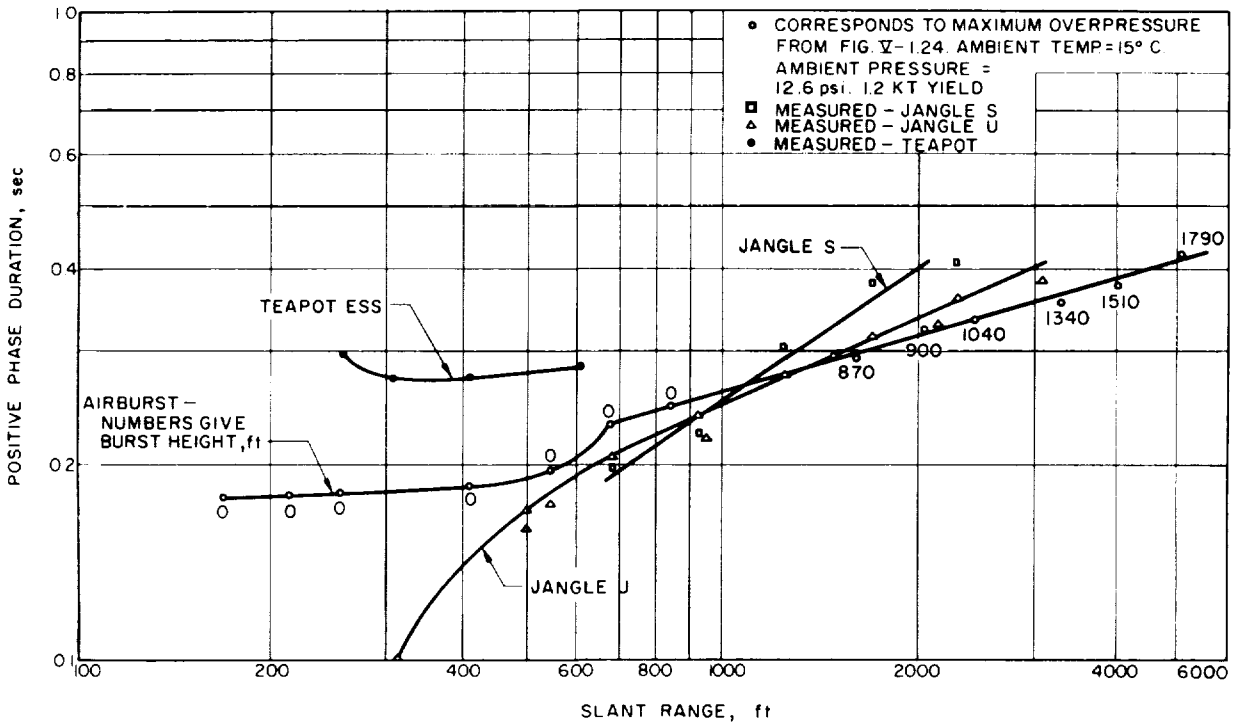

FIG. V-2.13 POSITIVE PHASE DURATION OF OVERPRESSURE FOR SEVERAL DETONATIONS AT YUCCA FLAT

depth in the data from gages at the same location but at different depths supports the hypothesis that a uniform stress was developed in the fluid column. In the Teapot ESS detonation the fact that the smaller slant ranges showed stresses larger than the overpressure might be explained by the near superposition of the airblast- and directly-induced stresses since at small slant ranges the arrival of the stresses of both types occur more nearly simultaneously than at large slant ranges. Although the values compared bear no real relation to one another, the fourth observation is important since it illustrates for the depths and soil type considered that the radial stress in the medium produced by airblast and direct effects combined is normally not greater than the overpressure and can be a relatively small fraction of the overpressure.

Since structural response is a function of both the intensity and duration of stress, it is also necessary to investigate the duration of the radial underground stress. Figure V-2.15 shows a comparison of measured durations of radial stress with positive phase duration of overpressure. An assumption that the airblast- and directly-induced horizontal stress near the surface would have a duration comparable to the positive phase duration of overpressure is supported by Figs. V-2.13 and V-2.15.

Where the seismic velocity of the medium greatly exceeds the average air-shock velocity, the directly-induced effects predominate. The maximum radial stress in a granite with seismic velocity of 12,000 ft/sec are compared with overpressure in Fig. V-2.16. These are compared directly based on the assumption (supported by the Boussinesq solution, cf. Section V-1.3.1) that the maximum radial stress induced by airblast cannot exceed the magnitude of the overpressure. Stresses in the medium are based on equations derived in Ref. V-1.17 by fitting equations to the data presented in Ref. V-1.25 and by specifying the energy equivalence between high explosive and nuclear charges from data obtained in the contained detonations in tuff (Ref. V-2.18). These data and equations are presented in Part IV of this book. The curve for overpressure was constructed from data summarized in Ref. V-1.24.

In Fig. V-2.16 it is apparent that the directly-induced effects predominate at high pressure levels if it is recalled that the radial stress induced by airblast cannot exceed the overpressure and that the seismic velocity of the medium exceeds the average air-shock velocity.

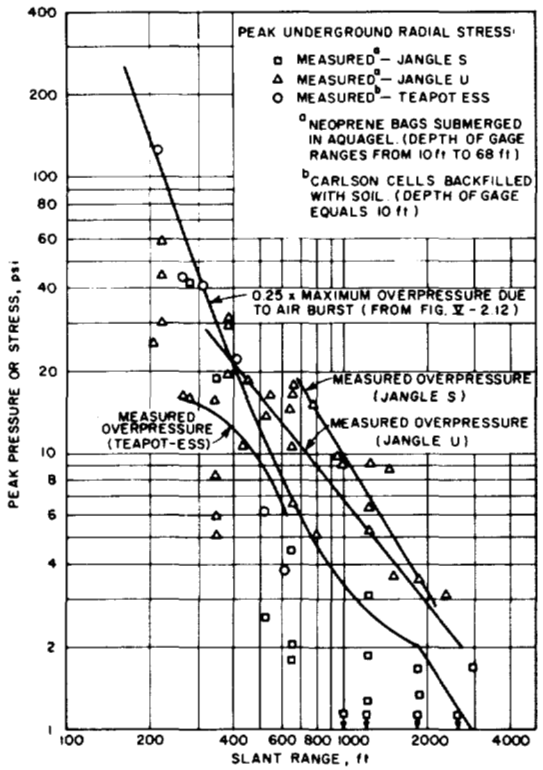

FIG. V-2.14 UNDERGROUND PRESSURES OR STRESSES MEASURED AT YUCCA FLAT

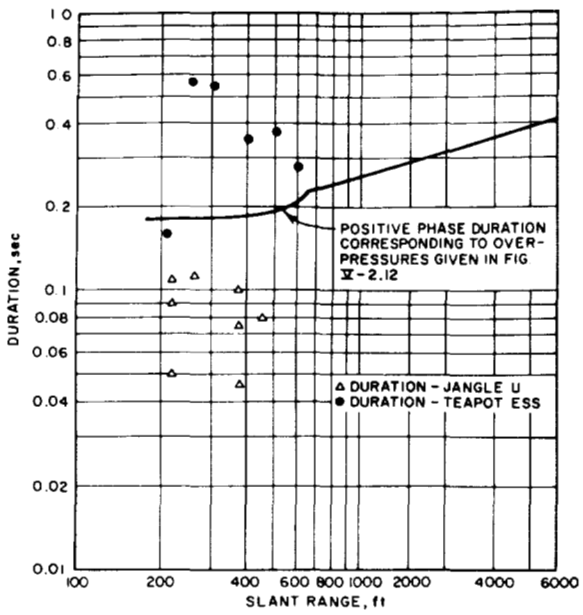

FIG. V-2.15 DURATION OF UNDERGROUND RADIAL PRESSURE OR STRESS MEASURED AT YUCCA FLAT

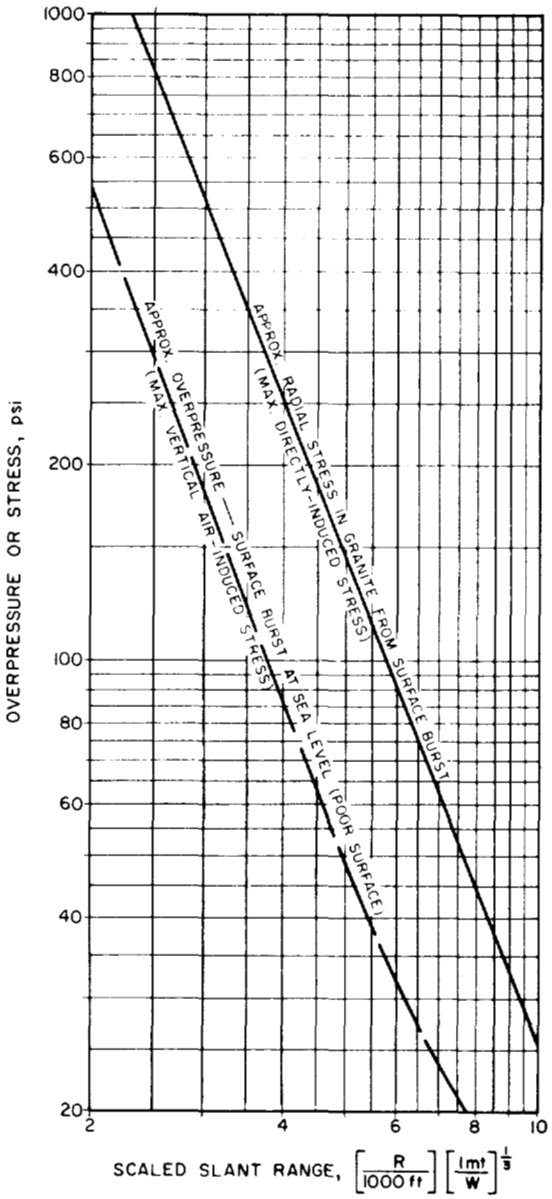

FIG. V-2.16 COMPARISON OF MAXIMUM DIRECTLY-INDUCED AND AIRBLAST-INDUCED STRESS FOR GRANITE

V-2.2.3 Arching

Dynamic arching, among other factors, probably depends upon the relative wavelength of the stress wave and length of the structure in the direction of stress wave propagation. If the structure is long compared to the wave length of the stress wave, the structure tends to remain stationary, and negative arching may develop. On the other hand a short structure relative to the length of the pulse probably would ride along with the soil, and arching effects on the overall structure may be small. For

that matter any structural characteristic which causes the structure to remain relatively stationary compared to the soil surrounding it may cause negative arching on the loaded elements. At the other extreme, if the structure can be forced by some means (such as by under-design of the foundations) to move away from the soil that is producing contact forces on it, positive arching may be enhanced. Positive arching also may be enhanced when certain parts of the structure are more flexible than other parts; here arching may occur across the more flexible parts causing increased loads on the more rigid elements.

Thus, whether the loading is static or dynamic, arching depends upon deflection of the loaded elements. For dynamic loads the initial deflection doubtless is caused by the stress wave striking the element. Thereafter a complex redistribution of stress occurs both in the medium and in the structure. The mechanism of redistribution is not understood, but it may not be of practical importance since to develop arching it is only necessary that deflections occur in the structure.

Theory. On the premise that structural deflections of some undefined magnitude exist in an element of a buried structure, extensions of concepts originally postulated by Terzaghi (Ref. V-2.4, Chapter X) qualitatively suggest a means by which arching may occur under dynamic conditions. These extensions were accomplished partially under the current contract and partially in another study (Ref. V-2.7). The complete derivation is given in Ref. V-2.7; thus only a summary is presented here.

A first look at the analyses summarized below may indicate that the phenomena apply to both static and dynamic arching; however as derived, it is believed to be more appropriate in explaining the dynamic case since it neglects the overburden of soil on the assumption that it is small compared to the overpressure existing on the surface. (An overburden producing the same magnitude of stress as the overpressure would normally be of the order of a hundred feet of soil fill on the surface.)

As shown in Fig. V-2.17, the deflection of the structure u_o causing the arch to develop in the soil produces planes of potential failure of the soil above the roof. The shearing forces τ acting along the planes of failure were assumed to be related to the relative movement u acting across the failure planes (Fig. V-2.18). Two cases were postulated: (1) the relative movement at some level above the roof is greater than some multiple α of the span L of the roof; and (2) the relative movement u was less than αL (From Terzaghi's results α would be of the order of 1%). In turn the relative movement u was assumed to vary exponentially between the surface and the roof (Fig. V-2.19).

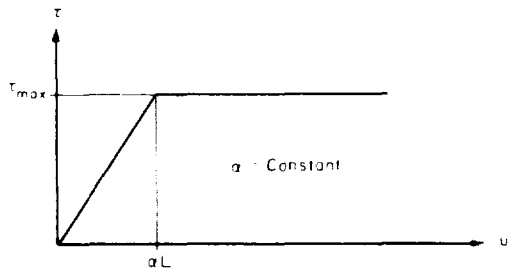

FIG. V-2.18 ASSUMED VARIATION OF SHEARING STRESS VERSUS DISPLACEMENT

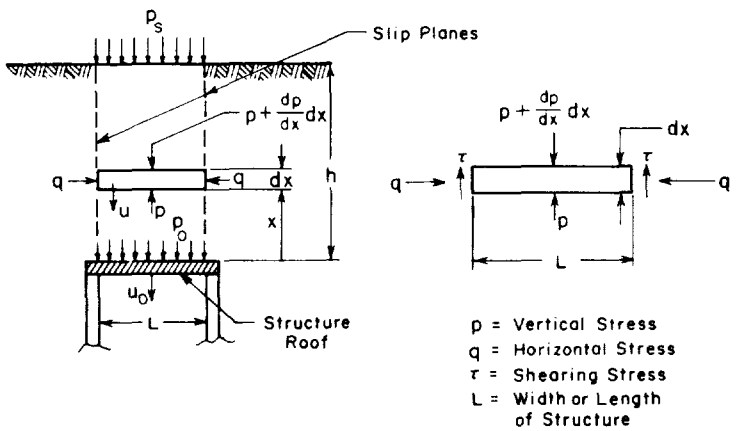

FIG. V-2.17 FORCE FIELD ASSUMED FOR UNDERGROUND STRUCTURE

From equilibrium of the element (Fig. V-2.17) the following equations are determined:

$$p = \frac{A}{B}(e^{\theta} - 1) + p_o e^{\theta} \qquad \text{(V-2.7)}$$

and

$$\theta = \log_e \frac{A + Bp}{A + Bp_o}$$

θ = Bx for Case 1: $u > \alpha L$, $\tau = \tau_{max}$

$$\theta = \frac{Bu_o}{\alpha\beta}\left(1 - e^{-\frac{\beta x}{L}}\right) \qquad \text{(V-2.8)}$$

for Case 2:

$$u \leq \alpha L, \quad \tau = \frac{u}{\alpha L}\,\tau_{max}$$

where p = vertical stress at any depth

p_o = vertical stress acting on roof of structure

e = base of natural logarithms (2.718....)

τ = shear stress at any depth

τ_{max} = limiting shearing stress

x = vertical coordinate measured from roof of structure

u = displacement at any depth

u_o = displacement of roof

β = constant for decay of displacement

α = limiting value of constant defining displacement at which shear failure occurs in soil

$A = \frac{c}{R}$

c = cohesive strength of soil

R = ratio of area of roof of structure to perimeter of roof lying between assumed planes of slip (Fig. V-2.17)

$B = \frac{K \tan \varphi}{R}$

K = ratio of horizontal to vertical stress in soil (q = Bp in Fig. V-2.17)

φ = angle of internal friction of soil

A qualitative comparison of the relative values of Eq. V-2.7 and V-2.8 (Fig. 2.20), shows that Case 1($u > \alpha L$) causes the arching factor θ to increase linearly with depth above the structure while Case 2 ($u \leq \alpha L$) causes the arching factor to reach an asymptote with a value of $Bu_o/\alpha\beta$. It is believed that arching in an actual case might lie between the two limits expressed by the two equations plotted in Fig. V-2.20. However, it is more likely that arching more nearly approaches Case 2 ($u \leq \alpha L$) than Case 1 ($u > \alpha L$) for buried structures subjected to airblast-induced stress because the lateral forces q can become large and because the maximum deflections obtainable in the roof of a buried structure tend to become small for overpressures normally considered in the design of buried protective structures.

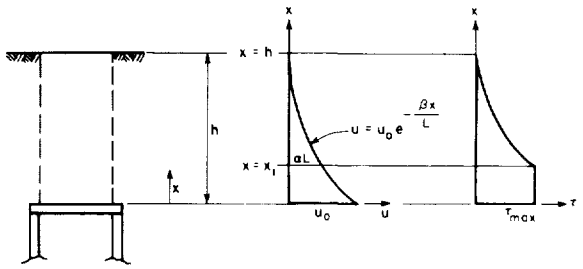

FIG. V-2.19 VARIATION OF DISPLACEMENT AND SHEARING STRESS WITH DEPTH

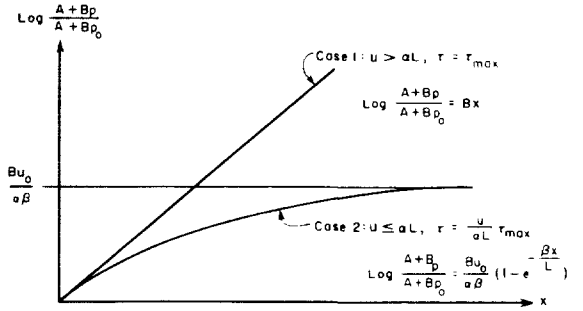

FIG. V-2.20 VARIATION OF STRESS WITH DEPTH

As is the case in static arching also, dynamic arching is critically dependent on the deflections of the structure which, because of the interaction, are not clearly understood as yet.

An analysis was performed (Ref. V-2.19) using the assumptions in Case 1, immediately above, except that the shearing force τ was taken as constant throughout the depth above the structure. Here however the dynamic motions and associated vertical stresses in the soil were accounted for by considering the mass of soil defined by the potential failure planes, the ground surface, and the roof of the structure (Fig. V-2.17) as a rigid body. The mass of this rigid body and the shearing forces acting on it increase very rapidly with depth; consequently the inertia force associated with motion of the rigid body and the shearing force increase very rapidly with depth causing a drastic reduction in vertical stress induced by airblast. In fact within a depth of the order of the span of the buried element the combined inertia and shearing forces equal the magnitude of the overpressure and the roof of the buried structure at a depth equal to its span feels essentially no dynamic load. This conclusion derived from the analysis (Ref. V-2.19) supports the observation by the authors (McKee, Selig and Vey) that their analysis probably is an upper limit for dynamic arching. From the preceding discussion, this upper limit probably develops because the shearing stresses along the planes of failure should not be constant

over the entire depth because the arching develops as a result of structural displacement and the effect of this displacement should diminish at points removed from the structure.

Experimental Results. Dynamic tests were conducted (Ref. V-2.6) with diaphragm or barium titanate gages (which for the scale of the experiments can be considered a simulated structure in a bounded medium) embedded in cylinders of Hysol or clay and loaded by means of a ballistic pendulum. A brief description of the diaphragm gage already has been presented in Section V-2.1.2. The dimensions of the barium titanate shell were 1/8 in. dia. x 1/8 in. high with a wall thickness of 0.020 in. This shell was mounted within a brass cylinder which was 5/16-in. dia. x 5/16-in. high. Load was distributed to the barium titanate through a 1/8-in. dia. lucite plate. Both types of gage were mounted at the center of a 3.0-in. dia. x 2-3/4-in. long cylinder of Hysol with the gage axis coincident with that of the Hysol cylinder. The depth ratio (distance from surface of the specimen to surface of embedded gage divided by the span of the sensitive element) was 1.7 and 3.9, respectively, for the diaphragm and barium titanate gages. In this configuration, the dynamic response for the diaphragm gage in Hysol was approximately 80% higher than the response produced by static air pressure of the same magnitude as applied to the end of the specimen, and 30% higher than the static response for the gage and Hysol for the full range of stresses applied. That is, when plotted on the same coordinates as used in Fig. V-2.3 the ordinates of the curve from the dynamic tests were 80% larger than those of the calibration curve. Characteristics of barium titanate preclude its being calibrated under a static condition; thus these gages were calibrated in a shock tube using air pressure. When embedded in Hysol the barium titanate registered a response for all values of stress applied to the specimen approximately 40% greater than the response produced by air shock applied to the gage alone. Roughly comparable results were obtained when the barium titanate gage was embedded in a cylinder of remolded clay with initial dimensions the same as the Hysol. However, the clay deformed significantly under each impact and the response of the embedded gage was a function of the number of impacts. The discrepancy between the response of the embedded gage and the gage in air became smaller with the number of impacts and also smaller as the magnitude of force applied to the specimen was increased.

The difference in response of these gages to static and dynamic loads might be attributed, among other things, to two facts: (1) a mismatch of acoustic impedance between the gage and embedding cylinder and (2) a change in the properties of the basic materials under dynamic loads. In the response records of the gages there is no evidence of stress reflection from the interface of the pendulum supporting the cylinder in which the gage was embedded. Because of the construction of the gages used, it is difficult to compute an acoustic impedance; nevertheless it appears probable that the gage has a higher impedance than the embedding material. In the diaphragm gage especially the modulus of elasticity of the brass may have increased as a result of the dynamic load causing the stiffness of this element to increase thereby causing a decrease in positive arching.

On the other hand, the fact that the gage response dynamically, for embedment in Hysol at least, was consistently greater than the static response for all applied stresses indicates qualitatively that arching may occur dynamically by a mechanism which is similar to that under static conditions. For the particular case considered here the arching is negative with the pressure felt by the simulated structure (or gage) being higher than the applied pressure.

Simulated structures like the diaphragm gages discussed above were tested in full-scale field operations in Operation Plumbbob (Ref. V-1.14) and at Eniwetok Proving Ground. A steel drum 2 ft in diameter with vertical stiffeners, and 2 ft long had aluminum diaphragms with five thicknesses in the range from 0.04 in. to 0.50 in. clamped across one or both ends (Fig. V-2.21). Two diaphragms of the same thickness were placed on either end of the drum in Operation Plumbbob; for the EPG experiments the bottom diaghragm was replaced by a steel plate.

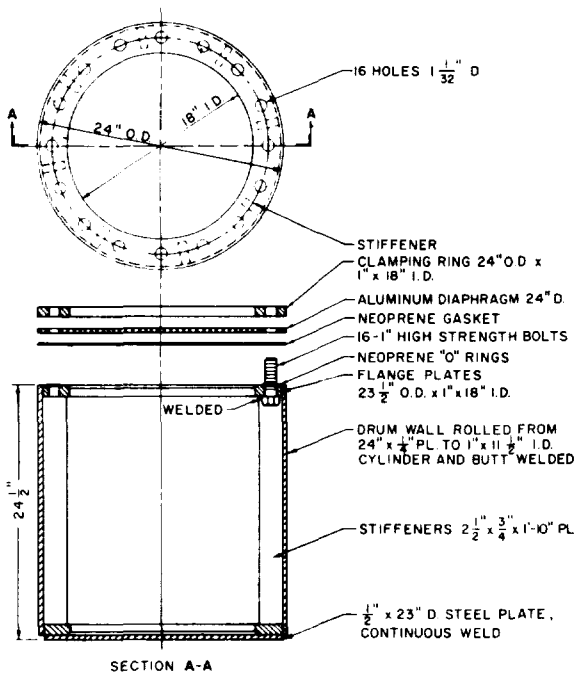

FIG. V-2.21 PLAN AND SECTION OF TEST DEVICE

These drums were buried in different locations at depths below the surface ranging from 0 to 20 ft. In a manner similar to the preceding experiments, the diaphragms were statically calibrated against gas pressure using strain and deflection at the center as a measure of effective pressure.

The results of these experiments are shown in Figs. V-2.22 through V-2.27 with each figure drawn for a single diaphragm thickness. A composite of these figures (Fig. V-2.28) summarizes the results. The curves at the top of each figure denoted theoretical stress-free field are defined by Eq. V-2.9. The theoretical attenuation of stress with depth was discussed in detail in Section V-1.3.1. In Ref. V-2.7 a semi-empirical equation was developed to approximate the theoretical results. Basis for the equation is that the attenuation of stress with depth depends upon the decay of overpressure with time. For overpressures greater than 30 psi the effective length of pulse (distance propagated in the duration of overpressure) can be related (Ref. V-2.7) to the peak overpressure p_s and the yield of the device W. With the use of this effective pulse length, Eq. V-2.9 was fitted to the theoretical curves:

$$p = \alpha p_s \qquad \text{(V-2.9)}$$

where p = vertical stress at depth y, psi

p_s = peak overpressure, psi

$$\alpha = \frac{1}{1 + \frac{y}{L}}$$

y = depth below surface, ft

$$L = 230 \text{ ft } \left(\frac{100 \text{ psi}}{p_s}\right)^{0.5} \left(\frac{W}{1 \text{ mt}}\right)^{1/3}$$

W = weapon yield, mt

The curve (Eq. V-2.26) is plotted on the various figures summarizing the results of the drum experiments to illustrate the amount of arching developed as distinguished from attenuation. In these figures, the data to a depth of 5 ft only are shown for tests at the Eniwetok Proving Ground (EPG) because the measurements below 5 ft (which corresponded approximately to the level of the water table at the time of the test) indicate pressures in excess of the overpressure. This increase has been attributed to a stress which was induced in the water at some point nearer the burst and propagated with little attenuation to the drum.

The existence of arching is apparent in the figures. This arching appears to be a function of the depth of burial and the stiffness of the diaphragm. It is interesting to note from Figs. V-2.22, V-2.24, and V-2.26 that there is no great effect of the size of weapon nor of the characteristics of the medium since the amount of arching on EPG 4 at EPG agrees reasonably with the results of EPG 3 also at EPG and of Priscilla at the Nevada Test Site (NTS). This relative lack of dependence on weapon yield tends to

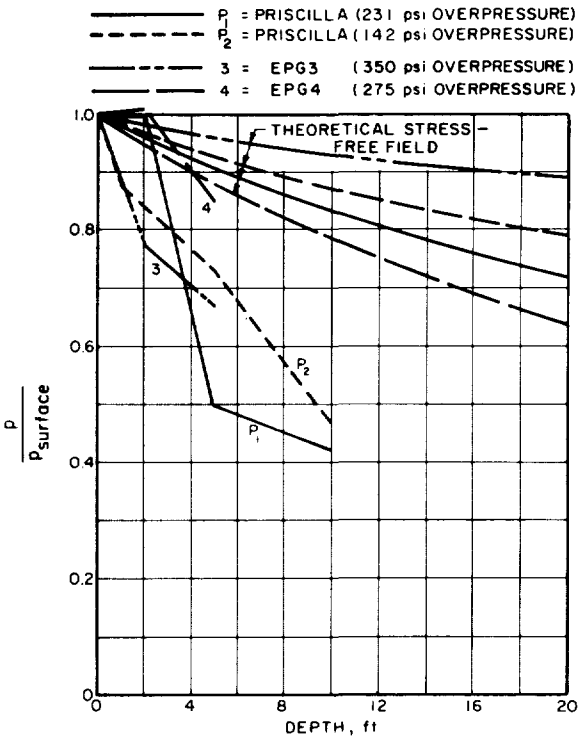

FIG. V-2.22 NORMALIZED STRESS VS DEPTH – DIAPHRAGM THICKNESS = 0.50 IN.

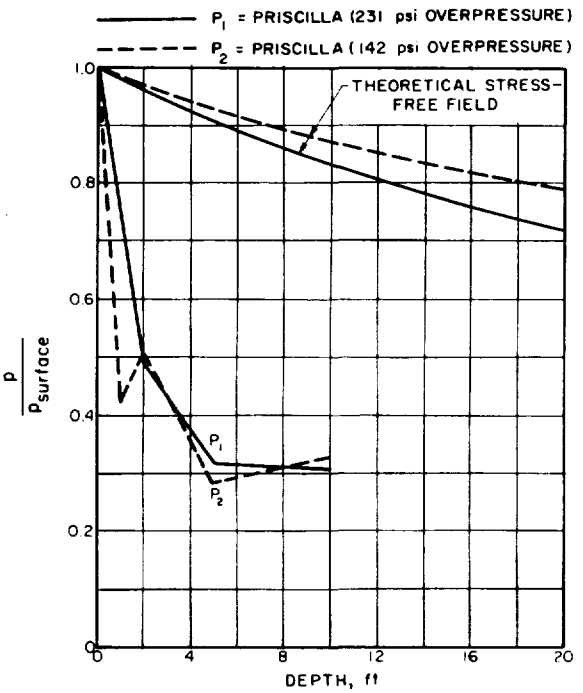

FIG. V-2.23 NORMALIZED STRESS VS DEPTH – DIAPHRAGM THICKNESS = 0.25 IN.

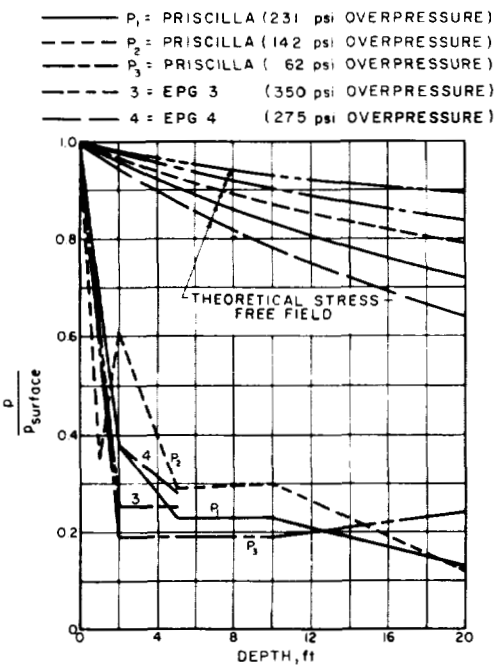

FIG. V-2.24 NORMALIZED STRESS VS DEPTH – DIAPHRAGM THICKNESS = 0.125 IN.

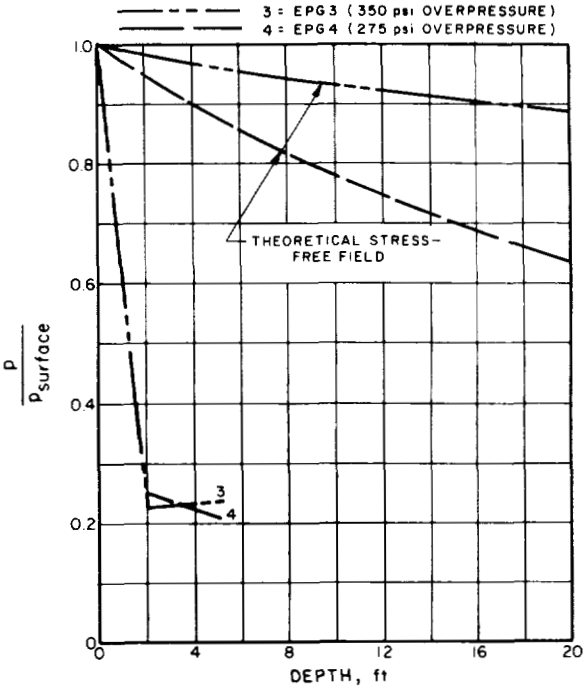

FIG. V-2.26 NORMALIZED STRESS VS DEPTH – DIAPHRAGM THICKNESS = 0.063 IN.

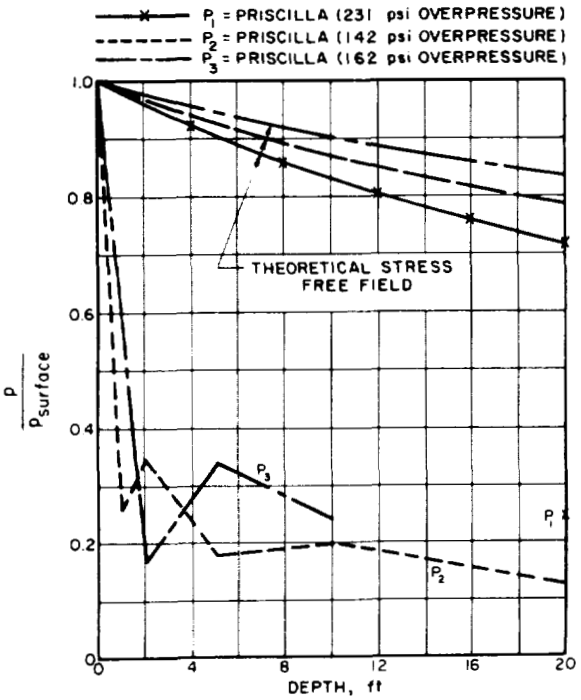

FIG. V-2.25 NORMALIZED STRESS VS DEPTH – DIAPHRAGM THICKNESS = 0.08 IN.

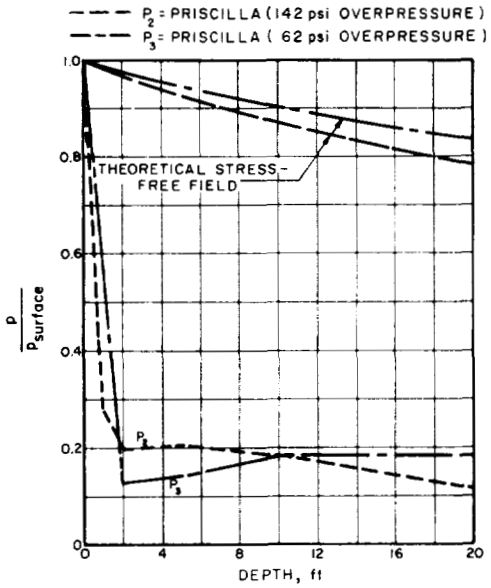

FIG. V-2.27 NORMALIZED STRESS VS DEPTH – DIAPHRAGM THICKNESS = 0.04 IN.

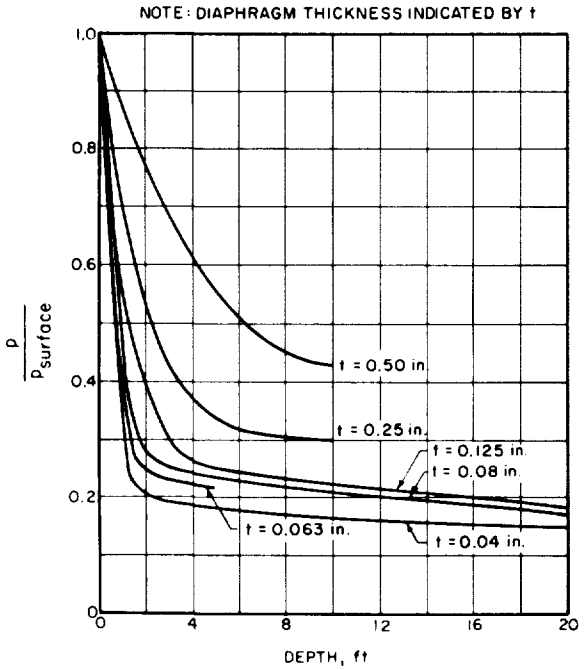

FIG. V-2.28 NORMALIZED AVERAGE CURVES FOR STRESS VS DEPTH

indicate that the measurements obtained from the drums does not correlate with the attenuation of vertical stress with depth which depends directly on the yield of the device and overpressure (cf. Eq. V-2.9). However, it is believed that the data are insufficient to make any conclusions on the existence of attenuation from these measurements; the existence of attenuation could be masked by the very rapid increase of arching with depth of burial. This belief is supported by the fact that vertical stresses measured by Carlson cells (cf. Fig. V-1.15) do exhibit attenuation; Carlson cells should not develop a major amount of arching because of their small size and because their sensitive element is relatively rigid (See Part III).

The degree of arching on these simulated structures depends on the thickness, and consequently stiffness, of the diaphragms; the thicker the diaphragm the smaller the arching (Fig. V-2.28). This dependence is perhaps more clearly shown in Figs. V-2.29 and V-2.30. In these figures the "major arching effect" is taken to correspond with the major break in the curves shown in Fig. V-2.28. As suggested by the curves (Figs. V-2.29 and V-2.30) it is believed that the degree of arching for the three thicker diaphragms is predominantly a dynamic effect while for the three thinner diaphragms a transition between dynamic and static arching developed; it is further suggested that static arching would have predominated for diaphragms thinner than any tested. This postulate results from knowledge that an unlined opening can be excavated if sufficient cohesion is present in the soil. Terzaghi (Ref. V-2.4) states that the insignificant effective cohesion provided by moisture (surface tension) in granular soils is sufficient to allow an opening to stand in the absence of vibrations. Furthermore, deflections of the order of 1% of the span are sufficient to develop a static arch in sands (Ref. V-2.4). Although the data obtained under static conditions existing immediately after completing the burial of the drums are inconclusive because of large scatter, these data tend to indicate that complete static arching developed for the thinnest diaphragms under the weight of overburden alone. The thinnest diaphragms did record vertical stress induced by airblast, but because the arch already had formed statically for these diaphragms the dynamic load recorded was much smaller than it was for the thicker diaphragms. Further investigation of this postulate has produced inconclusive quantitative results because of insufficient data. It is particularly important to note now, however, that the field data are qualitatively consistent with Case 2 of the theory summarized earlier in this section; that is, the case where the displacement and shear stress associated with arching decrease in magnitude with increase in distance measured from the roof of the structure. For this case the degree of arching changes rapidly with depth of structural burial and reaches a constant for relatively large depths.

V-2.2.4 Horizontal Stresses (Effect of Soil Moisture Content)

The horizontal stresses induced in soil appear to be critically dependent on the moisture content of the soil in which the structure is located. They also should be a function of the compressibility of the structure compared with the compressibility of the soil replaced by the structure. However, the effect of the compressibility of the structure is normally small compared to the uncertainties which exist in the ratio of lateral to vertical stress in the medium.

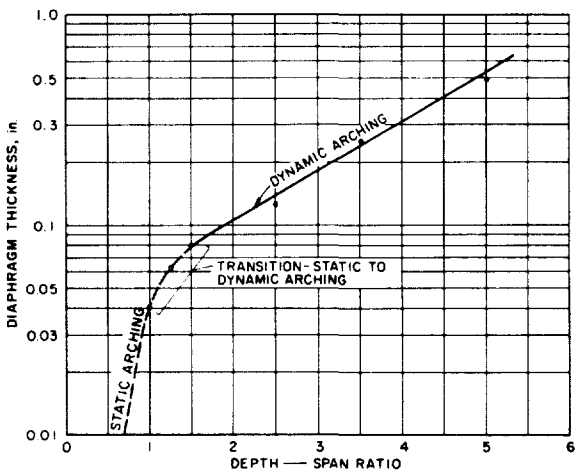

FIG. V-2.29 DEPTH-SPAN RATIO WHERE MAJOR ARCHING EFFECT OCCURS

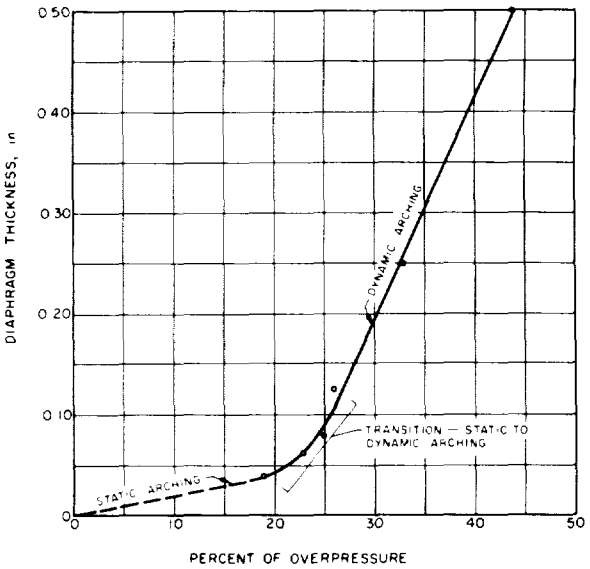

FIG. V-2.30 VARIATION OF MAJOR STRESS REDUCTION WITH DIAPHRAGM THICKNESS

A completely saturated soil should propagate a higher level of stress than a non-saturated soil. This can be explained on the basis of the manner in which the stress wave is generated and propagates in the soil. Within the time that the stress is acting it is doubtful that the pore pressure is a non-saturated soil can build up to equal the intensity of blast pressures existing either within the crater or in the air at the ground surface. Consequently for such a soil the stress wave develops and propagates by intergranular contact and the strengths of the soil developed during the passage of the shock are consistent with the characteristics of the soil matrix alone. When on the other hand the pores are completely filled with water, the stress wave must propagate as a hydrostatic pressure in the water because: (1) the water is much less compressible than the soil matrix; and (2) even for very porous soils, the water cannot drain to less saturated regions in the times associated with the loading. It is difficult to make generalizations regarding moisture contents between the limiting states because small changes in volume in the soil matrix for incomplete saturation could result in changing the condition of the soil to one of effectively complete saturation. At what point a soil which originally was unsaturated may be considered as completely saturated is unknown although it should be a direct function of the relative compressibility of the soil matrix to water and the degree of saturation.

It is important to note also that the peak intensity of the airblast-induced stress in a homogeneous medium cannot exceed the peak intensity of the overpressure at a given point; thus shock generally will propagate more rapidly and with less attenuation due to dispersion in a saturated soil. Yet the peak intensity of the directly-induced stress generally will be higher in saturated than in non-saturated soil (Ref. V-1.22 and Part IV). Thus, the moisture content can have an important influence in determining the relative importance of the airblast- and directly-induced effects.

Even though some clays may not be completely saturated, they may propagate stress in a manner approaching a hydrostatic condition. This develops because the moisture can effectively lubricate the particles, thereby eliminating internal friction. In such a case the seismic velocity may be low in comparison to that of a saturated soil, but the directly-induced effects can be comparable to those of a saturated soil.

Thus, the dynamic forces can be changed greatly if the soil surrounding the structure should become saturated. This results from the hydrostatic stress which may be induced in the water. If the hydrostatic condition is induced, the dynamic forces on all surfaces of the structure become equal. As already discussed, however, the development of a true hydrostatic state requires that the soil be saturated or nearly so over most of the region through which the shock must propagate. For example, if the water table is not very near the surface, the airblast-induced stress must propagate through unsaturated soil to reach the water table; in doing so the stress wave characteristics may be altered and some transition zone may develop before a hydrostatic condition is induced below the water table. The mechanism involved is not clear at the moment.

Empirical data related to this phenomenon are scarce. Data were obtained primarily from the field tests conducted in Frenchman Flat at the Nevada Test Site. The tests include measurements on one structure (Ref. V-1.13), on three horizontally oriented simulated structures (Ref. V-1.14) and from gages (Ref. V-1.12). Also three horizontal measurements below the water table were made at the EPG. The latter measurements, however, are very difficult to interpret because of the apparent strong directly-induced stress wave which propagated through the water between the point of burst and the simulated structure. The measurements on structures in Frenchman Flat also are difficult to interpret because of the very small number. Nevertheless they indicate the horizontal stress normally is a small fraction of the vertical stress. The measurements from gages (See Part IV) are more numerous, and they indicate a lateral stesss coefficient of from 0.15 to 0.20. The measurements below the water table at the EPG indicate the existence of essentially a hydrostatic state of stress. Finally the measurements and comparisons made in Section V-2.2 (cf. Fig. V-2.14) tend to support a lateral stress coefficient of approximately 0.25 in dry granular soil.

As a result of the relative absence of pertinent data, it has been recommended, on the basis of the preceding argument and small amount of data, that fixed values of the ratio of lateral to vertical stress in the medium be used for each of several general classifications of soil. Furthermore, it has been recommended that the stress acting on vertical surfaces of structures be taken equal to the lateral stress in the medium regardless of the compressibility of the structure. In Table V-2.4 are the recommended design values of the ratio of horizontal to vertical stress (Ref. V.1).

TABLE V-2.4 RECOMMENDED COEFFICIENTS OF LATERAL TO VERTICAL STRESS IN SOIL (STRESS ON VERTICAL SURFACES OF STRUCTURES)

SOIL TYPE	STRESS COEFFICIENT
Cohesionless soil, damp or dry	1/4
Unsaturated cohesive soils of stiff consistency	1/3
Unsaturated cohesive soils of medium consistency	1/2
Unsaturated cohesive soils of soft consistency	3/4
All saturated soils with the water table at the surface	1

When the water table is not at the surface, it is difficult to estimate what lateral stress coefficient should be applied. Since there is not sufficient time for pore pressures equal to the airblast overpressure to develop in unsaturated soil, it is doubtful that a hydrostatic pressure equal to the airblast overpressure can develop in the water. As an approximation to account for this effect the following has been recommended (Ref. V.1):

When the water table is more than 30 ft below the surface use the value of lateral stress coefficient for the unsaturated condition in the same type of soil. For intermediate levels of the water table, at depths between 0 and 30 ft, interpolate linearly for the value of lateral stress coefficient for points below the water table, and use the values from Table V-2.4 for points above the water table.

V-2.3 BEHAVIOR OF BURIED STRUCTURAL ELEMENTS

In this section the behavior of buried structural elements and the effects of this behavior on the loading and response of the elements is discussed in general terms. The parameters controlling the behavior for specific types of construction and for particular engineering materials are discussed in Chapter V-6. The current discussion is divided in accordance with the primary type of stress induced by the loading on the member. Detailed discussion of the strength and methods of analysis of structures located in soil are also included in Chapter V-6.

V-2.3.1 Direct Stress

Primarily direct stresses are induced in interior columns of rectangular structures and in the shells of fully-buried arches and domes. The failure of members under the action of direct stress normally occurs at relatively small ductility. Also it is generally true that members which are expected to be subjected to direct stress are stiffer than members subjected to other stress conditions. Greater stiffness implies a smaller natural period of vibration. Reference to Fig. V-1.31, which defines the resistance level required in a structural element for a given dynamic load, indicates that the reduction in ductility, x_m/x_y, and the reduction in natural period of vibration, T, combine to necessitate a larger resistance for a given dynamic load than the resistance required for the same load applied to a more ductile and less stiff structure. For example from Fig. V-1.31, if the ductility ratio for an arch is 2 and the effective duration of the equivalent triangular blast pulse is 20 times the natural period of vibration, the ratio of the peak applied pressure p_m to the resistance q_y of the structure is approximately 0.75. If on the other hand only the period T were increased five-fold the ratio, p_m/q_y, becomes approximately 0.80 while if only the ductility ratio were increased five-fold the ratio, p_m/q_y, increases to approximately 1.0.

Because interior columns generally are stiffer than the beams or slabs they support, the soil above the structure tends to arch across the beams while the columns form the abutments for the soil arch in addition to the supports for the beams. Yet the load on the columns from both sources should not exceed the load caused by the overpressure on the ground surface above the structure, but the time history of loading probably is modified by arching.

V-2.3.2 Flexure

Primarily flexural stresses develop in the roofs of box-shaped structures. Roofs of box-shaped structures can be subjected to direct stress in combination with flexure, but generally the direct stress is so small in comparison to the flexure that it may be neglected. An exception to this generality occurs when the span of the roof is nearly the same as the span of the wall and the structure is located in a soil where the lateral stress coefficient is large. Means of treating this exception will be considered in the following section.

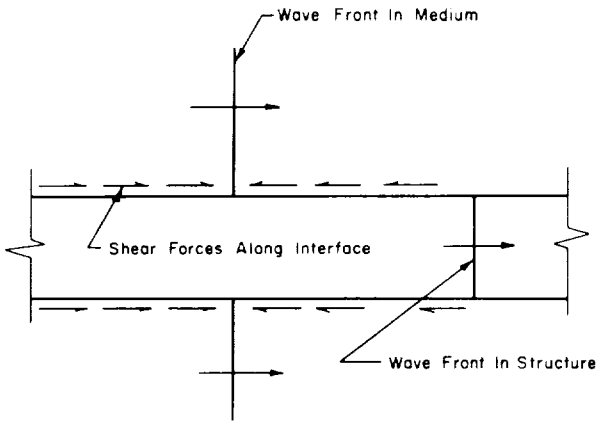

FIG. V-2.31 EFFECT OF RELATIVE MOTION BETWEEN SOIL AND STRUCTURE WITH LONGITUDINAL AXIS OF STRUCTURE PARALLEL TO DIRECTION OF SHOCK PROPAGATION

When members fail in flexure they usually exhibit large ductilities. Failure in flexure occurs if earlier failures in shear, lateral buckling, or related phenomena are precluded. Also excluded are reinforced concrete members with abnormally small or large amounts of flexural reinforcement or steel members with high local stress concentrations or members fabricated from materials which are susceptible to brittle fracture. The foregoing exclusions should be noted carefully because these are conditions which should be avoided insofar as possible in the design of protective structures. Through the large inherent ductilities usually available when flexural failures develop, the resistances required for a given loading can be smaller (Fig. V-1.31). Also these ductilities can imply potentially large compressibilities which may induce significant arching across the member.

V-2.3.3 Direct Stress and Flexure in Combination

The members which most frequently are subjected to combined flexure and direct stress are the exterior walls of a box-shaped structure. The problem associated with the analysis of such members lies in determination of the maximum stresses produced in the member by the loads applied. Normally the direct stress results from the reaction of the roof slab tributary to the wall. Because of the inertia of the roof this reaction builds up relatively slowly to a maximum value. The time at which this maximum value of the reaction develops is essentially equal to the time of maximum response, t_m, (Ref. V-1.35) which is specified as a ratio to the natural period of vibration in Fig. V-1.31. It is obvious from this figure that no generalizations can be made in terms of the absolute value of the time of maximum response. However, from consideration of the natural period of vibration of a wall when it is subjected to an axial force, it is apparent that the time of maximum response for the roof normally will be several times this natural period of vibration. It can be shown (e.g., Ref. V-2.20) that when the rise time of the loading (the time of maximum response for the roof in this case) is long in comparison with the period of vibration, the dynamic response is essentially the same as if the load were statically applied. Since, in addition, the duration of the loading on the roof will be long in comparison to the natural period of vibration of the wall, the maximum stress produced by the direct stress frequently can be assumed to remain unchanged until the maximum response of the wall in flexure is reached.

As a result of the foregoing reasoning the local stresses in the wall can be taken as a direct sum of the stress produced by direct force and the stress produced by flexure. Consequently the behavior of most members subjected to the effects of combined flexure and direct stress can be evaluated from an axial load-moment interaction diagram constructed for the member. The construction of such diagrams is discussed in Chapter V-6.

V-2.3.4 Combined Shear and Flexure

Failure in combined shear and flexure can take several forms depending upon the structural configuration and the type of material used in the structure. In steel members failure of this type is manifested by buckling of the web of a structural member, by crippling of the web near the support, and by lateral buckling of the compression flange. For reinforced concrete, failure in combined shear and flexure is manifested by pure shear near the support, by diagonal tension in the region of relatively high shear and moment, and by bond (slipping of the reinforcement relative to the concrete) either in the region of high shear or of high flexure. These types of failure can develop in any member in which the stresses induced by the loading are primarily flexural.

When failure by combined shear and flexure develops, both the strength and ductility of the member generally are reduced below the values which can develop if the same member fails in flexure alone. Frequently it is relatively easy and economical to prevent premature failure in combined shear and flexure. For example, web stiffeners can be added to individual steel beams or stirrups can be placed in individual reinforced concrete beams. In other cases, such as in flat slabs, it generally is not feasible to reinforce the member to preclude these premature failures. When this condition exists, the size of the member must be increased over the dimensions required for flexure to provide the necessary resistance. This required increase to resist a given loading results from: (1) the reduced strength; (2) the normally reduced ductility; and (3) the shorter natural period of vibration inherent in a member of greater depth or resisting capacity (cf. Fig. V-1.31).

Additionally, if the reduction in ductility is large, it is possible that the deformations might not be sufficiently large to mobilize arching in the soil in the vicinity of the element.

V-2.4 EFFECT OF GROUND MOTION

The behavior of the exterior elements of a buried structure depends upon the stresses acting on them or the relative motions which develop along the entire structure. In most cases these phenomena are paramount; other phenomena, as manifested by absolute acceleration, velocity, and displacement at a point, generally have a negligible effect on the exterior structure. Yet these last parameters are extremely important in assessing the behavior of interior elements and of equipment or personnel located within the structure. The characteristic of importance in visualizing this behavior is the mechanism by which the motion is transmitted to the contents.

Because of the additional motion induced by structural response of the exterior frame, it is unusual to find a structure with interior floors mounted directly to the exterior surfaces. More common is an interior frame which is separated insofar as possible from the exterior structure. Generally therefore motion reaches this interior frame by coupling of its footings with the medium. To reach these footings the stress wave must "travel around" the exterior structure, and it may be modified thereby. Also by design, or naturally, the coupling between the footings and the medium may not be perfect, thus changing the input to the footings as compared to the motions in the adjacent medium. Inherent energy absorbing or damping characteristics of the foundations seem to be the significant parameters which define the motion which reaches the interior elements.

The motion reaching the footings becomes the base motion to be applied to a mathematical model of the interior structure and the principal equipment it supports. It is emphasized that the mass and other characteristics of the principal equipment must be included in defining this mathematical model. Since heavy equipment can completely change the motions imparted to the entire system by the base motion, completely erroneous conclusions can be drawn if this equipment is omitted in the analysis. In formulating this model it also is extremely important that inherent ductility and damping, especially in the joints between individual members, be included. Otherwise the motions reaching personnel and equipment may be grossly overestimated.

If the shock motions imparted to personnel and equipment can be estimated, further analysis is required to determine whether particular equipment will be damaged. This analysis is complicated by the fact that much equipment is a highly complex assemblage of mechanical and/or electronic parts and that personnel in general are very mobile. This complexity and mobility make necessary certain generalities regarding the vulnerability of classes of items which might constitute the structural contents. In general these vulnerabilities are assessed in terms of a range of acceleration, of velocity, or of displacement.

Providing protection for the contents of a structure and designing interior framing which is physically separated from the protective shell are frequently the most difficult problems to attack. Much of the effort in this area has been devoted to defining the response spectra from the free field motion. In this section are presented the differences to be expected between the spectral motions in the free field and those effective in the behavior of structures and equipment.

To define the response spectra appropriate to the analysis of parts of the structure requires consideration of what happens when the free field motion acts on the structure. In this regard much can be learned from previous experience with earthquakes. Measurements which allow the determination of motions induced in the soil by an earthquake have been obtained in many earthquakes of various intensities. Analysis of structures (e.g., Ref. V-2.21) which withstood these earthquakes indicates that if the motions in the soil had had their full effect on the structure it could not have survived. In fact the structures which survived had response spectra significantly less than those which would be predicted on the basis of the ground motions measured by USCGS seismographs. There are several possible explanations for this reduction. Among these are: (1) There was imperfect coupling between the foundations and the medium such that the foundations do not receive the full effect of the medium motion; (2) Damping within the structure significantly reduced the motions transmitted through the structure; and (3) Minor plastic deformations were induced in certain parts of the structure and these reduced the motions in the structure.

Analyses currently are underway which are directed toward more detailed explanations of the effects of the structural properties on the motions imparted to structural elements. These analyses are summarized in Chapter V-4.

V-2.5 EFFECT OF RELATIVE MOTIONS

The behavior of a buried structure can be influenced greatly by relative motions which develop in the soil. These motions are produced primarily by the finite transit time of the load along the structure; one part is loaded while another part has no load acting on it. To resist these motions the structure must act somewhat like a box girder. Alternatively if the motions are relatively small, zones of weakness can be intentionally provided in the structure such that one part can move relative to another.

In either case it is necessary to estimate the magnitude of the motion to be expected. The following discussion is divided on the basis of the direction of the motion with respect to the longitudinal axis of the structure.

V-2.5.1 Longitudinal Motion

The effect of longitudinal motion already was mentioned in Section V-1.4.1. As developed there the motion itself is not as important as the shearing forces developed as a result of the relative motion. This results from the fact that frictional forces are largely independent of the amount of motion once motion has been established. Friction forces are dependent directly on the normal force acting on the surface of sliding and the angle of friction between the two materials which are sliding. Evaluation of the effects of longitudinal motion therefore reduces to estimating the magnitude of the frictional forces and investigating the section of the structure corresponding to the position of the shock front in the soil as shown in Fig. V-2.31.

Much more complex, but related, situations than those just described can occur when a shelter is located in a stratified medium. In such a case the action of the structure is similar, but the relative deformations can change direction or change in magnitude over relatively small lengths of the structure. With the shock hitting the structure end-on the direction of the shear forces pictured in Fig. V-2.31 conceivably could change for each stratum. For shock striking the structure side-on lateral displacements could change drastically in each stratum. For thin strata these differential displacements could induce large stresses in the walls of the shelter.

V-2.5.2 Differential Vertical Motion

Lateral motions in buried structures can develop as a result of the conditions shown in Fig. V-2.32. At point A on the structure the stress wave in soil has progressed to a point below the structure while for all points on the structure to the right of B the stress wave has not reached the structure. The length of stress pulse on a plane through point A is taken in the figure as approximately the product of the seismic velocity c and time t. This is not exact since the velocity of the portion of the wave shown must propagate with a velocity consistent with the air-shock and seismic velocities. However, for most soils and for magnitudes of overpressure generally considered for buried structures, the approximation used causes relatively small error in the computed displacements.

Because of the means by which the stress wave propagates, point A tends to deflect downward an amount compatible with the strain induced in the soil below the structure. This deflection steadily decreases between points A and B reaching zero at B. For times greater than t the deflection at A increases and the region over which deflection exists becomes larger. To resist this relative motion the structure must possess sufficient flexibility to allow it to deflect with the surrounding medium. Alternatively the structure must possess sufficient strength to resist the loads associated with the relative motion.

For stratified soils the differential displacement along the length of the structure becomes more complex, but the general ideas, just presented, remain valid.

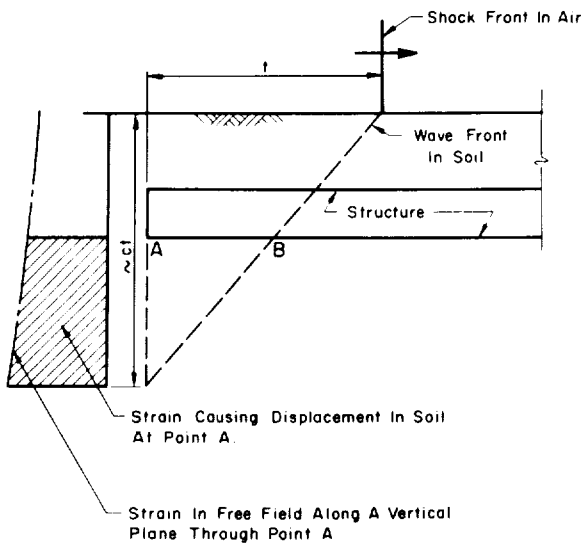

FIG. V-2.32 CONDITIONS PRODUCING LATERAL MOTION OF MEDIUM RELATIVE TO THE AXIS OF STRUCTURE

REFERENCES

V-2.1 Koenen, Berechnung des Seiten-und Bodendrecks Silozellen, Zentralblatt der Bauverwaltuns, 16, 446-447, (1896).

V-2.2 Terzaghi, Arching in Sands, Eng. News Rec., 116, 690-693 (1936).

V-2.3 Terzaghi, Stress Distribution in Dry and in Saturated Sand Above a Yielding Trap Door, First International Congress on Soil Mechanics and Foundation Engineering, 1, 307-311 (1936).

V-2.4 Terzaghi, Theoretical Soil Mechanics, New York: John Wiley & Sons, Inc., 1943.

V-2.5 Spangler, Underground Conduits - An Appraisal of Modern Research, Trans. ASCE, 113, 316-374, (1948).

V-2.6 Durelli and Riley, Research Studies of Stress Waves in Earth and Model Earth Media, ARF, AFSWC-TR-60-4, 1959.

V-2.7 Newmark and Hall, Preliminary Design Methods for Underground Protective Structures (1961 Revision), Currently being printed by AFSWC, prepared under Contract AF 29(601)-2837.

V-2.8 Moulton, Nuclear Weapons Blast Phenomena, DASA-1200, Washington, 3 vols., March 1960 (Secret).

V-2.9 Bleakney, A Shock Tube Study of the Blast Loading On Structures, Proceedings of the Symposium on Earthquake and Blast Effects on Structures, Los Angeles, June 1952.

V-2.10 Whipple, The Dynamic Response of Shallow-Buried Arches Subjected to Blast Loading, Ph.D. Thesis, Dept. of Civ. Eng., Univ. of Ill., Urbana, 1961.

V-2.11 Flatau, Blast Loading and Response of Underground Concrete - Arch Protective Structures, WES, Operation Plumbbob, ITR-1420, 1957, (Confidential).

V-2.12 Albright, Evaluation of Buried Corrugated-Steel Arch Structures and Associated Components, NCEL, Operation Plumbbob, WT-1422, 1961.

V-2.13 Whipple, Numerical Studies of Dynamic Response of Shallow Buried Arches Subjected to Blast Loading, Preliminary Draft Report on Contracts AF 29(601)-2591 and -4508 to AFSWC, August 1961.

V-2.14 Duberg, Appendix C: Analysis and Design of Flexible Underground Structures, by N. M. Newmark, et al, Contract DA-22-079-eng-225 with WES, Vol. I, Urbana, 1960.

V-2.15 Merritt, McDonough, and Newmark, Evaluation of Data from Underground Explosion Tests in Soil, Dept. of Civ. Eng., Univ. of Ill., SRS 152, Urbana, 1958, (Confidential).

V-2.16 Operation Jangle, Blast and Shock Measurements, I, II and III, Operation Jangle, WT-366, 367 and 368, 1952, (Secret Restricted Data).

V-2.17 Wells, Operation Teapot, Shot 7 - Data Report, Vols. I and II, SRI, 1955, (Secret Restricted Data).

V-2.18 Perret and Preston, Preliminary Summary Report of Strong-Motion Measurements from A Confined Underground Nuclear Detonation, ITR-1499, June 1958, (Unclassified).

V-2.19 Selig, McKee, and Vey, Underground Structures Subject to Air Overpressure, Journal, EMD, ASCE, 1960.

V-2.20 Melin and Sutcliffe, Development of Procedures for Rapid Computation of Dynamic Structural Response, Dept. of Civ. Eng., SRS 171, Univ. of Ill., Final Report on Contract AF 33(600)-24994 with PVD, 1958.

V-2.21 Anderson, Blume, et al, Lateral Forces of Earthquake and Wind, Trans. ASCE, 117, 716-780, 1952.

CHAPTER V-3

DEEPLY-BURIED STRUCTURES

For structures at shallow depths the predominant effects are produced by airblast-induced ground motion. Behavior of deeply-buried structures is predominantly controlled by the directly-transmitted motion. This is not because of the burial but because deeply-buried structures become economically feasible only if extreme protection is required; such hardness normally implies that the structure be located directly under the crater of the burst where the effects of most importance appear to be those induced by directly-induced motion.

The least costly means of providing structures at large depths would appear to be the use of abandoned mines or natural limestone caverns. Where such cavities do not exist in areas where strategic operations must be located, mining of tunnels in rock is required. It also is conceivable that some deeply-buried structures might be located in soil if the geologic and ground water conditions at a site are favorable. Even when the structure is located in soil at great depths (of the order of perhaps 1000 ft) it would appear that tunneling methods would be required.

Consequently the structures referred to in this chapter are those which have been placed by tunneling methods at great depths. Thus both the depth of burial and the method of construction distinguish the problems discussed here from those presented in the preceding chapter. For high degrees of hardness it would be desirable for the openings to be relatively small. Unlined tunnels in competent rock appear to afford a high degree of protection; yet even for static loads a lining must be provided for openings in soil. Still greater protection may be provided by placing protective linings within tunnels in rock or heavier linings than required for static loads in soil. Protective linings normally would be nearly cylindrical in shape since such configurations inherently provide greater strength than other types for long-narrow openings. Arched configurations also might be appropriate, but as will be developed later, it appears that a cylindrical structure can be conceived which will provide some degree of shock isolation to the contents of the structure; similar shock isolation cannot be as readily provided in arched configurations. Additionally for small operations a nearly spherical opening might be appropriate.

V-3.1 STRESSES AND DISPLACEMENTS AROUND UNLINED OPENINGS IN ROCK

V-3.1.1 Static Load

For many years the design of underground openings was accomplished largely by trial and error methods. Only relatively recently has the classical theory of elasticity been applied to the behavior of tunnels in rock. Now the use of this theory and the methods dictated by it seem to be widely accepted (Ref. V-3.1). Under elastic theory for static load, the opening in a massive rock formation is assumed to be a hole in an infinite plate. As long as the hole is located so that the cover over it is greater than approximately twice the largest lateral dimension and the hole is long compared with this lateral dimension, the usual assumption of plain strain is reasonably good (Ref. V-3.2). For layered formations, common to sedimentary deposits, each stratum is treated as a beam or plate loaded by its own weight (Ref. V-3.1). For most cases involving static loads this treatment is valid.

The discrepancies between the theory and observed behavior probably can be attributed more to difficulties in assessing the in situ strength and state of stress in the rock than to inappropriate interpretation of the theory. Because of the difficulties in defining the in situ conditions, rather large safety factors are applied in the design of mine workings. Safety factors ranging from 4 to 8 applied to the unconfined compressive strength or modulus of rupture appear to be relatively common.

It appears that some advantage of these safety factors can be taken in assessing the resistance of an abandoned mine to dynamic loads.

Determination of safety factors requires consideration of two primary variables: (1) variation in the computed loads (including effects of inaccuracies in the methods of analysis and of temperature, creep and related phenomena) and (2) variation in the strength of the materials. Although safety factors should be determined on the basis of statistical analysis, it has been common in this country to choose each parameter which enters a design conservatively

and to apply a safety factor to the over-all design in addition. The resulting compound value of safety factor frequently exceeds by some multiple the apparent safety factor so that the actual strength of a member often exceeds the actual load on the member by a large margin. Furthermore, an augmentation of the strength occurs under dynamic load because of the increased stress produced by high strain rates. Considering all of these combinations suggests that the reserve in strength over the static load might be on the order of the apparent safety factor. Since the member must resist the static load in addition to the dynamic load, it is conceivable that, for apparent safety factors ranging from 4 to 8, the reserve strength available to resist dynamic load might be 3 to 7 times the magnitude of the static load.

On this basis an existing mine might be capable of resisting a dynamic load in the vicinity of the opening which is 3 to 7 times the static load implied by the overburden. For example, a mine which proved safe at a depth of 1000 ft in massive rock with unit weight of 144 psf(1000 psi static load) might withstand dynamic loads of 3000 to 7000 psi. If some inelastic action is acceptable, even higher pressures may be resisted.

Openings in Homogeneous Rock. To design openings in competent-massive rock for static loads requires the definition of the stresses induced by the overburden. For openings located at some distance from the edges of the geologic formation or from major faults, the vertical stress, σ_v, can be defined in terms of the unit weight of the rock, w, and the depth, y:

$$\sigma_v = 1 \text{ psi} \left(\frac{w}{144 \text{ pcf}}\right)\left(\frac{y}{1 \text{ ft}}\right) \qquad \text{(V-3.1)}$$

If the opening is located in the hanging or foot wall of a fault the vertical stress may not be consistent with the above equation. Here the tectonic forces must be considered; these are discussed in Section V-3.1.3. However, since it generally is not desirable to locate a protective structure within a major fault or along a boundary between two geologic formations, the vertical stress defined by the above equation is applicable to the cases of interest.

The horizontal component of stress (σ_h) is more difficult to evaluate. Because the static load produces a strain in only one direction, the horizontal stress, σ_h, should be related to the vertical stress, σ_v, by the relation defined in Eq. V-3.2 where ν is Poisson's ratio.

$$\frac{\sigma_h}{\sigma_v} = \frac{\nu}{1 - \nu} \qquad \text{(V-3.2)}$$

In Ref. V-3.1 a value of Poisson's ratio ν of 0.25 is implicitly recommended. Thus:

$$\sigma_h = \frac{1}{3}\sigma_v \qquad \text{(V-3.3)}$$

However, for rock a range of values for Poisson's ratio from -0.5 to +0.5 have been measured with a few reported values as high as +0.95 (Ref. V-3.3). (A negative Poisson's ratio implies a lateral contraction of a specimen when it is subjected to longitudinal compression.) A value higher than +0.5 is theoretically impossible for elastic, isotropic, homogeneous material. The recommended value of 0.25 appears to be a reasonable average of the test results. Yet the problem of determining the horizontal intensity of stress is complicated additionally by tectonic forces; for example, if the rock opening is bounded laterally by open joints, the horizontal stress may be zero. On the other hand near the bottom of an anticline, the top of a syncline, or in the vicinity of a fault or intrusion, the horizontal stress may bear no relation to the vertical stress; in some cases the stress components may approach the ultimate strength of the rock.

If tectonic forces are neglected (these forces will be discussed later), a stress state in rock caused by static loads of the type shown in Fig. V-3.1 will result. Normally, the variation in stress over the height of an opening can be neglected because this change is small for the normally small height involved. Therefore, the stress state to which an opening (circular) is subjected can be represented as exemplified in Fig. V-3.2. Stress concentration factors, defined as the ratio of the tangential stress at the edge of a hole to the vertical stress in the medium at some distance from the hole, have been determined by several means for holes of various shapes. Analytical solutions exist for circular, elliptical, and certain ovaloidal openings while photoelastic and experimental studies have defined concentration factors for other shapes. These studies are summarized in Ref. V-3.1 in which three ratios of horizontal to vertical stress are considered, namely 0, 0.33, and 1. These results are summarized in Table V-3.1 for single openings and in Figs. V-3.3 and V-3.4 for multiple parallel openings.

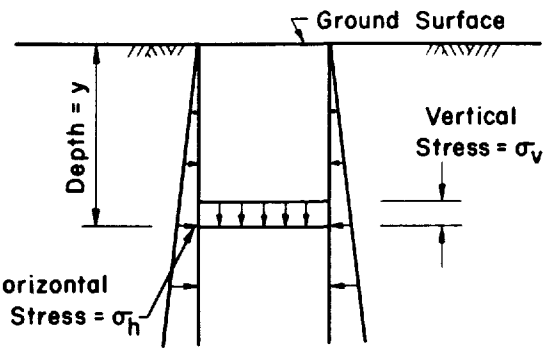

FIG. V-3.1 DEAD LOAD STRESSES IN HOMOGENOUS ROCK

TABLE V-3.1 MAXIMUM STRESS CONCENTRATION FACTORS FOR OPENINGS IN INFINITE ELASTIC, HOMOGENEOUS, ISOTROPIC PLATES (Ref. V-3.1)

Shape of Opening	*Ratio of Horiz. to Vert. Stress in Medium	Maximum Compressive Stress on Hole Boundary as Ratio to Applied Vert. Stress	Minimum Stress on Hole Boundary as Ratio to Applied Vert. Stress
Circular	0	3.00	-1.00
	1/3	2.67	0
	1	2.00	2.00
†Ellipse	0	0.75	-1.00
(Major Axis		(at ends of minor axis)	(at ends of major axis)
Vertical)	1/3	2.00	0.60
Width W to		(at ends of major axis)	(at ends of minor axis)
Height H Ratio = 1/4	1	8.00	0.25
		(at ends of major axis)	(at ends of minor axis)
Ellipse	0	2.00	-1.00
W/H = 1/2		(at ends of minor axis)	(at ends of major axis)
	1/3	1.70	0.70
		(at ends of major axis)	(at ends of minor axis)
	1	4.00	1.00
		(at ends of major axis)	(at ends of minor axis)
†Ellipse	0	5.00	-1.00
W/H = 2.00		(at ends of major axis)	(at ends of minor axis)
	1/3	4.60	-0.33
		(at ends of major axis)	(at ends of minor axis)
	1	4.00	1.00
		(at ends of major axis)	(at ends of minor axis)
†Ellipse	0	9.00	-1.00
W/H = 4.0		(at ends of major axis)	(at ends of minor axis)
	1/3	8.60	-0.50
		(at ends of major axis)	(at ends of minor axis)
	1	7.80	0.50
		(at ends of major axis)	(at ends of minor axis)
§Ovaloid:	0	1.90	-1.00
W/H = 1/4		(in fillet)	(at ends of major axis)
ξ = 1.19	1/3	2.05	0.70
η = 4.19		(in fillet)	(at ends of major axis)
ζ = 0.19	1	4.10	0.40
		(in fillet)	(at ends of minor axis)
§Ovaloid:	0	2.00	-0.90
W/H = 1/2		(in fillet)	(at ends of major axis)
ξ = 1.10	1/3	2.05	0.25
η = 2.10		(in fillet)	(at ends of major axis)
ζ = -0.10	1	3.15	0.70
		(in fillet)	(at ends of minor axis)

*Maximum stress in medium applied vertically

†Parametric equations for ellipse: $x = W \cos \theta$; $y = H \sin \theta$; $\theta = 0°$ is horizontal

§Parametric equations for ovaloids: $x = \xi \cos \theta + \zeta \cos 3\theta$; $y = \eta \sin \theta - \zeta \sin 3\theta$; $\theta = 0°$ is horizontal

TABLE V-3.1 (cont'd)

Shape of Opening	*Ratio of Horiz. to Vert. Stress in Medium	Maximum Compressive Stress on Hole Boundary as Ratio to Applied Vert. Stress	Minimum Stress on Hole Boundary as Ratio to Applied Vert. Stress
§Ovaloid:	0	3.40	-0.90
W/H = 2.0		(at ends of major axis)	(at ends of minor axis)
ξ = 2.10	1/3	3.20	-0.30
η = 1.10		(in fillet)	(at ends of minor axis)
ζ = -0.10	1	3.20	0.75
		(in fillet)	(at ends of minor axis)
§Ovaloid:	0	4.80	-0.90
W/H = 4.0		(at ends of major axis)	(at ends of minor axis)
ξ = 4.19	1/3	4.50	-0.50
η = 1.19		(at ends of major axis)	(at ends of minor axis)
ζ = -0.19	1	4.10	0.40
		(in fillet)	(at ends of minor axis)
†Rectangle	0	2.50 (in fillet)	-1.00
Width W to		1.50 (along long side)	(at ends of major axis)
Height H	1/3	3.50 (in fillet)	0
Ratio = 1/4		1.25 (along long side)	(at ends of major axis)
	1	6.15 (in fillet)	1.90
		0.70 (along long side)	(at ends of major axis)
†Rectangle	0	2.60 (in fillet)	-1.00
W/H = 1/2		1.75 (along long side)	(at ends of major axis)
	1/3	3.10 (in fillet)	-0.20
		1.50 (along long side)	(at ends of major axis)
	1	4.70 (in fillet)	1.00
		1.50 (at ends of major axis)	(along long side)
†Rectangle	0	3.05 (in fillet)	-1.00
W/H = 1.0		2.00 (along sides)	(along top and bottom)
	1/3	3.10 (in fillet)	-0.30
		1.65 (along sides)	(along top and bottom)
	1	3.80 (in fillet)	0
		0 (along sides)	(along top and bottom)
†Rectangle	0	4.00 (in fillet)	-0.70
W/H = 2.0		2.50 (center short side)	(along long side)
	1/3	4.00 (in fillet)	-0.20
		2.00 (center short side)	(along long side)
	1	4.60 (in fillet)	1.00
		1.50 (center short side)	(along long side)
†Rectangle	0	5.30 (in fillet)	-0.80
W/H = 4.0		2.90 (center short side)	(along long side)
	1/3	5.50 (in fillet)	-0.30
		2.65 (center short side)	(along long side)
	1	6.20 (in fillet)	0.80
		2.00 (center short side)	(along long side)

*Maximum stress in medium applied vertically

†All openings have rounded corners with fillet radius equal to 1/6 the short dimension

§Parametric equations for ovaloids: $x = \xi \cos\theta + \zeta \cos 3\theta$; $y = \eta \sin\theta - \zeta \sin 3\theta$; $\theta = 0°$ is horizontal

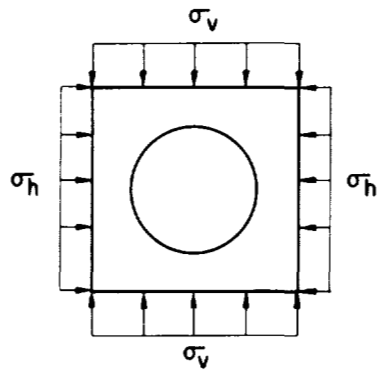

FIG. V-3.2 APPROXIMATE DEAD LOAD STRESSES ACTING ON TUNNEL

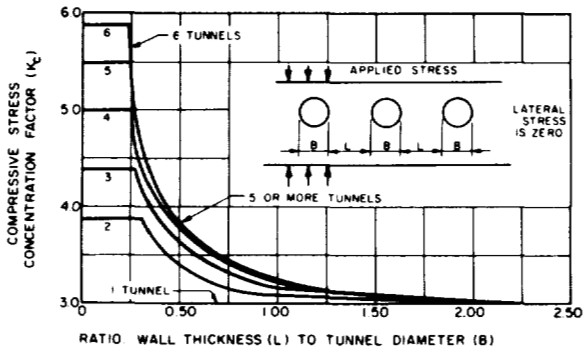

FIG. V-3.3 STRESS CONCENTRATION FACTOR FOR PARALLEL CIRCULAR OPENINGS

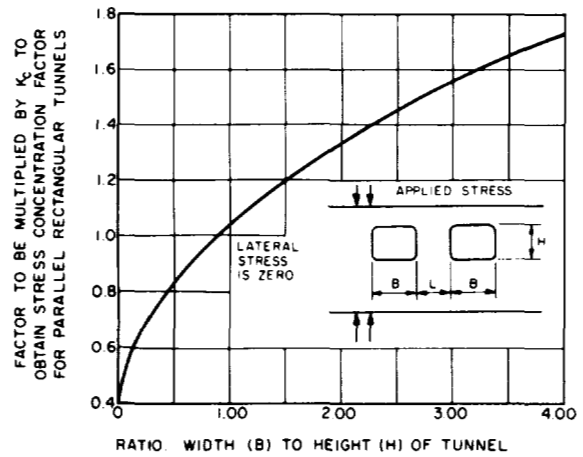

FIG. V-3.4 FACTOR RELATING COMPRESSIVE STRESS CONCENTRATION FACTOR FOR RECTANGULAR OPENINGS TO THOSE FOR CIRCULAR OPENINGS

The data in Fig. V-3.3 for multiple-cylindrical parallel openings are developed directly from Ref. V-3.1. On the other hand Fig. V-3.4 was developed by approximate procedures which involve a consideration of the difference between stress concentration factors for rectangular openings with rounded corners (Table V-3.1) and for circular openings (Fig. V-3.3).

The approximate procedure used in developing Fig. V-3.4 consisted of assuming that the ratio of stress concentration factor for a single rectangular opening to that for a single circular opening was also valid for parallel rectangular openings compared to parallel circular openings. Therefore, Fig. V-3.4 is merely a plot of the ratio of the maximum stress concentration factors for rectangular openings of varying dimensions from Table V-3.1 to the maximum stress concentration factor for a single circular opening. Choice of the maximum stress concentration factor for rectangular openings may not be realistic since this maximum occurs in the fillet at the corners; yet Fig. V-3.4 represents a set of approximate values, and similar curves can be constructed for other conditions summarized in Table V-3.1 if it is felt that other concentration factors are appropriate for rectangular openings.

The limiting conditions for the stress concentrations implied in Figs. V-3.1 and V-3.4 were imposed on the basis of the fact that when the walls separating individual openings become small in thickness they may be effectively considered as non-existent; thus, the upper limit was assumed to correspond to an ovaloid or rectangle which circumscribes the boundaries of the entire parallel tunnel configuration.

In Ref. V-3.1 the analysis or design of rooms and pillars for openings in homogeneous rock is based on the dimension of a pillar required to support the vertical stress applied to the tributary area of the pillar. This procedure merely corrects for the area reduction at the location of the room and pillar complex; that is, in forming a room and pillar configuration, a certain area of rock is removed. In plan view the reduction of area corresponds to the area of the rock removed as compared with the total area. As recognized in Ref. V-3.1 large stress concentrations must develop in the columns. An approximation to these stress concentrations can be developed by considering a room and pillar complex to be a set of intersecting parallel rectangular tunnels in two directions. This approximation employs the data shown in Figs. V-3.3 and V-3.4 to define stress concentration factors which might develop in pillars. For large pillars, the intersecting set of tunnels will have little effect on the stresses for the primary set of tunnels developed at some distance from the corners of the pillars. Use of this fact enables one to fix the lower limit of the stress concentration factor. This limit corresponds to the factor

for a single set of parallel rectangular tunnels subject additionally to the limitation that this stress concentration factor cannot be less than that consistent with the reduction in area alone. At the other extreme is the case involving small pillars where the stress concentration factor at the corner of the pillar might approach a magnitude equal to the product of the appropriate stress concentration factors for each set of parallel tunnels. Obtaining the approximation, therefore, reduces to defining a rule by which the stress concentration factor decreases from the product of the two appropriate values to the value for a single set of parallel rectangular tunnels. Study of the data presented in Ref. V-3.1 and theoretical solutions similar to those presented in Ref. V-3.2 suggest that the product of stress concentration factors would be appropriate for a ratio of pillar width to opening width less than 0.25. For values of this ratio greater than 2.25 the stress concentration factor for the single set of parallel tunnels might be appropriate. Finally by recognizing that for practical cases the individual stress concentration factors for each set of parallel rectangular tunnels which form a room and pillar configuration are nearly the same, the product of the two factors can be approximated as the square of either factor. Thus, to obtain values for the stress concentration factor in a pillar with dimensions between the extremes defined above, the value of the exponent applied to the maximum stress concentration factor for one set of parallel openings was assumed to vary from 2 to 1 as a linear function of the ratio of pillar to opening width. This approximation accounts both for the reduction in area and for the stress concentration; consequently it is somewhat more conservative than the procedure which accounts only for the reduction in area. The results of this approximation are presented in Fig. V-3.5 for equally-spaced pillars and in Fig. V-3.6 for unequally spaced pillars.

Whenever relatively long tunnels are constructed it is almost inevitable that some jointing and faulting will be encountered even in a homogeneous formation. When such geologic structures are encountered, safety dictates the provision of conventional rock supports such as rock bolts (with wire mesh if the area is highly jointed or brecciated), steel sets with steel or timber lagging, or reinforced concrete.

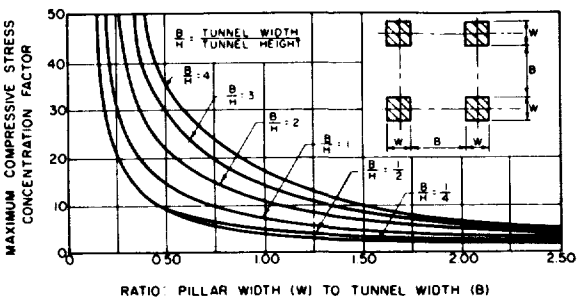

FIG. V-3.5 STRESS CONCENTRATION FACTOR FOR ROOM AND PILLAR CONSTRUCTION WITH EQUALLY SPACED PILLARS

Openings in Stratified Rock. In conventional mining practice openings in stratified formations follow either the strike or the dip of the individual strata whenever possible. Of these two it seems probable that following the dip (the angle which the planes of the strata form with reference to a horizontal plane) is preferable since the strata above the tunnel act as beams spanning the opening (see Fig. V-3.7). When the tunnel follows the strike (the azimuth of the planes of the strata), certain strata are made discontinuous by driving the tunnel; thus these strata must act essentially as cantilevers in the vicinity of the opening. Normal practice frequently requires that these discontinuous strata be fastened by rock bolts to adjacent strata. For protective structures located in these formations, rock bolts would appear to be mandatory.

In selecting a site for a protective tunnel in stratified rock advantage can be taken of the stability provided by the strata by running the tunnel in the direction of the dip of the beds. In this situation, and as long as the aspect ratio (the ratio of the long to short dimension in the planes of the strata) is greater than two, which normally would be true, each bed acts as a beam fixed at both ends spanning the roof (or back) of the tunnel. The end fixity is provided by the vertical stress produced by the overburden. When a bed which is more flexible than the one immediately above it forms the roof of the tunnel, this normally thinner stratum tends to deflect away from its neighbor so that if bond and shear between the strata are neglected the safety of the roof is defined by the resistance of the single stratum. The stresses and deflections in such a stratum can be defined in terms of the effective unit weight of the stratum, w_e, the span, L, the thickness, t_c, and the modulus of elasticity, E_c, of the critical stratum. The maximum stress produced by flexure is σ_{max}, the maximum shearing stress if τ_{max}, and the maximum deflection is δ_{max}. For elastic behavior these quantities as presented in Ref. V-3.1 become:

$$\sigma_{max} = \frac{w_e L^2}{2t_c} \qquad \text{(V-3.4)}$$

$$\tau_{max} = \frac{3w_e L}{4} \qquad \text{(V-3.5)}$$

$$\delta_{max} = \frac{w_e L^4}{32 E_c t_c^2} \qquad \text{(V-3.6)}$$

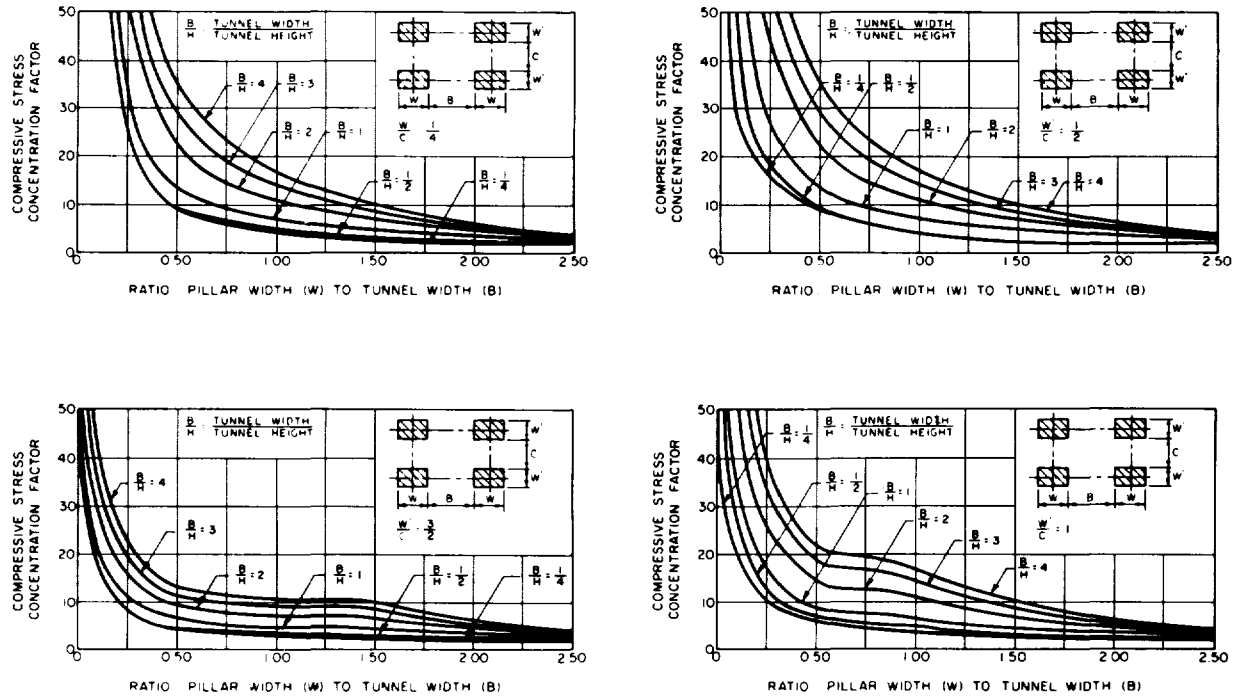

FIG. V-3.6 STRESS CONCENTRATION FACTOR FOR ROOM AND PILLAR CONSTRUCTION WITH UNEQUALLY SPACED PILLARS

In Ref. V-3.1 it is concluded, since the ultimate tensile strength is small compared with the ultimate compressive or shearing strength, that the resistance of a slab which is long compared with its thickness, is governed only by Eq. V-3.4 and thus the permissible width of tunnel opening is defined by setting σ_{max} equal to the modulus of rupture determined by laboratory tests of the rock.

Because the physical properties of rock are similar to those of plain concrete (Ref. V-3.4) the problem of defining the safe opening might be considerably more complicated for most tunnels than the procedure just described since their width generally would be small compared with the thickness of the overlying stratum. At certain spans, which are not clearly defined for beams of plain concrete, the ultimate resistance is governed by a complex function of the maximum principal tensile stress and not by the maximum shear or flexural stress alone (Refs. V-3.5 and V-3.6). This particular behavior has received much attention in the investigation of the static and dynamic characteristics of plain and reinforced concrete, but the actual phenomena controlling the behavior still are not clearly understood. This problem has not been studied in detail for rock, but the similarity between rock and plain concrete suggests that the materials might have comparable behavior.

A summary and extension of analyses of the principal stresses in elastic, homogeneous beams either simply supported or fixed at both ends is given in Ref. V-3.7. Yet experimental studies of concrete indicate that the maximum tensile principal stress alone is not the controlling parameter in defining the failure; a similar condition might be expected for rock so that the knowledge of the principal stresses may not be particularly valuable at this time. Nevertheless, certain design approximations used for plain or reinforced concrete may be helpful in defining the resistance of rock strata: (1) failure in pure shear, as defined by Eq. V-3.5, occurs when a maximum shear stress, τ_{max} develops which is equal to approximately 15 to 20 percent of the unconfined compressive strength; (2) failure in flexure can be expected when the maximum flexural stress, σ_{max}, defined by Eq. V-3.4, reaches the modulus of rupture; and (3) failure in combined shear and flexure (classically called diagonal tension) might occur at a stress (in psi) equal to $2\sqrt{\sigma_u}$ where σ_u is the unconfined compressive strength in psi. When this last limiting stress is related to the average stress, v_{max}, the following equation is obtained which defines the limiting conditions for "diagonal tension" (notation was defined for Eqs. V-3.4 to V-3.6).

$$v_{max} = 2 \text{ psi} \sqrt{\frac{\sigma_u}{1 \text{ psi}}} = \frac{w_e L}{2} \qquad \text{(V-3.7)}$$

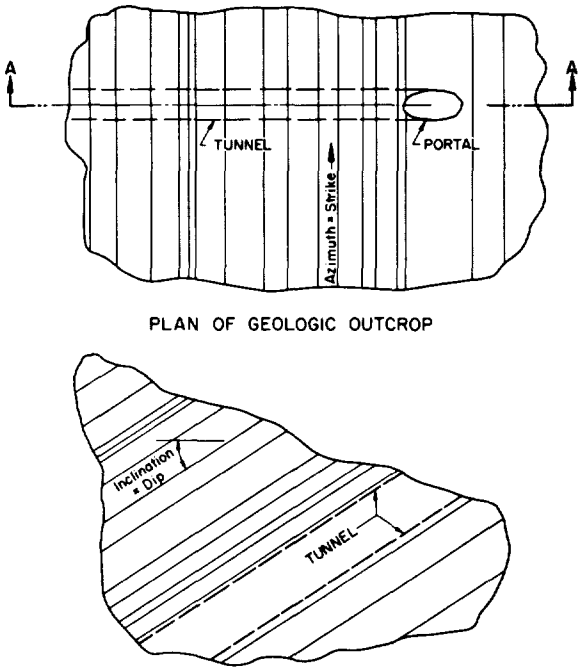

FIG. V-3.7 PREFERRED ORIENTATION OF PROTECTIVE TUNNELS IN STRATIFIED FORMATIONS

The study of the physical properties of rock in Ref. V-3.3 indicates that the modulus of rupture might be approximately 10% of the unconfined compressive strength. However the modulus of rupture may vary over wide limits from zero for a jointed formation to perhaps as high as 20% or more of the unconfined compressive strength. If 10% is taken as a reasonable average for an unjointed stratified formation, certain relations among the equations for strength can be derived to define the controlling conditions. These relations indicate that the safety of the roof is controlled by Eq. V-3.4 unless:

$$\left(\frac{\sigma_u}{1000\ \text{psi}}\right)\left(\frac{150\ \text{pcf}}{w_e}\right)\left(\frac{1\ \text{ft}}{t_c}\right) \leq \frac{1}{200} \qquad \text{(V-3.8)}$$

$$\text{or} \quad \left(\frac{150\ \text{pcf}}{w_e}\right)\left(\frac{1\ \text{ft}}{t_c}\right) \leq \frac{1}{80} \qquad \text{(V-3.9)}$$

Equation V-3.8 defines the conditions under which the safety of the roof is governed by Eq. V-3.5 ; i.e., by the maximum shearing stress. It is interesting to note that for the conditions assumed, the maximum shearing stress as a governing criterion for failure requires that L/t_c be less than unity. Equation V-3.9 defines the conditions under which the safety of the roof is governed by Eq. V-3.7; i.e., by resistance to "diagonal tension".

A first look at the last two equations indicates that the modulus of rupture would control the safety of any tunnel in a stratified formation. If only a single bed is involved this probably is true. However when a relatively stiff bed supports many layers which have less stiffness than the supporting stratum, pure shear or "diagonal tension" may become critical. For this situation, the previously derived equations may be valid provided that an effective unit weight of the critical stratum can be defined. This effective unit weight includes both the actual weight of the critical layer and the weight of the supported layers. By noting that the deflection of all layers must be equal if they remain in contact, an expression for the effective unit weight of the critical slab can be defined (Ref. V-3.1). In Eq. V-3.10 the subscript c refers to the critical slab and the subscript n refers to each supported slab; w_e is the effective unit weight on the critical slab.

$$w_e = \frac{E_c t_c^2 \sum_{n=c}^{n} w_n t_n}{\sum_{n=c}^{n} E_n t_n^3} \qquad \text{(V-3.10)}$$

Application of Eq. V-3.10 requires a trial and error procedure in which the number of slabs is successively increased between each trial until a maximum value for the effective unit weight is obtained. Equation V-3.10 should provide a conservative result since the span of all slabs is assumed the same while the span of each slab should decrease with increasing height above the tunnel as a result of the change in the radius of curvature for each successive slab. The failure and deflections of a roof consisting of several layers can be determined directly from Eqs. V-3.4 through V-3.9 by substituting w_e, calculated from Eq. V-3.10.

Parallel tunnels or room and pillar construction in stratified formations can be approached somewhat differently than it is for homogeneous formations. In stratified formations the rock between parallel tunnels or the pillars support the flat slabs of the roof. At first a moment distribution or another similar indeterminate analysis might suggest itself for analyzing the stress state in the columns. However, by virtue of the direction of stratification assumed here there probably would be an insignificant amount of moment transferred to the walls or pillars. Recognizing that the stiffness of the walls or pillars generally will be very large compared with the stiffness of the roof allows an analysis wherein the walls or pillars carry the total effective force on the portion of the roof tributary to them. This effective force already would have been found in the analysis of the roof slabs; i.e., by application of Eq. V-3.10.

V-3.1.2 Damage Mechanisms and Dynamic Load

In this section are discussed the analytical methods which define the damage mechanisms associated with tests of openings in rock. Most of the discussion pertains to tunnels located in homogeneous rock. If the acoustic properties of individual layers are similar, the problem should be similar for both stratified and homogeneous formations. If the acoustic properties of the layers are not similar shock transmission becomes extremely complex and generalizations cannot be made. However, a large reduction in the energy reaching the structure may occur as a result of reflections and refractions between individual strata of differing acoustic properties, so that locating a protective structure below these strata may be advantageous.

Stratified Formations. Based on the hypothesis presented in Section V-3.1.1 for the use of factors of safety inherent in the conventional design for static loads of tunnels in a stratified formation with matched acoustic impedance, a factor of safety of 4 to 8 or perhaps more, would imply a reserve in strength for resisting dynamic load in existing tunnels or openings of 3 to 7 times the effective unit weight in Eq. V-3.10. That is, the static load develops only a fraction of the strength available leaving a significant reserve in strength to resist the dynamic load. Yet consideration of the practical conditions normally encountered indicates a limit of effective unit weight of the order of 100 psi, which corresponds to an effective thickness of material above the tunnel of approximately 100 ft; consequently the apparent maximum intensity of dynamic stress to cause failure of a tunnel with a normal factor of safety of 8 would be of the order of only 700 psi. This limit of strength probably exists irrespective of the difference in loading mechanism associated with static and dynamic loads since normally a similar factor of safety would be used to define for static loading, the dimensions of the various components (roof, pillars, etc.) of the opening. The use of rock bolts to provide unity of action of several layers may somewhat increase the maximum intensity of dynamic stress.

On the other hand for new construction in stratified media where the maximum dimension of opening is smaller than the least dimension of the stratum in which the opening is located, the resistance to dynamic load can be evaluated in the same manner as it is for an opening in a homogeneous formation.

Homogeneous Formations. The analysis in Ref. V-1.31, which has been extended and corroborated with minor changes and with extensions in Refs. V-3.8 through V-3.11, indicates that the stress concentrations around circular openings caused by nuclear explosions and by static loads, which produce planar stress distributions in the vicinity of the opening, are practically identical. As long as the hole is small enough that the duration of the dynamic loading is several transit times across the hole this result of the analyses should be valid; this duration of loading is implicit in the analyses cited and such a duration would normally be required to provide equivalence between static and dynamic conditions if it exists. For nuclear explosions of even kiloton yield this criterion would imply openings of extraordinary dimensions. Consequently it may be assumed that stress concentrations comparable to those induced by static loads, summarized in Table V-3.1 and in Figs. V-3.3 through V-3.6, might be expected to develop for all dynamic loads considered here.

Furthermore, tests of many materials indicate that the strains retain a distribution consistent with elastic theory even after Hooke's law no longer applies (see for example Ref. V-3.12). This suggests that the theoretical stress concentration factor is directly equivalent to a strain concentration factor even as the material approaches failure.

Based on this postulate and observations of the behavior of materials in general, simple procedures can be developed for defining the limiting ranges at which the types of damage observed in tunnels develop. The limits of these types of damage were defined in Section V-1.5.1, and they are summarized here:

- Limit of Closure
- Limit of General Compression Failures
- Limit of Local Compression Failures
- Limit of Damage

The limit of closure develops when the rock surrounding the opening can begin to sustain the stress wave without crushing in a partially-confined state. The rock is not totally confined because of the presence of the opening. Partial confinement, however, is developed because of the finite time required for the rock, as it crushes, to move into the opening. The effect of this partial confinement can be accounted for by assuming a strain (in the free field at a range corresponding to the location of the opening) at failure which is approximately three times the strain corresponding to the unconfined compressive strength of the rock. At least such an assumption gives results consistent with the results in Ref. V-1.25. Also the assumption is justified by tests on concrete (Ref. V-3.13), assuming that concrete behaves in a manner similar to rock. Normally for most types of rock, this strain is between 0.5 to 1.0%.

The limit of general compression failure occurs where the local compressive strains around the opening equal the strain at ultimate conditions in partially-confined compression. If ϵ_u is the strain corresponding to the ultimate strength in unconfined compression and K_c is the maximum compressive

strain concentration around the opening, general compression failure ceases when the strain in the free field ϵ is:

$$\epsilon \cong \frac{3\epsilon_u}{K_c} \qquad \text{(V-3.11)}$$

As it is in the case immediately preceding, $3\epsilon_u$ for most rock types is between 0.5 to 1.0%.

Local compression failure develops as long as the local compressive strain around the opening exceeds the strain corresponding to the ultimate strength in unconfined compression. With the notation previously defined the limit of this type of damage occurs when:

$$\epsilon = \frac{\epsilon_u}{K_c} \qquad \text{(V-3.12)}$$

For most types of rock ϵ_u is between 0.2 to 0.4%.

Finally the limit of damage develops when the local tensile strains around the opening equal the strain ϵ_t corresponding to the effective tensile strength of the rock; thus if K_t is the appropriate maximum strain concentration factor for tension, the limit of damage occurs when:

$$\epsilon = \frac{\epsilon_t}{K_t} \qquad \text{(V-3.13)}$$

Normally for most types of rock ϵ_t is between 0.03 to 0.06%.

The stress concentration factors in Table V-3.1 and in Figs. V-3.3 through V-3.6 are approximately consistent with a dilatational wave with a duration of at least several transit times (Ref. V-1.31). For a tunnel located directly below the burst, it would appear that the dilatational wave would be most important in causing damage. Even for tunnels located at great depths but removed from the point of detonation, the dilatational wave, whether it be directly- or airblast-induced, probably is of greater importance in causing damage than the shear or Rayleigh waves. This assumption is based on the empirical observation that the initial part of the stress wave has a greater intensity than the later parts, and the dilatation wave propagates with the highest velocity.

Experimental evidence (Ref. V-1.53) from Operation Hard Hat (a contained nuclear detonation in granite), supports the preceding postulate. In Ref. V-2.7 approximate relations based on high explosive tests and nuclear tests (Rainier and Hardtack) are developed for the directly-induced stress wave in rock produced by a nuclear surface burst. The peak radial strain, ϵ, in the free field is defined in this reference in terms of the distance, R, from the center of a surface burst and the weapon yield, W:

$$\epsilon \cong 0.001 \text{ in./in. } \left(\frac{1000 \text{ ft}}{R}\right)^{5/2} \left(\frac{W}{1 \text{ mt}}\right)^{5/6} \qquad \text{(V-3.14)}$$

This expression is independent of the seismic velocity in the medium; however, other parameters (such as stress, particle velocity, etc.) are not independent of seismic velocity. Using this strain in Eqs. V-3.4 through V-3.13 with $\epsilon_u = 0.003$ in./in. and $\epsilon_t = 0.0005$ in./in. (Ref. V-3.4) and with $K_c = 3$ and $K_t = -1$ (for a circular tunnel with Poisson's ratio of zero which it would approach for a jointed formation) gives ranges measured from the point of detonation of approximately 420, 640, 1000 and 1300 ft for each of the successively larger limits of damage for openings in granite subjected to the effects of a 1-mt surface burst. These limits mean that an unlined tunnel in granite would be completely closed by the detonation of a 1-mt burst at the surface if it were 420 ft or less below the surface, damaged beyond usefulness at 640 ft or less, damaged but repairable at 1000 ft or less, and undamaged at 1300 ft below the surface.

Comparison of these ranges with data obtained in high explosive tests of nearly circular tunnels in granite (Ref. V-1.25) is presented in Table V-3.2. The high explosive data in the table are scaled using a nuclear-high explosive yield equivalence of 0.06 as derived in Ref. V-2.7. This yield equivalence was obtained from empirical data obtained in granite and sandstone for high explosive charges and in tuff for nuclear detonations. The Hard Hat event indicates the equivalences in Ref. V-2.7 are reasonable, but there now exist only limited theoretical information on the problem of nuclear-high explosive yield equivalence.

Spalling. In addition to the types of failure just described, experiments indicate that damage may occur by spalling when the stress wave strikes the free surface of the tunnel. Laboratory experiments (Ref. V-3.14) confirm the possibility of spalling for certain tunnel configurations which have nearly plane surfaces but indicate that spalling might not occur for circular or nearly circular openings. However, in an actual circular tunnel spalling might also occur because of the inherent irregularities in the shape and because of the possible weakening of the rock in the vicinity of the tunnel resulting from the construction. Thus, the possibility of spalling should always be considered.

TABLE V-3.2 COMPARISON OF MEASURED* LIMITS OF DAMAGE IN GRANITE (SCALED TO A 1-mt SURFACE BURST) WITH THOSE COMPUTED BY METHODS DEVELOPED IN SECTION V-3.1.2

	Limit of Closure (ft)	Limit of General Compression Failure (ft)	Limit of Local Compression Failure (ft)	Limit of Damage (ft)
Measured*	440	800	1200	1300
Computed	420	640	1000	1300

*The measured values are from high explosive tests (Ref. V-1.25) converted to be equivalent to a 1-mt surface burst using a yield equivalence of 0.06 (Ref. V-2.7).

Definition of the conditions under which a spall might form is shown in Fig. V-3.8a in which a compressional wave is intersecting a free surface thereby generating a tensile wave in the opposite direction. For the geometry and notation in the figure, the thickness of the spall, D, is given by:

$$D = \frac{\bar{\epsilon}}{2\epsilon} L_p \qquad (V\text{-}3.15)$$

The case shown in Fig. V-3.8a represents a plane compressive stress wave of triangular shape intersecting a plane surface. In such a case the boundary conditions require that a tensile wave be generated which travels back into the medium from the free surface. Whenever the tension exceeds the compression by an amount equal to approximately the ultimate tensile strength of the rock in situ a spall will form. Multiple spalls can form by the same process since, after one spall forms, a new free surface is formed and if the length of the compressive pulse is sufficient the net tension can again exceed the ultimate tensile strength causing a new spall of depth, D, to form for the triangular incident wave.

In Fig. V-3.8a a simple triangular shape is used to approximate the incident compressive stress wave. The actual stress wave normally decays exponentially with time, and it may exhibit a finite rise time as well as high frequency variations of stress superimposed on the decaying wave. The length of the triangle shown in the figure is adjusted such that the impulse of the triangular approximation equals the impulse of the actual curve. The rise time is neglected which results in spall thickness which may be smaller than the actual thicknesses if the presence of high frequency components are neglected. Consideration of the effect of high frequency variations of stress in the incident wave, however, complicates the over-all picture; at the moment there appears to be no theory which predicts accurately these high frequency effects.

Finally it should be noted that the representation of the spalling process in Fig. V-3.8a also illustrates what tends to happen locally for tunnel cross-sections with curved surfaces.

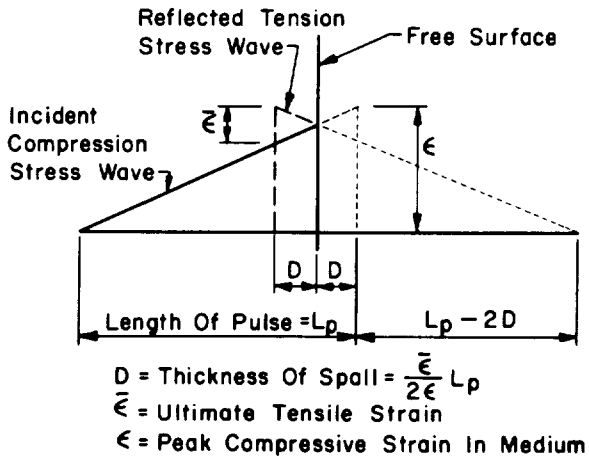

FIG. V-3.8a ASSUMED CONDITIONS PRODUCING SPALLING

Unless the characteristics of the medium and of the explosion are such that they produce a stress wave which approaches a true shock (Fig. V-3.8a), it is highly doubtful that a spall* can form. This results from the thickness of spall, D, becoming, for finite rise times (Fig. V-3.8b), so large in comparison to the size of the opening that the potential spall cannot enter the opening. Most rocks are not capable of developing and sustaining a true shock wave; thus this mechanism generally does not develop for the cases considered here.

When spalling can occur, the spalls produce a loading on the lining which is consistent with the kinetic energy of the spall, or if several spalls can form the sum of the kinetic energies in the individual spalls. The kinetic energy in each spall is defined by the mass and by the momentum trapped in it at the time it forms.

*This doubt is supported by the absence of pieces of rock embedded in the packing in Event Hard Hat. The work on which this evidence is based has just been completed, and a detailed report is under preparation at the time of this writing.

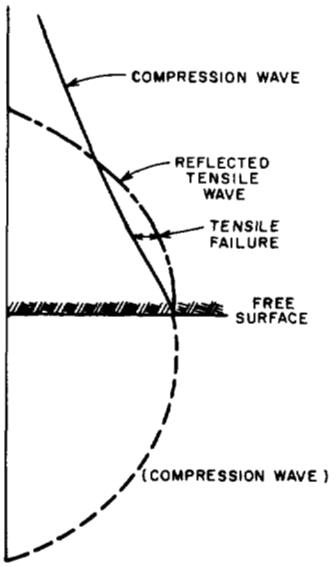

FIG. V-3.8b SPALLING WITH FINITE RISE TIME

V-3.1.3 Tectonic Forces

Tectonic forces are those associated with the diastrophism producing geologic formations and those generated through the subsequent history of the formation. For example, when an igneous intrusion is formed, large compressive stresses exist in the molten rock as a result of the confinement offered by the surrounding material. As the intrusion cools however large tensile stresses can develop through shrinkage and differential solidification. The folding of the earth's crust as a result of igneous intrusions and/or shifting of the earth's mantle produces large residual stresses in the rock. These residual stresses subsequently may be modified through erosion or faulting.

Residual stresses in any rock formation can impair its ability to resist static and dynamic stresses around tunnels located in it. Therefore it is important to have some measure of the natural state of stress to determine the effect of these stresses on the behavior of any tunnel located in the rock. In general it is impossible to estimate quantitatively these stresses from surface and subsurface studies of the geology. Instead it is necessary actually to measure these stresses. Methods are constantly being developed for making these measurements (see for example Ref. V-3.15).

If the tectonic forces are measured, their effect should be considered in assessing the behavior of a tunnel. When these forces cannot be measured beforehand, an estimate of their magnitude should be made to assess the behavior of tunnels. It should be kept in mind, however, that current methods for designing underground openings are based on strengths of cores of rock determined in the laboratory. Frequently the variation in strength between individual specimens is greater than the stress associated with the tectonic forces. Furthermore, the laboratory specimens might not be representative of the in situ conditions because removal of the core releases stresses trapped in it and this stress relief might affect the strength of the core. This speculation is based on the often observed Bauschinger effect in metals in which overstraining in one direction significantly alters subsequently observed strength properties when a test is conducted on the same specimen with stresses applied in the opposite direction. Therefore, although the effect of tectonic forces should always be considered, it frequently will be found that their influence is less than the uncertainties in the controlling strength parameters. Consequently it seems reasonable to include tectonic forces in the analysis only when it is suspected that their influence is larger than the uncertainties in the strength properties used in the over-all analysis.

V-3.2 STRESSES AND DISPLACEMENTS AROUND LINED TUNNELS IN SOIL AND ROCK

V-3.2.1 Dead Loads

Linings for tunnels in competent rock normally will not be subjected to any static load except the weight of the lining itself and of any backpacking placed around the lining. For tunnels in soil or in heavily fractured rock the lining must often support a relatively large static load.

Whether the lining is located in soil or highly fractured rock, it would appear that the forces reaching the lining would be similar. According to Terzaghi (Refs. V-2.4 and V-3.16) the vertical component of stress, $\bar{\sigma}_v$, acting on a tunnel with horizontal span B, height h, and in soil (or rock) with an angle of internal friction, φ, unit weight, w, and cohesive strength, $\bar{c}$, is:

$$\bar{\sigma}_v \leq w\left(0.50B + 0.58h - \frac{\bar{c}}{w}\right)\frac{1}{\tan\varphi} \qquad \text{(V-3.16)}$$

If the tunnel is rectangular the vertical walls can be treated as if they were retaining walls of height h subjected to an additional surcharge equal to $\bar{\sigma}_v$. For circular or nearly circular tunnels the static load produces a nearly uniform stress around the tunnel which is equal to $\bar{\sigma}_v$.

Any structural lining must resist these static stresses. Also the circular linings must have sufficient flexural strength to account for any nonuniformity of loading which might develop as a result of nonhomogeneities in the soil or the construction procedures used. These nonuniformities cannot be generalized so that in design practice a percentage of

the vertical stress depending upon the site conditions normally is assumed. Normally the nonuniform stress is taken as 10% of the vertical stress but in plastic soil or so-called squeezing ground it may be several times the vertical stress.

V-3.2.2 Dynamic Loads

In addition to the static load, the structural lining must resist the effects of the dynamic loading produced by the blast. The blast loading on the lining may be of extreme intensity near the crater. On the other hand as the limit of damage is approached, the loading on a lining in competent rock might consist only of the weight of a block of rock which was dislodged from the roof with zero initial velocity. Providing structural integrity against this latter hazard, frequently termed rock drops, is a simple problem. Normally wire mesh held in place by conventional rock bolts will protect against this hazard.

Also at great depths below the surface in soil the stress wave may attenuate significantly as a result of dispersion or dissipation so that the intensity of stress reaching the tunnel is relatively insignificant.

Therefore, of primary concern in this section are the loads imparted to liners in rock and soil at ranges relatively close to the center of the burst. In rock the loads imparted to the linings are those associated with crushing and spalling of the rock around the tunnel surface. In soil the range in loads to be considered is not as clearly defined as in rock.

Relative Compressibility. Although it is inherently important, an interesting limiting condition can be approximated by neglecting the acoustic impedance between a lining and the surrounding material. This condition might be determined by considering the compressibility of the lining relative to the compressibility of the material replaced by the lining. This approach is most easily formulated for a cylindrical configuration. For a uniform hydrostatic stress field in the vicinity of a tunnel, equating the circumferential strain in the cylinder of material removed to the approximate circumferential strain in the lining yields (Ref. V-3.2):

$$\frac{t}{r} = \frac{E_m}{E_\ell} \frac{1}{1 - \nu_m} \cong \frac{E_m}{E_\ell} \qquad \text{(V-3.17)}$$

where t is the thickness of a solid lining, r is the mean radius of the lining, E_m is the modulus of elasticity of the medium, E_ℓ is the modulus of elasticity of the lining material and ν_m is Poisson's ratio for the medium. If, as is likely, the stress in the medium surrounding the tunnel is not hydrostatic, a much thicker lining is required to obtain matched compressibility since the lining would be subjected to relatively large flexure.

From Eq. V-3.17 it may be seen that the ratio of thickness to radius for a solid lining would have to be very large for a structure located in competent rock since E_m and E_ℓ would be of the same order of magnitude. On the other hand, for soil, E_m probably would be at least an order of magnitude less than E_ℓ or the ratio of thickness to radius for a solid lining might be of the order of 10%. As discussed in Section V-3.1.3, increasing the compressibility of a structure in soil might significantly enhance the arching. However, at the moment it is not clear how arching in soil depends on the compressibility. Because of the much smaller compressibility required to match the rock replaced as compared to soil, it is doubtful that increasing the compressibility of a lining in rock would significantly influence the forces acting on the lining. Also, it is difficult to place a lining in competent rock which will be in continuous contact with the rock face. Therefore, it would appear that a concept other than compressibility must be used to evaluate the behavior of a lining in competent rock.

Loads Produced by Deformation of Rock Openings. If a lining in rock is placed such that sufficient clearance is provided between the outer surface of the lining and the surface of the rock cavity to allow deformations of the rock to occur without contacting the lining, the load reaching the lining will be only that imparted by the spalls which might form. However, at ranges from the detonation approaching those associated with closure of the rock opening it appears impossible to provide sufficient space to prevent the deformed surfaces of the cavity from contacting the lining; an energy absorbing filler, or packing, must be provided in the space between rock and lining to resist the deformation and, in doing so, to act with the lining in absorbing the energy in the failed rock and to distribute the load more uniformly over the surface of the lining. At longer ranges, well beyond where closure of a tunnel is expected, an integral lining in contact with the rock can provide sufficient resistance to prevent the failed rock from entering the tunnel.

As a means of determining the properties required in the total lining system (the interior lining and the packing, if any, surrounding it), it appears adequate to provide in the lining system sufficient energy absorbing potential and sufficient thickness of packing to accommodate both the energy associated with the failure and the deformations of the surrounding rock. The energy associated with the failure of the surrounding rock, whether it be part of a homogeneous or stratified geologic formation, may be taken approximately as the total strain energy which would have been induced by the stress wave in the core of rock replaced by the total lining system. Computation of the total strain energy requires first estimating the effective, compressive stress-strain relation for the rock in situ; the area under this stress-strain curve between zero strain and the strain consistent with the distance from the detonation to the tunnel (computed from Eq. V-3.14) is multiplied by the total volume of the rock replaced

by the structural system. It appears adequate to take for the effective, compressive stress-strain curve that curve defined by unconfined compressive tests on small, sound cylindrical cores taken from the rock; at the moment it appears that the effect of jointing on the strength so defined and the confinement which exists in situ are largely compensating.

The inward displacement of the rock surrounding an opening accompanying the failure of the rock is difficult to estimate from the data now available (Ref. V-1.25 or V-1.53). Yet it seems clear (Ref. V-3.17) that this displacement is caused by the bulking, or increase in volume, of some volume of rock extending beyond the surfaces of the opening. This bulking increases from essentially zero at the limit of local compression failure to large values at the limit of closure. Therefore, because this bulking, and the associated deformation, cause the more severe loading on the lining, integral linings in contact with the rock can be expected to survive at a range slightly greater than that associated with the limit of local compression failure. At lesser ranges the deformations accompanying the bulking are larger than can be accommodated without failure of a conventional integral lining. Thus, energy absorbing packing must be interposed between the surface of the rock and the outer surface of the lining if survival without structural damage is to be provided at ranges less than the limit of local compression failure. Limited data now available (Ref. V-3.17) indicate that for structural survival the packing thickness must range from approximately one-tenth of the radius of the rock opening at the limit of local compression failure to approximately one-half the radius of the rock opening at the limit of general compression failure. Also it appears sufficient for design purposes to assume a maximum deformation of the rock caused by bulking of one-half the required thickness of the packing. The minimum deformation of the rock caused by bulking occurs on a line nearly perpendicular to a line through the axis of the tunnel and the point where maximum deformation of the rock occurs. This minimum deformation is small, and for design purposes, it frequently may be assumed to be zero.

These deformations produce strains in the packing which, in turn, develop the stress on the interior structural lining. However, the subsequent deformation of the interior lining alters the strain in the packing and consequently the stress distribution on the structural lining. This complex problem of interaction is discussed briefly in the following section.

V-3.2.3 Lined Tunnels with Energy Absorbing Packing

Lined tunnels with highly energy absorbant packing interposed between the lining and the rock are required to survive structurally the effects within the range defined by the limit of general compression failure and the limit of local compression failure. This structural system must resist the energies and deformations associated with the failure of the surrounding rock. For design purposes these phenomena may be treated separately: (1) the thickness of the packing required to accommodate the deformation is defined in the discussion preceding; and (2) the required strength of the packing is defined by the energy in the volume of rock replaced by the total lining system.

To provide an optimum amount of energy absorption the packing material should ideally have a rigid-plastic stress-strain curve of the type shown in Fig. V-3.9. Also shown in Fig. V-3.9 are the types of stress-strain curve which are obtained in the tests of granular materials (confined in a cylinder), and of certain foamed plastics (such as rigid polyurethane). (The curves shown are derived from tests conducted at the University of Illinois which are not yet published.) Some lightweight concretes (such as cellular neat cement and vermiculite concrete) have resistance characteristics similar to those of plastic foam. However, the lightweight concretes generally are highly permeable, and precautions must be taken to prevent their becoming saturated if they are used as packing materials.

Because the packing should have a much higher potential to absorb energy than the interior structural lining, little error is introduced if the energy absorption of the structural lining is ignored in computing the required energy absorption in the system. For an ideally rigid-plastic material (or approximately for plastic foams up to locking), the energy absorption per unit of surface area E_f can be written in terms of the thickness t_f, the strain ϵ_f (at locking in plastic foams) and the plastic resistance:

$$E_f = r_f \epsilon_f t_f \qquad \text{(V-3.18)}$$

The resistance required in the packing material r_f is defined by equating Eq. (V-3.18) to the total strain energy defined by the effective stress-strain for the rock expressed in terms of the unit surface area for the core of rock replaced by the total structural system.

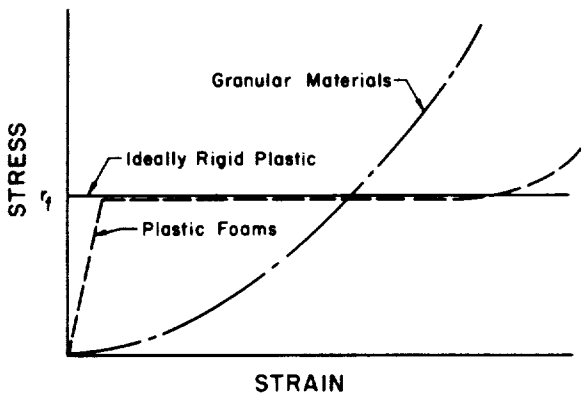

FIG. V-3.9 SCHEMATIC REPRESENTATION OF STRENGTH PROPERTIES OF MATERIALS FOR TUNNEL ISOLATION

The interior structural lining enclosed in the packing must possess sufficient strength and buckling resistance to develop the strength of the packing. Evaluation of the required strength requires assuming the proportions of the interior lining and computing the resistance of this lining to combined axial load and flexure. To provide optimum resistance this lining normally will be a right-circular cylinder or a capsule consisting of a right-circular cylinder with hemispherical ends. Because the deformations of the bulking rock are nonuniform, the deformation, and consequently the stress, in the packing is nonuniform. Thus, the interior lining is subjected initially to a nonuniform stress distribution. For design purposes this nonuniformity may be assumed to cause the lining to deform in the pattern of a sine wave with two complete waves developing in the circumference (Fig. V-3.10). Further the stress may be divided into two components, one a uniform component q and the other a sinusoidal component p. The sinusoidal component p, causes the dominant flexure, but as a result of the curvature, the uniform component also produces bending. If the total deflection of the lining is δ while the maximum deformation of the surface of the rock is Δ_m and the minimum deformation Δ, then the strains produced in the packing and the associated stresses are as shown in Fig. V-3.11 wherein t_f is the thickness of the packing. As indicated in the figure (Fig. V-3.10) the strain in one direction is $\frac{\Delta_m - \delta}{t_f}$ while at a point 90° removed the strain is $\frac{\Delta + \delta}{t_f}$; the corresponding stresses are the sum of p and q and the difference between q and p, respectively. The deformations δ and the stresses in the packing and in the adjacent lining must be compatible. Thus, a solution is determined by assuming various values of δ and computing the corresponding values of p, for the

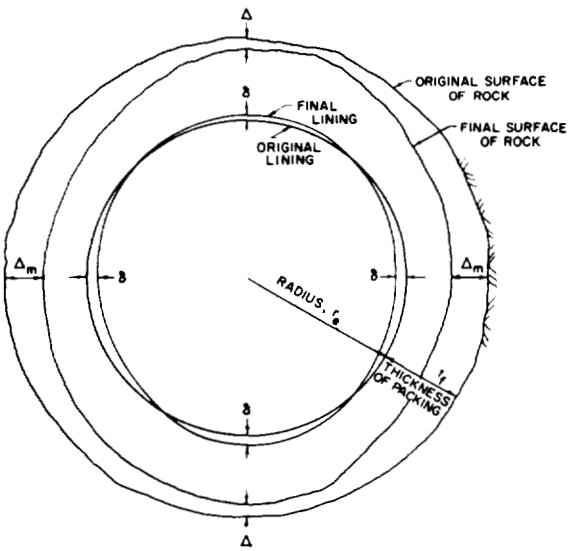

FIG. V-3.10 DEFORMATION OF LINING AND PACKING

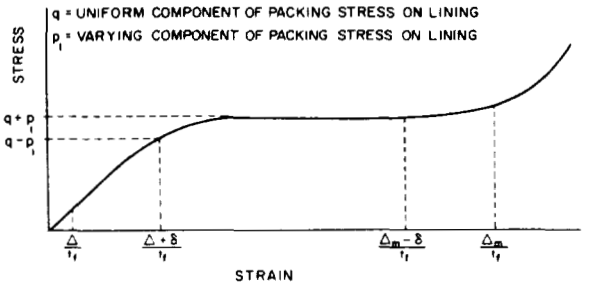

FIG. V-3.11 LOAD-COMPRESSION RELATION FOR PACKING

packing. This defines a curve of p, as a function of δ, which is plotted on the same coordinates as the load-deformation diagram for the interior lining (Fig. V-3.12). The solution is defined by the point (p_1, δ_1) where the two curves cross as indicated in Fig. V-3.12.

Buckling of the interior lining may be investigated conservatively, (possibly too conservatively), as if the interior lining were a cylinder subjected to a uniform external pressure equal to the plastic resistance of the packing. For this case (Ref.V-3.18)

$$q_{cr} = \frac{3\,EI}{r^3} = r_f \qquad \text{(V-3.19)}$$

where

q_{cr} = uniform pressure causing buckling to be imminent

E = modulus of elasticity of lining material

I = moment of inertia of lining

r = mean radius of lining

r_f = plastic resistance of packing

Since the lining must have at least this buckling resistance an initial trial section for the lining can be obtained by computing the section required to provide the requisite buckling resistance and increasing the thickness or moment of inertia of this section by an arbitrary amount.

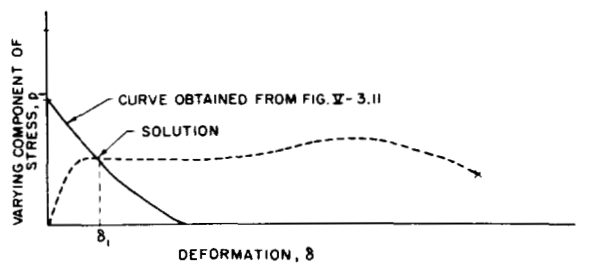

FIG. V-3.12 LOAD-DEFORMATION RELATION FOR LINING

The buckling load defined by Eq. V-3.19 is conservative since it neglects completely the elastic restraint provided by the surrounding packing. A brief study has been made of this problem by the writers (Ref. V-3.17), and the equations are highly nonlinear.

The use of a packing material to surround the lining has some advantage in reducing the peak accelerations and velocities imparted to the interior lining; however limited data (Ref. V-3.19) indicate that any reduction is relatively small, being at the most a factor of 2 reduction in acceleration with essentially no reduction in displacement or velocity.

REFERENCES

V-3.1 Design of Underground Installations in Rock, Manual prepared by APRL of BuMines for U. S. Army, Corps of Engineers, EM 1110-345-432, Wash., D.C., 1961.

V-3.2 Timoshenko and Goodier, Theory of Elasticity, New York: McGraw-Hill, Book Co. Inc., 2nd ed., 81, 1951.

V-3.3 Judd and Huber, Correlation of Rock Properties by Statistical Methods, International Symposium on Mining Research, Rolla, Mo., Feb. 1961.

V-3.4 Physical Properties of Some Typical Foundation Rocks, U. S. Department of Interior, Bureau of Reclamation, Denver, Colo., Aug. 1953.

V-3.5 Laupa, Siess, and Newmark, Strength in Shear of Reinforced Concrete Beams, Engineering Experiment Station, Univ. of Ill., Bulletin 428, Urbana, Ill., 1955.

V-3.6 Guralnik, Strength of Reinforced Concrete Beams, Transactions, ASCE, 125, 603-643, (1960).

V-3.7 Caudle and Clark, Stresses Around Mine Openings in Some Simple Geologic Structures, Engineering Experiment Station, Univ. of Ill., Bulletin 430, Urbana, Ill., 1955.

V-3.8 Pao and Mow, Dynamic Stress Concentrations in an Elastic Plate with Rigid Circular Inclusion, Mitre Corporation, Bedford, Mass., SR-41, Dec. 1961.

V-3.9 Logcher, A Method for the Study of Failure Mechanisms in Cylindrical Rock Cavities Due to the Diffraction of a Pressure Wave, School of Engineering, MIT, Cambridge, Mass., Report T62-5, July 1962.

V-3.10 Paul, Interaction of Plane Elastic Waves with a Cylindrical Cavity, Ph.D. Thesis, Dept. of Civ. Eng., Univ. of Ill., Urbana, Feb. 1963.

V-3.11 Yoshihara, Robinson, and Merritt, Interaction of Plane Elastic Waves with an Elastic Cylindrical Shell, Univ. of Ill., Dept of Civ. Eng., Urbana, Ill., SRS 261, Jan. 1963.

V-3.12 Seelye and Smith, Advanced Mechanics of Materials, New York: John Wiley & Sons, Inc., 2nd ed., 511-581, 1952.

V-3.13 Richard, Brandtzaeg, and Brown, Study of the Failure of Concrete Under Combined Compressive Stresses, Univ. of Ill., Col.of Eng., Urbana, Ill.,Bul. 185, Nov. 1928.

V-3.14 Rinehart, Model Experiments Pertaining to the Design of Underground Openings Subjected to Intense Ground Shocks, Res. Found., Colo. Sch of Mines, Golden, Colo., Jan. 1960.

V-3.15 Merrill, Static Stress Determinations in Salt-Site, Cowboy, BuMines, App. Phys. Res. Lab., Report APRL 38-3.1, July 1960.

V-3.16 Proctor and White, Rock Tunneling with Steel Supports, (Especially Section 1 by Terzaghi), The Commercial Shearing and Stamping Co., Youngstown, Ohio, 1946.

V-3.17 Newmark and Merritt, Design of Tests of Nearly Invulnerable Structures in Granite, DASA-1399, Urbana, Ill., July 1963 (Secret Formerly Restricted Data).

V-3.18 Timoshenko, Theory of Elastic Stability, New York: McGraw Hill Book Co, Inc., 1936.

V-3.19 Barton and Lindahl, Displacement Spectrum Measurements, STL, Operation Nougat, Shot Hard Hat, POR-1806, 1963 (Confidential).

CHAPTER V-4

SINGLE-DEGREE-OF-FREEDOM SYSTEMS

V-4.1 INTRODUCTION AND GENERAL PHILOSOPHY

This chapter presents the methods of solving for the dynamic response of single-degree-of-freedom systems (Fig. V-4.1), and indicates the important conclusions which may be drawn from these solutions. At first it might appear that the development in this chapter is backward: The conclusions are presented prior to the detailed discussion of the methods of solution. The emphasis here is used to circumvent some of the potential misconceptions frequently inherent in the classical procedures. The source of these possible misconceptions can be illustrated by enumerating the steps normally followed in the solution of a particular problem:

First, most structures and individual elements are so complex that certain idealizations are needed to reduce the design to a tractable problem. Usually the idealization results in a relatively simple mathematical model. Second, the physical properties of the element are characterized in some way based on an estimate of the manner in which the structure responds to the forces and motions. Most often these characterizations require the specification of the strength, ductility, and other physical properties of the materials used in the structure. Next, the forces and motions imposed on the structure must be inferred. Finally an analysis is performed using the model, the estimated structural characteristics, and the inferred forces and motions. The model of the structure selected, which frequently depends upon the loading and motion, may not represent the actual member under its actual loading. Estimates of strength and stiffness may err by a large amount since it is well documented that the strength characteristics of structural materials made under the same specification can have a variation of commonly 25 to 30% from a minimum value. Variations may be even larger between the forces and motions actually sustained and those inferred. At first glance all of these factors may suggest a hopeless situation, but actually it is little, if any, worse than the perhaps more familiar cases normally encountered by the engineer. Instead, these factors dictate against the use of analyses which are quite sensitive to changes in the controlling parameters; most classical methods of analysis possess this sensitivity. Furthermore, most classical procedures require that the detailed dimensions and characteristics of the element be known; thus, the properties of the element must be literally guessed at before the analysis can proceed. This last observation is the crux of the problem: If a shrewd assumption can be made for the properties required in a structure, then no further analysis need be made. The damage-pressure-level equation and associated methods, including the use of the "response spectrum" analysis, provide systematic means of determining the properties required in a structure. At the same time they allow rapid appraisal of the effects of changes in the controlling parameters.

On the other hand, classical methods cannot be dismissed as unimportant since they are the basis of the damage-pressure-level equation and associated methods. In fact the damage-pressure-level equation represents the complete spectrum of solutions gained from application of methods of conventional dynamic analysis to single-degree-of-freedom systems.

At this point, it also is important to emphasize a basic premise of the field of protective construction in general: Except in those relatively rare instances where large deflections will compromise the functional character of the element, some inelastic action of structural components must be allowed in the design. Justification of this premise can be illustrated by a simple example: If a simple oscillator (Fig. V-4.1) is subjected to a step-pulse of force with infinite duration and if elastic behavior is maintained, the minimum resistance required at yielding is nearly twice that required when large inelastic action is allowed in the same oscillator. Generally providing twice the resistance at yielding in a given structure constitutes a luxury which may, in terms of total cost, mean that the structure cannot be built; other solutions may prove significantly less expensive.

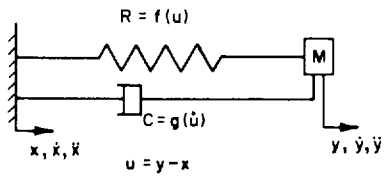

FIG. V-4.1 SINGLE-DEGREE-OF-FREEDOM SYSTEM OR SIMPLE OSCILLATOR

V-4.2 MATHEMATICAL MODELS OF COMPLEX STRUCTURAL SYSTEMS

Detailed study of the single-degree-of-freedom (SDF) system or model is important for two reasons: (1) Many complex structural systems can be idealized as simple oscillators provided that care is taken in

specifying the properties of the idealized model; and (2) a wealth of knowledge has been developed for the simple oscillator. Once the structure is designed by assuming it to act as a SDF system, an analysis using a more complex model is possible if it is desired.

V-4.2.1 Approximation of Loading and Response, Elastic Systems

Consider a simply-supported beam subjected to a uniformly distributed load as shown in Fig. V-4.2. Ideally the uniform loading develops, for example, when airblast is traveling in a direction perpendicular to the axis of the member. (For beams of practical length it has been shown (Ref. V-4.1) that the air shock velocity is such that little error is introduced if a uniform loading is assumed even when the airblast is traveling parallel to the axis of the member.) At any instant of time, it is easily shown that the loading is represented by the following Fourier series

$$p_n = \frac{4p}{\pi} \sum_{n=1,3,5...}^{\infty} \frac{1}{n} \sin\frac{n\pi x}{L} \qquad \text{(V-4.1)}$$

wherein p is the magnitude of the applied load, x is the coordinate measured from the support, and L is the span of the beam. Use of the familiar differential equation developed in strength of materials for elastic behavior:

$$\frac{p_n}{EI} = \frac{d^4y}{dx^4} \qquad \text{(V-4.2)}$$

leads to the following series defining the deflection at the center of the beam, y_b, if the load is statically applied.

$$y_b = \frac{4pL^4}{\pi^5 EI} \sum_{n=1,3,5...}^{\infty} \frac{1}{n^5} \sin\frac{n\pi}{2} \qquad \text{(V-4.3)}$$

where

E = modulus of elasticity of material in beam

I = moment of inertia of cross section of beam.

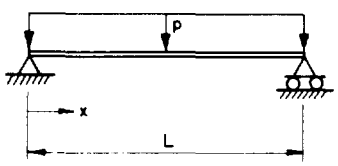

FIG. V-4.2 SIMPLY SUPPORTED BEAM SUBJECTED TO A UNIFORMLY DISTRIBUTED LOAD

Incidentally this series, for the case under consideration, must yield

$$y_b = \frac{5pL^4}{384EI}$$

Now consider two limiting conditions for the variation of the loading with time: (1) a step pulse of force with infinite duration (Fig. V-4.3) and (2) an impulse (Fig. V-4.4). From the solutions developed in Section V-4.3.1 it can be shown that Eqs. V-4.4 and V-4.5 represent the solutions for these two limits respectively, when there is no damping.

$$\bar{y}_b = \frac{4pL^4}{\pi^5 EI} \sum_{n=1,3,5...}^{\infty} \frac{1}{n^5}\left(1 - \cos\frac{2\pi t}{T_n}\right) \sin\frac{n\pi}{2} \qquad \text{(V-4.4)}$$

$$\bar{\bar{y}}_b = \frac{4pL^4}{\pi^5 EI} \sum_{n=1,3,5...}^{\infty} \frac{2\pi t_1}{n^3 T_n} \sin\frac{2\pi t}{T_n} \sin\frac{n\pi}{2} \qquad \text{(V-4.5)}$$

where

$\bar{y}_b$ = deflection at center line for step pulse of infinite duration

$\bar{\bar{y}}_b$ = deflection at center line for impulsive loading

t = time

t_1 = duration of impulse

T_n = natural period of vibration in the nth mode

$= \frac{2L^2}{n^2\pi}\sqrt{\frac{m}{EI}}$, in which m = mass of beam per unit of length.

Alternatively Eq. V-4.5 can be written in terms of the impulse i:

$$\bar{\bar{y}}_b = \frac{8iL^4}{\pi^4 EI} \sum_{n=1,3,5..} \frac{1}{n^3 T_n} \sin\frac{2\pi t}{T_n} \sin\frac{n\pi}{2} \qquad \text{(V-4.5')}$$

It should be noted that Eq. V-4.5 is valid only when t_1 is much less than T_n.

The maximum values of deflection from Eqs. V-4.4 and V-4.5 can be determined by combining the effects of all of the modes, of which there is an infinite number. When only the first mode is considered, the maximum deflection for the step pulse has the magnitude

$$\bar{y}_{b1} \text{ (first mode)} = \frac{8pL^4}{\pi^5 EI} \qquad \text{(V-4.6)}$$

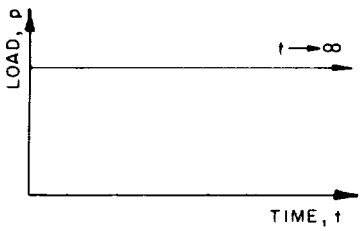

FIG. V-4.3 STEP-PULSE LOADING OF INFINITE DURATION

When there is no damping, there may be a time t for which all of the infinite modal components are in phase. Then the additional deflection due to the higher modes, as a ratio of the first mode component expressed in Eq. V-4.6, is equal to or less than

$$S_{\bar{y}} = \sum_{n = 3,5,7\ldots}^{\infty} \frac{1}{n^5} = 0.00452 \qquad (V\text{-}4.7)$$

since the coefficient in front of the summation sign is the same, and precisely equal to the right-hand side of Eq. V-4.6.

Similarly, the additional deflection due to the higher modes for a purely impulsive loading, as a ratio of the first mode component, is equal to or less than

$$S_{\bar{\bar{y}}} = \sum_{n = 3,5,7\ldots}^{\infty} \frac{1}{n^3} = 0.0518 \qquad (V\text{-}4.7')$$

The relative error in bending moment can be obtained by comparing the absolute values of the sums of the higher terms in the second derivatives of Eqs. V-4.4 and V-4.5 with the first term in the second derivative. One finds, for a step pulse of loading, the result

$$S_{\bar{M}} = \sum_{n = 3,5,7..}^{\infty} \frac{1}{n^3} = 0.0518 \qquad (V\text{-}4.7'')$$

However, for a purely impulsive loading the series given by this elementary theory, when there is no damping, diverges and the ratio is meaningless.

From Eqs. V-4.7 and V-4.7' it is apparent that neglecting all modes higher than the fundamental mode causes an error of less than 0.5% in deflection and less than 5.2% in bending moment if the beam is subjected to a step pulse of infinite duration. At the other extreme of variation of loading with time, impulsive loading, the error by neglecting all but the fundamental mode in deflection is less than 5% but the error in bending moment can be much larger. For most structures subjected to the effects of nuclear weapons of current operational size, the loading approaches the case of a step pulse of loading with infinite duration for which the errors inherent in the beam considered become generally insignificant.

Results similar to those just illustrated are obtained for most structural elements which respond elastically, have a uniform cross section (uniform distribution of mass), and are subjected to a uniformly distributed loading. In these of course, the mode shape excited dynamically will be the fundamental mode of vibration for the particular element. The fundamental mode of vibration is defined uniquely by the fundamental period of vibration, and the associated mode shape (fundamental Eigenvalue and Eigenvector), values of which are available in most standard references on vibrations (for example, Ref. V-1.35). Also values of fundamental periods of vibration for the more common structural configurations are given in Eqs. V-1.14 through V-1.17 in Chapter V-1. When structural elements have a distribution of mass which deviates significantly from uniform and/or the load does not approach a uniform distribution, then more complex responses, involving several modes being excited simultaneously, are involved, and more complex methods are required to define a model; these cases are discussed in Chapter V-5.

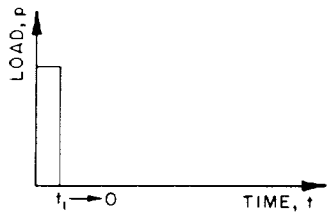

FIG. V-4.4 IMPULSIVE LOADING

V-4.2.2 General Procedures for Defining Characteristics of Model Including Effects of Plastic Action

In general, definition of a mathematical model which represents the essential characteristics of a specific structural element requires an equality to be established between the model and the prototype of (1) the external work done, (2) the internal work (or strain energy), and (3) the kinetic energy. To obtain these equalities requires a knowledge of the mode shape. Sometimes, as with the example in the preceding section, this will be known; other times it may have to be assumed. From these equalities are defined the mass M, the load P, and the stiffness K of the simple oscillator (or SDF system) in terms of the total mass, load, and stiffness of the actual structure.

Again it is helpful to take a specific example to illustrate the procedure. Consider again the simple beam loaded as shown in Fig. V-4.2. It is desired first to define the characteristics of a single-degree-of-freedom model which behaves similarly to the beam when it responds elastically. Second, the same structure will be considered, but the beam will be allowed to respond with some degree of plastic behavior.

In the first case, it was shown in the preceding section that the deflected shape is closely approximated by the fundamental mode or:

$$y \simeq c \sin\frac{\pi x}{L} \qquad \text{(V-4.8)}$$

It is to be noted that c is a function of time which defines the amplitude of the deflection at the center of the beam. By equating the work done by the force p acting over the entire beam (Fig. V-4.2) to the work done by the concentrated force P acting on the mass of the replacement oscillator (Fig. V-4.1) and by specifying that the deflections of the two systems must be equal, one can define the force which must act on the oscillator:

$$P = \frac{2}{\pi} pL$$

Similarly, from the internal work done (or the strain energy), the stiffness K is defined by

$$K = \frac{\pi^4 EI}{2L^3}$$

or alternatively in terms of the maximum moment M_c developing at the center of the beam

$$K = \frac{\pi^2 M_c}{2L}$$

Finally the mass M of the model is defined from the kinetic energy in each system:

$$M = \frac{1}{2} mL$$

When only plastic deformation occurs, the deflected shape can be approximated by assuming all curvature is restricted to a short length s at the center of the beam (Fig. V-4.5). In the same manner as in the case immediately preceding, the characteristics of the model are defined for plastic deformation in the beam:

$$P' = \frac{1}{2} pL$$

$$K' = \frac{16EI}{sL^2} = \frac{4 M'_c}{L}$$

$$M' = \frac{1}{3} mL$$

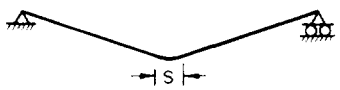

FIG. V-4.5 APPROXIMATE DEFLECTED SHAPE FOR BEAM DEFORMED PLASTICALLY

Thus, it is readily verified that the differential equation of motion for the model of a simple beam subjected to a uniformly distributed loading for deformations in the elastic range is

$$\frac{1}{2} mL\,\ddot{y} + \frac{\pi^4 EI}{2L^3} y = \frac{2}{\pi} pL$$

or rearranging:

$$\frac{\pi}{4} m\ddot{y} + \frac{\pi^5 EI}{4L^4} y = p \qquad \text{(V-4.9)}$$

For the same conditions but for only plastic deformations, the differential equation of motion for the model is:

$$\frac{2}{3} m\ddot{y} + \frac{32EI}{sL^3} y = p \qquad \text{(V-4.10)}$$

where

$\ddot{y}$ = the acceleration (second derivative with respect to time) of the mass (or the acceleration of the beam at the centerline).

p = the amplitude of the uniform loading at any instant of time

Taking ratios of the appropriate coefficients in Eqs. V-4.9 and V-4.10, one finds

$$\frac{M}{M'} = \frac{3\pi}{8} = 1.18$$

$$\frac{K}{K'} = \frac{\pi^3 M_c}{32 M'_c} \simeq 0.97 \text{ for } M_c = M'_c \qquad \text{(V-4.11)}$$

$$\frac{\omega}{\omega'} = 0.91$$

where M, K and ω are the mass, stiffness and circular natural frequency respectively for the model representing the beam responding elastically; M', K' and ω' have the same definition for the model representing the beam responding plastically.

It should be noted that $\omega = \sqrt{\frac{K}{M}}$ and that the natural period of vibration $T = \frac{2\pi}{\omega}$.

Normally a structural element will undergo both elastic and plastic deformation in resisting the load; therefore, the model theoretically must be changed as the deformation progresses from a system consistent with Eq. V-4.9 to a system consistent with Eq. V-4.10. However, it is apparent from the ratios defined by Eq. V-4.11 that little error will exist if the "elastic" model is not modified at the onset of plastic deformation. It is true that these ratios are computed above for only one case, but the values of the ratios given are comparable to those for the structural systems normally encountered. Of course, the coefficients for the mass, stiffness and load for the model representing a structural element other than a simply supported beam usually are different from those given above. Values of these coefficients are tabulated in Ref. V-1.52.

V-4.3 SELECTED METHODS FOR SOLVING THE DIFFERENTIAL EQUATION OF MOTION

Numerous texts treat in detail methods for solving the differential equation of motion for a single-degree-of-freedom system. Here no effort will be made to give all of the detailed solutions or methods of solution; instead limiting cases particularly useful in formulating design concepts will be considered. Also those procedures which give valuable insight into the response will be mentioned. In general, presence of viscous damping in the system will be ignored except, particularly in shock isolation systems, when consideration of damping is important. Although some damping (both viscous and Coulomb) exists in all physical systems, it generally is so small, unless conscious effort is made to increase it, that insignificant errors are introduced in the response to transient loads if it is neglected. Yet, one must not ignore the presence of damping in drawing conclusions about the total response of a structure since damping will modify the steady-state response significantly.

The limiting cases emphasized in the following discussion include: (1) the response to a step pulse in time with infinite duration and (2) the response to an impulse. Many solutions of practical importance are bounded by the response of systems subjected to these loads. Other important cases which are not bounded generally by these types of loading include loads which have a finite rise time; these will be treated separately in Section V-4.4.2. Finally, the system can be acted upon by motions of the support, and important cases of this type are treated in Section V-4.5.

V-4.3.1 Direct Solution of Differential Equation

In its general form, the differential equation of motion for the single-degree-of-freedom system (Fig. V-4.1) is (neglecting Coulomb damping)

$$M\ddot{u} + g(\dot{u}) + f(u) = P(t) - M\ddot{x}$$

where

- u = relative displacement between centroid of mass and the support with $\dot{u}$ and $\ddot{u}$ the successive derivatives with respect to time of this relative displacement.
- M = total mass supported by spring.
- $g(\dot{u})$ = a function of the relative velocity defined by the characteristics of the dashpot in the system. For a linear dashpot $g(\dot{u}) = c\dot{u}$ with c the constant for the dashpot.
- $f(u)$ = a function of the relative displacement defined by the resistance characteristics of the spring in the system. For an elastic system $f(u) = Ku$ with K the stiffness.
- $P(t)$ = the total force, as a function of time, acting on the mass.
- $\ddot{x}$ = the acceleration of the support or "ground."

For the base of the oscillator fixed, the governing equation becomes, for no damping and with y the absolute displacement of the centroid of the mass:

$$M\ddot{y} + f(y) = P(t) \qquad \text{(V-4.12)}$$

and for an elastic system:

$$M\ddot{y} + Ky = P(t) \qquad \text{(V-4.12')}$$

Although solutions of Eq. V-4.12 are rather easily obtained, there are other methods, to be discussed shortly, which are, to many engineers, more straightforward. Thus, in this section the discussion will be restricted to solutions of Eq. V-4.12'. It is readily shown that the homogeneous solution of Eq. V-4.12' is

$$y = c_1 \cos \omega t + c_2 \sin \omega t$$

where

- c_1 = a constant defined by the initial value of the displacement
- c_2 = a constant defined by the initial value of the velocity
- t = time

The particular solution for a step pulse of force with infinite duration is $y = \frac{P}{K} = y_s$, the static deflection caused by the load P. Combining the two solutions one obtains

$$y = y_s \left(1 - \cos \frac{2\pi t}{T}\right) \qquad \text{(V-4.13)}$$

when initial displacement and velocity are both zero. When an impulse is applied, the mass attains an initial velocity defined by equating the impulse and momentum. Thus for this case

$$y = \frac{2\pi\ Pt_1}{TK} \sin\frac{2\pi t}{T} \qquad \text{(V-4.14)}$$

where Pt_1 equals the impulse, i.

V-4.3.2 The Phase-Plane Diagram or Gyrogram

Taking the first derivative with respect to time of Eq. V-4.13 and multiplying both sides by $\frac{T}{2\pi}$, one obtains,

$$\frac{T\dot{y}}{2\pi} = y_s \sin\frac{2\pi t}{T} \qquad \text{(V-4.15)}$$

Equations V-4.13 and V-4.15 represent the parametric equations of a circle with radius y_s in rectilinear coordinates, y' (=y_s - y) and $\frac{T\dot{y}}{2\pi}$. The circle has its center at y = y_s and at $\frac{T\dot{y}}{2\pi}$ = 0. This coordinate system defines what is generally referred to as the phase plane and the diagram formed of connected circular arcs, developed as described below, is frequently referred to as a gyrogram. The general interpretation apparently was given first in Ref. V-4.2, and it is extended in Ref. V-4.3. The gyrogram represented by Eq. V-4.13 is a circle as shown in Fig. V-4.6(a), and the actual solution in a more familiar coordinate system constructed directly from the gyrogram is shown in Fig. V-4.6(b). It should be obvious that real time is represented by angles measured to any radius counterclockwise from the positive y'-axis. The angle has a value in radians which is set equal to $\frac{2\pi t}{T}$ or to ωt, an identical quantity.

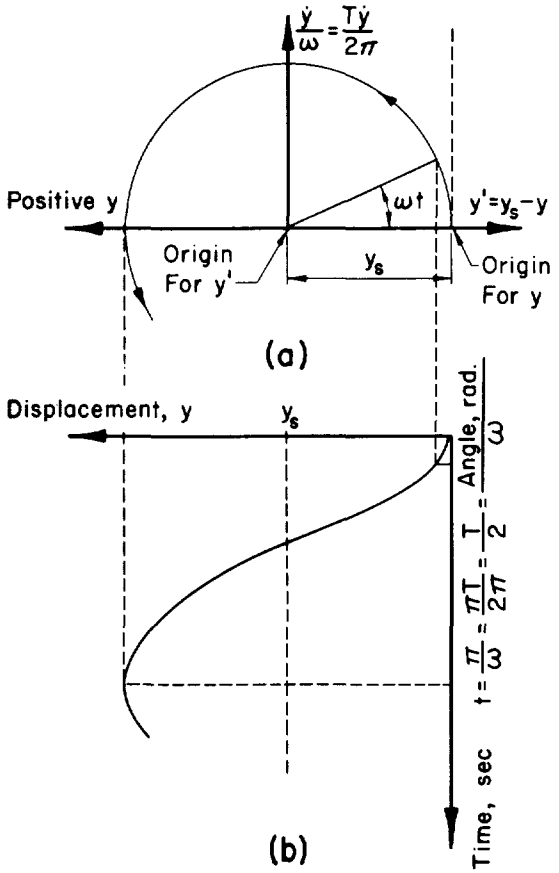

(a) Gyrogram.

(b) Displacement–Time Diagram.

FIG. V-4.6 GYROGRAM CONSTRUCTION FOR STEP PULSE ACTING ON SIMPLE ELASTIC OSCILLATOR

If it is now recognized that Eqs. V-4.13 and V-4.15 represent solutions for a step pulse with any duration, it follows that the gyrogram can be used to construct approximately the response of a system to any forcing function. To accomplish this approximate solution the forcing function is divided into a series of steps in which each step averages the area under the curve representing the actual force (Fig. V-4.7). Of course, the proper values of displacement and velocity must be used to begin each new step used to approximate the curve. Herein lies the significant advantage in the use of the gyrogram: (1) Each step (i) has a finite amplitude which defines the value y_{si} $\left(= \frac{P_i}{K}\right)$ which, in turn, is the radius of the circle for this step; and (2) each step has a finite duration t_i which defines the central angle of the arc through which the circle of radius y_{si} is to be drawn. The initial displacement and velocity of the system are normally zero; however, other values of initial velocity can be plotted on the phase-plane coordinates. From this initial point the radius y_{so} is laid off so that the center of the circle falls on the y'-axis. Then a circle is drawn through the point corresponding to the initial values of displacement and velocity until an arc subtending a central angle equal to $\omega\Delta t_o$ (in radians) is formed. The terminus of this arc defines the initial values of displacement and velocity for the next step used to approximate the actual forcing function, and the steps just outlined are repeated. This process is continued until the entire forcing function has been approximated.

The discussion so far has been restricted to a consideration of elastic response. When the resistance function for the system is monotonically increasing with a concave downward curvature, the gyrogram also is a useful tool for describing approximate response. The procedure to be followed is very similar to that just described: Since y_s is by definition $\frac{P}{K}$, successive reductions in K representing a

piecewise-linear approximation to the resistance function (Fig. V-4.8) have the same effect as successively larger steps in an approximation of a forcing function. However, it must be noted that all displacements from the gyrogram associated with values of K which do not pass through the origin of the resistance diagram are larger than they should be by an amount defined by the intercept, such as y_c in Fig. V-4.8, on the displacement axis of the particular straight-line portion considered.

The gyrogram can be used for solutions involving resistance functions other than that pictured in Fig. V-4.8, but they become quite complex and other methods are simpler to apply. For example, the parametric equations define parabolas and equilateral hyperbolas for the gyrogram representing a resistance function which is ideally plastic and unstable, respectively.

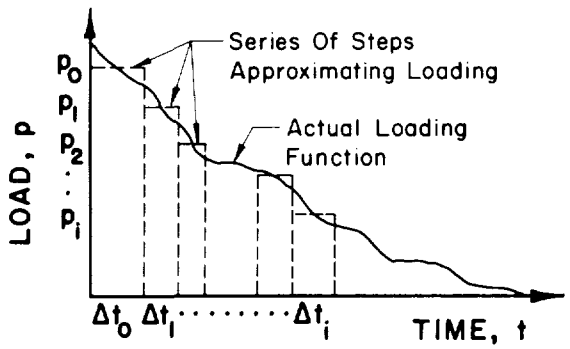

FIG. V-4.7 METHOD FOR APPROXIMATING LOADING FUNCTION FOR SOLUTION BY GYROGRAM

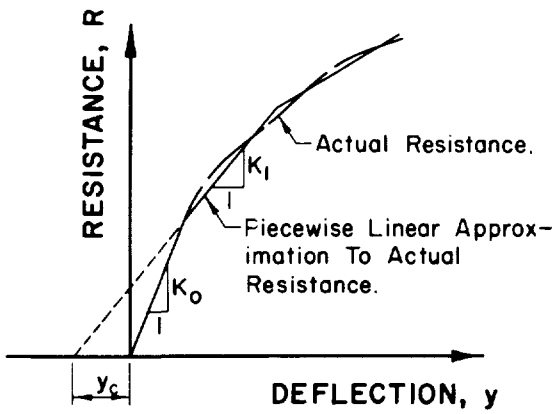

FIG. V-4.8 METHOD OF APPROXIMATING RESISTANCE FOR SOLUTION BY GYROGRAM

V-4.3.3 Another Useful Graphical Method

When the gyrogram solution becomes quite complex another graphical method can be used. If the governing differential equation (Eq. V-4.12) is rewritten in the form

$$\ddot{y} = \frac{P(t)}{M} - \frac{f(y)}{M}$$

It is apparent that the true acceleration of the mass is defined by the algebraic difference between the acceleration caused by the applied force and the acceleration resulting from the resistance developed. For elastic systems, this observation is not particularly helpful since generally the dependence of y on time is unknown. However, if the resistance function f(y) for the element is elasto-plastic (Fig. V-4.9), a rapid approximate solution for the response can be constructed graphically. Consider the conditions shown in Fig. V-4.10 wherein an arbitrary curve for $\frac{P(t)}{M}$ is drawn on the same coordinate system as the curve $\frac{f(y)}{M}$ for the resistance function f(y) shown in Fig. V-4.9. Means will be developed later for determining approximately the time t_y at which yielding begins. If the initial values of velocity and displacement of the system are zero, the maximum displacement occurs at time t_M where the cross-hatched area labeled 2 equals the cross-hatched area labeled 1 in Fig. V-4.10. The magnitude of the maximum displacement, which normally is the quantity desired, is then found by taking first moments of the areas labeled 1 and 2 in Fig. V-4.10 using time t_M as the center of moments. Since, by definition, the two areas are equal, this moment is equal to the couple defined by the product of the area under one portion (either 1 or 2) and the distance between the centroids of the two areas. In structural engineering this technique is directly analogous to finding the maximum bending moment in a beam on which the entire loading consists of the net acceleration in the system.

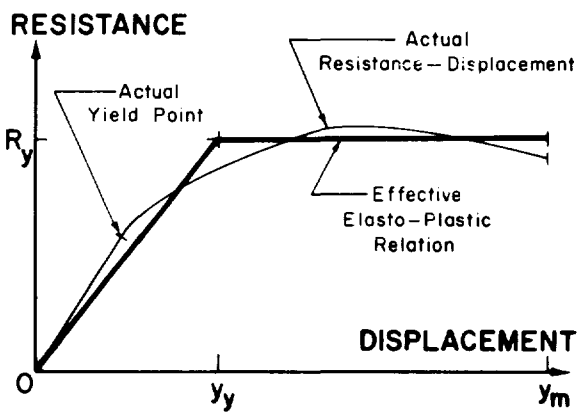

FIG. V-4.9 RESISTANCE–DISPLACEMENT RELATIONSHIP

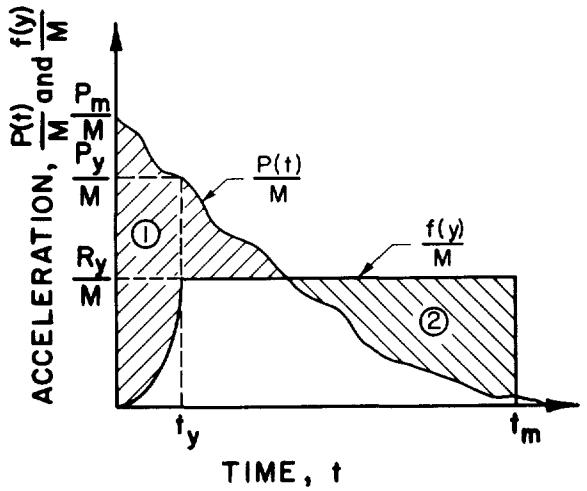

FIG. V-4.10 GRAPHICAL SOLUTION FOR RESPONSE OF SYSTEM WITH ELASTO-PLASTIC RESISTANCE

Now consider the problem of finding t_y. The deflection at yielding y_y is numerically equal to the moment (about t_y) of the net area to the left of t_y in Fig. V-4.10. Since only an approximate value is generally required, the area may be neglected under the resistance curve up to t_y. Thus if $\overline{P}$ is the "effective" average force acting on the structure during the time to t_y,

$$y_y \cong \frac{\overline{P}\, t_y^2}{2M}$$

But $R_y = Ky_y$ and $\frac{K}{M} = \frac{4\pi^2}{T^2}$; therefore

$$\frac{t_y}{T} \cong \frac{1}{\pi\ 2}\sqrt{\frac{R_y}{\overline{P}}} = 0.226\sqrt{\frac{R_y}{\overline{P}}} \qquad \text{(V-4.16)}$$

and if P_{max} and P_y are the forces acting at time zero and at the time yielding occurs respectively

$$\overline{P} \cong \frac{2\,P_{max} + P_y}{3} \qquad \text{(V-4.17)}$$

The interdependence between t_y and $\overline{P}$ precludes a direct solution for t_y. Usually, however, it is sufficient to take $\overline{P} = P_{max}$. The approximations used in the above derivation are justified by observing that the length of the moment arm for the couple defining the maximum displacement is relatively insensitive to changes in t_y.

V-4.3.4 Numerical Integration

Numerical methods of integration of the response of structures to dynamic loading are capable of application to structures as complicated as one wishes to consider, with any relationship between force and displacement ranging from linear elastic behavior through various degrees of inelastic behavior or plastic response, up to failure (Refs. V-4.4, 4.5, 4.6 and 1.52). Any type of loading or motion can be considered such as that due to blast, impact from a moving object, or foundation motion due to an earthquake.

There are many methods of numerical integration of differential equations. Among those described, for example, in Chapter 8 of Ref. V-1.52 are the Taylor Series Method, Milne's Methods, and the Method of Runge and Kutta. An alternative method is described here that has certain advantages in dynamics problems, and in particular avoids certain difficulties in starting the procedure, or in checking the steps involved in the calculation. The method is described in Ref. V-4.4. It can be used in the same way for both hand calculation or with a high-speed digital computer. The discussion here is related to a single-degree-of-freedom system; however, the method is readily applicable to more complicated systems.

Consider the structure shown in Fig. V-4.11, which consists of a weightless but deformable element supporting lumped masses. Each mass is acted upon by an external force, and the structure as a whole may be subjected to prescribed motion of the foundation or there may even be a prescribed motion of some particular point on the structure. The complete structure, shown in Fig. V-4.11(a), is separated into two parts: in Fig. V-4.11(b), the structure is isolated as a free body with resisting forces R acting on it which represent the reactions from the masses on the structural framework itself; in Fig. V-4.11(c) the masses are isolated with the

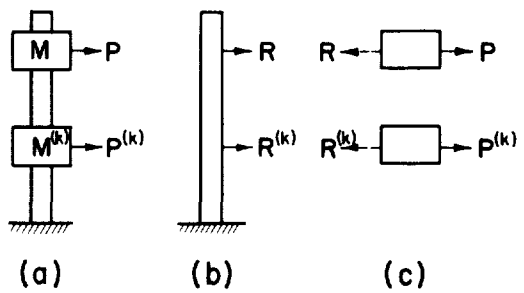

(a) Structure With Lumped Masses.

(b) Structure, With Masses Removed, Acted on by Resisting Forces, R.

(c) Masses Acted on by External Loads and Structural Resistances.

FIG. V-4.11 STRUCTURE ANALYZED

external loads acting on them, and with the structural resistance R opposing the action of the external loading P. The positive directions of P and R are the same on the structure, and these directions, which may be defined arbitrarily, are taken also as the positive directions for displacement y, velocity $\dot{y}$, and acceleration $\ddot{y}$. In the general case the mass may also be acted on by a damping force which is generally a function of the velocity of the mass, but it may be any function whatsoever. This can in general be considered as an additional external force which, however, is not known in advance. The structural resistance R is defined as that system of forces which corresponds at any time to the displacement of the structure at that time.

The sign convention and notation are chosen so as to make it apparent that the masses M modify or filter the forces P and transmit them to the structure in modified form as R. If the force P is applied very slowly, there is very little or no acceleration, and R = P. If the forces are applied quickly, the acceleration removes much of the force or changes it. Under these conditions, R is different from P. The structure, however, responds only to the forces R. It has static deflections which are just those generated by the forces R, and the stresses within the structure can be computed from these forces. Therefore, the structure can be analyzed statically, once we have determined the "modified" forces R. The forces P may become zero after a short time, but in general the system will still continue to deflect. The relationships which determine the motion remain unchanged. The maximum deflection and the maximum values of R, or those which correspond to the maximum stresses in the structure, may occur at a time at which the forces P are zero.

Let us consider one of the masses $M^{(k)}$, at a time t_n. Since we are dealing with the particular mass and the forces acting on it, we can drop the superscript designation for this mass in the equations which follow. We assume that we know the acceleration, velocity, and displacement of the mass at the time t_n. We wish to find these quantities at the time t_{n+1} which differs from t_n by the time interval h. The subscripts n and n + 1 indicate the values at either t_n or t_{n+1}, respectively, for the quantities $\ddot{y}$, $\dot{y}$ and y.

In general, for any time, the acceleration, as in the preceding section but replacing f(y) by R and P(t) by P, is given by the relation:

$$\ddot{y} = (P - R)/M \qquad \text{(V-4.18)}$$

Let us define the displacement and the velocity at the end of the time interval by the following equations:

$$y_{n+1} = y_n + \dot{y}_n h + \left(\frac{1}{2} - \beta\right) \ddot{y}_n h^2 + \beta \ddot{y}_{n+1} h^2 \qquad \text{(V-4.19)}$$

$$\dot{y}_{n+1} = \dot{y}_n + (1 - \gamma) \ddot{y}_n h + \gamma \ddot{y}_{n+1} h \qquad \text{(V-4.20)}$$

For $\gamma = \frac{1}{2}$, this becomes:

$$\dot{y}_{n+1} = \dot{y}_n + \ddot{y}_n h/2 + \ddot{y}_{n+1} h/2 \qquad \text{(V-4.21)}$$

In these equations, the parameters β and γ are those which can take on assigned values (as discussed later) so as to lead to the type of result which we desire. It can be seen that Eqs. V-4.19 to V-4.21 give correct results for displacement and velocity when the acceleration does not vary during the time interval. The values of the parameters will be chosen so as to give the best representation under conditions when the accelerations within the time interval do vary.

The numerical procedure is used in the following way: For each of the masses an assumption is made of the value of $\ddot{y}_{n+1}$. This can be taken as the same as $\ddot{y}_n$, or from a plot of successive values, an estimate can be extrapolated. By the application of Eq. V-4.19 to each mass in turn, the displacement at the end of the interval is computed. This gives a first estimate for the configuration of the structure at the end of the interval. Then the forces $R^{(k)}_{n+1}$ are computed, corresponding to this configuration. With the known values of $P^{(k)}_{n+1}$, the estimated values of R, and with the aid of Eq. V-4.18, derived values of $\ddot{y}_{n+1}$ are obtained. These are in general different from the assumed values. The calculation is therefore repeated until a close enough agreement is obtained between the assumed and derived values. At this point the calculation for the time interval is completed, and one can proceed with the next time interval.

Unless the calculations converge quickly, the method is tedious. Usually, fairly rapid convergence is required to insure accuracy also, as will be demonstrated in the following sections.

Convergence and Stability of Numerical Procedure. Consider a system of one degree of freedom or a more complex system loaded in such a way that its motion is in the shape of one of the modes of vibration of the system. It will suffice to consider the former simplification, in which case the quantity R can be stated in terms of the spring constant K times the displacement x, for linear elastic behavior. For such a system, the circular frequency of vibration ω is given by:

$$\omega^2 = K/M$$

It is apparent from Eqs. V-4.18 and V-4.19 that if the assumed acceleration is in error, the derived acceleration will generally also be in error. The true value of the acceleration is that which leads to the same value of acceleration from Eq. V-4.18

that one assumes in starting the calculation with Eq. V-4.19. With this observation, one can derive the result:

$$\frac{\text{error in derived acceleration}}{\text{error in assumed acceleration}} = S_a = -\beta\,\omega^2\,h^2 = -\beta\theta^2 \qquad \text{(V-4.22)}$$

The rate of convergence of the calculations is measured by the quantity S_a which is seen, therefore, to be a function of the square of the time interval. It is also apparent that the sequence of errors oscillates. Each error is opposite in sign to the preceding one.

It is clear that the formal numerical process of solution will converge only if the quantity S_a is numerically less than one. The critical value of time interval for which the numerical process formally converges can easily be determined from Eq. V-4.22.

For practical purposes the time interval would ordinarily be taken to be somewhat smaller than that which corresponds to pure oscillation (or $S_a = -1$), to insure rapid enough convergence for practical purposes. If $S_a = -0.32$, the errors will be reduced to 1% of their original value in four steps or four cycles of calculation. Of course, it can be seen that the convergence is more rapid the smaller the value of β. For $\beta = 0$, the ratio S_a is always zero. This would appear then to be the best value of β. However, other considerations affect the choice of β, and these are considered later.

Let us consider further the special case of a simple system such as that previously considered, but with the additional simplification that the external force P is zero. For such a condition, the motion of the system should be a pure oscillation. We can study easily what the results are from the relationships given by Eqs. V-4.19 and V-4.20 to determine whether our procedures can be made sufficiently precise. With the assumptions described, Eq. V-4.18 reduces to the following

$$\ddot{y} = \omega^2 y \qquad \text{(V-4.23)}$$

If one expresses y_n in terms of y_{n-1}, $\dot{y}_{n-1}$, $\ddot{y}_{n-1}$ and $\ddot{y}_n$, by use of Eq. V-4.19 for the preceding interval, and if one expresses y_n in terms of $\dot{y}_{n-1}$ and the corresponding accelerations from Eq. V-4.20 for the preceding interval, one can derive by use of Eqs. V-4.19, V-4.20 and V-4.23 the following difference equation in terms only of the displacements at three successive time intervals:

$$y_{n+1} - \left(2 - \alpha^2\right) y_n + y_{n-1} + \left(\gamma - \frac{1}{2}\right)\alpha^2 \left(y_n - y_{n-1}\right) = 0 \qquad \text{(V-4.24)}$$

For $\gamma = \frac{1}{2}$, this equation can be rewritten as:

$$y_{n+1} - \left(2 - \alpha^2\right) y_n + y_{n-1} = 0 \qquad \text{(V-4.25)}$$

In these equations, α^2 represents the expression:

$$\alpha^2 = \frac{\theta^2}{1 + \beta\,\theta^2} \qquad \text{(V-4.26)}$$

Equations V-4.24 and V-4.25 are difference equations for which the exact solutions can be obtained. However, it is unnecessary to write the exact solution to study the effect of γ on the result. It is immediately apparent that if γ is different from 1/2, the difference equation corresponds to the motion of a system with damping, even though our assumed system had no damping. Furthermore, if γ is less than 1/2, the damping is negative. This means that the system can build up self-excited vibrations if it starts to vibrate at all.

It is of interest to observe that if both β and γ are taken as zero, Eqs. V-4.19 and V-4.20 reduce to the very simple and commonly used form that corresponds to a numerical integration process which assumes that the acceleration in each step remains the same as its value at the beginning of the interval. It turns out from Eq. V-4.24 that such a procedure leads to a spurious oscillatory response with constantly increasing amplitude, which arises from the fact that negative damping is introduced by this type of procedure. It follows, therefore, that this simple process is not a desirable one. Furthermore, the best value of γ in Eq. V-4.20 is 1/2 although there may be a reason for taking γ greater than 1/2 since this introduces a real and positive damping in the results. Under these conditions one may be able to damp out undesirable higher mode response. However, this introduces other complications and is not in general a convenient or promising procedure. Consequently, it appears best to take γ always as 1/2.

When $\gamma = 1/2$, the solution of Eq. V-4.25 is a periodic one for α^2 less than 4. Under these conditions, the solution can be expressed in the following form:

$$\text{For } \alpha^2 < 4, \text{ let } \alpha = 2 \sin \psi/2, \qquad \text{(V-4.27)}$$

then

$$y = A \cos \psi\, t/h + B \sin \psi\, t/h \qquad \text{(V-4.28)}$$

Equation V-4.28 indicates that the displacement is periodic with a period T_s given by

$$T_s = 2\pi h/\psi \qquad \text{(V-4.29)}$$

The pseudo-period T_s can be stated in terms of the true period T by the relation

$$T_s/T = \theta/\psi \qquad \text{(V-4.30)}$$

It appears that the relationship between the pseudo-period and the real period depends on the time interval, which in turn is a function both of α^2 and β as indicated by

$$\theta^2 = \frac{\alpha^2}{1 - \beta\alpha^2} \qquad \text{(V-4.31)}$$

For α^2 greater than 4, Eq. V-4.25 will not have a periodic solution. Actually under these conditions the solution will be a divergent oscillatory one. Consequently, $\alpha^2 = 4$ is the limiting condition for "stability" of the solution. The limiting value of θ^2 can be obtained from Eq. V-4.31. It can be seen by comparison with Eqs. V-4.22 and V-4.31 that for values of β less than 1/8 the limiting value of time interval for stability is smaller than that for convergence. However, for values of β greater than 1/8, the reverse is true. Consequently, when β is less than 1/8, the results of the calculations may be unstable, and the instability may not be immediately apparent. However, when β is greater than 1/8, the sequence of calculations will diverge before the instability occurs, and the inadequacy of the procedure, or the excessive length of the time interval, will be immediately apparent.

Errors in Amplitude and Period from Numerical Calculation. For the simplified conditions considered in the previous sections, the exact solution for the problem, given by y, and the approximate solution, $\bar{y}$, are shown in Eqs. V-4.32 and V-4.33:

$$y = y_o \cos 2\pi t/T + \frac{\dot{y}_o}{\omega} \sin 2\pi t/T \qquad \text{(V-4.32)}$$

$$\bar{y} = y_o \cos 2\pi t/T_s + B \sin 2\pi t/T_s \qquad \text{(V-4.33)}$$

It should be recognized, of course, that the approximate solution, Eq. V-4.33, is defined only at specific times. The maximum values may not occur at the times at which the calculations are made.

It is apparent from a comparison of the last two equations that the approximate solution is similar in form to the exact solution but differs in the periodicity. The approximate period is measured by the quantity T_s which is different from T in general. However, the maximum displacement that corresponds to a given value of initial displacement is identical in these two equations. In other words, there is no error in maximum response corresponding to an initial displacement. There is, however, an error in the response corresponding to an initial velocity. This is indicated by:

$$\frac{B}{\dot{y}_o/\omega} = \left[1 + (\beta - \frac{1}{4})\,\theta^2\right]^{-1/2} \cong 1 + \frac{1/4 - \beta}{2}\theta^2 + \ldots \qquad \text{(V-4.34)}$$

It will be noted that if $\beta = 1/4$, then there is no error in maximum response due to an initial velocity.

The relation given in Eq. V-4.30 can be expressed more conveniently by the following approximate formula for the ratio of the pseudo-period to the actual period of vibration:

$$T_s/T \cong 1 - (1 - 12\beta)\,\theta^2/24 - (17 - 120\beta + 720\beta^2)\,\theta^4/5760 - \ldots \qquad \text{(V-4.35)}$$

Here it is apparent that the error in period varies as the square of the time interval. However, for $\beta = 1/12$, the term involving the square of the time interval vanishes and the error in period varies as the fourth power of the time interval. Consequently, the error in pseudo-period of the response is considerably smaller when $\beta = 1/12$ than it is for any other value of β.

For convenience, the magnitude of S_a which measures the rate of convergence is summarized in Table V-4.1(a) and the errors in velocity response and in period are summarized in Tables V-4.1(b) and V-4.1(c), for a number of values of β ranging from zero to 1/4, for several values of time interval h ranging from 0.05 T to the limiting values for stability or convergence.

To complete the presentation, there is given in Table V-4.2 a summary of the time intervals for stability and for convergence for the different values of β.

It can be seen from Tables V-4.1 and V-4.2 that divergence is obtained before the limit of stability is reached, when β is greater than 1/8, and that the solution becomes unstable while the numerical solution is still convergent when β is less than 1/8. The fact that the response due to initial displacement is exact for all values of β, within the range of stability, means that numerical errors that inevitably creep into the calculations will not cause the computed results to increase without limit. However, above the range of stability this observation no longer applies and the response even to initial displacement becomes excessively large.

The response to initial velocity is always greater than it should be, and becomes infinitely large, also, at the limit of stability. Below this range of stability, the errors that occur in the calculations have the effect of magnifying the response. However, these errors are relatively small for values of h/T less than 0.2 and are very small for h/T less than 0.1.

It is interesting to note to what type of variation of acceleration during the time interval

TABLE 4.1 EFFECTS OF LENGTH OF INTERVAL ON ERRORS DUE TO NUMERICAL PROCEDURE

	Values of β				
h/T	0	1/12	1/8	1/6	1/4
		(a) Rate of Convergence			
0.05	0	0.008	0.012	0.016	0.025
0.10	0	0.033	0.049	0.066	0.099
0.20	0	0.132	0.197	0.263	0.395
0.25	0	0.206	0.308	0.411	0.617
0.318	0	0.333	0.500	0.667	1.000
0.389	*	0.500	0.750	1.000	1.500
0.450	*	*	1.000	1.333	2.000
		(b) Relative Errors in Maximum Response to an Initial Velocity			
0.05	0.012	0.008	0.006	0.004	0
0.10	0.052	0.034	0.025	0.017	0
0.20	0.209	0.166	0.116	0.073	0
0.25	0.614	0.306	0.202	0.122	0
0.318	inf.	0.732	0.414	0.225	0
0.389	*	inf.	1.000	0.414	0
0.450	*	*	inf.	0.732	0
		(c) Relative Errors in Period			
0.05	-0.004	-0.0001	0.002	0.004	0.008
0.10	-0.017	-0.0003	0.008	0.017	0.033
0.20	-0.076	-0.006	0.028	0.059	0.121
0.25	-0.130	-0.015	0.038	0.087	0.179
0.318	-0.363	-0.045	0.047	0.129	0.273
0.389	*	-0.220	0.035	0.170	0.382
0.450	*	*	-0.100	0.195	0.480

*Values indicated are beyond limit for stability.

TABLE 4.2 STABILITY AND CONVERGENCE LIMITS

	$\beta = 0$	$\beta = 1/12$	$\beta = 1/8$	$\beta = 1/6$	$\beta = 1/4$
Stability Limit, h/T	0.318	0.389	0.450	0.551	inf.
Convergence Limit, h/T	inf.	0.551	0.450	0.389	0.318

some of the different values of β correspond. If Eqs. V-4.19 and V-4.21 are considered, the type of variation of acceleration during the time interval that corresponds to the values of $\beta = 1/4$, $1/8$, and $1/6$, is shown respectively in Fig. V-4.12. For $\beta = 1/4$ the acceleration during the time interval is constant and has a value which is the average of the values at the beginning and the end of the interval. For $\beta = 1/8$, the acceleration has a constant value equal to the initial value for the first half of the time interval and a constant value equal to the final value for the second half of the time interval. However, for $\beta = 1/6$, the acceleration varies linearly during the time interval from the initial to the final value.

Since the effect of the external loading can be taken into account in the same way, it appears that if the external loading varies linearly during the time interval, the value of $\beta = 1/6$ should give the best results. However, this is not entirely true if the linear relationship changes from one interval to the next. Nevertheless, because the various errors appear to be more nearly balanced, and because of the convenience in dealing with external loadings which vary linearly or nearly linearly, it is recommended that for practical purposes the value of $\beta = 1/6$ be used. It is also clear that this choice gives a large value of S_a in comparison with the limit of stability, and therefore a convergent sequence of calculations will always insure stability for this choice of β.

Choice of β for Practical Use of Numerical Method. In addition to the considerations just outlined, there is another reason for using a value of β different from zero for practical calculations. In any set of calculations it is desirable to have a self-checking procedure. If β is taken as zero, no check is possible except one which involves some other criterion to check the results, since the calculation does not require repetition in each time interval. However, where a convergent system of calculations is developed, then during the process of converging to an answer the calculations are inevitably repeated, and repeated with slightly different values of the numbers involved. A close agreement between the results of successive calculations is in general a sufficient check on the accuracy of the numerical work. With a value of $\beta = 1/6$, a time interval of the order of $1/5$ to $1/6$ the shortest natural period of vibration of the structure will give a high enough rate of convergence for practical purposes and will also give errors small enough to be tolerable. It should be noted that the natural periods generally become longer as inelastic action develops. For purely plastic resistance, the period is infinitely long. Therefore the time interval can become longer as plastic action develops in the structure.

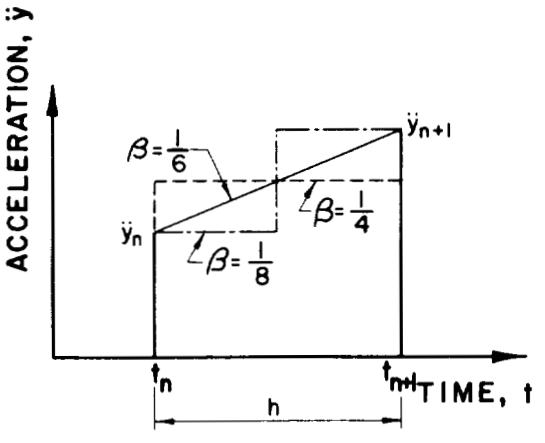

FIG. V-4.12 CONSISTENT VARIATIONS OF ACCELERATION WITH β IN A TIME INTERVAL

With the errors in the results and also with the criteria of convergence and stability, it is necessary at this point to indicate the results for systems with more than one degree of freedom. It is clear that the general relationships which described above apply independently to each of the modes of vibration of the structure. Consequently, the most critical conditions are generally found in the highest mode of vibration or in the mode which has the shortest period. Both the stability and the convergence are affected primarily by this mode. All the other modes are more stable, converge more rapidly, and introduce smaller errors in the results.

It is not necessary that the individual modes be separated and computed in the calculations. The results are determined by the numerical procedure, applied without consideration of the individual modes, and the numerical results obtained in the calculations will be a combination of those which pertain to the individual modes. However, the stability of the results and the convergence is determined by the component of the highest mode in the structural response. Because of the effect of the stability limitations, and also because of convergence difficulties, it is necessary to take a time interval somewhat less than the maximum for stability or convergence. If the convergence difficulty can be overcome, any time interval, however long, can be taken for $\beta = 1/4$.

In many cases, although the higher modes exist in the problem, the proportion of the highest mode in the response of the structure is relatively small. Consequently, a much greater error is permissible in the calculation for the higher modes than for the lower modes. This means that in general the errors in the total response of the structure will be considerably less than those indicated in Tables V-4.1(a), (b), and (c) when a system with several modes is considered. However, this does not mean that the criteria for length of time interval can be disregarded since a value of time interval greater than the limit for stability will introduce eventually errors which approach infinite values in the structural response. The only simple way of avoiding errors of this sort is to introduce artifical damping in the procedure to avoid the instability. This can be done by a choice of γ different from $1/2$ in Eq. V-4.20, but it does not appear to be practicable to use a value

different from 1/2, because such a choice introduces other errors. It is probably more convenient to reduce the number of masses and thereby reduce the shortest period considered.

In structures which change their flexibility with deformation, it is clear that the frequency or period of the highest mode changes as the flexibility changes. It is that frequency which corresponds to the particular condition of the structure which is important in any state of the calculation. Since it is inconvenient to compute the shortest period of the structure in a structure in which this value is constantly changing, it is probably sufficiently accurate and in most cases convenient to use as a criterion for value of the time interval the rate of convergence of the results. This can be done in the following way:

With a given choice of β, say $\beta = 1/6$, the calculation is carried out until convergence in the assumed and derived accelerations is reached in three to four steps. If this convergence, say to the order of about 1% or less, is not reached in four steps, the time interval is reduced by a factor of 2, and the calculation is repeated. This process is carried on until a time interval is found which gives rapid enough convergence. The time interval so obtained is used until convergence is obtained in one or two intervals. When this condition is obtained, the time interval is doubled for the next step. With this procedure of changing the time interval in accordance with the rate of convergence, one is assured that the time interval is sufficiently long to give a reasonable rapidity. A similar criterion can be established with more rapid and more accurate computing equipment.

Solutions by High-Speed Digital Computer. The results of a great many solutions obtained either by exact integration of the equations of motion, or by numerical methods, are summarized in detail in Ref. V-1.37 and Fig. V-1.31. Also the problem of rebound of a structural element was studied by use of computer solutions. The results of this study (Ref. V-1.17) are presented in Fig. V-1.32 and in Table V-1.2. Table V-1.2 indicates that rebound can be significantly modified by the presence of relatively little damping. Values of t_m in Fig. V-1.32 are obtained directly from Fig. V-1.31.

Figure V-1.31 presents results for only one type of idealized resistance and one type of idealized loading. Computer solutions were also obtained for other loading and resistance functions. However, the approximations developed in the following sections present the results of these studies with sufficient accuracy to make it unnecessary to discuss the "exact" results.

Approximation for Complex Loading Curves. For more complex loading curves, it is possible to use Fig. V-1.31 with a reasonably accurate degree of approximation by the following procedure.

Assume a loading curve of the form given in Fig. V-4.13 where, for convenience, only three separate triangular elements are considered. More or fewer triangles can be treated in exactly the same way. For each elementary triangle there is a "partial loading" P_1, P_2, or P_3. One can designate the general component of loading as P_n. For each triangle there is also a duration, with a corresponding subscript, t_1, t_2, t_3, or for the general case t_n. It is assumed that the value of the effective period of vibration of the structure T, and the ductility factor μ, are known. It is required to determine the required yield resistance R_y.

For any component of loading having a duration t_n, acting alone, use Fig. V-1.31 to determine, for the given period of vibration and the ductility factor desired, the ratio of the peak pressure to R_y. Let this quantity be denoted by the symbol F_n. For the loading diagram in Fig. V-4.13, one may determine values of F_1, F_2, and F_3. These will all be determined for the same ductility factor and the same period of vibration, of course. Now apply the general approximate relationship:

$$\Sigma \frac{P_n/R_y}{F_n} = 1 \qquad \text{(V-4.36)}$$

For three component loadings this reduces to

$$\frac{P_1/R_y}{F_1} + \frac{P_2/R_y}{F_2} + \frac{P_3/R_y}{F_3} = 1$$

If both sides of the latter equation are multiplied by R_y one obtains the result:

$$R_y = \frac{P_1}{F_1} + \frac{P_2}{F_2} + \frac{P_3}{F_3}$$

In the general case one would use the relation:

$$R_y = \Sigma\, P_n/F_n \qquad \text{(V-4.37)}$$

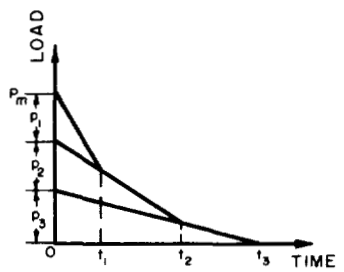

FIG. V-4.13 TYPICAL LOAD-TIME RELATION CONSIDERED

The maximum error in this procedure arises when an extremely short pulse is combined with an infinitely long one. Under this circumstance, where the subscript 1 refers to the impulse component, and the subscript 2 to the infinitely long duration, the true relation becomes

$$\left(\frac{P_1/R_y}{F_1}\right)^2 + \frac{P_2/R_y}{F_2} = 1$$

However, the error, even in this case, of using Eq. V-4.36 is not serious.

V-4.3.5 Energy-Momentum Considerations

A simple method of developing general relations for a single-degree-of-freedom system, based on the concepts of energy and momentum, is described here (Ref. V-1.4 and V-4.7).

It is possible to plot from a curve such as Fig. V-4.9, or for any actual resistance displacement curve, a diagram (Fig. V-4.14) which shows the energy absorbed by the structure as a function of its displacement. For the initial elastic part, the energy curve is a parabola and it is concave upward as long as the resistance of the structure does not decrease with deflection. The curve always rises, of course, but becomes concave downward when the resistance is decaying.

Using this curve one can find two cases where exact relationships can be derived for the peak dynamic force which can be applied to a structure having a given resistance. These two cases correspond to (1) a sudden rise of the dynamic force to a maximum value that remains constant for all deflections of the structure, generally called a "step-pulse"; and (2) the application of the force as an impulse before the structure deflects appreciably. The first of these corresponds in Fig. V-4.14 to a line such as OB drawn from the origin having a constant slope corresponding to the maximum dynamic force P_m. The work done on the structure by the dynamic force is of course the force P_m multiplied by the deflection, and a straight line through the origin represents this quantity. Where it intersects the curve the absorbed energy is equal to the external energy, and one has the maximum deflection y_m produced in the structure by the step-pulse of loading.

In the second instance one can consider that the impulse i from the loading is applied to the structure so that the mass of the structure acquires an instantaneous velocity. The magnitude of the instantaneous velocity at each mass is equal to the impulse divided by the mass. From this one can derive the fact that the initial kinetic energy of the mass is equal to the square of the impulse divided by twice the mass. This kinetic energy is plotted as a

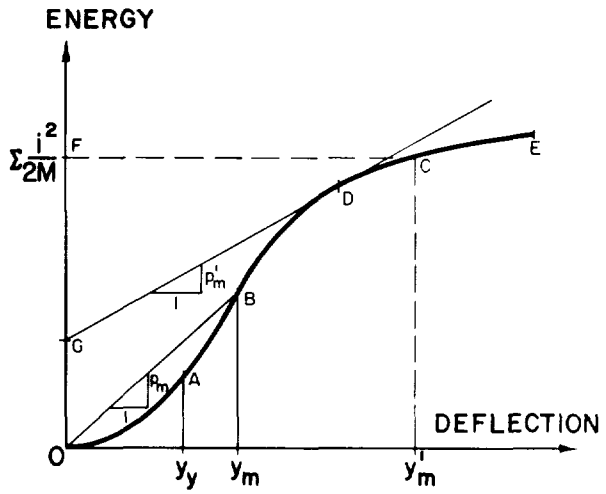

FIG. V-4.14 ABSORBED ENERGY VS DEFLECTION

quantity of input energy such as at F in Fig. V-4.14. A straight horizontal line drawn from this point, such as FC, will intersect the curve defined by the resistance at an absorbed energy equal to this initial kinetic energy and will therefore give the maximum displacement y_m' produced by the impulsive loading.

The maximum deflection can also be obtained directly when a long duration load is combined with an initial impulse. Here one draws a line of constant slope, equal to the magnitude of the long duration loading, from a point such as G that corresponds to the initial kinetic energy produced by the initial impulse.

There are some minor points to be considered with this kind of graphical solution. The most important of these is that in an unstable resistance curve, it is possible that some particular point on the curve such as E cannot be reached by a line drawn from a particular point on the vertical axis such as G without such a line passing through some intermediate point of the energy-displacement curve. This situation merely means that the line GD from the initial point G tangent to the energy absorption curve, as at D, is the one that must be used, as all deflections beyond this point will be produced by a loading infinitesimally greater than the one corresponding to the intersection at D.

V-4.4 DESIGN RELATIONS FOR APPLIED FORCE

The general procedure outlined in the section, immediately preceding, can be formalized into equations which are useful in the design of systems subjected only to force. The general equation (Ref. V-1.4)has become known as the damage-pressure-level equation.

V-4.4.1 Damage-Pressure-Level Equation

For an elasto-plastic resistance (Fig. V-4.9) the relations shown in Fig. V-4.14 can be stated in the form of equations as follows.

If the force is of infinitely long duration, the external work done is equal to the internal energy absorbed at maximum deflection. Then,

$$P_m y_m = R_y (y_m - 0.5\, y_y)$$

or

$$\frac{P_m}{R_y} = 1 - \frac{0.5}{\mu} \qquad \text{(V-4.38)}$$

where μ = the "ductility factor" or the ratio of y_m/y_y.

On the other hand, if a triangular forcing function acts for a very short time t_d, the positive impulse is $0.5\, P_m t_d$ and the initial kinetic energy of the mass is $0.25\, P_m^2 t_d^2/2M$. However, this energy is equal to the stored energy at maximum deflection, as before. Hence, with use of the relation,

$$M = \frac{M}{K}\frac{Ky_y}{y_y} = \frac{R_y T^2}{4\pi^2 y_y}$$

one can derive the result

$$\frac{P_m}{R_y} = \frac{\sqrt{(2\mu - 1)}\ T}{\pi t_d} \qquad \text{(V-4.39)}$$

Equation V-4.39 applies when t_d is very small and Eq. V-4.38 when t_d is very large. Trials with various combinations of the equations led to the following generally applicable empirical result (slightly different from the previous versions of the same equation, but with some theoretical advantages, as will be shown later):

$$\frac{P_m}{R_y} = \frac{T}{\pi t_d}\sqrt{2\mu - 1} + \frac{2\mu - 1}{2\mu\left(1 + \frac{2T}{\pi t_d}\right)} \qquad \text{(V-4.40)}$$

Equation V-4.40 is in error (compared with the exact solution in Fig. V-1.31) by less than 8.4% over the whole range of values of t_d from zero to infinity and of μ from 1 to infinity. The error is less than 5% for all values of t_d if μ is less than 100.

A more general relation has been derived in Refs. V-4.7 and V-1.4 which is accurate for any nonlinear resistance-deflection curve that is not unstable. If we designate by the symbol $\overline{A}$ the ratio of the absorbed energy up to a deflection y_m, relative to the elastic energy up to the deflection y_y, then the following equation can be derived directly from the procedure described in the foregoing discussion leading to the derivation of Eq. V-4.40.

$$\frac{P_m}{R_y} = \frac{T}{\pi t_d}\sqrt{\overline{A}} + \frac{\overline{A}/2\mu}{1 + \frac{2T}{\pi t_d}} \qquad \text{(V-4.41)}$$

Note that for the elasto-plastic case,

$$\overline{A} = 2\mu - 1 \qquad \text{(V-4.42)}$$

The following relations are derived for the general case, but can be adapted to the elasto-plastic case by use of Eq. V-4.42.

In Eq. V-4.41 let t_d approach infinity, and designate the value of P_m for this case as P_∞, where

$$\frac{P_\infty}{R_y} = \frac{\overline{A}}{2\mu} \qquad \text{(V-4.43)}$$

Then compute P_m/P_∞, as follows:

$$\frac{P_m}{P_\infty} = \frac{2T}{\pi t_d}\frac{\mu}{\sqrt{\overline{A}}} + \frac{1}{1 + \frac{2T}{\pi t_d}} \qquad \text{(V-4.44)}$$

Since $\overline{A}$ must always be less than μ^2, for a load-deflection relation which does not involve hardening or locking, for such conditions P_m/P_∞ will always be greater than unity.

Now in Eq. V-4.41, multiply both sides of the equation by $t_d/2$ so that we obtain on the left the quantity i_m/R_y. Then when t_d is allowed to approach zero, $i = i_o$, and one finds

$$\frac{i_o}{R_y} = \frac{T}{2\pi}\sqrt{\overline{A}} \qquad \text{(V-4.45)}$$

If we compute the ratio i/i_o, we find:

$$\frac{i}{i_o} = 1 + \frac{2T}{\pi t_d}\frac{\sqrt{\overline{A}}/\mu}{1 + \frac{2T}{\pi t_d}} \qquad \text{(V-4.46)}$$

where i = the area under the force-time curve. Note, by comparison of Eqs. V-4.44 and V-4.46, that

$$\frac{P_m}{P_\infty} = \frac{2T}{\pi t_d}\frac{\sqrt{\overline{A}}}{\mu}\frac{i_m}{i_o} \qquad \text{(V-4.47)}$$

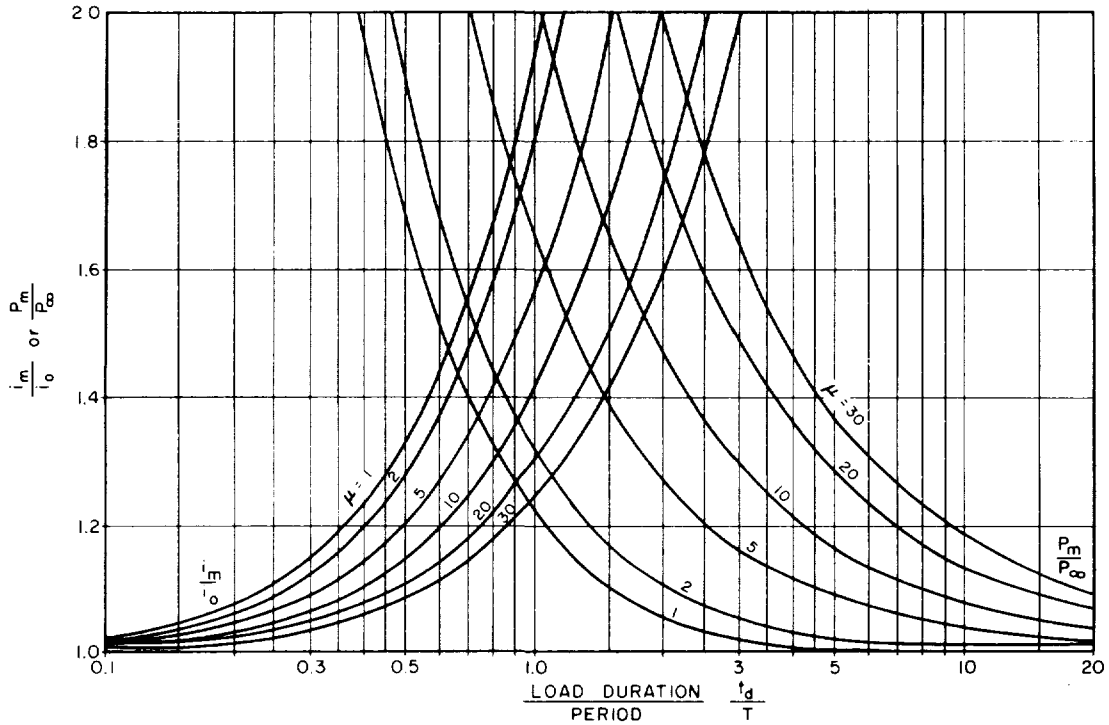

FIG. V-4.15 CORRECTION FACTORS $\frac{P_m}{P_\infty}$ AND $\frac{i_m}{i_o}$ FOR ELASTO-PLASTIC RESISTANCE

A plot of Eqs. V-4.44 and V-4.46 for values of t_d/T greater than about 0.5, leads to small correction factors (having a numerical value less than 1.8 for μ less than 30) to be applied to the values of P_∞ in order to obtain P_m. Such a plot is shown in Fig. V-4.15 for the elasto-plastic case where $\overline{A} = 2\mu - 1$.

Also in Fig. V-4.15 are shown correction factors to be applied to the values of i_o, always less than 1.8, for values of μ less than 30, to be used for values of t_d/T less than 3.

In other words, by use of the correction factors derived here, one can obtain accurate results with only small correction factors, by using as a datum the conditions for infinite duration loads when t_d/T is greater than 1/3 to 1.0, and by using as a datum the conditions for pure impulse when t_d/T is less than 1 to 3.

The advantage in the use of the preceding approximate procedure lies in the ease with which a solution can be obtained for a resistance function of any shape. Also with certain exceptions, the most notable being that of a finite rise time, any loading function can be accounted for by using Eq. V-4.46 and the appropriate correction from Fig. V-4.15; that is, the impulse defined by an irregularly-shaped loading function is computed and set equal to i. When the duration t_d of the irregularly-shaped loading function is greater than 3 times the period T, an approximate solution can be obtained by replacing the actual loading function by an initially-peaked-triangular-force pulse with maximum amplitude P_m such that the replacement triangle averages the force under the actual curve; the solution is then obtained from Eq. V-4.44 and the appropriate correction from Fig. V-4.15.

V-4.4.2 Effect of Finite Rise Times in Loading Function

The response of an SDF system to a loading function with a finite rise time provides one graphical illustration of the point made so frequently before in this part: Calculation of the response of a given system to a particular loading can lead to gross misinterpretation of the general behavior of the system. For example, consider Fig. V-4.16 which shows the variation of response with rise time of the loading function: Relatively small changes in the ratio of rise time to natural period of vibration, particularly in the vicinity of integer values of this ratio, can cause large changes in the maximum deflection. Similar behavior is portrayed in Figs. V-4.17a and b wherein plastic behavior of the system and more general loading functions are considered.

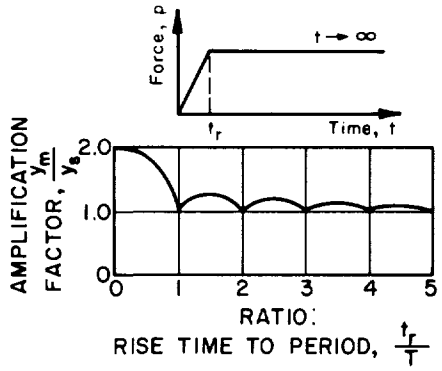

FIG. V-4.16 EFFECT OF RISE TIME OF LOAD PULSE ON RESPONSE OF SIMPLE ELASTIC OSCILLATOR

The last group of figures allow some generalization to be made with regard to design. As the ratio of rise time to period of vibration increases, the maximum displacement y_m exceeds by successively smaller amounts the static displacement y_s (Fig. V-4.16) or the yield displacement y_y (Fig. V-4.17). Frequently in design the rise time of the loading pulse is not known with precision, and if it is known precisely, the precise value applies only to a given loading function; there is no assurance that the given loading function will actually be achieved during the life of the structure. In addition the properties of the structure can frequently vary significantly (of the order of 25%) from the characteristics ascribed to it in the design. Therefore, it is likely that the best a designer can do is to stipulate the limiting conditions associated with the loading and the resistance of the structure. If it can be reasonably assured that the ratio of rise time to natural period cannot be expected to be less than approximately 3, the yield resistance of the structure R_y can be set equal to the peak value of the loading P_m. Using this as a design rule one finds from Fig. V-4.17a that the maximum response y_m of the structure will correspond to a ductility factor between 1 and approximately 2. Of course this is a large range in response, but even the upper limit can hardly be expected to produce failure unless the structure is an unusually brittle one.

Similarly a second rule for design to take account of the ratio of rise time to natural period can be expected reasonably to be below 3. Because the ductility factor μ can become quite large for small values of t_r/T, it is safest, and reasonable in view of the unknowns entering the problem, to assume a zero rise time.

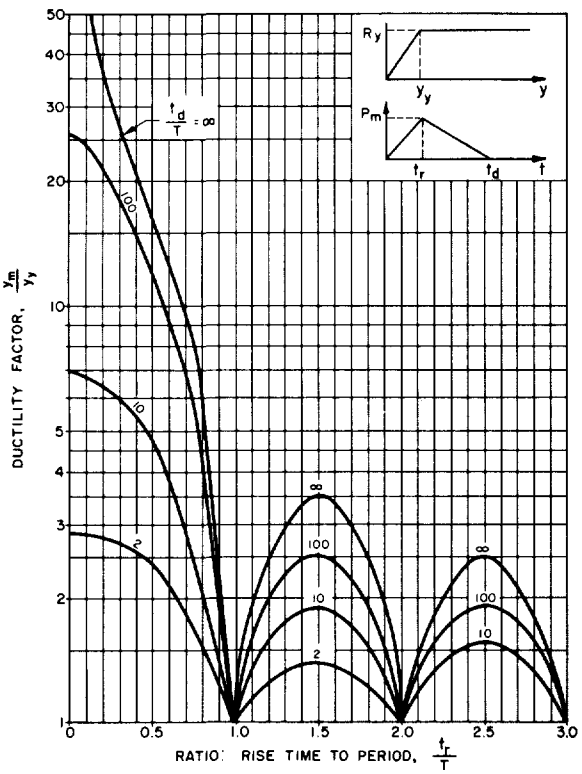

FIG. V-4.17a APPROXIMATE EFFECT OF RISE TIME ON RESPONSE OF SIMPLE OSCILLATOR FOR A DAMAGE-PRESSURE LEVEL (P_m/R_y) OF 1.0; LOADS OF LONG DISTANCE

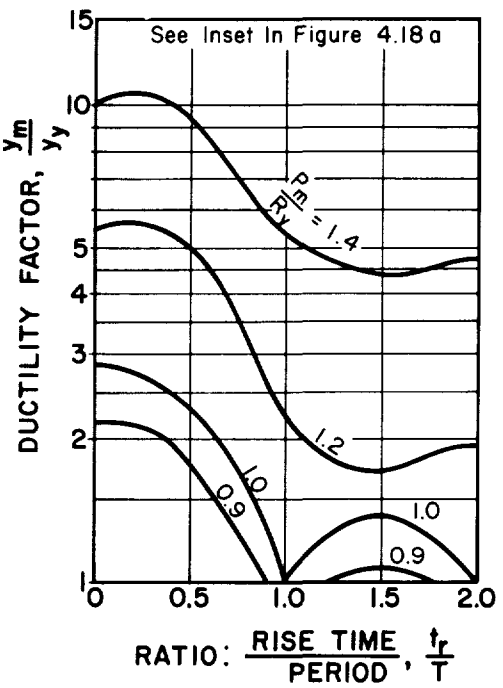

FIG. V-4.17b APPROXIMATE EFFECT OF RISE TIME ON RESPONSE OF SIMPLE OSCILLATOR FOR A RATIO OF PULSE DURATION TO PERIOD OF 2

V-4.5 DESIGN INVOLVING BASE MOTIONS (GROUND MOTION)

V-4.5.1 Shock Response Spectra

The time history of the actual motions of the earth caused by the passage of a shock wave over the surface is very complex and subject to considerable uncertainty. However, the principal effects on equipment and structural components can be described quite readily by use of the concept of the shock response spectrum (Refs. V-4.8 and V-4.9), which has been used successfully in studies of response of structures subjected to earthquake ground motions (Refs. V-4.10, V-4.11, and V-4.12). Further aspects of the response spectrum applied to shock problems arising from blast have been published for elastic systems (Refs. V-4.13 and V-4.14), and extensions of the spectrum concept to elasto-plastic systems have been made for earthquake ground motions (Ref. V-4.15). In these references solutions were obtained generally by methods discussed in Section V-4.3. A preliminary attempt to summarize design procedures for shock isolation systems has been made in Ref. V-4.16.

Consider a piece of equipment or an internal element of a structure supported at a point on an underground structure which is subjected to motion from blast. The equipment or element can be represented as a simple oscillator as shown in Fig. V-4.18 (or V-4.1).

Let the motion of the mass M be designated by y, the ground motion or support motion by x, and the motion of the mass relative to the support by u. The resistance of the supporting spring connecting the mass to the ground is R, where for an elastic system

$$R = Ku$$

in which K is the constant for the spring.

The natural frequency f of the oscillator is given by the equation

$$f = \frac{1}{2\pi}\sqrt{\frac{K}{M}} = \frac{1}{T}$$

For a given transient ground motion x(t), the mass M will be set into motion, with a resulting displacement u which is a function of time. The maximum value of the displacement u relative to the support is called the response spectrum displacement, denoted herein by the symbol D. The maximum value of the absolute acceleration of the mass M is called the response spectrum acceleration, and is denoted by Ag, where g is the acceleration of gravity. The maximum value of the velocity of the mass M relative to the support is approximately equal to the following more useful quantity called the response spectrum pseudo-velocity V,

$$V = 2\pi fD$$

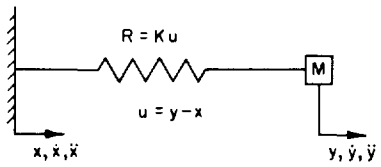

FIG. V-4.18 SIMPLE MASS-SPRING SYSTEM SUBJECTED TO GROUND MOTION

For a system with zero damping, the relation between D and A is as follows:

$$Ag = (2\pi f)^2 D$$

The same equation applies, approximately, if damping of the motion occurs. The quantity D has dimensions of length, V of length per unit of time, and A is dimensionless. These quantities designate the same maximum response of the oscillator in slightly different ways.

For a given input motion and a given oscillator, the values of D, V, and A are functions of the frequency f of the oscillator (or system) considered, modified slightly by the damping in the system. A single plot of the values of D, V, and A can be drawn, as functions of frequency, by use of the type of chart shown in Fig. V-4.19a. The actual values form, generally, a jagged curve having roughly the shape of the upper part of the trapezoid marked out by the heavy lines on the figure. A typical response spectrum for a simple parabolic velocity pulse is shown in Fig. V-4.19b. A typical response spectrum for a much more complex input, corresponding to a strong motion earthquake (the El Centro earthquake of May 18, 1940) is shown in Fig. V-4.19c, for several different values of damping. The parameter β in the figure corresponds to the amount of damping in terms of the critical value for the system.

From studies of many earth shock response spectra, it has been found that the general characteristics and approximate magnitudes can be plotted on the chart if the maximum values of ground displacement, ground velocity, and ground acceleration are known. One does not need to consider the precise time history of the ground motions. (Actually there are discrepancies which may occasionally be as high as a factor of 2, but are generally much smaller. However, the actual ground motions are not known even this accurately, and the simplification of the spectrum in this way is usually permissible.) Rules for simple construction of spectra for even complicated ground motions are given in Ref. V-4.16.

The spectra in Figs. V-4.19b and V-4.19c are typical of response spectra for elastic systems subjected to simple input motions and to complex input motions. For simple input motions, damping has only a small effect on the response, (Fig. V-4.19b).

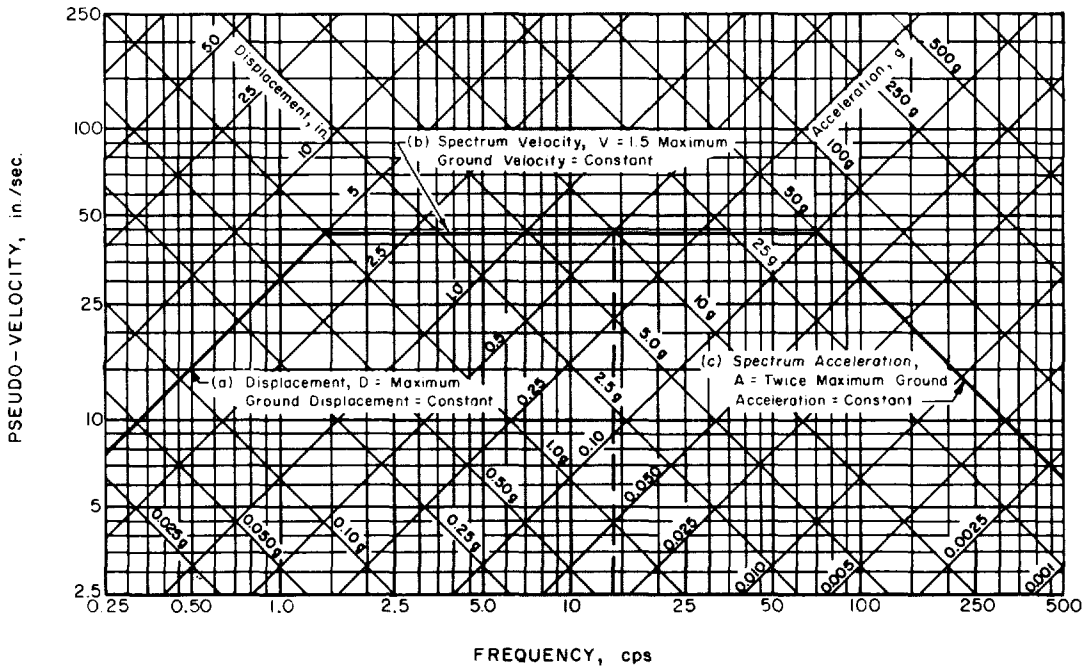

FIG. V-4.19a COMBINED SHOCK SPECTRUM ENVELOPE FOR EARTH MOTION

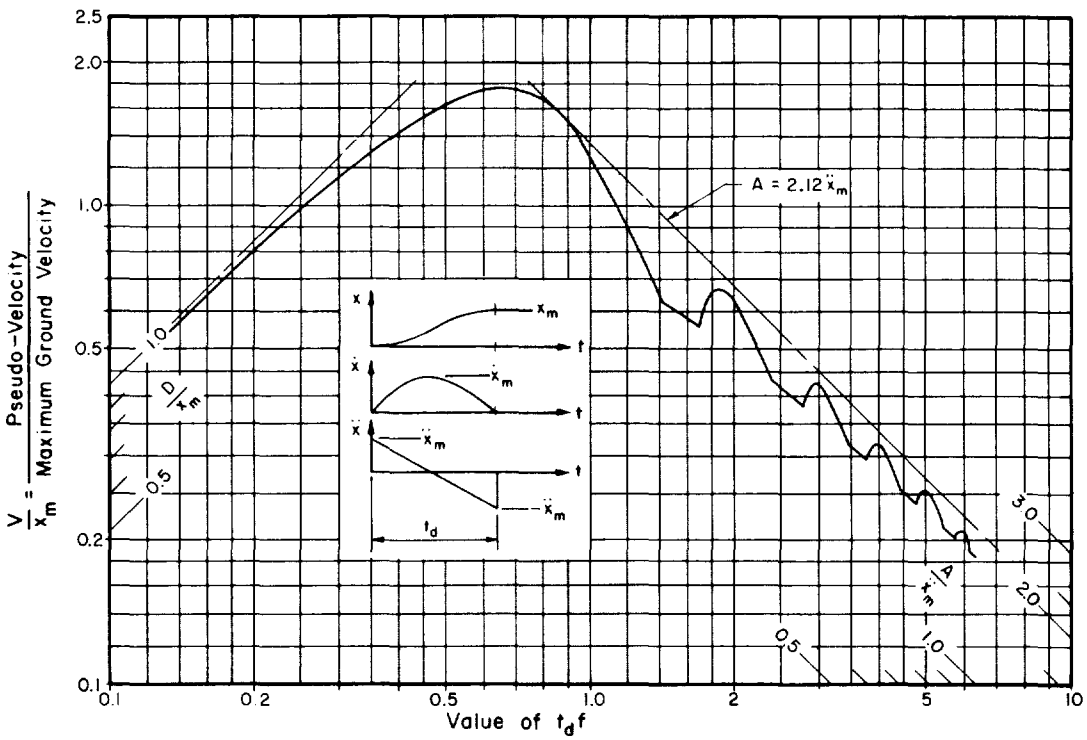

FIG. V-4.19b DEFORMATION SPECTRUM FOR UNDAMPED ELASTIC SYSTEMS SUBJECTED TO A PARABOLIC VELOCITY PULSE

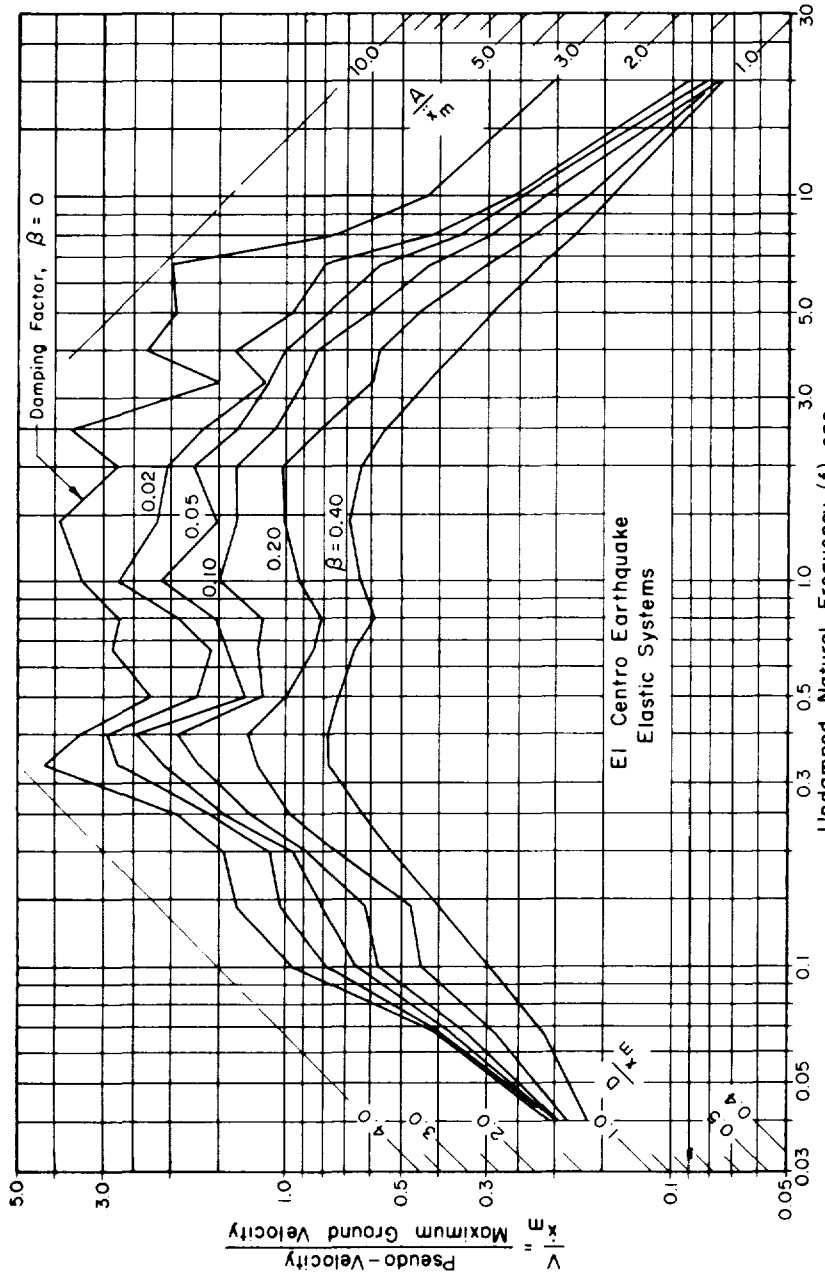

FIG. V-4.19c DEFORMATION SPECTRA FOR ELASTIC SYSTEMS SUBJECTED TO THE EL CENTRO QUAKE

For complex inputs, damping may have a relatively large effect, especially in the intermediate range of frequencies (Fig. V-4.19c).

The following comments are made to assist in the interpretation of response spectra in general. They arise from the definitions of the quantities defining the spectra, as limits or bounds are considered.

As the frequency of the responding system decreases, eventually it becomes so small that the disturbance takes place practically as a static motion of the ground, without motion of the mass of the oscillator. Hence, in the limit the maximum relative displacement in the oscillator spring, D, must be precisely equal to the maximum ground displacement, X_m. Both figures show this tendency. Also, they indicate that damping has little effect on response at the very low frequency region of the spectrum.

At the other extreme, when the frequency of the oscillator is very high, then the spring is relatively so stiff and/or the mass so light that the mass moves with the same motion as the ground, and the force in the spring must be precisely equal to the product of mass times acceleration of the mass, which is the same as the acceleration of the ground. If there are no discontinuities in the acceleration input (corresponding to infinite frequencies of excitation), then the maximum acceleration of the mass, A, must be precisely equal to the maximum ground acceleration $\ddot{x}_m$, and approaches this value more rapidly as the damping increases. However, for only moderately large frequencies, there is a substantial amplification in the response acceleration, as shown on the right-hand sides of Figs. V-4.20b and V-4.20c.

For intermediate frequencies there is generally a greater amplification in response, especially in the cases where there is any large number of input pulses and where damping is small. Damping changes the amplifications and reduces them greatly. With no damping, even for only one input pulse, the maximum response, for example, for a single sine pulse of velocity input, reaches a magnitude of more than 1.7, and for a single rectangular block pulse of input velocity, the maximum response is twice the input. Damping changes these amplifications somewhat but not as much as in the case where there is a large number of input pulses.

Although fairly precise rules can be given for sketching approximate response spectra for any input motions, primarily from consideration of the shapes of the input curves of displacement, velocity, and acceleration, the relations involved are fairly complex. These rules are embodied in Figs. V-4.21a and b, taken from Ref. V-4.17. A simplification of these rules, suitable for use in ordinary situations corresponding to ground motions arising from nuclear blasts, is described here, in terms of an "envelope" to the response spectrum.

The approximate spectrum "envelope" is defined as follows:

(a) A line D = constant, parallel to the displacement scales, drawn with a magnitude equal to the maximum ground displacement.

(b) A line V = constant, drawn with a magnitude of 1.5 times the maximum ground velocity.

(c) A line A = constant, parallel to the acceleration scales, drawn with a magnitude equal to twice the maximum ground acceleration.

The heavy spectrum lines in Fig. V-4.19a are consistent with a typical set of conditions at or near the surface of a soil having seismic velocity of about 2,000 ft/sec, with an overpressure of 200 psi, and a yield of device of about 8 mt (cf Part IV). From the plot it can be seen, for example, that the maximum response of a piece of equipment having a frequency of 14 cps would be 0.50 in., with a maximum acceleration of 10 g.

V-4.5.2 Shock Mounting

This section is concerned with the problem of attachment of equipment (mechanical, electrical, hydraulic, etc.) to the protective structure. The equipment must remain attached throughout a blast and must function in the post-blast state. It is obvious that the attachments must have sufficient strength to transmit the forces which are associated with the equipment accelerations and with the relative distortions of structure and equipment. The stiffness of attachments must be considered not only in relation to its influence on the magnitudes of transmitted forces but also from the point of view of possible limits of acceptable relative displacements and accelerations of equipment and structure.

Since the problem relates to the mounting of equipment, rather than to the design of major structural components, it can be assumed that the attached mass is relatively small compared with the mass of the structure. It follows that the attachment forces are negligible in comparison with the direct effects of the blast, and the motion of the structure is nearly independent of the forces transmitted through the attachments. Motion of the structure is taken as the basic input for which the mounting must be designed. These input data must be obtained from an analysis of the response of the structure to ground shock and air blast, or must be assumed.

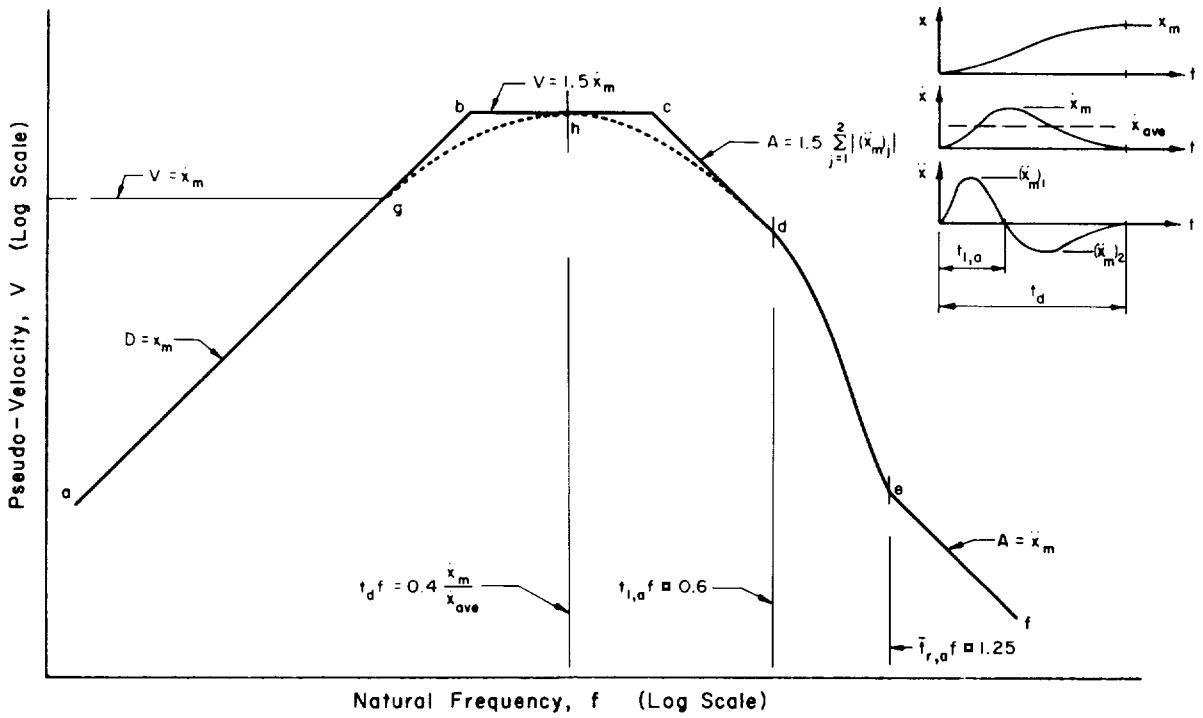

FIG. V-4.20a DESIGN SPECTRUM FOR THE APSOLUTE MAXIMUM DEFORMATION OF SYSTEMS SUBJECTED TO A HALF-CYCLE VELOCITY PULSE–UNDAMPED ELASTIC SYSTEMS; CONTINUOUS INPUT ACCELERATION FUNCTIONS

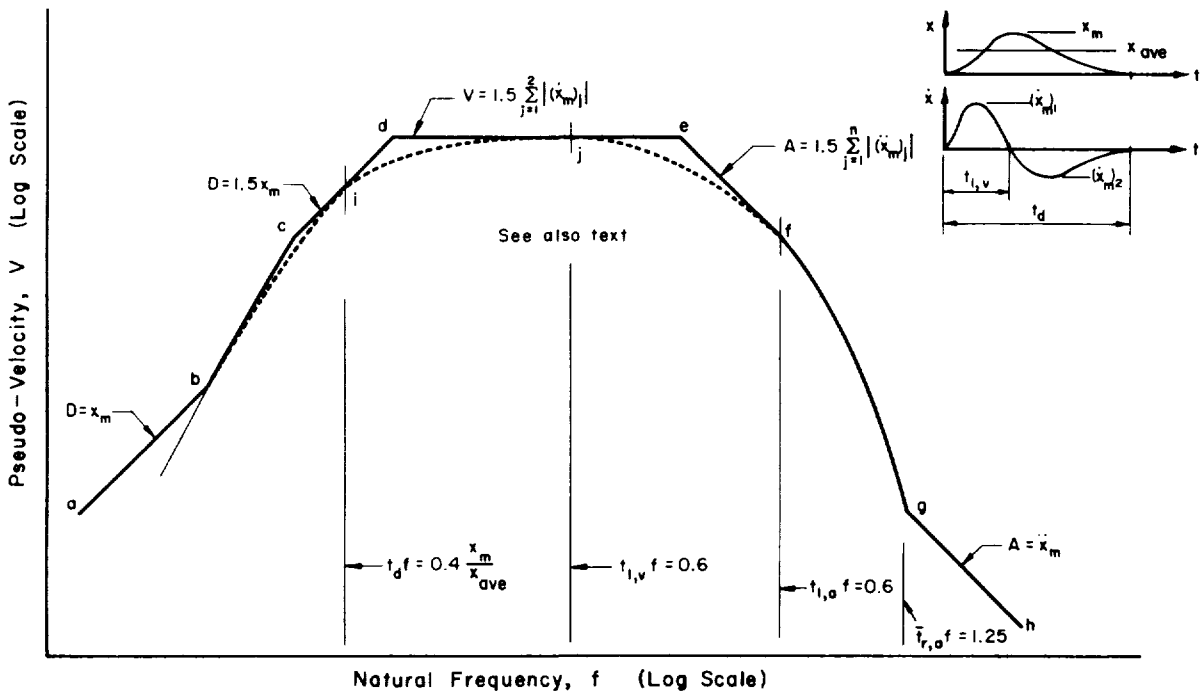

FIG. V-4.20b DESIGN SPECTRUM FOR THE ABSOLUTE MAXIMUM DEFORMATION OF SYSTEMS SUBJECTED TO A HALF-CYCLE DISPLACEMENT PULSE–UNDAMPED ELASTIC SYSTEMS; CONTINUOUS INPUT ACCELERATION FUNCTIONS

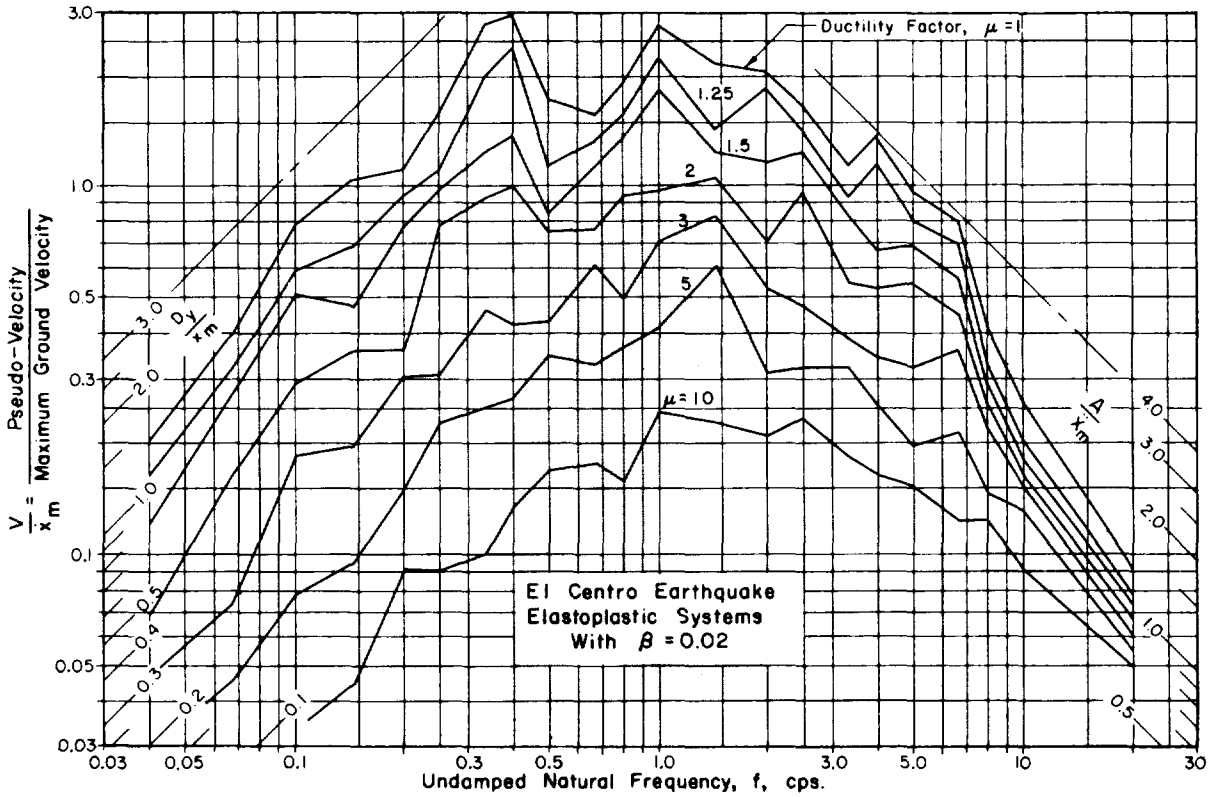

FIG. V-4.21 DEFORMATION SPECTRA FOR ELASTO-PLASTIC SYSTEMS WITH 2% CRITICAL DAMPING SUBJECTED TO THE EL CENTRO QUAKE

Maximum accelerations or displacements which can be tolerated by the equipment must be known or computed. For complex items, such as electronic equipment, this information should be supplied by the manufacturer. The permissible accelerations and distortions of many other items, such as piping, ductwork, machinery bases, etc., often can be investigated directly by the mounting designer.

In general the conditions which cause damage to equipment correspond to maximum values of relative displacement, relative velocity change, or acceleration, but in all cases these must be considered as a function of frequency. In other words, one can draw a sort of spectrum, like a response spectrum, which defines damage to specific equipment items. At high frequencies, a particular level of acceleration can be defined as causing damage or failure. This level can usually be defined from knowledge of the stresses within the equipment and the factor of safety used in its design. Accelerations of the order of 1.5 to 2.5 g are not uncommon for fairly delicate electronic equipment such as cathode ray tubes, or for high speed rotating equipment with small tolerances, such as magnetic drums, etc. Accelerations of the order of 5 to 10 g are not uncommon for more rugged items of equipment such as motors, generators, ventilating fans, and the like. And values of the order of 20 to 50 g can be attained for small and rugged items.

For intermediate and low frequencies, a velocity step can usually be defined as causing damage. This can be related to the height of free fall onto a hard surface which the equipment might sustain without failure. Values of 12 to 24 in./sec are not unreasonable for moderately resistant items or for very heavy pieces of equipment, and values of several times this much might be reached for equipment with well-protected vulnerable parts.

General rules cannot be given, unfortunately, for all items of equipment. However, comparison with damage under conditions such as in transport by truck or rail often furnishes a valuable basis for judgment as to the vulnerability of specific items. Some further discussion of this and presentation of data are to be found in Ref. V-4.16.

Provision for Relative Distortion of Equipment and Structure. When equipment must be connected to the structure at two or more points, and when significant relative displacements of these points

are anticipated, the capacity of the equipment and attachments to accommodate such displacements must be investigated. Cases of this kind are not limited to the obvious situation in which the equipment is attached to two structures having independent motion components. Quite often structures are designed to undergo substantial distortion, particularly in flexure modes. A few examples are shown in Fig. V-4.22; in each example, points a and b undergo significant relative displacements. This displacement may be either elastic or elasto-plastic. If some plastic distortion is anticipated its magnitude may be very sensitive to small changes in the assumed loading on the structure. If this is the case, relative displacements should be computed on the assumption of maximum structural distortion; i.e., distortion corresponding to conditions when the structure is at the point of collapse.

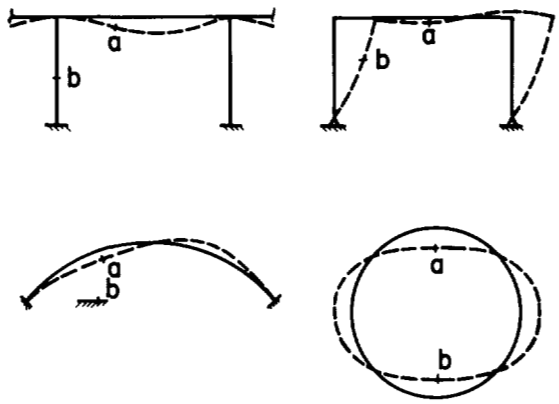

FIG. V-4.22 RELATIVE DISPLACEMENTS WITHIN A STRUCTURE ASSOCIATED WITH STRUCTURAL DISTORTION

It should be emphasized that relative displacement of attachment points may be accommodated by elastic or elasto-plastic distortion of the equipment, by flexible joints, slip-couplings or other devices incorporated in the equipment, by elastic or elasto-plastic distortion of the attachment, or by some combination of these factors. It may be quite unrealistic to attempt to supply all of the required accommodation in the attachments. In piping or conduit, for example, provision of bends or loops rather than a straight run between the connected points may permit the entire relative motion to be absorbed by flexural distortion of the pipe.

Nature of Elastic Systems Comprised of Mounted Equipment. In general any piece of mounted equipment comprises a multi-degree-of-freedom elastic system (or elasto-plastic system) which responds to the motion of its support points (points of attachment to the structure). If the equipment is so connected to the structure that relative distortions of the structure can be accommodated without serious stresses in equipment and attachments, a desirable condition, the stresses in the equipment and forces transmitted through the attachments will be primarily a function of accelerations of the equipment. The major problem of analysis thus is determination of equipment accelerations. The products of equipment masses (concentrated or distributed) and corresponding accelerations represent a loading for which the corresponding stresses and support forces can be found by conventional methods of stress analysis.

Every system has many degrees of freedom and corresponding modes of motion, and the total motion is comprised of the sum of the responses in each mode. Fortunately most systems have only a very few, easily recognized modes of predominant significance which contribute most of the response to a specified direction of support motion. Consequently, it usually is sufficient to determine the response in each (often only one) of these predominant modes. When it is deemed necessary to determine the response in more than one mode, advantage should be taken of the fact that peak values of stresses and reactions in the separate modes are unlikely to occur simultaneously. Thus the combination of values from the separate modes should be based on probability considerations.

In some instances the flexibility of a piece of equipment and its attachments may be limited almost entirely to the latter. This would be the case, for example, if an electric motor were attached to the structure by relatively soft spring mountings. In other cases the attachments may be very rigid and the equipment may be relatively flexible. An example of the latter would be piping having a relatively small ratio of diameter to distance between points of support.

In many instances for which the equipment has a mass distributed over considerable length, or area, it is convenient to approximate the distributed mass by one (or a few) mass concentrations.

Design of Mounted Equipment to Resist Shock. In a typical case, an underground structure may be considered to move with the ground in accordance with the free-field motions at or near the base of the structure. Consider a situation where the motions are such as to lead to the response spectrum for design shown in Fig. V-4.19a. If a piece of equipment is to be mounted in the structure, the equipment must be designed for the response it would receive. This response is determined by the frequency of the system composed of the piece of equipment, its mounting bracket or connections, and the part of the structure to which it is attached. In general the structure is rigid enough so that all parts of the structure have the same motions and consequently the input motion for which the equipment is to be designed is the free-field earth motion.

If the equipment is a heavy, compact element mounted on a bracket, one must make an estimate of the natural frequency of the system. It will be possible in most cases to assume that the point of attachment of the bracket to the wall of the structure is a fixed point of support. Then from the flexibility of the bracket and the magnitude of the supported mass, one can compute the natural frequency. This can be estimated fairly well by determining what the static deflection of the system would be in the direction of motion due to a force equal to the weight of the supported element. If this deflection is y_s', then the frequency f is approximately:

$$f = \frac{1}{2\pi}\sqrt{\frac{g}{y_s}} \qquad \text{(V-4.48)}$$

where g is the acceleration of gravity.

For example, consider a piece of equipment which with its attachment plates and bolts weighs 1,000 lb, bolted to a plate which is welded to the flanges of two channels, and attached to the wall of a structure as shown in Fig. V-4.23.

The channels have a web thickness of 0.51 in. and a net height of web of 11.0 in. The spring constant for the two channels, each 1 ft long, considered as deflecting without end rotation, because of the fixity of the web by the flanges, may be computed. The deflection y_s due to a weight of 1,000 lb turns out to be 0.014 in., and by use of Eq. V-4.48, one obtains

$$f = 26.5 \text{ cps}$$

The maximum static stress in the web is 5,300 psi.

For the input data given, one finds from Fig. V-4.19a that the acceleration response at a frequency of 26.5 cycles is about 20 g. This means that the equipment mass will be subjected to a maximum acceleration of 20 g, and it also means that the bracket will have a stress of 20 times the stress computed for the weight of the equipment, or 106,000 psi, in addition to the static stress, or a total of 111,000 psi. The bracket is clearly overstressed.

It is not necessarily true that strengthening the bracket will work with full effectiveness in reducing the stress, because adding to the strength at the same time adds to the stiffness and attracts more force because of the consequent increased acceleration response. For example, doubling the number of channel supports increases the frequency to 37.6 cps and gives an acceleration response of 28 g, which results in a stress, including static stress, of 77,000 psi.

On the other hand, if the bracket were subjected to an input motion only one-third as great, the spectrum response values would be decreased to one-third their value and the net stress would correspond to an acceleration of about 6.7 g, or 38,000 psi, plus the static stress of 5,300 psi, which would be acceptable.

In general, it is desirable to provide as much flexibility in the mounting as possible without sacrificing strength, to keep the response as low as possible, both for the equipment and the mounting itself.

One may use the shock spectrum in very nearly the same way to design for a limiting condition of acceleration, relative velocity, or displacement relative to ground.

Design Stresses in Shock Mountings. If the forces transmitted through the attachments are determined on the basis of elastic behavior, it should be safe to proportion the attachments for yield stresses at peak transmitted forces. If brittle materials are avoided the plastic distortion available generally will be substantially larger than the elastic distortion which occurs up to the point of yield. Consequently, actual fracture is not likely.

It is not feasible to recommend general stress levels for use in the equipment itself since these depend on the function of the equipment and the extent to which that function would be impaired by large strains. For those items involving ductile materials and where plastic strains would not impair the post-blast function, yield values of stress will be acceptable.

V-4.5.3 Response Spectra for Inelastic Systems

It is often possible to permit yielding to take place in the shock mounting in order to achieve an economical design, or in order to limit the acceleration imposed on the equipment supported by the shock mounting.

Studies that have been reported in Refs. V-4.15 through V-4.20* indicate that for an elasto-plastic system, a response spectrum can be obtained for the elastic component of displacement, and hence also the acceleration, from the response spectrum applicable to an elastic system having the same parameters (namely spring constant and frequency) as the initial elastic part of the elasto-plastic system.

*It should be noted that Refs. V-4.18 through V-4.20 consider nonlinear, but elastic systems. The latter restriction to the results is not present in the studies of Refs. V-4.15 and V-4.17.

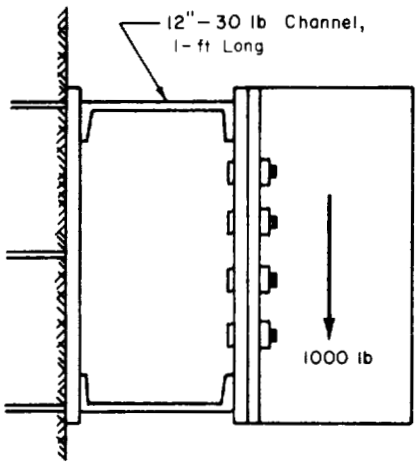

FIG. V-4.23 EXAMPLE OF BRACKET MOUNTING

Numerous data have been tabulated for the response of nonlinear systems. The results obtained are in general similar to those shown in Fig. V-4.21 which illustrates the elastic component of response in an elasto-plastic system having a ductility factor μ ranging from purely elastic ($\mu = 1$) to highly plastic ($\mu = 10$). The input motion considered is that for the El Centro earthquake, for which response spectra for an elastic system were reported in Fig. V-4.19c. A viscous damping coefficient of 2% of critical, in the elastic range, was used. Similar results are obtained for simpler input motions.

Elementary considerations of the sort described in the latter part of Section V-4.5.1 suggest that even for an inelastic system, when the "frequency," defined, for example, for the elastic initial portion of the resistance curve, is very low, the maximum relative displacement D must be the same as the maximum ground displacement x_m. Hence for elasto-plastic resistance, the elastic component of maximum relative displacement must be $\frac{1}{\mu}$ times the maximum ground displacement. The data in Fig. V-4.21, and similar data for other inputs, demonstrate the validity of this conclusion.

Also, for an inelastic system, when the "frequency," however defined, is very high, the mass must move with the same motion, and hence the same acceleration, as the ground. Therefore A must approach $\ddot{x}_m$. In other words, for a very high frequency oscillator, the force transmitted to the mass is independent of the force-displacement relation for the spring. This conclusion is verified by the trend at the extreme right-hand side of Fig. V-4.21. Other data for simpler inputs confirm the conclusion also.

It appears that for the intermediate range of frequencies the displacement for an inelastic system is virtually the same as for an elastic system having the same "frequency," as defined for the elastic portion of the resistance-displacement relationship for the spring. However, from some point corresponding to the peak or apex of the pseudo-velocity response spectrum, and extending over to the region at the extreme right, where force is preserved, heuristic reasoning suggests that energy is constant in both the inelastic and elastic systems.

It is conservative to use this relationship, of constant energy rather than constant displacement, for the entire mid-range of frequencies.

The above reasoning can be summarized in quantitative form for elasto-plastic systems, as follows:

If the ductility factor for the elasto-plastic system is μ, the location of the modified spectrum can be given as a function of μ relative to the elastic spectrum.

In the left-hand part of the spectrum, for low frequencies, the total displacement of the elasto-plastic system is the same as for the elastic system; hence the elastic component of displacement, and therefore the acceleration, is reduced by a factor $1/\mu$ in the elasto-plastic system.

In the right-hand part of the spectrum, for high frequencies, the acceleration of the elasto-plastic system is nearly the same as for the elastic system; hence the total displacement of the elasto-plastic system is increased by a factor μ times that of the elastic system.

In the central part of the spectrum, the total energy absorbed in the elasto-plastic system is the same as that absorbed in the elastic system. Hence the total displacement is reduced by the ratio $\mu/\sqrt{2\mu - 1}$, and the acceleration reduced by the ratio $1/\sqrt{2\mu - 1}$ for the elasto-plastic system.

REFERENCES

V-4.1 Townsley, The Response of Flexibly Supported Simple Beams to Dynamic Loads, Particularly Appendix A, USA, EWES, Misc. Paper No. 2-344, Vicksburg, July 1959.

V-4.2 Lamoën, Etude Graphique des Vibrations de Systèms à un Seul Degré de Liberté, Revue Universelle de Mines, Paris (May 1935).

V-4.3 Jacobsen, On a General Method of Solving Second Order Ordinary Differential Equations by Phase Plane Displacements, Jour. Appl. Mech., 19, 6 (Dec. 1952).

V-4.4 Newmark, A Method of Computation for Structural Dynamics, Trans., ASCE, 127, 1, 1406-1435, New York (1962). See also: Newmark, Analysis and Design of Structures to Resist Atomic Blast, Bul. of the Virginia Poly. Institute, XLIX, 3, Part 2 (Jan. 1956).

V-4.5 Newmark, Methods of Analysis for Structures Subjected to Dynamic Loading, Report to Physical Vulnerability Division, Directorate of Intelligence, U. S. Air Force, 17 Nov. 1949, revised 18 Dec. 1950.

V-4.6 Proceeding of the Symposium on Earthquake and Blast Effects on Structures, Earthquake Engineering Research Institute and University of California, June 1952.

V-4.7 Design of Structures to Resist Nuclear Weapons Effects, Manual of Engineering Practice No. 42, ASCE, New York, 1961.

V-4.8 Jacobsen and Ayre, Engineering Vibrations, New York: McGraw-Hill Book Co., Inc., 1958, esp. Chapter 4.

V-4.9 Fung and Barton, Some Shock Spectra Characteristics and Uses, Jour. Appl. Mech., 25, 3, 365-372 (Sept. 1958). See also: Fung and Barton, Some Characteristics and Uses of Shock Spectra, Ramo-Wooldridge Report No. GMTR-82/AM No. 6-14, 15 Oct. 1956.

V-4.10 Biot, Analytical and Experimental Methods in Engineering Seismology, Trans. ASCE, 108, 365-408 (1943).

V-4.11 Hudson, Response Spectrum Techniques in Engineering Seismology, Proc. World Conf. on Earthquake Engineering, Earthquake Engineering Research Inst., Berkeley, California, pp. 4-1 to 4-12 (1956).

V-4.12 Housner, Behavior of Structures During Earthquakes, Jour. Eng. Mech. Div. ASCE, 85, EM-4 109-129 (Oct. 1959).

V-4.13 Fung, Shock Loading and Response Spectra, Colloquium on Shock and Structural Response, ASME, p. 1-17, Nov. 1960.

V-4.14 Barton, Ground Shock and Missile Response, Colloquium on Shock and Structural Response, ASME, p. 69-79 (1960).

V-4.15 Veletsos and Newmark, Effect of Inelastic Behavior on the Response of Simple Systems to Earthquake Motions, Proceeding Second World Conference on Earthquake Engineering, Science Council of Japan, Ueno Park, Tokyo, Japan (1960).

V-4.16 A Guide for the Design of Shock Isolation Systems for Underground Protective Structures, prepared by Ralph M. Parsons Co. for Air Force Special Weapons Center, AFSWC-TDR-62-64, December 1962.

V-4.17 Veletsos and Newmark, Vol. III, Response Spectra Approach to Behavior of Shock Isolation Systems, Newmark, Hansen and Associates under subcontract to Mechanics Research Division, General American Transportation Corp., for Air Force Weapons Laboratory, Kirtland Air Force Base, June 1963.

V-4.18 Fung and Barton, Shock Response of a Non-Linear System, EM 10-22, Space Technology Laboratory TR-60-0000-19317, Los Angeles, Oct. 1960.

V-4.19 Fung and Schreiner, Tables and Charts of the Loading Ratio of the Shock Response of a Non-Linear System, EM 10-23 Space Technology Laboratory TR-60-0000-19362, Los Angeles, February 1960.

V-4.20 Fung and Barton, The Performance and Design of Non-Linear Systems Subjected to Ground Shock, EM 11-6, Space Technology Laboratory, Los Angeles, July 1961.

CHAPTER V-5

MULTI-DEGREE-OF-FREEDOM SYSTEMS AND MODAL ANALYSIS

Most structures consist of a complex assemblage of individual elements such as beams, columns, trusses, and slabs; therefore their response to time-dependent loading or motion involves multiple frequencies and corresponding multiple modes of vibration. Further each structural element and the components of each element may be of themselves complex members. For example, as shown in Section V-4.2 even a simple beam has an infinite number of frequencies and mode shapes, any or all of which may be present in the general response to a dynamic loading. Fortunately, in many instances, a reasonable approximation to response for a given loading can be obtained by consideration of a single mode. However, in some cases, either because of the complexity of the structure or the nature of the loading, it is essential to consider responses in which a number of possible modes of vibration may be involved. Consideration of a number of modes is referred to as modal analysis.

Important as it is, it must be noted that modal analysis or any of the other classical analytical methods are not very useful in the design of the structure; to perform these analyses one must know the distribution of mass and flexibility in the structure. For that reason, these analyses are useful after, and not before, specific proportions of the structure are selected.

The emphasis in this chapter will be placed on modal analysis and on the concepts directly useful in performing a modal analysis. Since various references describe modal analysis in detail, only a brief and heuristic treatment will be given here. More information may be found in standard references dealing with classical vibration theory, for example Refs. V-1.35, V-4.8, V-4.12, V-4.16, and V-5.1.

An example of a structure which can be approximated well as a multi-degree-of-freedom system (MDF system) with a finite number of degrees of freedom* is a multi-storied building with girders that are much stiffer in flexure than are the columns (Fig. V-5.1a). In this figure the structure consists of several interconnected frames, of the type shown, arrayed along a line normal to the plane of the figure. These several frames constrain the motion to occur predominantly in the plane of the figure. Furthermore, the extension and compression of the columns produce deflections which are generally very small compared with the relative translation occurring horizontally between stories; thus, the rotation of each floor normally is negligible compared with the relative translation. All of these observations are necessary to reduce even this simple structure to the model shown in Fig. V-5.1b.

In the model (Fig. V-5.1b), which is frequently referred to as a shear-beam, the lumped masses, M_1 through M_4, represent the individual floors; the springs, K_1 through K_4, between the masses or between M_1 and the ground represent the bending stiffness of the columns; and the coordinates, y_1 through y_4 represent the absolute horizontal displacements of the masses. These displacements are shown as vertical in the model (Fig. V-5.1b) since it is easier to symbolize with meaning extensional rather than rotational springs and vertical rather than horizontal constraint to the motion, but it is obvious, despite the lack of correspondence in the direction of motion, that the model (Fig. V-5.1b) represents the structure (Fig. V-5.1a). Since four coordinates, y_1 through y_4, are needed to define the motion of the model, it is by definition a system with four degrees of freedom.

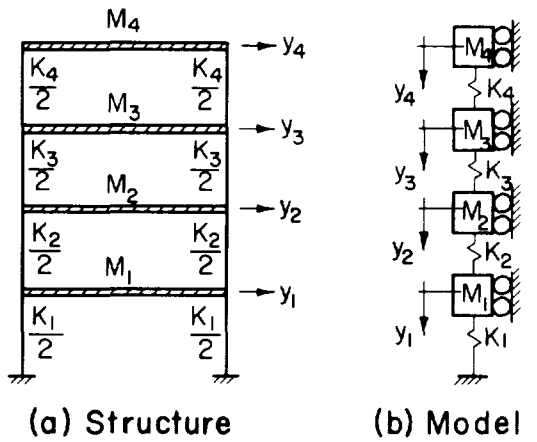

FIG. V-5.1 STRUCTURE WITH STIFF FLOORS AND FLEXIBLE COLUMNS AND MULTI-DEGREE-OF-FREEDOM MODEL

*The number of degrees of freedom is defined as the number of independent generalized coordinates required to define completely the motion of a system. For example a rigid body in space has six degrees of freedom, three translational and three rotational. Thus, a coordinate system using three variables is required to define the position of the body if it translates without rotation while a coordinate system using three other variables is required to define the position of the body if it rotates without translation.

In general, a model of a structure with several degrees of freedom may be defined by an extension of the methods described in Section V-4.2. However, it must be emphasized that a model having fewer degrees of freedom than the prototype can be developed only after a particular configuration or set of configurations for the prototype is selected; for example in Fig. V-5.1, the actual structure has an infinite number of degrees of freedom. If only the lateral deflections at each floor are of interest, however, one can choose only the masses lumped at each floor level, and the magnitude of each lumped mass, the force acting on each mass, and the stiffness of each spring in terms of the mass, force and stiffness of the actual structure can readily be determined. In the particular example considered here the model is characterized as follows: (1) The lumped mass in each case is the total mass* of the floor and of the items supported by the floor; (2) the force acting on each mass is the total concentrated force acting at each floor level**; and (3) the stiffness of each spring is the sum of the flexural stiffness of the two actual columns represented by the spring in the model. Care must be exercised in selecting the particular characteristics of the model. Normally an appropriate and reasonably simple model can be specified by observing the physical constraints on the motion present in the actual structure.

V-5.1 GENERAL METHODS OF SOLUTION

Vibrations of structures constitute a type of problem mathematically similar to other problems such as elastic buckling, beams on elastic foundations, and the like, in which under certain conditions the distortion of the structure is zero except when some parameter, such as vibration frequency, buckling load, etc., reaches a critical value. Such problems are said to have Eigenvalues (natural frequency), and the configuration associated with an Eigenvalue is called an Eigenfunction or Eigenvector.

The approach to determining the response of complex systems is conveniently divided into two parts: (1) Defining the characteristics of the particular system when no loads are applied to it, and (2) solving for the response of the system to a given transient load. The following development is so divided.

* Approximately one-half of the mass of the columns framing into the floor should be added to the mass of the floor.

** For a force distributed in some manner over the height of the actual structure, the force acting on each mass is approximately equal to the intensity of pressure multiplied by the wall area tributary to the floor.

V-5.1.1 Determination of the Eigenvalues and Eigenvectors

In vibration analysis of a multi-degree-of-freedom system the values of the circular frequencies of free vibration constitute a series or set of eigenvalues, and the associated deflected shape for each frequency is referred to as an eigenvector (or mode shape). Sometimes exact solutions of the governing differential equaltions can be obtained, at other times exact solutions are impractical and approximate methods must be used. There are two principal approximate methods generally in use: (1) The Rayleigh-Ritz or energy method and (2) the Vianello-Stodola method. Both of these methods are described below. Both methods become quite cumbersome for complex systems unless a computer is used for the solutions. For simple systems or for solution of the fundamental frequency of complex systems either method can be easily handled using hand computation.

Rayleigh-Ritz Method. This method was suggested initially by Lord Rayleigh (Ref. V-1.18), but at the same time he stated reservations about the method except when it was used to compute the fundamental frequency. The procedure was further developed by Ritz (Ref. V-5.2) to allow its use in computing frequencies for higher modes. It can be shown formally that the method leads to frequencies which are equal to (only if the precise modal shape is assumed) or higher than the true values. A simple physical explanation for this has been given (Ref. V-1.35): If any deflected shape other than the exact one is assumed, a restraint on the motion of the system is imposed; this leads to higher frequencies than the exact ones.

The method consists of: (1) Assigning a deflected shape to the structure in the form of a finite series, each term of which satisfies the boundary conditions; (2) solving for the maximum potential energy (strain energy) stored in the system; (3) solving for the maximum kinetic energy in the system; and (4) equating the difference of the maximum values of the potential and kinetic energies to zero. Using the criterion that the coefficients of the series selected in (1) must be such that the total energy is a minimum produces the characteristic equation to be solved for the various frequencies.

This procedure is based on the assumption that there is no energy lost in the system. Since there is no external force to do work, the maximum potential energy which develops when the system is deflected to an extreme position must equal the maximum kinetic energy which develops when the system passes through its equilibrium position; i.e., the difference of these energies must be zero. By definition, the motion must be periodic so that the kinetic energy is proportional to the square of the circular frequency.

As an illustration, consider the simple beam shown in Fig. V-5.2. Although it is known that the true deflected shape is represented by a sine function, take as an approximation the deflected shape caused by the weight of the beam:

$$y_x = \frac{wx}{24EI}(L^3 - 2Lx^2 + x^3) \text{ for } 0 \leq x \leq \frac{L}{2} \qquad \text{(V-5.1)}$$

where

y_x = deflection caused by weight of beam

w = weight of beam per unit of length

L = total span

EI = flexural stiffness of beam

First apply the Rayleigh method alone to obtain the fundamental frequency. The maximum strain energy U is

$$U = 2\int_0^{\frac{L}{2}} \frac{M_x^2\,dx}{2EI} = \frac{w^2}{4EI}\int_0^{\frac{L}{2}} (x^2 - Lx)^2\,dx \qquad \text{(V-5.2)}$$

since $M_x = EI\dfrac{d^2y_x}{dx^2}$ = bending moment caused by weight of beam.

The maximum kinetic energy V is

$$V = \frac{2w}{2g}\int_0^{\frac{L}{2}} (\dot{y}_x)^2\,dx = \frac{\omega^2 w^3}{576gE^2I^2}\int_0^{\frac{L}{2}} (L^3x - 2Lx^3 + x^4)^2\,dx \qquad \text{(V-5.3)}$$

since $\dot{y}_x = \omega y_x$ = the maximum velocity of the beam if ω is the circular natural frequency of vibration, and g is the acceleration of gravity.

If the indicated integrations are performed and the last two equations are set equal to one another,

$$\omega^2 = 97.59\frac{EIg}{wL^4} \qquad \text{(V-5.4)}$$

compared with the precise value of

$$\omega^2 = \pi^4\frac{EIg}{wL^4} \cong 97.41\frac{EIg}{wL^4} \qquad \text{(V-5.5)}$$

To apply the Rayleigh-Ritz procedure, we must express the deflected shape as a series, each

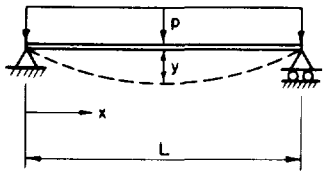

FIG. V-5.2 SIMPLY SUPPORTED BEAM WITH UNIFORMLY DISTRIBUTED LOADING

term of which must satisfy the boundary conditions. Instead of using the deflected shape caused by the weight of the beam as a basis for the series in this case, it is desirable to choose an expression which is less cumbersome to integrate. Thus, take the series

$$y_x = \frac{w}{EI}\sum_{n=1}^{n} a_n \sin\frac{n\pi x}{L} \qquad \text{(V-5.6)}$$

and select only the first two terms. Then

$$U = \frac{1}{2}\int_0^L \frac{M_x^2\,dx}{ET} = \frac{w^2}{2ET}\int_0^L \left[a_1\frac{\pi^2}{L^2}\sin\frac{\pi x}{L} + a_2\frac{4\pi^2}{L^2}\sin\frac{2\pi x}{L}\right]^2 dx$$

and

$$V = \frac{\omega_n^2 w^3}{2gE^2I^2}\int_0^L \left[a_1\sin\frac{\pi x}{L} + a_2\sin\frac{2\pi x}{L}\right]^2 dx$$

Integrating, taking the difference in the last two expressions and setting the difference equal to zero, yields

$$U - V = a_1^2 + 16a_2^2 - \frac{\omega_n^2 L^4 w}{\pi^4 EI\, g}\left[a_1^2 + a_2^2\right] = 0$$

For a minimum of the energy:

$$\frac{\partial(U-V)}{\partial a_1} = a_1 - \frac{\omega_n^2 L^4 w}{\pi^4 EI\, g}a_1 = 0 \qquad \text{(V-5.7)}$$

and

$$\frac{\partial(U-V)}{\partial a_2} = 16a_2 - \frac{\omega_n^2 L^4 w}{\pi^4 EI\, g}a_2 = 0 \qquad \text{(V-5.8)}$$

From these expressions it is obvious that either $a_1 = a_2 = 0$, a trivial case, or from Eq. V-5.7

$$\omega_n^2 = \omega_1^2 = \frac{\pi^4 EIg}{wL^4}$$

and from Eq. V-5.8

$$\omega_n^2 = \omega_2^2 = \frac{16\pi^4 EIg}{wL^4} = \frac{n^4\pi^4 EIg}{wL^4}$$

Each of these values for the circular frequency are precise since Eq. V-5.6 represents the exact deflected shape of a simple beam undergoing free vibration.

Vianello-Stodola Method. Although this method is useful for finding the characteristic values λ for any equation of the type indicated in Eq. V-5.9, it will be applied here to find the circular natural frequencies of complex systems

$$\frac{d}{d}\left[a(\xi)\frac{d\eta}{d\xi}\right] + b(\xi)\eta = 0 \qquad \text{(V-5.9)}$$

Since by definition the motion is periodic the maximum acceleration $\ddot{y}_n$ is related to the displacement y_n by

$$\ddot{y}_n = -\omega_n^2 y_n \qquad \text{(V-5.10)}$$

Accordingly the maximum d'Alembert force, acting in a direction opposing the maximum acceleration, associated with the motion of any mass M_n is

$$M_n \ddot{y}_n = M_n \omega_n^2 y_n \qquad \text{(V-5.11)}$$

Therefore, the Vianello-Stodola method, as applied to the problem of finding circular natural frequencies, consists of: (1) Assuming a deflected shape for the system y_{m-1}, (2) finding the d'Alembert forces consistent with the assumed deflections, (3) computing the deflections y_m caused by the d'Alembert forces, and (4) finding the coefficient which must be multiplied by the assumed deflected shape to make it equal to the computed shape. This coefficient is the square of the circular natural frequency ω^2. A constant value of this coefficient, found by considering selected points along the structure, is obtained only if the assumed deflected shape is the exact one. If a constant value is not obtained, a closer approximation to the deflected shape of the fundamental or lowest mode is obtained by using the deflected shape computed in step (3) as the assumed shape and repeating the steps. In fact it can be shown (Ref. V-5.3) that the iterative method will converge to the fundamental frequency; that is

$$\omega^2 = \lim_{m\to\infty} \frac{y_{m-1}}{y_m} = \frac{K}{M} \qquad \text{(V-5.12)}$$

where K is the "scale factor" for stiffness and M is the "scale factor" for mass. That is, the actual mass (or stiffness) is defined as the product of a scale factor times a distribution or pattern of mass (or stiffness).

As an example, consider the problem of determining the fundamental natural circular frequency of the simply supported beam in Fig. V-5.2. Assume as a deflected shape the deflection produced by the weight of the member (identical to the illustration of the Rayleigh Method).

$$y_{m-1} = \frac{wx}{24\ EI}(L^3 - 2Lx^2 + x^3) \text{ for } 0 \leq x \leq \frac{L}{2} \qquad \text{(V-5.1)}$$

Since $\frac{d^4y}{dx^4} = \frac{p}{EI}$ and $p = \frac{w}{g}\omega^2 y_{m-1}$ from Eq. V-5.11, successive integration with substitution of the appropriate boundary conditions yields

$$y_m = \frac{w^2\omega^2 x}{40320\ E^2I^2g}(17L^7 - 28L^5x^2 + 14L^3x^4 - 4Lx^6 + x^7) \qquad \text{(V-5.13)}$$

If the last expression is evaluated at $x = \frac{L}{2}$ and the result is set equal to Eq. V-5.1 also evaluated at $x = \frac{L}{2}$,

$$\omega^2 = \frac{26880}{277}\frac{EIg}{wL^4} = 97\frac{EIg}{wL^4}$$

Similarly for the expressions evaluated at $x = \frac{L}{4}$

$$\omega^2 \cong \frac{34.4 \times 10^6}{0.251 \times 10^6}\frac{EIg}{wL^4} = 137\frac{EIg}{L^4}$$

Since the values obtained by considering points ($x = \frac{L}{2}$ and $x = \frac{L}{4}$) along the structure are not equal, it is apparent that the deflected shape assumed is not the correct one. In accordance with Eq. V-5.12, a better approximation to the deflected shape is represented by Eq. V-5.13. Therefore, this would be used as the assumed deflected shape in the second iteration.

It is apparent from the foregoing discussion that formal solution of the equations in this iterative process can become cumbersome; the integrations become more tedious with each iteration. Consequently, it is frequently helpful to make use of numerical integration of the type developed in Ref. V-5.4 in the solution of the deflections caused by the d'Alembert forces. Numerical integration is also a particularly useful technique to use when a structure, such as a beam, supports several concentrated masses and/or contains several step discontinuities in its cross section (which produce step discontinuities in the distribution of mass and stiffness).

The Vianello-Stodola method is a particularly powerful technique to be used in finding circular natural frequencies of systems with lumped masses

connected by massless springs (Fig. V-5.1b). For such systems the method can be used to find all of the natural frequencies, and the computations can be carried out neatly in a tabular form for which the essential characteristics were suggested first in Ref. V-5.4. A single mass from the system (Fig. V-5.3a) is isolated as a free body in Fig. V-5.3b. The d'Alembert force on each mass associated with an assumed deflected shape is defined uniquely by Eq. V-5.11. From knowledge of the d'Alembert force acting on each mass, one can find the forces in the springs of the system. From the forces in each spring, the deflection of each spring is determined since

$$\Delta y_n = \frac{\Delta F_n}{K_n} \qquad \text{(V-5.14)}$$

where

Δy_n = deflection of nth spring

ΔF_n = force in nth spring

K_n = stiffness of nth spring

Knowing the deflection of each spring, one can find the deflected shape consistent with the d'Alembert forces, and as before an approximation to the circular natural frequency is determined by taking the ratio of the magnitude at each mass of the assumed deflected shape to the computed deflected shape. If these ratios are not equal, the process is repeated using as an assumed deflected shape the computed shape from the preceding trial.

As an example, consider the specific system shown at the top of Table V-5.1. The calculations for one trial are shown in Table V-5.1. In the table: (1) The first column defines the operation being performed in the rows; (2) the subsequent columns immediately below the structure give the numerical values; and (3) the last column summarizes the units which are common to the numerical values in each row.

Specifically, the structure (Table V-5.1) has a spring constant for the first story (cf. Fig. V-5.1) which is four times that for the top story; the spring constant for the second story is three times that for the top story. The mass distribution is not quite uniform, with the mass of the second floor (M_1) twice that of the third floor or of the top floor.

It is noted that M and K can have any magnitudes assigned to them, and they are kept in general form throughout the calculations. The mass is given in terms of the weight divided by the acceleration of gravity. Consequently, the units used in the calculation have to be taken with consistent values. If the mass is stated in terms of a weight in pounds divided by an acceleration of gravity in inches per second squared, and if the spring constant is given in terms of pounds per inch, the period T will be in units of seconds. Another set of consistent units involves displacement in feet, weight in kips, acceleration of gravity in feet per second squared, and spring constant in kips per foot.

It is also apparent that the assumed deflection y_{m-1} can have any units whatsoever, and the derived deflection y_m will have the same units. Consequently, it is convenient to take y_{m-1} as dimensionless. This does not affect the results at all and makes it more clear that the modal displacements are quantities that give the shape of the deflection pattern rather than the absolute magnitudes.

The calculations for the fundamental mode in Table V-5.1 for an assumed shape of the mode correspond to deflections at the first, second, and third story, respectively, of magnitudes 2, 3, and 3. The inertial forces F_n are computed from Eq. V-5.11. At the first mass adjacent to the base, the magnitude of the mass being 2M, the value of the assumed deflection y_{m-1} (= 2) is multiplied by 2M whereas the assumed deflections at the second and third levels are multiplied by M only.

The shears or spring forces ΔF_n in the various stories are obtained by summing the forces from right to left, since there is no force applied at the right. These shears, divided by the spring constants for the various floors, give the tabulated values of the increment in story displacement Δy_n. From these, by starting with the known value of zero deflection at the support one obtains directly the values of the derived deflection y_m. The final row shows ratios of y_{m-1} to y_m. These give the values of ω^2 at the particular mass points for which the derived curve and the assumed curve agree exactly.

It can be noted that if ω^2 has the smallest of these values, namely 0.400 for the third mass M_3, the derived curve will lie everywhere inside the assumed curve or, in other words, between it and the original undeflected position. This indicates that the quantity 0.400 is an absolute lower limit to the value of ω^2 for the first mode. It also can be noted that if the value of ω^2 has the magnitude 0.800, as for the first mass M_1 in this case, the derived curve will lie everywhere outside the assumed value and therefore this is an upper limit to the value of ω^2 for the first mode. In other words, any value of ω^2 between 0.400 and 0.800 can make the two curves agree in part, although not completely; but values outside these limits cannot make the curves agree at all. Consequently, the true value of ω^2 must lie between the limits described.*

*These observations are applicable only when the assumed curve and the derived curve of deflections have no modal points or points of zero deflection.

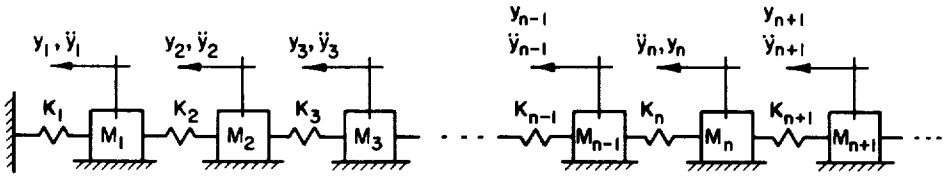

(a) Multi-Degree-of-Freedom System With Lumped Masses.

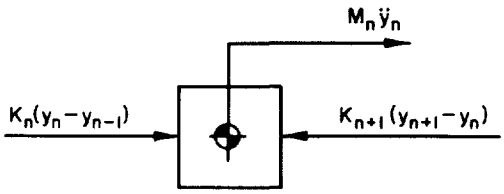

(b) Free-Body Diagram of n^{th} Mass.

FIG. V-5.3 ANALYSIS OF SYSTEMS WITH LUMPED MASSES

TABLE V-5.1 — ILLUSTRATION OF COMPUTATION OF FUNDAMENTAL CIRCULAR NATURAL FREQUENCY BY VIANELLO-STODOLA METHOD

Operation	Spring 1	Mass 1	Spring 2	Mass 2	Spring 3	Mass 3	Common Units
Assumed Deflection	0	2		3		3	y_{m-1}
d'Alembert Force, F_n		4		3		3	$M\omega^2 y_{m-1}$
*Force in Spring, ΔF_n	10		6		3	0	$M\omega^2 y_{m-1}$
Deflection of Spring, Δy_n	2.5		2		3		$\frac{M}{K}\omega^2 y_{m-1}$
†Computed Deflection, $y_m = \Sigma \Delta y_n$	0	2.5		4.5		7.5	$\frac{M}{K}\omega^2 y_{m-1}$
Ratio, $\frac{y_{m-1}}{y_m}$		0.800		0.667		0.400	$\frac{K}{M\omega^2}$

$$\omega^2 = \frac{\Sigma M_n y_{m-1} y_m}{\Sigma M_n y_m^2} \frac{K}{M} = \frac{46}{89} \frac{K}{M} = 0.517 \frac{K}{M} \text{ from Eq. V-5.15.}$$

*A compression of the spring is taken as positive; note that there is no external force applied to M_3.

†Note that the left support of the entire system does not deflect.

Since the individual ratios between assumed and calculated deflections are not constant, the assumed deflected shape is not the correct one. A new trial, using the values of y_m computed as assumed deflections, would improve the correspondence between the individual ratios. Frequently, however, it is sufficiently accurate (Ref. V-5.5) to use the approximation shown at the bottom of the table to find the natural frequency; that is, for any step in the iteration process

$$\omega^2 \cong \frac{\sum_n^{\Sigma} M_n y_{m-1} y_m}{\sum_n^{\Sigma} M_n y_m^2} = \frac{K}{M}$$

where K is the "scale factor"* for stiffness and M is the "scale factor"* for mass.

From this equation, as shown in Table V-5.1, $\omega_1^2 = 0.517 \frac{K}{M}$. It will be shown later that the exact value is $0.500 \frac{K}{M}$.

The pattern of derived deflections, 2.5, 4.5, and 7.5, relative to a deflection of unity at the first mass above the base, has the values 1.0, 1.8, and 3.0. The true pattern for the first mode has the values 1, 2, 4. The derived pattern is much closer to the first mode than is the assumed set of values corresponding to 1.0, 1.5, 1.5 relative to a deflection of unity for the first mass. It is noted that the deflection pattern for the first mode is not, however, nearly as accurate after one cycle as is the best value for the first mode frequency.

For systems with lumped masses (Fig. V-5.3), the method also can be used to find the highest circular natural frequency directly. This is accomplished by performing the computations discussed immediately above in the reverse order; an example is given in Table V-5.2. Specifically, from the assumed deflections (y_m in this case because the computations are reversed), the change in length of each spring Δy_n is computed. In turn the shear or force ΔF_n in each spring is computed. From a free body diagram of each mass (starting from M_3) the d'Alembert force F_n on each mass is determined. Deflections of each mass y_{m-1} are computed from the d'Alembert force from Eq. V-5.11. As before ratios of y_{m-1} to y_m are computed at each mass and ω_3^2 is the required circular natural frequency which causes the assumed and computed displacements to be equal at each mass. Again the ratios are not constant which means that the assumed deflected shape is not correct. As in the case of calculating the fundamental frequency a good estimate of ω_3^2 can be obtained by applying Eq. V-5.15. In this case (Table V-5.2) $\omega_3^2 = 5.94 \frac{K}{M}$ compared with the exact value of $6.00 \frac{K}{M}$.

Because the Vianello-Stodola method converges to the lowest mode for which any component exists in the assumed deflection, the method can be used in principle to compute higher frequencies than the fundamental by removing or "sweeping" the fundamental and the next computed mode or modes from the assumed deflections. However, for systems with more than three or four degrees of freedom the sweeping method is impractical. The removal process makes use of the fact that the mode shapes or eigenvectors are "orthogonal." (See, for example, Refs. V-5.5 to V-5.11.)

The orthogonality for any two modes having deflections or eigenvectors y_i and y_j with a component at each mass point n in the structure of y_{ni} or y_{nj} is expressed as follows:

$$\sum_n^{\Sigma} M_n y_{ni} y_{nj} = 0 \qquad \text{(V-5.15)}$$

provided that the frequencies for the ith and the jth mode are different.

Since any arbitrary deflection can always be expressed as a series of modal deflections (Refs. V-5.1, V-5.5 to V-5.11), one can express an assumed deflection y_a, having a value at mass point n of y_{na}, as a series of modal deflections, with the coefficients c_i, in the form

$$y_{na} = \sum_n^{\Sigma} c_i y_{ni}$$

If this equation is multiplied on both sides by $M_n y_j$, where y_j is different from y_i, and summed over all the mass points, one obtains

$$\sum_n^{\Sigma} M_n y_{na} y_{nj} = c_j \sum_n^{\Sigma} M_n y_{nj}^2$$

because all the values of c_i other than for $i = j$ will be multiplied by a term which equals zero, owing to the relation expressed by Eq. V-5.15.

Then the coefficient of the jth mode in the assumed configuration, y_a, is determinable directly from the equation

$$c_j = \frac{\sum_n^{\Sigma} M_n y_{na} y_{nj}}{\sum_n^{\Sigma} M_n y_{nj}^2} \qquad \text{(V-5.16)}$$

Now one may use Eq. V-5.16 to remove any modal component from the assumed deflection for which one has values of the modal displacements. If

*In accordance with carrying the common factors separately in the tabular computations as shown in Table V-5.1, it is appropriate to take the stiffness of one spring K (and the mass M at one point) as a common factor and express all other stiffnesses (or masses) in terms of this common factor.

the first mode has already been determined, one may remove it and use the Vianello-Stodola procedure to compute the second mode frequency and deflection; and after doing so, one may remove both the second and first modes, and compute the third mode, etc. Any mode can be removed if its shape is known; the modes need not be removed in order. However, the procedure will always yield a result that converges toward the lowest mode remaining in the assumed deflection.

For example, the second circular natural frequency is computed in Table V-5.3 for the system considered in Tables V-5.1 and V-5.2. Any deflection configuration is assumed as shown in the first row of Table V-5.3. The components or values of c_j for the first and third modes are computed from Eq. V-5.16 using for y_n or y_j the computed deflections in Tables V-5.1 and V-5.2. These components are

$$c_1 = \frac{2 \times 2.5 \times 1 + 1 \times 4.5 \times 1 + 1 \times 7.5 \times \left(-\frac{1}{2}\right)}{2 \times 2.5^2 + 1 \times 4.5^2 + 1 \times 7.5^2}$$

$$= \frac{5.75}{99} = 0.0578$$

$$c_3 = \frac{2 \times 16.5 \times 1 + 1 \times (-26) \times 1 + 1 \times 5 \times \left(-\frac{1}{2}\right)}{2 \times 16.5^2 + 1 \times 26^2 + 1 \times 5^2}$$

$$= \frac{4.5}{1246} = 0.00361$$

The product of the component and the corresponding deflection is subtracted from the assumed deflection as shown in Table V-5.3. The computations in the table then proceed in a manner identical to that in Table V-5.1. However, if any deflection corresponding to the first mode is present, the procedure inherently converges to the fundamental mode. Therefore, the first mode must again be removed from the computed deflections. This is accomplished by computing a new component c_1' as follows:

$$c_1' = \frac{2 \times 2.5 \times 0.342 + 1 \times 4.5 \times 6.301 + 1 \times 7.5 \times (-0.653)}{2 \times 2.5^2 + 1 \times 4.5^2 + 1 \times 7.5^2}$$

$$= \frac{-1.84}{99} = -0.0186.$$

The product of this new factor and the computed deflections from Table V-5.1 are used to remove the first mode. It should be noted that the computations in Table V-5.3 should converge to the precise value in a single iteration since the contributions of the first and third modes were removed from the deflections. (The deflection here is totally defined by three modes since the system has three degrees of freedom.) That it did not converge is a result of the relatively inaccurate values used for the first and third mode shapes.

To summarize; higher modes may be computed by the process of (1) computing the modal deflections for the fundamental mode, (2) assuming an arbitrary deflected shape for the second mode, (3) subtracting from the assumed shape the components of deflection for the fundamental mode by using Eq. V-5.16, (4) computing the deflections for the second mode by the Vianello-Stodola method, (5) removing, by use of Eq. V-5.16, the first mode deflections, which invariably creep in as a result of round off, from the computed deflections, and (6) taking ratios of the corrected assumed deflections to the corrected computed deflections (of Table V-5.3). Similarly, to compute the natural frequency for the third mode, the same steps are followed, but now the components of deflection corresponding to the first and second modes must be subtracted in Steps (3) and (5). Although this method is theoretically valid, its application becomes quite tedious especially if several modes must be considered. Moreover, because of inevitable errors, including round-off even in machine calculations, the method loses accuracy rapidly as more modes are computed.

Other Methods. Application of the Vianello-Stodola Method to systems with lumped masses, using the computational format indicated, is directly equivalent to matrix iteration (see pp. 196-204, Ref. V-5.1). Although use of formal matrix algebra is preferred by many, the writers believe the form of computations suggested in the preceding discussion is less tedious to perform especially for systems with several degrees of freedom.

Another method which has been used frequently for lumped-mass systems is Holzer's method (Refs. V-4.8 and V-5.12). This is an iterative technique of a nature different from those previously discussed because it requires assuming a value of the frequency. The calculations generally result in an external force being applied to the terminal mass. In the physical problem this external force does not exist; therefore several values of the circular natural frequencies are assumed until the external force is eliminated. The process is expedited by making a plot of the external force as a function of assumed frequency; a continuous curve is obtained, and a value of the natural frequency for the system exists wherever the curve crosses the frequency axis. Obviously this method can define all natural frequencies of the system. A convenient format for the computations and the order in which they are made is diagrammed in Fig. V-5.4 wherein the encircled numbers denote the steps in the calculations. The assumed value of the deflection at Step (1) is completely arbitrary; similarly the value of the square of the circular frequency ω^2 assumed in any iteration may be arbitrary although, after the first set of computations is completed, values are chosen using the plot of P as a function of ω^2 as a guide. A specific example is given in Table V-5.4 applying this method to the structure considered above.

TABLE V-5.2 — ILLUSTRATION OF COMPUTATION OF HIGHEST CIRCULAR NATURAL FREQUENCY BY VIANELLO-STODOLA METHOD

Operation		Spring 1	Mass 1	Spring 2	Mass 2	Spring 3	Mass 3	Common Units
Assumed Deflection, y_m	0		3		-4		1	y_m
*Deflection of Spring, Δy_n		3		- 7		5		y_m
Force in Spring, ΔF_n		12		-21		5	0	Ky_m
d'Alembert Force, F_n			33		-26		5	Ky_m
Computed Deflection, y_{m-1}	0		16.5		-26		5	$\frac{K}{M\omega^2} y_m$
Ratio, $\frac{y_{m-1}}{y_m}$			5.50		6.50		5.00	$\frac{K}{M\omega^2}$

$$\omega_3^2 \cong \frac{\Sigma M_n y_{m-1} y_m}{\Sigma M_n y_m^2} \frac{K}{M} = \frac{208}{35} \frac{K}{M} = 5.94 \frac{K}{M} \quad \text{Eq. V-5.15.}$$

*Note that the left support of the entire system does not deflect; a compression is positive.

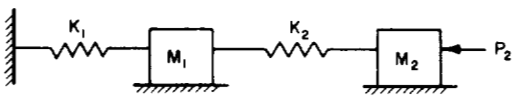

OPERATION	SPRING 1	MASS 1	SPRING 2	MASS 2	APPARENT APPLIED FORCE P_2
Deflection of Mass, y_m		*(0) Assume (1)	ω^2	(7)	
Deflection of Spring, Δy_m	(2)		(6)		
Force in Spring, $\Delta F_n = K \Delta y_m$	(3)		(5)		(9)
d'Alembert Force, $F_n = M_n \omega^2 y_m$		(4)		(8)	
(10) Plot value of apparent applied force, P_2, against assumed value of square of circular frequency, ω^2.					

* Encircled numbers indicate the order in which the calculations are performed.

FIG. V-5.4 DIAGRAMMATIC ILLUSTRATION OF APPLICATION OF HOLZER'S METHOD

TABLE V-5.3 — ILLUSTRATION OF COMPUTATION OF SECOND CIRCULAR NATURAL FREQUENCY BY VIANELLO-STODOLA METHOD

Operation	Spring 1	Mass 1	Spring 2	Mass 2	Spring 3	Mass 3	Common Units
Assumed Deflection, y_{m-1} 0		1		1		-0.500	y_{m-1}
*Remove Contribution of First Mode, $-c_1y_1$		-0.145		-0.262		-0.436	y_{m-1}
*Remove Contribution of Third Mode, $-c_3y_3$		-0.060		+0.094		-0.018	y_{m-1}
Net Deflection, $y_{m-1}-c_1y_1-c_3y_3$ y'_{m-1}		0.795		0.832		-0.954	y_{m-1}
d'Alembert Force, F_n		1.590		0.832		-0.954	$M\omega^2 y_{m-1}$
Force in Spring, ΔF_n	1.368		-0.122		-0.954	0	$M\omega^2 y_{m-1}$
Deflection of Spring, Δy_n	0.342		-0.041		-0.954		$\frac{M\omega^2}{K} y_{m-1}$
Computed Deflection, $y_m = \Sigma\Delta y_n$ 0		0.342		0.301		-0.653	$\frac{M\omega^2}{K} y_{m-1}$
*Remove Contribution of First Mode, $-c'_1y_1$		+0.046		+0.084		+0.140	$\frac{M\omega^2}{K} y_{m-1}$
Net Deflection, $y_m - c'_1y_1$ y'_m		0.388		0.385		-0.513	$\frac{M\omega^2}{K} y_{m-1}$
Ratio, $\frac{y_{m-1}-c_1y_1-c_3y_3}{y_m-c'_1y_1}$		2.05		2.16		1.86	$\frac{K}{M\omega^2}$

$$\omega_2^2 = \frac{\Sigma M_n y'_{m-1} y'_m}{\Sigma M_n y'^2_m} \frac{K}{M} = \frac{1.425}{0.714} \frac{K}{M} = 2.00 \frac{K}{M} \quad \text{Eq. V-5.15.}$$

*See text.

TABLE V-5.4 — ILLUSTRATION OF ONE STEP OF COMPUTATIONS BY HOLZER'S METHOD

Operation	Spring 1	Mass 1	Spring 2	Mass 2	Spring 3	Mass 3	Apparent Applied Force	Common Units
Assume $\omega^2 = 1.0\frac{K}{M}$								
Assumed Deflection, y_{m-1}	0	1		5/3		2		y_{m-1}
Deflection of Spring, Δy_n	1		2/3		1/3			y_{m-1}
Force in Spring, ΔF_n	4		2		1/3		-5/3*	Ky_{m-1}
d'Alembert Force, F_n		2		5/3		2		$M_n \omega^2 y_{m-1} = Ky_{m-1}$

*Since this did not vanish, a new step in the computations must be made starting with a new value for ω^2.

TABLE V-5.5 — MODAL DEFLECTIONS AND PARTICIPATION FACTORS FOR ILLUSTRATIVE STRUCTURE OF TABLE V-5.1

Quantity	Mode 1	Mode 2	Mode 3
ω^2	0.5 K/M	2 K/M	6 K/M
ω	$1.0\sqrt{K/2M}$	$2\sqrt{K/2M}$	$3.464\sqrt{K/2M}$
T	$1.0(2\pi\sqrt{2M/K})$	$0.5(2\pi\sqrt{2M/K})$	$0.289(2\pi\sqrt{2M/K})$
Defl. 3rd floor (roof)	4	-1	1
Defl. 2nd floor	2	1	-5
Defl. 1st floor	1	1	3
$\Sigma M_n u_{nj}$	8	2	2
$\Sigma M_n u_{nj}^2$	22	4	44
γ_j	8/22	11/22	1/22

Another method of computing the natural frequencies which is popular employs the use of finite differences to generate the characteristic equation (see pp. 151-157, Ref. V-5.13).

The characteristic equation also is defined directly by use of Lagrange's equations which are discussed in the following section. However, the characteristic equation normally is tedious to solve for systems with several degrees of freedom since the characteristic equation is a polynominal, in the square of the circular frequency, of degree equal to the number of degrees of freedom. The approximate methods presented above frequently are more easily solved.

V-5.1.2 Lagrange's Equations

Solutions of the response of a system with several degrees of freedom acted upon by forces with a complicated variation with time and with complicated resistance functions, and possibly damping characteristics, can be obtained in a straightforward manner using numerical integration which was discussed in detail in Section V-4.3.4. The approximate procedures in the preceding section are used in conjunction with numerical methods to define the period and, in turn, the time interval to be used.

Another method, presented by Lagrange in 1788 (Refs. V-5.1 and V-5.14), is fundamental to the development of modal analysis; the general concepts underlying its use are discussed below.

The equations of motion (n equations) for a conservative system of n degrees of freedom can be written in terms of the generalized velocity $\dot{y}_i$, the generalized displacement y_i, and the Lagrangian function of the system L with L the difference in kinetic (V) and potential (U) energies.

$$\frac{d}{dt}\frac{\partial L}{\partial \dot{y}_i} - \frac{\partial L}{\partial y_i} = 0 \qquad \text{(V-5.17)}$$

Generalized coordinates in terms of three-dimensional Cartesian coordinates, ξ, η, ζ * are defined by:

$$\begin{aligned} \xi_i &= \xi_i \ (y_1, y_2, y_3 \cdots\cdots y_n) \\ \eta_i &= \eta_i \ (y_1, y_2, y_3 \cdots\cdots y_n) \\ \zeta_i &= \zeta_i \ (y_1, y_2, y_3 \cdots\cdots y_n) \end{aligned} \qquad \text{(V-5.18)}$$

*ξ, η, ζ are used for Cartesian coordinates here to avoid confusion with x and y which were previously defined as the displacement of the base (or ground) and y_n the displacement of a given mass in the system, respectively.

Use of Lagrange equations for conservative systems requires: (1) Choosing generalized coordinates in such way that each coordinate provides for a minimum of total energy in the system; (2) writing an expression for the potential energy U for the system in terms of the generalized coordinates; (3) writing an expression for the kinetic energy V for the system in terms of the generalized coordinates; and (4) substituting these into Lagrange's equations to obtain n linear homogeneous differential equations with constant coefficients. Solution of these equations produces the characteristic equation, mentioned above, from which the natural frequencies and mode shapes of the system can be determined.

The procedure is illustrated by a simple example. Consider the system shown at the top of Table V-5.1. It is apparent that y_1, y_2, y_3 represent the generalized coordinates. The potential energy U is

$$U = \frac{1}{2}\left[4Ky_1^2 + 3K(y_2 - y_1)^2 + K(y_3 - y_2)^2\right] \qquad \text{(V-5.19)}$$

The kinetic energy V is

$$V = \frac{1}{2}\left[2M\dot{y}_1^2 + M\dot{y}_2^2 + M\dot{y}_3^2\right] \qquad \text{(V-5.20)}$$

Since in this case, U is independent of $\dot{y}_i$ and V is independent of y_i, Lagrange's equations become

$$\begin{aligned} 2M\ddot{y}_1 + K y_1 - 3Ky_2 &= 0 \\ M\ddot{y}_2 + K y_2 - Ky_3 - 3Ky_1 &= 0 \\ M\ddot{y}_3 + Ky_3 - Ky_2 &= 0 \end{aligned} \qquad \text{(V-5.21)}$$

It is easily verified that Eqs. V-5.21 are correct by isolating each mass in the system as a free-body.

It is easily shown that

$$y_i = c_i \sin(\omega t + \alpha) \qquad \text{(V-5.22)}$$

is a solution of Eqs. V-5.21 if $c_1 = c_2 = c_3 = 0$, a trivial ease, or

$$\begin{vmatrix} \frac{K}{2M} - \omega^2 & -\frac{3K}{2M} & 0 \\ -\frac{3K}{M} & \frac{K}{M} - \omega^2 & -\frac{K}{M} \\ 0 & -\frac{K}{M} & \frac{K}{M} - \omega^2 \end{vmatrix} = 0 \qquad \text{(V-5.23)}$$

Equation V-5.23 is the characteristic equation, a cubic in ω^2; it has three real roots: $0.500\,\frac{K}{M}$, $2.00\,\frac{K}{M}$, and $6.00\,\frac{K}{M}$, which may be compared with the values obtained in Tables V-5.1 to V-5.3.

Each of the differential equations above is analogous to the homogeneous part of the equation of motion for the single-degree-of-freedom system Eq. V-4.12. Now if $P_i(t)$ is the ith component of the generalized force applied to the system, Lagrange's equations become

$$\frac{d}{dt}\frac{\partial L}{\partial \dot{y}_i} - \frac{\partial L}{\partial y_i} = P_i(t) \qquad \text{(V-5.24)}$$

each of which is directly analogous to Eq. V-4.12. If expressions can be written for the potential and kinetic energies in terms of the generalized coordinates and if $P_i(t)$ is analytic, direct solutions to the series of equations in some cases can be found. More often however it is simpler to add to the homogeneous solutions of Eq. V-5.24 particular solutions which are written in the form of trigonometric series. Use of this technique is the basis for modal analysis.

V-5.1.3 Computation of Modal Response

In any structure having several degrees of freedom and subjected to a transient loading and to time-dependent boundary conditions an analysis may be made by numerical methods, for either elastic or inelastic response. (See Refs. V-4.4, V-5.9, and V-5.11.) If the structure remains elastic, analysis by use of the normal modes is usually most convenient, making use of the fact that the loading, boundary displacement, and response, all may be divided into modal components by the procedure described in the derivation of Eq. V-5.16. General methods of making this type of analysis are discussed in practically all textbooks on vibration of systems having more than one degree of freedom. Details of the method, with examples, are given in Refs. V-4.8, V-4.12, V-4.16, and V-5.1 through V-5.11 and will not be repeated here.

A discussion of complex time-dependent boundary motions is contained very briefly in Ref. V-4.4 Most of the other references describe relatively simple boundary motions.

An illustration of the computations for a simple boundary motion of a structure supported at only one boundary point, for only the boundary or support motion effects, is contained in the following section. The procedure for handling transient loading is similar, and can be taken from almost any of the references cited above.

V-5.2 ILLUSTRATIVE EXAMPLE—THREE-DEGREE-OF-FREEDOM SYSTEM

In a multi-degree-of-freedom system that has independent or uncoupled modes of deformation (this condition is generally satisfied for buildings), each mode responds to the base motion or excitation as an independent single-degree-of-freedom system. Since the modal patterns can be multiplied by arbitrary scale factors, a scale factor γ may be defined by which to multiply the modal quantities that are of interest. The factor γ must be such that the response to the base excitation in the particular mode desired is given by the product of the modal excitation factor γ_j, the modal quantity desired α_j, and the deflection response u(t), for a single-degree-of-freedom system subjected to the same ground motion. The quantity α may be the deflection at a particular floor in the mode considered, the relative story deflection in a particular story, the story shear in a particular story, the stress at a particular point in the structure, or any other such quantity it is desired to compute. To keep the presentation general, the sumbol α will be used to designate any of these various quantities that are of interest.

It is then possible, by proper definition of the modal participation factor γ_j, to write the following expression for the response at the particular point or in the particular manner considered, as a function of time

$$\alpha(t) = \sum_j \gamma_j \alpha_j u(t) \qquad \text{(V-5.25)}$$

In order for this relationship to be applicable, the following equation for γ_j must be used (see Refs. V-4.8, V-4.12, V-5.5 to V-5.11):

$$\gamma_j = \frac{\sum_n M_n u_{nj}}{\sum_n M_n u_{nj}^2} \qquad \text{(V-5.26)}$$

where u_{nj} gives the deflection at the nth mass point in mode j. It is apparent from a comparison of Eq. V-5.26 with Eq. V-5.16 that γ_j is the coefficient for the expansion of a constant unit deflection at all mass points into a modal series of deflections.

The calculations for γ_j, in accordance with Eq. V-5.26, are shown in Table V-5.5 for the structure of Table V-5.1.

Because of the complexities in computing the response as a function of time, and because the maximum responses in the various modes do not necessarily occur at the same time, one is generally interested only in the maximum possible response. An upper bound to this maximum response is obtained by taking

the sum of the numerical values of the maximum modal responses. In other words, an upper limit can be written for the particular function under consideration, designated by α, as follows:

$$\alpha_m \leqq \sum_j \left| \gamma_j \alpha_u D_j \right| \qquad \text{(V-5.27)}$$

where the individual modal terms are the product of the participation factor γ_j, the modal quantity desired α_j, and the spectral value of the displacement of the single-degree-of-freedom structure D_j, where the subscript j refers to the value of D for the particular modal frequency or period. Two additional equivalent forms of Eq. V-5.27 are convenient in certain cases to permit use of the spectral velocity response for the single-degree-of-freedom system V_j, or the spectral acceleration response A_j. These are shown in the following equations:

$$\alpha_m \leqq \sum_j \left| \frac{\gamma_j}{\omega_j} \alpha_j V_j \right| \qquad \text{(V-5.28)}$$

or

$$\alpha_m \leqq \sum_j \left| \frac{\gamma_j}{\omega_j^2} \alpha_j A_j \right| \qquad \text{(V-5.29)}$$

Of the three preceding equations the one that is most convenient to use is generally that in which the spectrum values are most nearly constant for the range of modal frequencies considered. Consequently, Eq. V-5.27 might be used where the spectral displacement is nearly constant, Eq. V-5.28 where the spectral velocity is nearly constant, and Eq. V-5.29 where the spectral acceleration is nearly constant.

If the modal displacements are chosen appropriately, the values of γ_j can be made unity. In other words, the modal deflections computed in the general case can be modified by multiplying them by the quantity γ_j, and it will be found that these modified modal values will have a modal participation factor of unity. This has been done for the values shown in Table V-5.5 and the modified modal values are given in Table V-5.6. Tabulated in this table, in addition to the deflections of the three floors, are the accelerations of the three masses, the relative story displacements in each of the three stories, and the shears in each story. These may be considered as values of α for the three modes. With these quantities as given in Table V-5.6, the quantities γ_j, will be 1.0.

It will be noted that the modal deflections are taken as dimensionless, and therefore the dimensions of the responses are determined by the dimensions of the single-degree-of-freedom spectrum response values.

V-5.3 APPLICATIONS TO DESIGN

V-5.3.1 Approximations for Design-Applied Loads

The basic procedure used in design requires making a reasonable estimate of the predominant mode or modes excited by the applied force. In this section a method is suggested which is sufficiently accurate for most cases.

Consider the loading applied to a complex structure. The peak magnitudes of the forces at various points have a certain distribution over the structure. Define the resistance R of the structure for any deflection, related in magnitude to the "static" load applied over the structure with the same relative distribution as the peak dynamic load that produces the given deflection. Now select some point on the structure where the deflection will be large. This need not be the point of greatest deflection, but it must not be a point of very small deflection relative to the maximum deflection. Let the deflection of this point be the quantity y. The value of y when the structure first yields "generally," not at just one or more isolated places, is y_y, and the maximum acceptable distortion of the structure is associated with $\bar{y}_m$.

Now select some other point on the structure where the largest or nearly largest forces act. This may be the same point defined for deflection but it need not be. Let the applied static pressure at this point be P, and the peak value $\bar{P}_m$. Then define the resistance R as a force applied at the same point, as $\bar{P}$, but of course having the same distribution as the forces P. The value of R_y is then the value of R which corresponds to general yielding (cf. Fig. V-4.12).

In determining the period one is concerned with the vibration of the structure in a mode most nearly like that which corresponds to the shape in which it fails. For uniform loading corresponding to blast loading this is generally about the same as the fundamental mode of vibration of a complex structure. In those instances where it is not, one can make an estimate of the period of vibration in the mode corresponding most nearly to the configuration as it approaches failure. With these definitions the structure is now treated as a simple system and Fig. V-1.31 can be used for determining response.

In some instances an additional step is necessary. Where a structure has nearly independent modes of deformation which may be excited in such a way as to produce a possibility of failure in more than one mode, special consideration is required. Such a

TABLE V-5.6 — MODIFIED MODAL VALUES (FOR UNIT VALUES OF MODAL PARTICIPATION FACTORS) FOR ILLUSTRATIVE STRUCTURE OF TABLE V-5.1*

Quantity	Mode		
	1	2	3
$\ddot{u}_3$ = accel. 3rd floor (roof)	+16 K/M	-22 K/M	+ 6 K/M
u_3 = defl. 3rd floor (roof)	+32	-11	+ 1
$u_3 - u_2$ = displ. 3rd story	+16	-22	+ 6
S_3 = shear 3rd story	+16 K	-22 K	+ 6 K
$\ddot{u}_2$ = accel. 2nd floor	+ 8 K/M	+22 K/M	-30 K/M
u_2 = defl. 2nd floor	+16	+11	- 5
$u_2 - u_1$ = displ. 2nd story	+ 8	0	- 8
S_2 = shear 2nd story	+24 K	0	-24 K
$\ddot{u}_1$ = accel. 1st floor	+ 4 K/M	+22 K/M	+18 K/M
u_1 = defl. 1st floor	+ 8	+11	+ 3
u_1 = displ. 1st story	+ 8	+11	+ 3
S_1 = shear at base	+32 K	+44 K	+12 K

*The constant factor 1/22 in the γ_j values of Table V-5.5 is factored out of the values of this table so that only whole numbers appear. All of the tabulated values are to be divided by 22.

case is that of an arch which may fail in one of two ways, almost independently: (1) by compression corresponding to symmetrical loading, and (2) by flexure corresponding to antisymmetrical loading. For this situation it is possible to treat each mode separately and to investigate the two types of failure independently. Another case of practical importance is a dome, for which both symmetrical and antisymmetrical loading must also be studied.

V-5.3.2 Procedures for Design — Base or Ground Motion

In general, the analysis for a multi-degree-of-freedom linear system subjected to base motion can be accomplished with a procedure which involves a number of steps:

1. Find the normal modes and associated frequencies for the system. For each mode, find the response parameter (displacement, velocity, stress, strain, etc.) at the point desired. This may be where a piece of equipment is to be mounted.
2. Find the excitation coefficient for each mode. This step is defined as the expansion of a unit deflection of all the masses, in the direction of the base motion, into a series of modal deflection shapes, as indicated in Section V-5.2.1.
3. Now determine the response spectrum for the displacement, pseudo velocity, and acceleration for a single-degree-of-freedom system.
4. The modal response is then determined as the product of the stress or particular response in each mode, times the excitation coefficient for that mode, times the single-degree-of-freedom response spectrum value for the frequency of the mode, using the terms in Eqs. V-5.27, V-5.28, or V-5.29, whichever equation is most convenient.
5. The maximum response of the system for the particular response quantity that is desired is less than the sum of the modal maxima, as indicated by the above equations.

6. For a system with several degrees of freedom, the actual maximum response will not ordinarily exceed greatly the square root of the sums of the squares of the modal responses (see Ref. V-5.15). Even in a two-degree-of-freedom system the excess will be less than 40%. Consequently, the square root of the sum of the squares can be used as a design basis rather than the sum of the modal maxima, particularly where the number of modes is large.

V-5.3.3 Multi-Degree-of-Freedom Inelastic Systems

When the multi-degree-of-freedom system is inelastic, and when the properties of the system are determinable, the method of analysis described in Ref. V-4.4 can still be used, although it is usually tedious to make the calculations in this way. It certainly would be too complex to make a complete analysis of a system for the purposes of designing it, because the system would have to be reanalyzed a number of times before a final design is reached. Based on the procedures described in Section V-4.5.3, the following procedure appears to give a reasonable approximation to the response of an elasto-plastic system of two or more degrees of freedom.

1. Determine the response as if the system were elastic, with modes and frequencies corresponding to those obtained from the initial elastic part of the inelastic load-deflection relationships for the system.

2. Take the maximum response, in terms of internal forces or stresses as given by the corresponding quantities for the elastic system multiplied by a factor depending on μ, the ductility factor or the ratio of the maximum permissible displacement to the elastic limit displacement.

3. The factor for force or acceleration used should be chosen as the value most nearly representative of the locations of the several lowest frequencies of the structure with reference to the response spectrum, as for the single degree of freedom considered in Section V-4.5.3. That is, use $1/\mu$ for the extreme left-hand side, or for low frequencies; $1/\sqrt{2\mu - 1}$ for intermediate frequencies; and 1 for high frequencies.

4. For displacements or strains, the factors used should be those in step 3 multiplied by μ, or respectively 1, $\mu/\sqrt{2\mu - 1}$, and μ.

REFERENCES

V-5.1 Karman and Biot, Mathematical Methods in Engineering, New York: McGraw-Hill Book Co., Inc., 1940.

V-5.2 Ritz, Gesammelte Werke, Paris, 1911.

V-5.3 Stodola, Dampf-und Gasturbinen, 6th ed., Berlin: Springer, 1924.

V-5.4 Newmark, Numerical Procedure for Computing Deflections, Moments and Buckling Loads, Trans., ASCE, 108, 1943.

V-5.5 Blume, Newmark, and Corning, Design of Multistory Reinforced Concrete Buildings for Earthquake Motions, Chicago, Portland Cement Association, 1961.

V-5.6 Crossley, Systems of Several Degrees of Freedom, Chapter 57, Handbook of Engineering Mechanics, edited by W. Flügge, New York: McGraw-Hill Book Co., Inc., 1962.

V-5.7 O'Hara and Cunniff, Elements of Normal Mode Theory, U. S. Naval Research Laboratory, Washington, D. C., NRL Report 6002, November 15, 1963.

V-5.8 Blake, Basic Vibration Theory, Chapter 2, Vol. 1, Shock and Vibration Handbook, edited by C. M. Harris and C. E. Crede, New York: McGraw-Hill Book Co., Inc., 1961.

V-5.9 Norris, et al, Structural Design for Dynamic Loads, Chapter 4, New York: McGraw-Hill Book Co., Inc., 1959.

V-5.10 Housner, Vibration of Structures Induced by Seismic Waves, Part I, Earthquakes, Chapter 50, Volume 3, Shock & Vibration Handbook, edited by C. M. Harris and C. E. Crede, New York: McGraw-Hill Book Co., Inc., 1961.

V-5.11 Crandall and McCalley, Numerical Methods of Analysis, Chapter 28, Vol. 2, Shock and Vibration Handbook, edited by C. M. Harris and C. E. Crede, New York: McGraw-Hill Book Co., Inc., 1961.

V-5.12 Holzer, Die Berechnung der Drehschwingungen, Berlin: Springer, 1921.

V-5.13 Salvadori and Baron, Numerical Methods in Engineering, New York: Prentice-Hall, Inc., 1952.

V-5.14 Lagrange, Mechanique Analytique, Paris, 1788.

V-5.15 Goodman, Rosenblueth, and Newmark, Aseismic Design of Firmly Founded Structures, Trans. ASCE, 117, 1952.

CHAPTER V-6

STRUCTURAL BEHAVIOR—EQUATIONS FOR DESIGN

Although some equations useful in the design of certain structural elements are presented in this chapter, the presentation here is neither a specification nor a design handbook; rather it is a summary of the basis for equations which have become more or less generally used in the field. Detailed specifications for steel structures are presented in Ref. V-6.1, and for reinforced concrete structures in Ref. V-6.2. Concepts of structural design are presented in many texts such as Ref. V-6.3 for steel and Ref. V-6.4 for reinforced concrete.

Because the properties of most steel sections commonly used are summarized in Ref. V-6.1, the emphasis in this chapter will be on structural elements of reinforced concrete. However, many of the general concepts applicable to the behavior of reinforced concrete are equally applicable to the behavior of comparable sections fabricated of steel and of prestressed concrete. The latter type of structure generally has not been considered suitable for use in protective structures mainly because of the widely held suspicion that its small resistance to rebound, primarily, and its reduced ductility, secondarily, placed it at a distinct disadvantage compared with conventional reinforced concrete. Recent data (Ref. V-6.5) indicate that reservations concerning reduced resistance to rebound may not be significant for loads with relatively long duration. Nevertheless it is likely that more studies of the behavior of prestressed concrete will be required before it is widely considered for use in protective construction.

The expressions and concepts developed subsequently are used as the basis for the analysis of several common structural configurations in the charts presented in Refs. V.1 and V-6.6. Since these references give methods for quickly evaluating the behavior or vulnerability of structures and structural components, the reader may find them useful for making a trial design or a rapid evaluation of a completed design. Each of these references is voluminous; thus it is impractical to attempt to make a detailed summary of their contents here.

V-6.1 RESISTANCE FUNCTIONS

The resistance of a given structural element is most usefully characterized as a resistance-deflection diagram. Normally two values of resistance are important: (1) The effective yield resistance where the general yielding of a member or of a material takes place, and the member begins to show an increase in deflection with little or no accompanying increase in resistance; and (2) the ultimate resistance which is the maximum resistance developed before failure of the member is imminent. For statically determinate structures, the effective yield resistance develops when the material in the element begins to yield generally at a single point or isolated region; in statically indeterminate structures, on the other hand, the effective yield resistance develops when the material in the element yields generally at single points or isolated regions, the number of which is one more than the degree of indeterminacy; i.e., the element becomes a mechanism or deforms without limit for an infinitesimal increase in load. The formation of a mechanism in a statically indeterminate structure must be taken into account or the effective yield resistance will normally be grossly underestimated.

V-6.1.1 Flexure Alone

Beams and One-Way Slabs (Concrete). An under-reinforced concrete beam* will begin to yield generally at an isolated region when the steel reinforcement acting in tension reaches its yield point. Test results (Ref. V-6.7, for example) indicate that the "classical" straight-line theory provides a realistic basis for estimating the strength when the steel first begins to yield. This doubtless is a result of the stress distribution in the concrete in compression remaining nearly linear for the strains associated with initial yielding of the tensile reinforcement. The same tests indicate that adding compressive reinforcement without making a corresponding addition of tensile reinforcement does not change the resistance, a fact attributable to the change in internal forces caused by the addition of the compression reinforcement (with a corresponding decrease in volume of concrete) being comparable to the inaccuracies in the knowledge of the properties of the materials. The straight-line approximation applied to rectangular cross-sections (Fig. V-6.1) results in

$$M_y = f_y\, pjbd^2 = f_y A_s jd \qquad \text{(V-6.1)}$$

*An under-reinforced beam (ultimate strength concept of behavior) is one in which the amount of tensile reinforcement is such as to result in yielding of the steel before crushing of the concrete occurs.

where

M_y = bending (or resisting) moment at general yielding

f_y = yield stress for tensile reinforcement

p = tensile reinforcing ratio = $\frac{A_s}{bd}$

j = dimensionless parameter defining the distance between the centroid of the internal compressive and tensile forces; i.e., the internal moment arm divided by the effective depth.

b = width of member or of compression flange

d = effective depth of member which is the distance from the surface of the member subjected to the largest compressive strain to the centroid of the tensile reinforcement (see Fig. V-6.1).

A_s = cross sectional area of tensile reinforcement

In the preparation of Ref. V-1.36 the value of j was formally evaluated for variations in parameters normally encountered in construction, and it was shown that Eq. V-6.1 can be approximated to within ±5%, for values of p between 0.003 to 0.02, by

$$M_y = 0.9\, pf_y\, bd^2 \qquad \text{(V-6.2)}$$

Furthermore, Eq. V-6.2 is valid for one-way slabs, plates in which the reinforcement (excluding temperature reinforcement) is placed in only one direction, and approximately for T-sections (Fig. V-6.1).

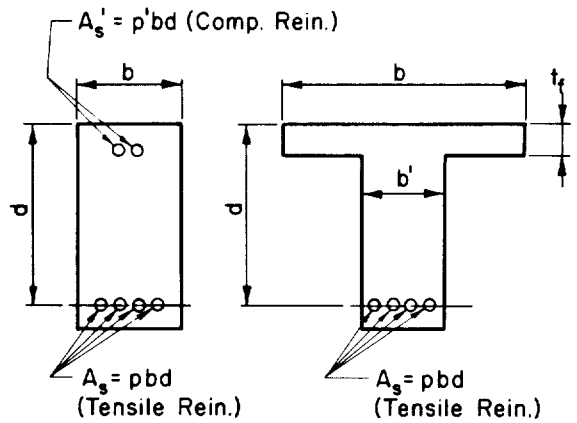

(a) Rectangular (b) T-Section

FIG. V-6.1 COMMON SHAPES OF CROSS SECTION FOR ISOLATED REINFORCED CONCRETE BEAMS

The ultimate resisting moment of an under-reinforced beam or one-way slab develops when (Ref. V-6.4)

$$M_u = f_y pbd^2 \left(1 - 0.6\frac{pf_y}{f'_c}\right) = f_y A_s d \left(1 - 0.6\frac{pf_y}{f'_c}\right) \qquad \text{(V-6.3)}$$

where

M_u = bending (or resisting) moment at ultimate conditions.

f'_c = ultimate strength of concrete.

Formal evaluation of this expression leads to an approximation which is identical to Eq. V-6.2; i.e., the ultimate resisting moment is equal to the resisting moment at general yielding in under-reinforced beams or slabs. That this equality should exist is easily explained: For an under-reinforced beam in which the possibility of strain hardening of the reinforcement is neglected, the internal forces do not change as deformations in excess of those existing when general yielding develops; thus any change in resistance must result from a change in internal moment arm $\left(j \text{ as compared to } \left(1 - 0.6\frac{pf_y}{f'_c}\right)\right)$, and this change must be small.

Since the internal resistance does not change with deflections in excess of those corresponding to yielding, the effective yield resistance of a statically indeterminate beam (one continuous over several supports or one fixed against rotation at either or both supports) subjected to a uniformly distributed loading can be directly evaluated. For a given beam, f_y, b, and d are constant; thus the yield moment M_y at any point is directly proportional to the reinforcing ratio p at the same point. If p_1 is the tensile reinforcing ratio at one support, p_2 is the tensile reinforcing ratio at another support and p_c is the tensile reinforcing ratio at (or near)* mid-span, the uniformly distributed load per unit of length bR_y acting on the beam which produces general yielding is

$$bR_y = 7.2\, f_y b \left(\frac{d}{L}\right)^2 \left[p_c + \frac{1}{2}(p_1 + p_2)\right] \qquad \text{(V-6.4)}$$

or

$$R_y = 7.2\, f_y \left(\frac{d}{L}\right)^2 \left[p_c + \frac{1}{2}(p_1 + p_2)\right]$$

since for static equilibrium the maximum change in moment along the beam must equal $\frac{R_y L^2}{8}$ where L is the span of the member.

*For a beam fixed against rotation at one support and simply supported at the other end, the maximum positive moment does not occur at mid-span. However, the error associated with assuming a maximum at mid-span is less than 3%.

Equation V-6.4 is valid for isolated rectangular beams or for one-way slabs. Because concrete is assumed to carry no tension, a T-section is effectively a rectangular section near the supports. Consequently, the comparable expression for T-sections, for which the effective width of the member over the support is* b' rather than b (See Fig. V-6.1), becomes

$$bR_y = 7.2\, f_y b \left(\frac{d}{L}\right)^2 \left[p_c + \frac{b'}{2b}\,(p_1 + p_2)\right]$$

$$\text{or}\quad R_y = 7.2\, f_y \left(\frac{d}{L}\right)^2 \left[p_c + \frac{b'}{2b}\,(p_1 + p_2)\right] \qquad \text{(V-6.5)}$$

Minimum Amount of Reinforcement. In presenting Eq. V-6.2 above, it was noted that the accuracy of the approximation was evaluated for a specific range of values of reinforcing ratio p. In general, any value of reinforcing ratio would be acceptable between the limits given. However, one must be careful to insure that he inadvertently does not limit the ductility of the member by using a value of p which is too small. In this regard we recall that the resistance deflection diagram obtained in a conventional static test (wherein deformation rather than load is applied to the member) of a beam with very small amounts of tensile reinforcement, the load corresponding to initial cracking of the concrete in tension may exceed the ultimate capacity of the member (Fig. V-6.2). For this type of resistance diagram, a step-pulse loading of infinite duration with magnitude P_m just slightly larger than $R_y/2$† would cause the member to collapse. On the other hand a magnitude of force P_m slightly less than $R_y/2$ would not crack the member.

Although there are important questions relating to the possibility of having a totally uncracked beam since shrinkage and temperature stresses may cause cracking, the situation just described could result in disastrous failures both for static and dynamic loads. Thus, it is important to insure that the ultimate resistance of the member is at least equal to the cracking resistance. Such insurance is provided by finding that minimum value of reinforcing ratio p_{min} which causes the ultimate resistance R_u to equal the cracking resistance R_c. Alternatively since R_c and R_u are directly proportional to M_c and M_u, the corresponding moments respectively, these moments can be equated. The cracking moment M_c can be approximated very closely by:

$$M_c = f_r \frac{I_g}{c}$$

where

f_r = modulus of rupture of concrete

I_g = gross moment of inertia of the section neglecting the presence of the reinforcement

c = half the total depth of the member (or the distance from the neutral axis to the "extreme fiber")

Thus from Eq. V-6.2:

$$0.9\, p_{min}\, f_y b d^2 \cong f_r \frac{I_g}{c} = f_r \frac{bh^2}{6}$$

and (V-6.6)

$$p_{min} = \frac{1}{5.4}\,\frac{f_r}{f_y}\left(\frac{h}{d}\right)^2 \cong 0.2\,\frac{f_r}{f_y}$$

since the ratio of h^2 to d^2 is nearly unity. For normal values of f_r and f_y, p_{min} is in the range from 0.002 to 0.003.

Maximum Amount of Reinforcement. At the other extreme, there is so much tensile reinforcement that crushing of the concrete occurs before the reinforcement yields.* Normally this is not a problem since it is uneconomical, and frequently impossible, to place such an amount of reinforcement in the beam. However, for unusually high yield strengths of the reinforcement, crushing of the concrete can precede yielding of the reinforcement. This phenomenon has long been recognized, and the limiting value is defined by Eq. 16.2 of Ref. V-6.2. In general the expression is

$$p_{max} \cong 0.7\,\frac{f'_c}{f_y}\cdot\frac{\epsilon_u}{\epsilon_u + \epsilon_y} \qquad \text{(V-6.7)}$$

where

p_{max} = maximum reinforcing ratio or the "balanced reinforcing ratio" in ultimate strength concepts.

ϵ_u = maximum compressive strain at which crushing of the concrete begins.

ϵ_y = strain in reinforcement corresponding to initial yielding.

*Note that b' is the width of the so-called compression flange at the supports and conventionally p_1 and p_2 would be defined as $A_{s1}/b'd$ and $A_{s2}/b'd$ respectively. If instead p_1 and p_2 are defined as A_{s1}/bd and A_{s2}/bd (unconventional), Eq. V-6.4 would be valid directly for T-sections, provided that R_y is interpreted correctly.

†The precise magnitude of P_m depends upon the area under the actual resistance curve to the ultimate deflection y_y, cf. Eq. V-4.38.

*Such a condition is referred to as an over-reinforced beam.

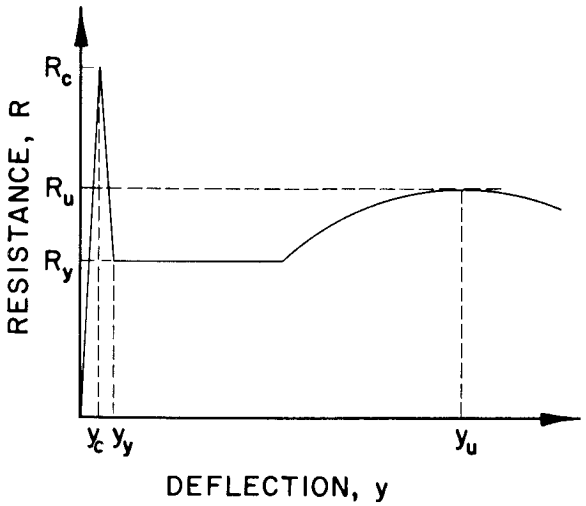

FIG. V-6.2 RESISTANCE-DEFLECTION DIAGRAM FOR A GROSSLY UNDER-REINFORCED BEAM

The comparable expression in Ref. V-6.2 results from setting ϵ_u = 0.003 in./in., $\epsilon_y = f_y/29{,}000$ ksi,* and the coefficient (0.7) as a function of f'_c. Equation V-6.7, above has the advantage of being applicable for any value of ϵ_u, and for deep beams the maximum strain at crushing ϵ_u might be as high as 0.006 to 0.008 in./in. (Ref. V-6.8).

Two-Way Slabs (Concrete). A two-way slab is a term used to describe a flat rectangular plate of reinforced concrete which is supported at its perimeter by beams. The beams supporting the slab are proportioned by methods given above taking cognizance of the distribution of loading from the adjacent slab or slabs (Ref. V-6.9). Although it is possible to estimate the resistance of a given slab well, once its dimensions and reinforcing details are known (Ref. V-6.10), it is sufficiently accurate in most cases to take a standardized approximate pattern of the "yield lines" as shown in Fig. V-6.3. The "yield lines", corresponding to the lines of cracking in Fig. V-6.3, are the isolated regions at which general yielding occurs to reduce the slab to a mechanism. It is shown (Ref. V-6.9) that the approximate resistance of a two-way slab is equal numerically to the product of the following factor β and the resistance of a one-way slab, as given by Eq. V-6.4, with a span L_s equal to the shorter span of the two-way slab.

$$\beta = 1 + \alpha\left[\frac{1}{6 - 4\alpha} + \frac{3}{2}\left(\frac{p_{Lc} + p_{Le}}{p_{sc} + p_{se}}\right)\right] \quad \text{(V-6.8)}$$

*ksi = kilopound (or kip)/in^2.

where

α = ratio of shorter span L_s to longer span L_L of the slab, the aspect ratio

p = reinforcing ratio with the first subscript (s or L) denoting whether the steel is parallel to the shorter (s) or longer (L) edge and the second subscript denoting the location in the slab (c for near mid-span and e for near the edge).

V-6.1.2 Flexure and Shear in Combination

Normally a structural member is not subjected to flexure (or bending) alone; flexure usually is produced by loads applied to the surface of the member, and these loads produce shear, acting in combination with flexure. Unfortunately, no completely rational explanation exists of the behavior of reinforced concrete subjected to this combination although a recent approach (Ref. V-6.11)* appears more promising than earlier ones. Because of the absence of theory, there are numerous empirical equations which define the behavior of particular structural configurations. A sufficient number of structural types have been tested to provide enough confidence in the empirical approaches for them to be used. Nevertheless, it is likely that factors of safety different from the intended ones exist in these empirical approaches since they probably do not provide a correct appraisal of behavior for all possible configurations.

The fundamental basis of the equations in Ref. V-6.2 attempts to prevent diagonal cracking of concrete members, which is a manifestation of distress under combined flexure and shear, or if such cracks occur, to prevent them from opening when the member is subjected to its design load. For the general purpose of this code, this is a sound basis since the structure, normally designed under this

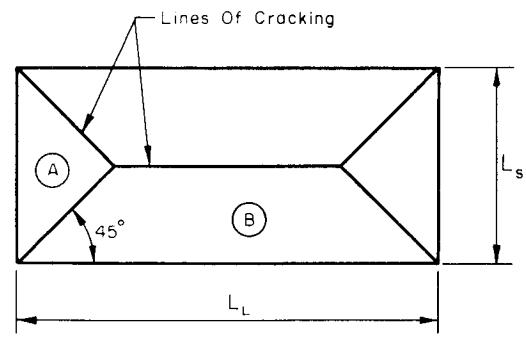

FIG. V-6.3 ASSUMED CRACK PATTERN FOR TWO-WAY SLABS

*It should be noted that the study in Ref. V-6.11 at the moment is more qualitative than quantitative, but the qualitative conclusions are consistent with the observed behavior.

code, may, during its lifetime, be loaded to the vicinity of design capacity many times; if cracks develop, there immediately exists an aesthetic problem which may also have psychological ramifications, and over a period of time a structural problem can develop from corrosion of the reinforcement. In a protective structure, the design load may never be realized, but if it is there is a low probability that the full design load will be applied several times. Furthermore for a protective structure the loads associated with the daily use of the structure are normally a small fraction of the design load. These observations indicate that a basis for design requiring that no diagonal cracks develop may be entirely too conservative. In many cases, reinforced concrete members possess a significant reserve in strength after a diagonal crack is formed. Except in those rare instances where the loads imposed by daily use of a protective structure are comparable to the design loads, it is desirable to take advantage of this reserve in strength.

In Ref. V-1.36 empirical equations are derived which appear to estimate realistically the resistance of members failing under the action of combined shear and flexure. The basic premise underlying this derivation involves an assumption wherein the concrete fails in compression at a limiting (fixed) value of strain or at a limiting (variable) value of bending moment. An expression is derived for this moment as a complicated function of the strength of the concrete and the properties of the cross section. Subsequently this expression was modified by finding an equivalent approximate expression, and this expression can be stated (Ref. V-6.9) in the following form.

$$bR_{ys} = 1000 \text{ psi } b\left(1 + \frac{3}{2}\frac{p_a}{p_c}\right)\left(\frac{1}{2+\varphi}\right)\sqrt{p_c f'_c}\left(1 + \frac{2 p_v f_y}{10^3 \text{ psi}}\right)\left(\frac{d}{L}\right)^2$$

or (V-6.9)

$$R_{ys} = 1000 \text{ psi}\left(1 + \frac{3}{2}\frac{p_a}{p_c}\right)\left(\frac{1}{2+\varphi}\right)\sqrt{p_c f'_c}\left(1 + \frac{2p_v f_y}{10^3 \text{ psi}}\right)\left(\frac{d}{L}\right)^2$$

where

R_{ys} = resistance at general yielding and at ultimate conditions for a beam subjected to combined shear and flexure.

p_a = average value of tensile reinforcing ratio over the supports.

p_v = volumetric reinforcing ratio of web reinforcement (vertical stirrups).*

f'_c = cylinder strength of concrete, in psi.

*Because the possibility of rebound is always present, only vertical stirrups are effective in elements of protective structures.

Use of an argument similar to that presented in the discussion associated with Eq. V-6.6 leads to a minimum value for p_v of 0.005 which must be used if the web reinforcement is to be effective.

From comparison of Eqs. V-6.4 and V-6.9 it is apparent that values R_y and R_{ys} can be coincident for certain combinations of the variables. When R_{ys} exceeds R_y the member will fail in flexure; when the converse is true the mode of failure is not clear. However, in the studies made in preparing Refs. V-1.36 and V-6.2, it became apparent that failure will occur by flexure if the required resistance, for a given depth d and span L, is less than that defined by Eq. V-6.10. If the required resistance exceeds the value given by Eq. V-6.10, failure is defined by the lesser of the two values, R_y or R_{ys}.

$$\frac{V_{max}}{bd} = \sqrt{2\ f'_c} \qquad \text{(V-6.10)}$$

where*

V_{max} is maximum shear in member, which is directly proportional to the load R_y on the member.

f'_c is in psi

Another mode of failure may theoretically occur when a member is subjected to flexure and shear in combination. This has been referred to as pure shear, and it is characterized by a nearly vertical cleavage (as distinguished from diagonal cracking) at the face of the support. Definition of the resistance associated with this type of failure (Ref. V-1.36) has utilized the value of the intercept on the shear axis of the Mohr envelope of rupture for plain concrete. This intercept (Ref. V-6.4) ranges from 0.2 f'_c to 0.6 f'_c. Use of the lower value and the internal forces in the beam leads to

$$\frac{V_{max}}{bd} = 0.2\ f'_c \qquad \text{(V-6.11)}$$

Resistance to pure shear can be enhanced by providing inclined bars near the support. No tests of this system have been made, and the evaluation of resistance has been made heuristically (Ref. V.1 and V-6.9). The approach involves defining a critical section which is taken as d/2 or 0.1 L, whichever is smaller, from the face of the support. The shear at this critical section is then distributed equally (arbitrary) to the concrete and the inclined steel.

*Conventionally a numerical factor 7/8 (or j) would appear in the denominator on the left side of this equality. However, the experimental variation of the coefficient makes inclusion of this factor academic.

V-6.1.3 Axial Load Alone

The resistance at general yielding and at ultimate conditions for reinforced concrete columns is defined in Ref. V-6.2; however, the specific procedures applicable are not explicit therein. Therefore, it is of value to review and to summarize the conclusions of Ref. V-6.12.

General yielding of either a short tied or a short spiral column occurs when the axial load reaches the value N_y*

$$N_y = 0.85 f'_c (A_g - A_{st}) + f_y A_{st}$$

Since A_{st}, the total cross sectional area of longitudinal steel, is small compared to A_g, the gross cross sectional area of the column, it normally is sufficiently accurate to use

$$N_y \cong A_g (0.85 f'_c + f_y p_g) \qquad \text{(V-6.12)}$$

where

$$p_g = \text{gross reinforcing ratio} = \frac{A_{st}}{A_g}.$$

The ultimate capacity of a tied column occurs at the same load and nearly at the same deflection as that corresponding to general yielding. On the other hand a spiral column possesses more ductility than a tied column, and the ultimate load depends upon the volumetric spiral reinforcing ratio p_s. The ultimate load can be defined explicitly (Ref. V-6.12), but it has become common practice to provide a sufficient quantity of spiral (actually helical) reinforcement to make the ultimate load equal to the yield load. This quantity of spiral reinforcement is obtained by equating the ultimate capacity† to the capacity at general yielding which yields (by rounding the coefficient slightly upward)

$$p_s \geq 0.45 \frac{f'_c}{f'_s} \left(\frac{A_g}{A_c} - 1 \right) \qquad \text{(V-6.13)}$$

where

f'_s = yield strength of spiral reinforcement

A_c = core area of column = cross sectional area enclosed within the spiral.

Equation V-6.13 is identical to Eq. 9.1 of Ref. V-6.2.

*Defined by equating the contribution of force from each of the component materials to the load. A short column is one which is assumed to be unaffected by buckling.

†The ultimate capacity as in the case of the yield capacity is determined by equating the contributions to the force of each of the component materials to the applied load; i.e.,

$$N_u = 0.85 f'_c (A_c - A_{st}) + f_y A_{st} + 2 f'_s p' A_c$$

In most cases of interest here buckling is considered to be unimportant for a ratio of unsupported height h to least lateral dimension d_m of approximately 15 (cf. Section 916, Ref. V-6.2). The strength is degraded linearly to zero for values h/d_m of approximately 50. This provision of the code appears to have no really rational basis except for the important rationale associated with the successful performance of thousands of columns proportioned on this basis. A study of long columns has been made (Ref. V-6.13).

Recent studies (Ref. V-6.14) indicate that under dynamic loads, buckling might be inhibited or even precluded. This probably is a result mainly of the finite time required for deflections associated with buckling to occur. However, until more information on this subject is gained, it is probably unwise to ignore the possibility of buckling.

V-6.1.4 Flexure and Axial Load in Combination

Many of the components of a structure are subjected simultaneously to bending and axial force. The behavior of such members is concisely described by an interaction diagram (Fig. V-6.4). The coordinate axes and any curve $\left(\text{parametric in } \frac{pf_y}{f'_c}\right)$ define a region which will sustain the combined loads without failure. Each parametric curve defines the limiting combinations which will cause failure to be imminent. A group of interaction diagrams are presented for many variations in reinforced concrete columns in Ref. V-6.15. Figure V-6.4 provides a summary of these diagrams for rectangular tied columns with equal amounts of longitudinal reinforcement on each face and with a ratio of effective depth h to total depth D of 0.9. The procedure used to establish the diagrams (Fig. V-6.4) consists of: (1) Assuming successive particular values for the strain in the longitudinal reinforcement on one face of the member*; (2) using the Stüssi or Whitney theories (Ref. V-6.4) which are basically equivalent to find the internal forces consistent with each particular value of strain assumed in (1); (3) applying the conditions of equilibrium to find the axial force and moment consistent with the internal forces computed in (2); (4) plotting the resulting values on the diagram; and (5) normalizing the completed diagram by dividing the ordinate scale by the appropriate axial load acting alone (Eq. V-6.11) and the abscissa scale by the appropriate moment acting alone (Eq. V-6.2). For a given cross section each diagram can be defined by a set of equations (cf. Section 1902, Ref. V-6.2). However, the procedure described above has the distinct advantage that the process is self checking; if an error is made, the value in error will be obvious since it will not fall on a smooth curve. Further the process is not as tedious as one might suppose since only three

* The strain distribution through the depth of the section is assumed to be linear.

or four points need be computed: The interaction diagram is so nearly a straight line that it is assumed to be straight between the intercept on the ordinate and the so-called "balance point";* the curve between the balance point and the intercept on the abscissa is nearly a parabola with approximately a vertical tangent at the "balance point."

Two points of major importance should be made regarding the interaction diagrams for under-reinforced members: (1) Any radial line, passing through the origin, has a slope consistent with the reciprocal of eccentricity of a force applied parallel to but at a distance e (eccentricity) from the gravity axis (Fig. V-6.5); and (2) for an under-reinforced member, the addition of an axial load can significantly increase the moment capacity. The latter is a result of the decrease in internal tensile force in the reinforcement attending the application of an external compressive force to a member subjected initially to bending alone. Such increases in resistance do not occur in symmetrical members fabricated of a single material (such as a steel beam) since the material on both surfaces of such a member is imminently failing under the action of moment alone.

V-6.2 DEFLECTIONS

To complete the definition of approximate resistance functions it is necessary to obtain expressions for the deflection at general yielding and at ultimate conditions.

V-6.2.1 Deflections at General Yielding Beams and Slabs.

If it is noted that Eq. V-6.1 is identically equivalent to the familiar flexure formula, $M = f\frac{I_c}{c}$,** it is easily shown that the deflection at the center y_b of a simply-supported beam is given by

$$y_b = \frac{5M\,L^2}{48EI_c} = \frac{5fL^2}{48Ec} \qquad \text{(V-6.14)}$$

where

- M = bending moment at mid-span
- L = span
- E_c = modulus of elasticity of the material
- c = distance from the gravity axis to the extreme "fiber" of the member

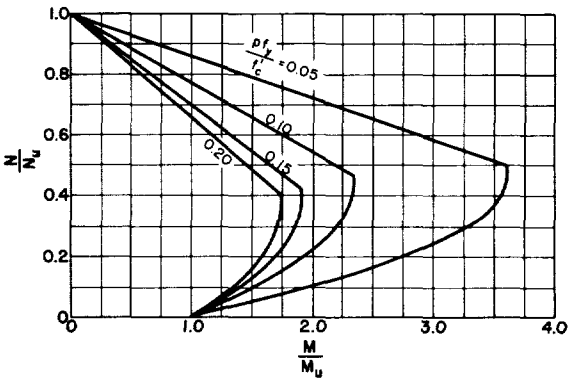

FIG. V-6.4 INTERACTION DIAGRAM FOR REINFORCED CONCRETE BEAM-COLUMNS

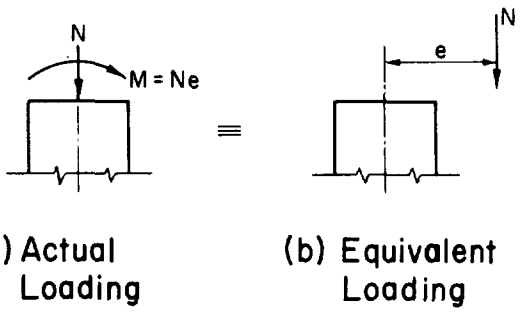

FIG. V-6.5 DEFINITION OF ECCENTRICITY OF NORMAL LOADING ON COLUMN

Interpreted in terms of the stress in the tensile reinforcement, the deflection at yielding y'_y is given by the following since $f_y/E = \epsilon_y$ by definition.

$$y'_y = \frac{5\,\epsilon_y L^2}{48c}$$

For normal variations in the properties of the materials, c, which identically equals (1-k), is very nearly equal to 5/8 d where d is the effective depth of the member. Thus,

$$y'_y \cong \frac{\epsilon_y L^2}{6d}$$

or alternatively, to avoid confusion in units

$$\frac{y'_y}{L} = \frac{\epsilon_y}{6} \cdot \frac{L}{d} \qquad \text{(V-6.15)}$$

Since for most reinforcing steels currently in use ϵ_y averages approximately 0.0015 in/in., Eq. V-6.15 can be written as

$$\frac{y'_y}{L} \cong \frac{L}{4000\,d} \qquad \text{(V-6.15')}$$

* That combination of axial load and moment which causes the concrete to crush and the "tensile" reinforcement to begin to yield simultaneously.

** I_c is the moment of inertia of the so-called "transformed section."

Study of the data on simply-supported members failing under the action of combined flexure and shear (For example, Ref. V-3.5) indicates that Eq. V-6.15 also is valid for such cases.

Equation V-6.15 used in conjunction with the basis for Eq. V-6.4 allows the definition of the effective deflection at yielding for beams with other support conditions. The "effective yield deflection" is used to reduce the rather complex resistance function to an effective elasto-plastic one, and this deflection is defined as that which causes the area under the effective resistance curve to equal the area under the actual curve approximately. For example in Fig. V-6.6, the area $\frac{1}{2} R_y y_y$ is set equal to the area $\frac{1}{2}\left[R_1 y_2 + R_y (y_2 - y_1)\right]$. If the curve in Fig. V-6.6 represents the conditions associated with a uniformly distributed loading on a beam fixed at both ends, the resistance R_1 and associated deflection y_1 represent yielding of the member at the supports; the deflection R_y and associated deflection y_2 represent yielding at mid-span. The actual initial stiffness of such a beam is one-fifth* of that of an equivalent simply supported beam as defined by Eq. V-6.15. The incremental stiffness between y_1 and y_2 is the same as that for the equivalent simply supported beam. Use of these values of stiffness and the value of resistance for the points where yielding occurs as defined by Eq. V-6.2 defines the following corrections, for the conditions of support indicated, to be applied to Eqs. V-6.15 or V-6.15':

$$y_y = \frac{y_y'}{4} \cdot \frac{5 - 2\theta + 2\theta^2}{1 + \theta}$$ for equal restraint at supports (V-6.16)

$$y_y = \frac{y_y'}{2} \cdot \frac{5 - \theta + \theta^2}{2 + \theta}$$ for partial restraint at one support and pinned at other support

where

θ = ratio of tensile reinforcing ratio at the supports to that at mid-span

The effective yield deflection for two-way slabs is not at this time well-documented by either theory or experiment. It is apparent that this deflection must be smaller than the similar deflection of a one-way slab with the same dimensions and reinforcement. In the absence of more definitive data, an approximation to the effective yield deflection can be obtained by dividing the effective yield resistance as defined by Eq. V-6.8 by the appropriate stiffness given in Table V-6.1. The data in this table are computed from information contained in Ref. V-6.16 for elastic plates on rigid supports.

*The deflection of a beam fixed at both ends is $y_y = \frac{ML^2}{48\,EI_c}$ which should be compared with Eq. V-6.14.

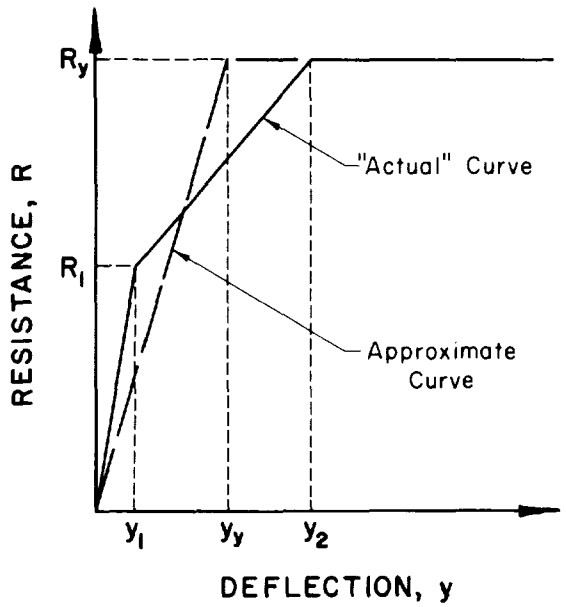

FIG. V-6.6 "ACTUAL" AND EQUIVALENT RESISTANCE FUNCTIONS FOR A STATICALLY INDETERMINATE BEAM

Columns. Because the strain* corresponding to initial crushing of concrete subjected to axial load alone is nearly coincident with the strain corresponding to initial yielding of the longitudinal reinforcement, general yielding of a reinforced-concrete column (or a steel column) occurs approximately when the strain in the steel reaches its yield value ϵ_y. Thus the yield deflection y_{ya} is

$$y_{ya} = \epsilon_y L_a$$ (V-6.17)

or alternatively to avoid confusion of units

$$\frac{y_{ya}}{L_a} = \epsilon_y$$

where

y_{ya} = effective yield deflection of column

L_a = total length of column

Since the concentric application of a normal force to a member subjected already to bending, does not theoretically alter the angle change (curvature), the effective yield deflection for members subjected to axial load and bending in combination is the same as that for the member with no axial load applied. Consequently, for these conditions of loading the effective yield deflection is defined by Eqs. V-6.15 or V-6.16.

*Experimental values range from 0.0015 to 0.0020 in/in. (Ref. V-6.4)

TABLE V-6.1 — STIFFNESS OF ELASTIC PLATES ON RIGID SUPPORTS

Ratio: Short to Long Span ($\alpha = \frac{L_S}{L_L}$)	Stiffness Expressed as Coefficient of $\frac{E_c \bar{I}^*}{(L_S)^3 L_L}$	
	Simple Supports	Fixed Supports
1.0	252	810
0.9	230	742
0.8	212	705
0.7	201	692
0.6	197	724
0.5	201	806

* $\bar{I}$ is defined as the average for the uncracked and transformed sections which is used in an attempt to approximate the true stiffness (Ref. V-6.9).

V-6.2.2 Approximation for Maximum Ductility Factors Flexure Failures (Concrete)

Although methods exist (Ref. V-6.7) for calculating the deflection associated with the ultimate strength, these procedures are at best approximate; this occurs because the load-deflection curve, obtained in a static test of an under-reinforced beam, exhibits little curvature in the range approaching failure. More meaningful values are obtained directly from the experimental results. Because, as shown in Chapter V-4, the resistance of a member loaded dynamically can be defined by the ratio (the ductility ratio μ) of the maximum displacement y_m to the yield displacement y_y, it is convenient to evaluate the experimental results in terms of the ductility ratio.

Figure V-6.7 portrays the maximum value of the ductility ratio obtained in static tests of beams failing in flexure, as distinguished from diagonal tension, pure shear, or bond, (Refs. V-6.7 and V-6.17 to V-6.19). The maximum value of the ductility ratio is defined as the ratio of the maximum deflection observed prior to imminent collapse of the member and the observed deflection at yielding; thus, the values shown are the maximum values of ductility which can be used in design. All members except two* with a single load at mid-span actually had this load applied through a stub column, an arrangement simulating the two beams framing into a column in an actual structure. Although the results from tests on this type of specimen appear to indicate larger ductilities generally then the results from simple beams with equal loads applied at the third-points (Fig. V-6.7), the number of tests are too limited to draw a definite conclusion. Also as indicated in the legend, several of the beams were subjected to flexure and axial load in combination.

From the data presented (no other data could be located with all the needed deflection information), the following purely empirical expression is suggested to define the maximum ductility factor μ_m.

$$\mu_m = \frac{1}{10\,(p - p')} \leq 20 \qquad \text{(V-6.18)}$$

where

p = tensile reinforcing ratio at mid-span

p' = compressive reinforcing ratio at mid-span, but not to be taken as greater than p in the equation.

In many cases it is desirable to proportion protective structures such that collapse is imminent under the design loading; therefore, use of the value μ_m should be considered in applying the methods given in Chapter V-4 to concrete members failing in flexure.

*The results from these two tests cannot be distinguished from the results of the tests of the similar members loaded through the stub column.

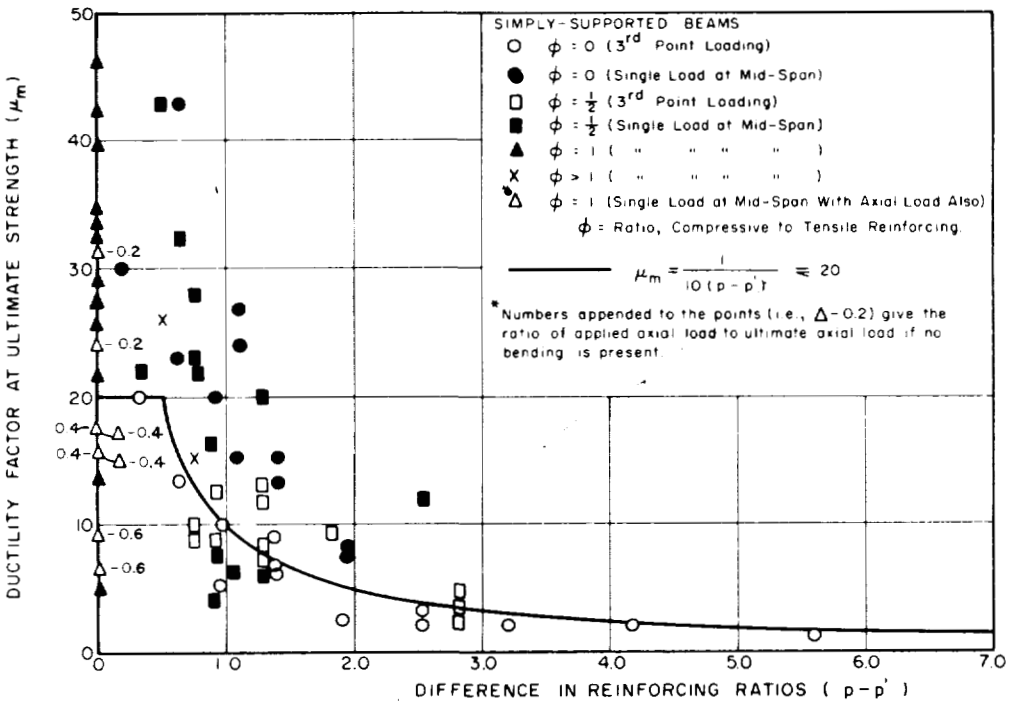

FIG. V-6.7 DUCTILITY FACTOR AT ULTIMATE STRENGTH OF REINFORCED-CONCRETE BEAMS

Concrete Failing by Combined Flexure and Shear or by Axial Load. Failure is relatively brittle when it is produced by either of these types of loading in a mode associated with crushing of the concrete prior to or simultaneously with yielding of the tensile reinforcement. It must be emphasized that failure caused by combined flexure and shear is ductile and defined by Eq. V-6.18 if the resistance is defined by Eq. V-6.4; the failure is relatively brittle if the resistance is defined by Eqs. V-6.9 and V-6.10.

Data from tests of beams failing in a shearing mode (Ref. V-3.5, for example) indicate that there is no apparent correlation between the properties of the member and the maximum ductility. It appears safe from the data to assume a maximum ductility ratio of 1.5 to 2.0.

A similar lack of correlation between maximum ductility and properties of the section exists for tied columns. Data in Ref. V-6.12 and associated reports indicate a maximum ductility ratio of approximately 2 can be safely assumed for tied columns. It has long been recognized that spiral columns are much more ductile than tied columns. This ductility is doubtless a function of the ductility of the steel used in the spiral and of the pitch of the spiral. Although one can argue that such a functional relation should exist, the data are too limited to investigate it. Nevertheless, it is clear that spiral columns have a maximum ductility ratio of at least 4.

V-6.3 SYNTHESIS FOR DESIGN

Practically every element encountered in a protective structure is subjected to combinations of forces. As examples consider: (1) A roof or wall slab of a rectangular structure in soil is subjected to lateral load (producing flexure and shear) and to axial load; (2) an arch will be subjected to a hoop compression, of uniform amplitude around the rib, and even if it is fully buried, to local flexures, at least, caused by non-uniformities in backfill or to the transients attending the envelopment of the structure by the stress wave; and (3) a cylindrical structure surrounded with soft packing in rock is subjected to both hoop compression and to bending. The designer must in every case determine the relative magnitudes of each of the forces (moment, axial force, shear, etc.). Thus, all of the preceding material in this chapter for a given structural configuration must be considered. Fortunately, the different forces cause responses of the structure which are in most cases weakly coupled; therefore, they frequently can be treated separately and directly combined in a pseudo-static analysis.

The force to be considered in the trial design is defined normally by Eq. V-4.38.* Use of this equation

*For large yield weapons and the blast forces normally considered in the design of underground structures the duration of loading is usually long compared to the natural period of vibration. Thus, the assumption of a step-pulse of infinite duration is justified.

requires an estimate to be made of only the ductility factor μ. Choice of μ is normally left to the designer's discretion, and larger values should always be considered since they reduce the value of force to be used in the design. The largest value selected, of course, cannot exceed, for each type of loading, μ_m given in the preceding section. Members are designed by the concepts presented in Section V-6.1. With the trial design completed, the resulting structure is analyzed by methods given in Chapters V-4 and V-5.

REFERENCES

V-6.1 American Institute of Steel Construction, Manual of Steel Construction, 6 ed., New York, 1963.

V-6.2 Committee 318, American Concrete Institute, Building Code Requirements for Reinforced Concrete, (ACI 318-63) Detroit, 1963.

V-6.3 Gaylord and Gaylord, Design of Steel Structures, New York: McGraw Hill Book Co., Inc., 1957.

V-6.4 Ferguson, Reinforced Concrete Fundamentals, New York: John Wiley & Sons, Inc., 1958.

V-6.5 Miyamoto and Allgood, Blast Load Tests on Post-Tensioned Concrete Beams, Port Hueneme, USNCEL Report TR 116, DASA-1198, 1961.

V-6.6 Newmark, Hansen and Associates, Vulnerability Handbook for Hardened Installations, Vols. 1 and 2, prepared for Defense Intelligence Agency under Contracts AF 33(657)-10287 and -7472, Urbana, 1963. (S)

V-6.7 Gaston, Siess and Newmark, An Investigation of Load-Deformation Characteristics of Reinforced Concrete Beams up to the Point of Failure, Univ. of Ill., Structural Research Series No. 40, Urbana, 1952.

V-6.8 Untrauer and Siess, Strength and Behavior in Flexure of Deep Reinforced Concrete Beams under Static and Dynamic Loads, Univ. of Ill., Structural Research Series No. 230, Report to AFSWC, Urbana, 1961.

V-6.9 Newmark and Haltiwanger, Air Force Design Manual: Principles and Practices for Design of Hardened Structures, AFSWC-TDR-62-138, Urbana, 1962.

V-6.10 Hognestad, Yield Line Theory for the Ultimate Flexural Strength of Reinforced Concrete Slabs, Journal, ACI, Detroit, 1953.

V-6.11 Krahl, An Analytical Study of the Behavior of Reinforced Concrete Beams without Web Reinforcement Under Combined Shear and Bending Moment, Ph.D. thesis, Department of Civil Engineering, Univ. of Ill., Urbana, 1963.

V-6.12 Richart and Brown, An Investigation of Reinforced Concrete Columns, Eng. Exp. Sta., Univ. of Ill., Bull. 267, Urbana, 1934.

V-6.13 Richart, Draffin, Olson, and Heitman, The Effect of Eccentric Loading, Protective Shells, Slenderness Ratios, and other Variables in Reinforced Concrete Columns, Eng. Exp. Sta., Univ. of Ill., Bull. 368, Urbana, 1948.

V-6.14 Yang and Reinschmidt, The Dynamic Behavior of Reinforced Concrete Columns, Part III, Department of Civil Engineering, MIT, DASA-1333, 1962.

V-6.15 Whitney and Cohen, Guide for Ultimate Strength Design of Reinforced Concrete, Journal, ACI, Detroit, 1956.

V-6.16 Timoshenko, Theory of Plates and Shells, New York: McGraw Hill Book Co., Inc., 1940.

V-6.17 McCollister, Siess and Newmark, Load-Deformation Characteristics of Simulated Beam-Column Connections in Reinforced Concrete, Univ. of Ill., Structural Research Series No. 76, Urbana, 1954.

V-6.18 Burns and Siess, Load-Deformation Characteristics of Beam-Column Connections in Reinforced Concrete, Univ. of Ill., Structural Research Series No. 234, Urbana, 1962.

V-6.19 Yamashiro and Siess, Moment-Rotation Characteristics of Reinforced Concrete Members Subjected to Bending, Shear, and Axial Load, Univ. of Ill., Structural Research Series No. 260, Urbana, 1962.

DISTRIBUTION

	Nr. of Copies
Director of Defense Research & Engineering, Washington, D. C. Attn: Tech. Library	1
Assistant to the Secretary of Defense (Atomic Energy) Washington, D. C. 20330	1
Advanced Research Projects Agency, Attn: T. A. George, Washington, D. C. 20301	1
Institute for Defense Analysis, 1666 Connecticut Ave. N. W., Washington, D. C. For Mr. F. B. Porzel and Dr. Frank Adelman	2
Director, Weapons Systems Evaluation Group, OSD, Room 1E880, The Pentagon, Washington, D. C. 20301	1
Department of Defense, Defense Intelligence Agency (DIAAP-1K2) Washington, D. C. 20301	1
Chief, Defense Atomic Support Agency, Washington, D. C. 20301 Attn: Document Library Attn: Blast & Shock Division	5 10
Commander, Field Command, DASA, Sandia Base, Albuquerque, New Mexico 87115 Attn: FCWT Attn: FCTG	2 1 1
Commander-in-Chief, Pacific, Fleet Post Office, San Francisco, California 94129	1
U. S. Documents Officer, Officer of the United States National Military Representative-SHAPE, APO-55, New York, New York	1
Commandant, National War College, Washington, D. C. Attn: Class Rec. Library	1
Commandant, The Industrial College of the Armed Forces, Ft. McNair, Washington, D. C. 20310	1
Commandant, Armed Forces Staff College, Norfolk 11, Virginia Attn: Library	1
Defense Documentation Center (DDC) Cameron Station, Alexandria, Virginia 22314 Attn: TISIA-21 (No TOP SECRET to this address)	50
Director, Defense Atomic Support Agency, Washington, D. C. 20301 Attn: Security Directorate	5

ARMY

Chief of Research and Development, D/A, Washington, D. C. 20310 Attn: Atomic Division	1
Commanding General, U. S. Army Materiel Command, Washington, D. C. 20310 Attn: AMCRD-DE-N	2
Commanding General, U. S. Continental Army Command, Ft. Monroe, Virginia 23351	1

	Nr. of Copies
Chief of Engineers, D/A, Washington, D. C. 20310	
Attn: ENGCW-NE	1
ENGTE-E	1
ENGMC-E	1
Director, Ohio River Division Laboratories, U. S. Army Engineer Division, Ohio River, 5851 Mariemont Avenue, Cincinnati, Ohio 45201	1
Division Engineer, U. S. Army Corps of Engineers, Missouri River Division, Omaha, Nebraska 68101	1
District Engineer, U. S. Army Engineer District, Omaha, Nebraska	1
Director, Waterways Experiment Station, U. S. Army Corps of Engineers, Vicksburg, Mississippi	
Attn: Library	3
Director, U. S. Army Corps of Engineers, Nuclear Cratering Group, Livermore, California	3
Commanding Officer, U. S. Army Corps of Engineers, Beach Erosion Board, Washington, D. C. 20315	1
Commanding General, The Engineer Center, Ft. Belvoir, Virginia 22060	
Attn: Asst. Commandant, Engineer School	1
Director, U. S. Army Research and Development Laboratory, Ft. Belvoir, Virginia 22060	
Attn: Chief, Tech. Support Branch	1
President, U. S. Army Air Defense Board, Ft. Bliss, Texas 79906	1
Commandant, Command & General Staff College, Ft. Leavenworth, Kansas 66027	
Attn: Archives	1
Commandant, U. S. Army Air Defense School, Ft. Bliss, Texas 79906	1
Director, Special Weapons Development, Hq, CDC, Ft. Bliss, Texas 79906	
Attn: Chester I. Peterson	1
U. S. Army Research Office, Box CM, Duke Station, Durham, North Carolina	
Attn: Mr. Alan Blade	1
Commandant, U. S. Military Academy, West Point, N. Y. 10996	
Attn: USMA Library	2
Commanding General, Aberdeen Proving Ground, Aberdeen, Maryland 21005	
Attn: Director BRL	4
Commanding Officer, U. S. Army Mobility Command, Center Line, Michigan 48015	1
Commanding Officer, Picatinny Arsenal, Dover, New Jersey 07801	
Attn: ORDBB-TK	1
Commanding Officer, Transportation Research Command, Ft. Eustis, Virginia 23604	
Attn: Chief, Tech. Info. Div.	1
Commanding General, U. S. A. Electronic R&D Lab., Ft. Monmouth, New Jersey 07703	
Attn: Technical Documents Center, Evans Area	1

	Nr. of Copies
Commanding General, USA Missile Command, Huntsville, Alabama (For Scientific Information Center)	1
Commanding General, USA Munitions Command, Dover, New Jersey	1
Commanding Officer, U. S. Army Nuclear Defense Laboratory, Edgewood Arsenal, Edgewood, Maryland 21040 Attn: Tech. Library	1
Commandant, Army War College, Carlisle Barracks, Pennsylvania Attn: Library	1

NAVY

Chief of Naval Operations, Navy Department, Washington, D. C. 20350	
Attn: OP-75	2
OP-03EG	1
Director of Naval Intelligence, Navy Department, Washington, D. C. Attn: OP-922V	1
Special Projects Office, Navy Department, Washington, D. C. 20360 Attn: SP-272	1
Chief, Bureau of Naval Weapons, Navy Department, Washington, D. C. 20360	2
Chief, Bureau of Ships, Navy Department, Washington, D. C. 20360	
Attn: Code 372	1
Code 423	1
Chief, Bureau of Yards and Docks, Navy Department, Washington, D. C. 20360	
Attn: Code D-400	1
Code D-440	1
Chief of Naval Research, Navy Department, Washington, D. C. 20390 Attn: Code 811	1
Commander-in-Chief, U. S. Pacific Fleet, FPO, San Francisco, California	1
Commander-in-Chief, U. S. Atlantic Fleet, U. S. Naval Base, Norfolk 11, Virginia	1
Commandant of the Marine Corps, Navy Department, Washington, D. C. Attn: Code A03H	4
President, U. S. Naval War College, Newport, Rhode Island	1
Commanding Officer, Nuclear Weapons Training Center, Atlantic, Naval Base, Norfolk 11, Virginia Attn: Nuclear Warfare Department	1
Commanding Officer, Nuclear Weapons Training Center, Pacific, Naval Station, North Island, San Diego 35, California	2
Commanding Officer, U. S. Naval Schools Command, U. S. Naval Station, Treasure Island, San Francisco, California	1
Superintendent, U. S. Naval Postgraduate School, Monterey, California	2
Commanding Officer, U. S. Naval Damage Control Training Center, Naval Base, Philadelphia 12, Pa. Attn: ABC Defense Course	1

	Nr. of Copies
Commander, U. S. Naval Ordnance Laboratory, Silver Spring 19, Maryland	
Attn: EA	1
EU	1
E	1
Commander, U. S. Naval Ordnance Test Station, China Lake, California	1
Commanding Officer & Director, U. S. Naval Civil Engineering Laboratory, Port Hueneme, California	
Attn: Code L31	2
Director, U. S. Naval Research Laboratory, Washington, D. C. 20390	1
Commanding Officer & Director, Naval Electronics Laboratory, San Francisco, California 94129	
Attn: Tech. Info. Division	1
Commanding Officer & Director, David W. Taylor Model Basin, Washington, D. C. 20007	
Attn: Library	1
Underwater Explosions Research Division, DTMB, Norfolk Naval Shipyard, Portsmouth, Virginia	1
Commanding Officer, U. S. Naval Radiological Defense Laboratory, San Francisco, California 94129	
Attn: Tech. Info. Div.	1
U. S. Naval Academy, Annapolis, Maryland	
Attn: USNA Library	2
Officer-in-Charge, U. S. Naval School, Civil Engineering Corps Officers, U. S. Naval Construction Battalion, Port Hueneme, California	1

AIR FORCE

Hq. USAF, Washington, D. C. 20330	
Attn: AFRNE	1
Deputy Chief of Staff, Plans and Programs, Hq, USAF, Washington, D. C. 20330	
Attn: War Plans Division	1
Director of Research and Development, DCS/D, Hq. USAF, Washington, D. C. 20330	
Attn: Guidance & Weapons Division	1
Air Force Intelligence Center, Hq. USAF, ACS/I (AFCIN-3K2), Washington, D. C. 22212	1
Commander-in-Chief, Strategic Air Command, Offutt AFB, Nebraska 68113	
Attn: OAWS	2
Commander, Tactical Air Command, Langley AFB, Virginia 23365	
Attn: Document Security Branch	1
ASD, Wright-Patterson AFB, Ohio 45433	1
Commander, Air Force Logistics Command, Wright-Patterson AFB, Ohio 45433	2
AFSC, Andrews Air Force Base, Washington, D. C. 20331	
Attn: RDRWA	1
Director, Air University Library, Maxwell AFB, Alabama 36112	2

	Nr. of Copies
AFCRL, L. G. Hanscom Field, Bedford, Massachusetts 01731 Attn: CRQST-2	1
AFWL, Kirtland AFB, New Mexico 87117 Attn: WLRS	4
Commandant, Institute of Technology, Wright-Patterson AFB, Ohio 45433 Attn: MCLI-ITRIDL	1
BSD, Norton AFB, California 92409	2
Director, USAF Project RAND, Via: U. S. Air Force Liaison Office, The RAND Corporation, 1700 Main Street, Santa Monica, California 90406 Attn: Document Librarian-1, Dr. H. Brode-1	2
Director of Civil Engineering, Hq. USAF, Washington, D. C. 20330 Attn: AFOCE	1
U. S. Air Force Academy, Colorado Springs, Colorado 80840 Attn: USAFA Library	2
SSD, U. S. Air Force Unit Post Office, Los Angeles, California 90045 Attn: BSRGA	1
AFTAC, Washington, D. C. 20330	1
AFOSR, Tempo Bldg., 6th & Independence Ave., Washington, D. C. 20333	1
Other Governmental Agencies	
U. S. Arms Control & Disarmament Agency, Dept. of State, Washington 25, D. C. Attn: Reference Research	1
U. S. Department of the Interior, Geological Survey, Washington 25, D. C.	1
Superintendent, Eastern Experiment Station, U. S. Bureau of Mines, College Park, Maryland Attn: Dr. Leonard Obert	1
Coast & Geodetic Survey, Washington 25, D. C. Attn: Seismology Branch	1
Scientific Publications Branch, USAEC, Germantown, Maryland Attn: Mr. Joseph Gratton	10
Division of Technical Information Extension (DTIE) USAEC, Oak Ridge, Tennessee Attn: Mr. Thomas Laughlin	20
Manager, Albuquerque Operations Office, U. S. Atomic Energy Commission, P. O. Box 5400, Albuquerque, New Mexico	1
Manager, Nevada Operations Office, USAEC, Las Vegas, Nevada	1
Lawrence Radiation Laboratory, Box 808, Livermore, California Attn: Technical Information Division	5
Los Alamos Scientific Laboratory, P. O. Box 1663, Los Alamos, New Mexico Attn: Report Librarian	5
Sandia Corporation, Sandia Base, Albuquerque, New Mexico 87115 Attn: Classified Document Division, For: Dr. M. L. Merritt	5

	Nr. of Copies
Administrator, National Aeronautics & Space Administration, 1512 H Street N. W., Washington, D. C. 20546	1
National Aeronautics & Space Administration, Man-Spacecraft Center, Space Technology Division, Box 1537, Houston, Texas	1
Langley Research Center, NASA, Langley Field, Hampton, Virginia 23365 Attn: Mr. Philip Donely	1
Other Distribution	
Allied Research Associates, Inc., Virginia Road, Concord, Mass. Attn: Mr. Alan D. Sapowith	1
Atlantic Research Corporation, Shirley Highway & Edsall Road, Alexandria, Virginia	1
Barry Controls, 700 Pleasant Street, Watertown 72, Massachusetts	1
DASA Data Center, General Electric Company, 735 State Street, Santa Barbara, California Attn: Mr. Warren Chan	1
Agbabian & Jacobsen Associates, 8939 South Sepulveda Boulevard, Los Angeles, California Attn: Dr. M. S. Agbabian	1
Dr. Joseph W. Berg, Jr., Department of Oceanography, Oregon State University, Corvallis, Oregon	1
Dr. George Clark, University of Missouri, School of Mines and Metallurgy, Rolla, Missouri	1
Dr. Vincent J. Cushing, Engineering Physics Company, 5515 Randolph Road, Rockville, Maryland	1
Dr. Robert C. DeHart, Southwest Research Institute, P. O. Box 28281, San Antonio 6, Texas	1
Dr. George Duvall, Washington State University, Pullman, Washington	1
Dr. Robert J. Hansen, Division of Industrial Cooperation, Massachusetts Institute of Technology, 77 Massachusetts Avenue, Cambridge, Massachusetts (Send TS to 244 Wood Street, Lexington, Mass.)	1
Dr. Bruce G. Johnston, The University of Michigan, University Research Security Office, Lobby 1, East Engineering Bldg., Ann Arbor, Michigan (Do not send TOP SECRET to this address)	1
Dr. Sidney Kaufman, Shell Development Co., Houston, Texas	1
Dr. G. Neidhardt, General American Transportation Corporation, 7501 N. Natchez Ave., Niles, Illinois	1
Dr. Nathan M. Newmark, University of Illinois, Room 207, Talbot Laboratory, Urbana, Illinois	3
Dr. T. H. Schiffman, Illinois Institute of Technology Research Institute, 10 West 35th Street, Chicago 16, Illinois	1
Dr. Robert L. Kondner, Northwestern University, Evanston, Illinois	1
Dr. Frank Shelton, Kaman Nuclear, Colorado Springs, Colorado	1

	Nr. of Copies
Edgerton, Germeshausen and Grier, Inc., 160 Brookline Avenue, Boston, Mass. 02129 Attn: Mr. D. F. Hansen	1
Edgerton, Germeshausen and Grier, Inc., 1622 "A" Street, Las Vegas, Nevada	1
Holmes & Narver, Inc., AEC Facilities Division, Highland Avenue, Las Vegas, Nevada	1
Massachusetts Institute of Technology, Cambridge 39, Mass. Attn: R. V. Whitman	1
Mitre Corporation, P. O. Box 208, Lexington 73, Massachusetts	1
Mr. J. F. Halsey, c/o Thiokol, P. O. Box 428, Brigham City, Utah	1
Mr. Kenneth Kaplan, United Research Services, 1811 Trousdale Drive, Burlingame, California	1
Mr. David N. Keast, Bolt, Beranek & Newman, Inc., 8221 Melrose Ave., Los Angeles 46, California	1
Mr. Marc Peter, Corporate Systems Center, United Aircraft, 940 Sepulveda Blvd., El Segundo, California	1
Mr. Fred M. Sauer, Department of Physics, Stanford Research Institute, Menlo Park, California	1
Mr. Sherwood Smith, Roland F. Beers, Inc., 2520 Oakville, Alexandria, Virginia	1
Mr. A. Wiedermann, Illinois Institute of Technology, Research Institute, 10 West 35th Street, Chicago 16, Illinois	1
Paul Weidlinger, Consulting Engineer, 770 Lexington Ave., New York 21, New York Attn: Dr. M. Baron	1
Professor M. G. Spangler, Iowa State University, Ames, Iowa	1
Professor J. Neils Thompson, University of Texas, Structural Mechanics Research Laboratory, Austin, Texas	1
Professor R. V. Whitman, Physics Div. Stanford Research Institute, Menlo Park, California	1
Space Technology Laboratories, Inc., One Space Park, Redondo Beach, California	2
United Electrodynamics, Inc., 314-16 Montgomery St., Alexandria, Virginia	1
Aerospace Corporation, P. O. Box 95085, Los Angeles, California 90012	1
Boeing Company, P. O. Box 3707, Seattle, Washington 98124 Attn: Mr. R. W. Hagger (5172); Mr. M. V. Anthony (2191)	2
The Ralph M. Parsons Company, Los Angeles, California Attn: Mr. Carl Flechman	1
The Martin Company, Sand Lake Road, Orlando, Florida Attn: Mr. Ralph Dudley (MP-492)	1
The Stanford Research Institute, Menlo Park, California 94025	10
Bell Telephone Laboratories, Structures Design Department, Whippany, New Jersey	1

Unclassified

Security Classification

DOCUMENT CONTROL DATA - R&D

(Security classification of title, body of abstract and indexing annotation must be entered when the overall report is classified)

1. ORIGINATING ACTIVITY *(Corporate author)*

Stanford Research Institute,
Menlo Park, California

2a. REPORT SECURITY CLASSIFICATION
Unclassified

2b. GROUP
None

3. REPORT TITLE

NUCLEAR GEOPLOSICS, A SOURCE BOOK OF UNDERGROUND PHENOMENA AND EFFECTS OF NUCLEAR EXPLOSIONS

4. DESCRIPTIVE NOTES *(Type of report and inclusive dates)*

Final

5. AUTHOR(S) *(Last name, first name, initial)*

Sauer, Fred M., Editor-in-Chief

6. REPORT DATE	**7a. TOTAL NO. OF PAGES**	**7b. NO. OF REFS**
May 1964	672	624

8a. CONTRACT OR GRANT NO.
DA-49-146-XZ-030

b. PROJECT NO.
NWER Subtask 13.036

c.

d.

9a. ORIGINATOR'S REPORT NUMBER(S)
DASA-1285 (I), (II), (III), (IV), (V)

9b. OTHER REPORT NO(S) *(Any other numbers that may be assigned this report)*
None

10. AVAILABILITY/LIMITATION NOTICES

This document not approved for open publication or distribution to the Office of Technical Services, Department of Commerce. Qualified requestors may obtain copies of this report from DDC. Foreign announcement and dissemination of this report by DDC is not authorized.

11. SUPPLEMENTARY NOTES
None

12. SPONSORING MILITARY ACTIVITY
Defense Atomic Support Agency
Washington, D.C. 20301

13. ABSTRACT

The sourcebook is comprised of five parts:

I Theory of Directly-Induced Ground Motion

II Mechanical Properties of Earth Materials

III Test Sites and Instrumentation

IV Empirical Analysis of Ground Motion and Cratering

V Effects on Underground Structures and Equipment

DD FORM 1 JAN 64 1473

Unclassified

Security Classification

Security Classification

14. KEY WORDS	LINK A		LINK B		LINK C	
	ROLE	WT	ROLE	WT	ROLE	WT
Nuclear Explosions, Ground Shock, Ground Motion Protective Structures, Dynamic Properties of Soil and Rock, Nuclear Test Data, Nuclear Test Sites, Dynamic Instrumentation						

INSTRUCTIONS

1. ORIGINATING ACTIVITY: Enter the name and address of the contractor, subcontractor, grantee, Department of Defense activity or other organization *(corporate author)* issuing the report.

2*a*. REPORT SECURITY CLASSIFICATION: Enter the overall security classification of the report. Indicate whether "Restricted Data" is included. Marking is to be in accordance with appropriate security regulations.

2*b*. GROUP: Automatic downgrading is specified in DoD Directive 5200.10 and Armed Forces Industrial Manual. Enter the group number. Also, when applicable, show that optional markings have been used for Group 3 and Group 4 as authorized.

3. REPORT TITLE: Enter the complete report title in all capital letters. Titles in all cases should be unclassified. If a meaningful title cannot be selected without classification, show title classification in all capitals in parenthesis immediately following the title.

4. DESCRIPTIVE NOTES: If appropriate, enter the type of report, e.g., interim, progress, summary, annual, or final. Give the inclusive dates when a specific reporting period is covered.

5. AUTHOR(S): Enter the name(s) of author(s) as shown on or in the report. Enter last name, first name, middle initial. If military, show rank and branch of service. The name of the principal author is an absolute minimum requirement.

6. REPORT DATE: Enter the date of the report as day, month, year; or month, year. If more than one date appears on the report, use date of publication.

7*a*. TOTAL NUMBER OF PAGES: The total page count should follow normal pagination procedures, i.e., enter the number of pages containing information.

7*b*. NUMBER OF REFERENCES: Enter the total number of references cited in the report.

8*a*. CONTRACT OR GRANT NUMBER: If appropriate, enter the applicable number of the contract or grant under which the report was written.

8*b*, 8*c*, & 8*d*. PROJECT NUMBER: Enter the appropriate military department identification, such as project number, subproject number, system numbers, task number, etc.

9*a*. ORIGINATOR'S REPORT NUMBER(S): Enter the official report number by which the document will be identified and controlled by the originating activity. This number must be unique to this report.

9*b*. OTHER REPORT NUMBER(S): If the report has been assigned any other report numbers *(either by the originator or by the sponsor)*, also enter this number(s).

10. AVAILABILITY/LIMITATION NOTICES: Enter any limitations on further dissemination of the report, other than those imposed by security classification, using standard statements such as:

(1) "Qualified requesters may obtain copies of this report from DDC."

(2) "Foreign announcement and dissemination of this report by DDC is not authorized."

(3) "U. S. Government agencies may obtain copies of this report directly from DDC. Other qualified DDC users shall request through

_____."

(4) "U. S. military agencies may obtain copies of this report directly from DDC. Other qualified users shall request through

_____."

(5) "All distribution of this report is controlled. Qualified DDC users shall request through

_____."

If the report has been furnished to the Office of Technical Services, Department of Commerce, for sale to the public, indicate this fact and enter the price, if known.

11. SUPPLEMENTARY NOTES: Use for additional explanatory notes.

12. SPONSORING MILITARY ACTIVITY: Enter the name of the departmental project office or laboratory sponsoring *(paying for)* the research and development. Include address.

13. ABSTRACT: Enter an abstract giving a brief and factual summary of the document indicative of the report, even though it may also appear elsewhere in the body of the technical report. If additional space is required, a continuation sheet shall be attached.

It is highly desirable that the abstract of classified reports be unclassified. Each paragraph of the abstract shall end with an indication of the military security classification of the information in the paragraph, represented as *(TS)*, *(S)*, *(C)*, or *(U)*.

There is no limitation on the length of the abstract. However, the suggested length is from 150 to 225 words.

14. KEY WORDS: Key words are technically meaningful terms or short phrases that characterize a report and may be used as index entries for cataloging the report. Key words must be selected so that no security classification is required. Identifiers, such as equipment model designation, trade name, military project code name, geographic location, may be used as key words but will be followed by an indication of technical context. The assignment of links, rules, and weights is optional.

Defense Threat Reduction Agency
45045 Aviation Drive
Dulles, VA 20166-7517

CPWC/TRC

May 6, 1999

MEMORANDUM FOR DEFENSE TECHNICAL INFORMATION CENTER
ATTN: OCQ/MR WILLIAM BUSH

SUBJECT: DOCUMENT REVIEW

The Defense Threat Reduction Agency's Security Office has reviewed and declassified or assigned a new distribution statement:

- AFSWP-1069, AD-341090, STATEMENT A — RD waiting for copy
- DASA-1151, AD-227900, STATEMENT A
- DASA-1355-1, AD-336443, STATEMENT A
- DASA-1298, AD-285252, STATEMENT A
- DASA-1290, AD-444208, STATEMENT A
- DASA-1271, AD-276892, STATEMENT A
- DASA-1279, AD-281597, STATEMENT A
- DASA-1237, AD-272653, STATEMENT A
- DASA-1246, AD-279670, STATEMENT A
- DASA-1245, AD-419911, STATEMENT A
- DASA-1242, AD-279671, STATEMENT A
- DASA-1256, AD-280809, STATEMENT A
- DASA-1221, AD-243886, STATEMENT A
- DASA-1390, AD-340311, STATEMENT A — FRD
- ~~DASA-1283,~~ AD-717097, STATEMENT A OK
- DASA-1285-5, AD-443589, STATEMENT A
- DASA-1714, AD-473132, STATEMENT A
- DASA-2214, AD-854912, STATEMENT A
- DASA-2627, AD-514934, STATEMENT A
- DASA-2651, AD-514615, STATEMENT A
- ~~DASA-2536, AD-876697, STATEMENT A~~
- DASA-2722T-V3, AD-518506, STATEMENT A
- DNA-3042F, AD-525631, STATEMENT A
- DNA-2821Z-1, AD-522555, STATEMENT A

If you have any questions, please call me at 703-325-1034.

Ardith Jarrett

ARDITH JARRETT
Chief, Technical Resource Center